November 2022

Quantifying Environmental Sensitivity of Marine Resources to Oil Well Blowouts in the Gulf of Mexico

Emily Chancellor
University of South Florida

Quantifying Environmental Sensitivity of Marine Resources to Oil Well Blowouts in the Gulf of Mexico

by

Emily Chancellor

A dissertation submitted in partial fulfillment
of the requirements for the degree of
Doctor of Philosophy
College of Marine Science
University of South Florida

Major Professor: Steven A. Murawski, Ph.D.
Ernst Peebles, Ph.D.
Claire Paris, Ph.D.
James Sanchirico, Ph.D.
David Naar, Ph.D.

Date of Approval:
November 21, 2022

Keywords: environmental sensitivity indices, vulnerability assessment, marine spatial planning

Acknowledgments

I am grateful for the support provided by my family, peers, and friends during the completion of this degree. My parents, Sam and Linda Chancellor, and my sister, Cara Chancellor, have been my supporters during their process and I am so thankful for it. I want to thank my fellow USF graduates for their friendship and motivation. I have met so many truly brilliant and talented peers during the completion of this degree and I am consistently inspired by them.

A large thank you goes to my advisor, Dr. Steve Murawski, for the opportunity to complete both my M.S. and my Ph.D. degrees at USF, and for his insightful expertise which has shaped so much of this dissertation. I want to thank the rest of my dissertation committee, Dr. Ernst Peebles, Dr. Claire Paris, Dr. James Sanchirico, and Dr. David Naar, for their invaluable assistance during this process. This research was made possible in part by financial support provided by the Gulf of Mexico Research Initiative/C-IMAGE I and II.

Table of Contents

List of Tables

List of Figures

Abstract

This dissertation focused on oil spill risk assessment techniques historically utilized for coastal resources (e.g., environmental sensitivity indices (ESIs), vulnerability assessments, species-specific vulnerability frameworks) and their application and expansion to offshore resources found in the Gulf of Mexico (GoM). Additional included techniques (e.g., multi-sector trade-off analysis, marine spatial planning (MSP) software) provide support in decision making processes regarding the potential siting of oil production sites and/or the withdrawal of areas from oil and natural gas production. Chapter 1 included an overview and justification for this study. Chapter 2 demonstrated an initial methodology for the creation of offshore ESIs and how vulnerability to marine resources might be estimated via the inclusion of an oil fate and transport model used to simulate oil well blowouts. Chapter 3 created spatial distributions of marine resources from disparate sources and transformed the distributions into quantifiably comparable grids via the use of standardized indices. These grids were combined via a multi-attribute utility model (MAUM) to create multiple cumulative ESIs (C-ESIs) identifying resource rich "hot-spots" within the GoM. Chapter 3 also explored dissimilarity and cluster mapping methods to identify sets of resources with similar distributions and estimate the degree of influence to the overall C-ESIs. Species-specific vulnerability rankings estimated under a preliminary trait-based framework were provided for use in this study and were added to a fish species C-ESI to illustrate how C-ESIs might be combined with similar frameworks to weight one resource or suite of resources more heavily. The C-ESI was impacted as expected by the heavy weighting of

one fish species with grid cells containing the weighted species being prioritized as resource "hot-spots". The C-ESI was rather robust to the inclusion of weights for the suite of fish species owing to the conflicting spatial distributions of the individual weighted species. In Chapter 4, surface oil distributions from four oil well blowout scenarios were modeled with the Connectivity Modeling System (CMS; Paris et al. 2013). These oil distributions were created to simulate likely conditions from the Deepwater Horizon oil well blowout (DWH) and three hypothetical oil well blowouts with origin points in the western GoM (WGoM), the west Florida slope (WFS), and at the DWH origin point with a September start date. The simulated distributions of surface oil from these four scenarios were used to create bounded areas, or polygons, of minimum oil concentration thresholds (MOCT) representing spatial areas exposed to at least the specified concentration of oil for at least one day. These MOCTs are intersected with the C-ESIs developed in Chapter 3 to compare potential vulnerability of resources to the oil well blowout scenarios. The WFS scenario was found to potentially have the largest impact on the suite of included species due to the large surface area of the modeled spill and the resources found in that area. While a spill off the continental slope near Texas (WGoM) would have the smallest overall footprint, it would affect some fisheries more severely than the other simulated spills. The MOCT polygons coupled with known PAH concentration toxicity endpoints and spatial distributions of marine resources can be used to predict the extent of the spatial overlap between marine resources and oil and the likely outcome of that interaction. In Chapter 5, a spatial distribution of 2018 oil production was overlaid with the C-ESIs created in Chapter 3 to form quantifiably explicit multi-sector tradeoff curves between resource sensitivity and oil production. These tradeoff curves represent the system-wide benefit of theoretical allocations of oil production to both sectors on a cell-by-cell planning unit basis. The C-ESIs and multi-sector

tradeoff functions were used to identify individual grid cells to potentially reserve from oil production. Marxan, an MSP zoning software, was used to create minimum-set "hot-spot" networks of areas to potentially reserve from oil production in both 1.) a hypothetical pristine system where future oil production siting is being planned and 2.) the current system with current levels and placement of oil production. In both scenarios, the "hot-spot" networks identified areas on the WFS as potentially valuable to reserve from oil production, with more "hot-spot" areas on the WFS when accounting for current oil production. This result indicates that in a hypothetical reserve sited around existing oil production and created to protect a significant proportion of offshore marine resources, the grid cells on the WFS would be the most valuable to include in that reserve. This study compares these "hot-spot" network solutions to the area in the eastern GoM currently withdrawn from oil production under Gulf of Mexico Energy Security Act (GOMESA) and the 2021 Congressional moratorium. The "hot-spot" networks overlap with the withdrawn area with 39.5% of the pristine "hot-spot" reserve network and 53.2% of the current oil production "hot-spot" reserve network being located within the withdrawn area. The "hot-spot" networks identified in this study can potentially be utilized in the decision-making process to continue the closure of these withdrawn areas.

The integrated collection of methods presented here were designed to add to the crucial knowledge base for planning and prioritizing oil spill response, predicting impacts from an oil spill to individual resources and groups of resources, and to assist in the decision-making processes for making new and existing sites available or unavailable to oil production. Impact estimates generated by these tools can be used in prioritizing oil spill cleanup and the acquisition or pre-positioning of oil spill response and supplies. The C-ESIs can be combined with actual or proposed oil production statistics to serve as a decision-making tool for justifying the reservation

of specific lease blocks from leasing or maintaining the status of areas temporarily withdrawn from oil production under the Congressional moratorium.

The tools in this study were designed, developed, and published as open source with the hope that they may be added to, improved upon, and utilized in real world scenarios to lessen the risk of impacts on marine resources from future blowout scenarios. The Python scripts used for the analyses and figures found in this dissertation can be found at github.com/echancellor/dissertation-scripts.

Chapter 1. Introduction

This dissertation focuses on oil spill risk assessment techniques historically utilized for coastal resources and their application and expansion to offshore resources found in the Gulf of Mexico (GoM). These applications are designed to add to the crucial knowledge base for planning and prioritizing oil spill response, predicting impacts from an oil spill to offshore resources, and to assist in the decision-making processes for making new and existing sites available or unavailable to oil production.

Offshore oil production in the Gulf of Mexico (GoM) provides about 15% of the total U.S. crude oil production and about 97% of the marine oil production (EIA 2018; EIA 2021) with estimated oil reserves of over 3.67 billion barrels (Kazanis et al. 2015). U.S. oil is produced in the GoM in the 200 miles beyond the U.S. coastline in the U.S. Exclusive Economic Zone (EEZ) and is divided into the Western Planning Area, Central Planning Area, and Eastern Planning Area (EIA 2021; BOEM 2021). Most of the GoM marine oil production occurs in the central and western planning areas as part of the Central Planning Area and most of the Eastern Planning Area are currently withdrawn from drilling until 2032 under the initial 2006 Gulf of Mexico Energy Security Act (GOMESA) and extended under the 2021 Congressional moratorium (Schwartz 2020; BOEM 2021). Most of this oil production occurs at depths between 1000 meters and 2000 meters with some production occurring at depths exceeding 3000 meters (BOEM 2018a, b). GoM oil production has focused on increasingly deeper sources to meet production goals and many of these deep-water sources are now more productive than

shallower fields (Murawski et al. 2020). As marine oil and gas production moves further offshore, marine resources in the deep GoM become increasingly vulnerable to oil spills and oil well accidents. The increased threat to these marine resources necessitates the knowledge of what resources are in these offshore areas and how they might respond to oil exposure from an oil spill accident. This knowledge is crucial for oil spill response, predicting long term impacts from an oil spill, and can also be used as part of the decision-making process regarding opening or closing areas to oil production.

The risks to marine resources from an oil spill depend on the degree of interaction between the resource and oil and the resource-specific vulnerability to that oil. The degree of interaction between a marine resource and oil varies by 1.) the degree of spatial intersection between the resource and the oil, 2.) the physical and chemical characteristics of the oil, and 3.) the concentration and duration of the exposure. Resource-specific vulnerability is the fragility and resiliency of that resource to an oil spill and varies due to resource-specific traits (e.g., life history traits in biological resources, physical traits between coastline areas; Polidoro et al. 2020; Peterson 2002).

Spatial vulnerability assessments include spatial distributions of sensitive resources and their specific vulnerability to create a vulnerability matrix (Matisziw and Grubesic 2013; Nelson et al. 2015). Spatial maps of sensitive natural resources called Environmental Sensitivity Indices (ESIs), are used to prioritize environmentally sensitive areas for oil spill cleanup, estimate impacts to marine resources from an oil spill, and to evaluate the potential environmental impacts caused by oil production (Jensen et al. 1990; Jensen et al. 1998; Kankara et al 2016). Coastal habitats and resources are not uniformly vulnerable to oil exposure due to differences in tidal energy, shoreline slope, and substrate type (Peterson 2002; Santos et al. 2012). ESIs have

therefore been created for much of the coastal areas in the United States and GoM to identify the locations of sensitive resources and habitats. Spatial vulnerability assessments can be incorporated with an oil fate and transport model to estimate interactions between the vulnerability matrix and oil, along with the chemical and physical traits of that oil. Environmental data, including ESIs, was combined to provide vulnerability assessments using the National Energy Technology Laboratory's (NETL) Blowout and Spill Occurrence Model (BLOSOM) model to provide an example assessment of coastal vulnerability in the GoM (Sim 2013; Nelson et al. 2015). A similar methodology to create an oil spill sensitivity analysis was applied in the Gulf of Kachchh through use of a previously published ESI for the coastal waters and an oil trajectory model to simulate oil spill scenarios (Kankara and Subramanian 2007).

This study applies similar methodology as described above to assess the risk to resources in the offshore waters in the GoM. Offshore waters in the GoM contain unique biological resources and habitats which are also threatened during large scale oil spills. The offshore waters of the GoM are important as they are home to multiple species of economically important fishes and shellfish (Felder et al. 2009; Sutton et al. 2017; Frasier et al. 2020; Perlin et al. 2020; Pulster et al. 2020) as well as ecologically important forage species and other animals of concern including mammals, turtles, seabirds, and deep-sea corals which all can experience lethal and significant sub-lethal effects from exposure to oil (Antonio et al. 2011; Carmichael et al. 2012; Schwacke et al. 2014; Tran et al. 2014; Etnoyer et al. 2016; Kinlan et al. 2016). Like coastal areas, which are not uniformly vulnerable to an oil spill, offshore marine resources are also not uniformly vulnerable to oil. A complete vulnerability assessment for the offshore resources would therefore include the resource-specific vulnerability to oil exposure. Resource-specific

vulnerability can be observed in the event of an oil spill, from toxicity tests, or estimated from life history traits via the use of a vulnerability framework.

Marine organisms are exposed to oil through four major pathways: absorption of bioavailable hydrocarbon compounds into skin via direct contact with oil (e.g., sea turtles and mammals surfacing and diving), inhalation and aspiration (air-breathing animals may breathe in aerosol compounds), and ingestion (ingestion of water or sediments containing oil; Westerholm and Rauch 2016). Polycyclic aromatic hydrocarbons (PAHs) are the most toxic compounds in crude oil. The concentration of PAHs and duration of exposure determine lethal and sublethal effects to biological resources through absorption. Toxicity tests are performed to identify critical thresholds (i.e., toxicity endpoints) of fish and invertebrate species to oil and dispersants used in oil cleanup (Westerholm and Rauch 2016). Species-specific vulnerability to petrochemical exposure is not known for all species (Bejarano and Barron 2014; Bejarano and Barron 2016; Bejarano and Mearns 2015; Bejarano and Wheeler 2020) but can be estimated by using a trait-based framework to rank relative vulnerability and identify sensitive species (Polidoro et al. 2020; Sarrazin et al. 2021). Species-specific vulnerabilities identified via these frameworks or by toxicity endpoints determined from experimental studies can be included when evaluating potential impacts to a resource due to oil exposure.

The Bureau of Ocean Energy Management (BOEM) within the U.S. Department of the Interior (DOI) produces and utilizes environmental impact assessments as part of their decision-making process on which areas to make available to oil drilling. Approved leases for oil drilling are then sold by the DOI. These environmental assessments consider the totality of natural resources and human activities within a region being considered for leases, as well as any particular hazards that might impact safe prospecting and production operations. Planners use a

number of qualitative and quantitative tools to consider these activities and hazards when identifying lease blocks to offer for sale. Ecosystem based marine spatial planning (MSP) is one such quantitative tool that has not heretofore been used in this regard but aims to maximize the combined benefit from the ecosystem to all sectors through use of quantifiably explicit tradeoffs between competing sectors (McLeod et al. 2005; White et al. 2012; Santos et al. 2013b). MSP divides the planning area into planning units and assigns a value to each planning unit for each sector. An optimization solver then finds a solution by assigning all planning units to sectors to maximize the system-wide benefit subject to grouping constraints. Quantifying offshore resources through use of ESIs allows for the mapping of these tradeoff functions between resources and oil production and the subsequent development of an MSP solution.

Chapters two-six of this dissertation explore the utility of spatially quantifying the distribution and abundance of offshore marine resources and creating Cumulative Environmental Sensitivity Indices (C-ESIs) for the offshore areas. These C-ESIs, coupled with an oil fate and transport model and MSP software are employed to identify particularly vulnerable offshore areas, or "hot-spots", as well as "hot-spot" networks that should potentially be reserved from oil production because the risks of oil production there create quantifiably greater risks than in other areas (Figure 1.1). In Chapter 2, the initial methodology is presented for creating the ESIs for offshore marine resources and intersecting them with fate and transport models of simulated oil well blowouts. In Chapter 3, C-ESIs are created from quantifiably comparable spatially distributed resource layers from initially disparate sources through use of scaling and data transformation. A species-specific vulnerability score based on a preliminary trait-based framework (Polidoro et al. 2020) is added to one C-ESI to demonstrate the utility of combining the C-ESIs with species-specific vulnerability to prioritize certain resources in the C-ESI due to

their vulnerability. In Chapter 4, surface oil distributions from four oil well blowout scenarios modeled by the Connectivity Modeling System (CMS; Paris et al. 2013) are used to create areas, or polygons, of minimum oil concentration thresholds (MOCT) representing areas exposed to at least the specified concentration of oil during these hypothetical blowouts. These MOCTs are intersected with the C-ESIs and comprising resource layers developed in Chapter 3 along with identified species-specific PAH concentration toxicity endpoints to compare potential vulnerability of resources to the oil well blowout scenarios. In Chapter 5, a spatial distribution of 2018 oil production is overlaid with the C-ESIs created in Chapter 3 to form quantifiably explicit multi-sector tradeoff curves between resource sensitivity and oil production. These tradeoff curves represent the system-wide benefit of theoretical allocations of oil production to both sectors on a cell-by-cell planning unit basis. These C-ESIs and multi-sector tradeoff curves are used to create minimum-set "hot-spot" networks of areas to potentially reserve from oil production in both 1.) a hypothetical pristine system where future oil production siting is being planned and 2.) the current system with current levels and placement of oil production. Finally, this study compares these "hot-spot" network solutions to the current areas withdrawn from oil production under GOMESA and the 2021 Congressional moratorium to provide additional support for the decision-making process of withdrawing these areas from oil production. A diagram representing of the datasets developed in this study, the deliverables created by chapter, and their corresponding inputs are found in Figure 1.1.

The tools developed in this study have useful applications for oil production planning and oil spill response. A complete risk and response assessment of marine resources in the event of an oil spill requires knowing what resources were exposed to oil, the characteristics of that exposure, and the resource-specific response to that oil. The techniques for quantifying and

combining disparate sources into C-ESIs helps to answer the question of what resources were potentially exposed. Creating MOCT polygons from fate and transport models of actual or hypothetical oil spills and intersecting them with the quantitative distributions of these resources provides details on the extent and characteristics of that exposure. While the calculation of resource-specific vulnerability lies outside the scope of this study, species-specific vulnerability rankings and published toxicity endpoints are combined with the C-ESIs and MOCT polygons to demonstrate how these tools could improve estimates of impacts on marine resources from oil spills. These impact estimates can be used in prioritizing oil spill cleanup and the acquisition or pre-positioning of oil spill response and supplies. The C-ESIs can be combined with actual or proposed oil production statistics to create tradeoff functions between sensitive resources and the oil production industry and serve as a decision-making tool for justifying the reservation of specific lease blocks from leasing or the status of areas temporarily reserved from oil production.

The tools in this study were designed, developed, and published as open source with the hope that they may be added to, improved upon, and utilized in real world scenarios to lessen the risk of impacts on marine resources from future blowout scenarios. The Python scripts used for the analyses and figures found in this dissertation can be found at github.com/echancellor/dissertation-scripts.

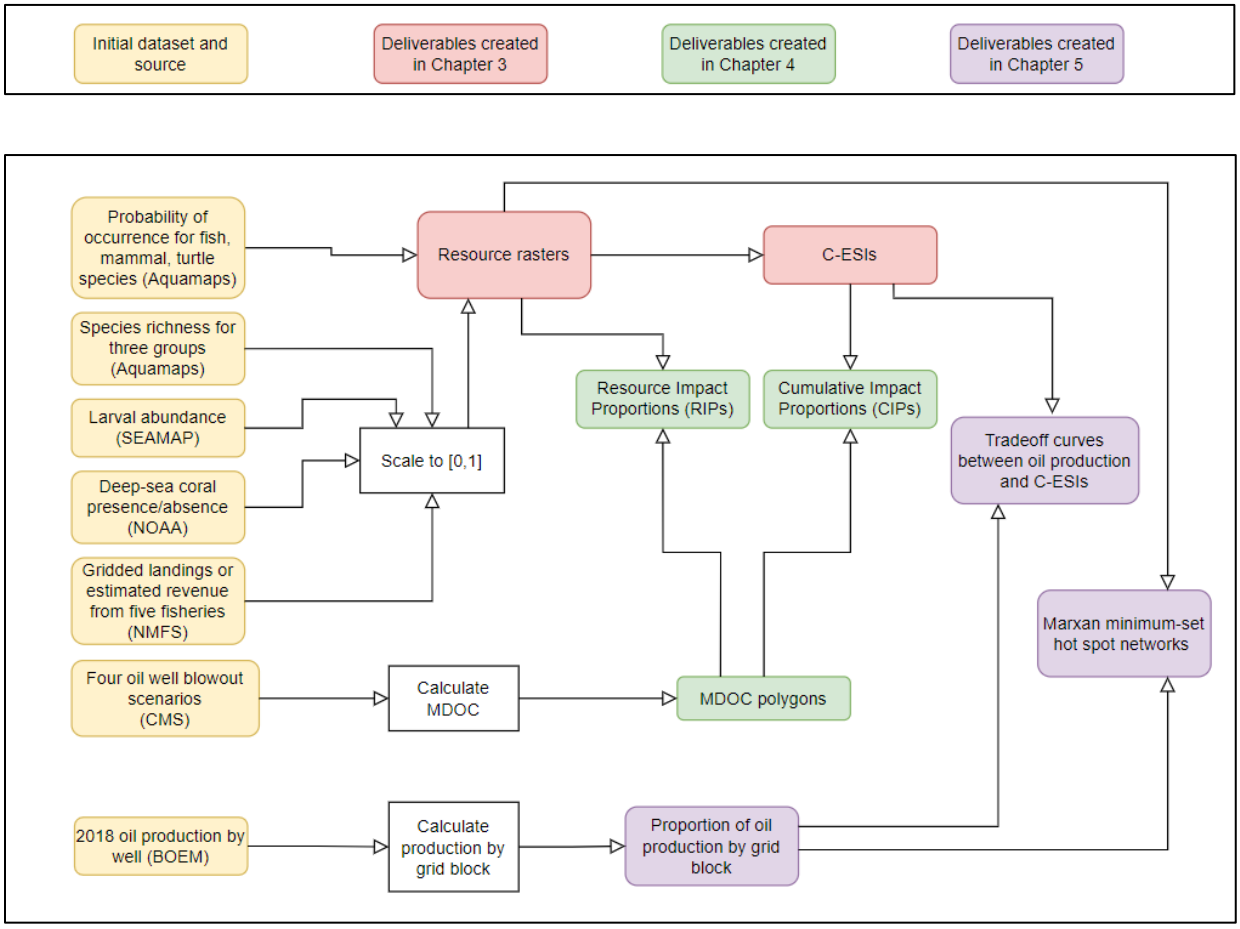

Figure 1.1 Design and organization of this dissertation.
Flowchart with data sources (yellow), data transformations(white), and deliverables by chapter (red – Chapter 3, green – Chapter 4, purple – Chapter 5).

Chapter 2. Comparative Environmental Sensitivity of Offshore Gulf of Mexico Waters Potentially Impacted by Ultra-Deep Oil Well Blowouts

2.1 Abstract

Environmental Sensitivity Indices (ESIs) have long been used to identify coastal and shoreline resources particularly vulnerable to oil spills and ensuing mitigation measures. In the Gulf of Mexico oil production by the USA and Mexico has increasingly focused on deep-water sources. As oil exploration and production continues further offshore, deep-water and open-ocean pelagic resources increasingly become the focus of susceptibility to oil well blowouts. Methodologies are proposed to spatially quantify ESIs specifically for offshore living marine resources. A multi-attribute utility model is proposed to integrate biological resource sensitivity measures and measures of potential economic losses to define spatially explicit environmental sensitivity. Model sensitivity is examined using three weighting schemes for various environmental attributes. The relative environmental sensitivities of four simulated deep-water blowouts in the Gulf of Mexico were analyzed and compared. While differences were found between four oil well blowout scenarios in terms of the overall sensitivity and the individual attributes, results were relatively insensitive to relative weights assigned to various attributes. The uses of ESIs in optimizing oil production locations to minimize potential impacts on sensitive ecological resources and economic uses are discussed.

2.2 Note to Reader

This chapter was published in the book: *Scenarios and Responses to Future Deep Oil Spills* and is included here in Appendix A.

The full citation is:

Chancellor, E., Murawski, S.A., Paris, C.B., Perruso, L., Perlin, N., 2020. Comparative environmental sensitivity of offshore Gulf of Mexico waters potentially impacted by ultra-deep oil well blowouts, in: Scenarios and Responses to Future Deep Oil Spills. Springer, pp. 443–466.

Chapter 3. A Quantitative Analysis of the Offshore Resources of the Gulf of Mexico and Creation of Cumulative Environmental Sensitivity Indices (C-ESIs)

3.1 Introduction

Offshore oil production in the Gulf of Mexico (GoM) provides about 15% of the total U.S. crude oil production and about 97% of the marine oil production (EIA 2018; EIA 2021). Most of this marine oil production occurs at depths between 1000 meters (m) and 2000 m with some production occurring at depths exceeding 3000 m (BOEM 2018a, b). GoM oil production has focused on increasingly deeper sources to meet production goals and many of these deep-water sources are now more productive than shallower fields (Murawski et al. 2020). The GoM contains many marine resources, both biological and human use, which can be negatively impacted in the event of an oil spill or oil well blowout such as occurred in the Deepwater Horizon blowout on April 20, 2010. As GoM oil production continues to move further offshore, it is necessary to assess the risk to these marine resources and habitats. Assessing this risk requires spatially quantifying the resources present in these offshore waters and combining the spatial distributions of these resources in a meaningful way to identify areas in the offshore waters which are especially vulnerable to a large oil spill event.

Spatial maps of the presence of sensitive natural resources called Environmental Sensitivity Indices (ESIs) are used to prioritize environmentally sensitive areas for oil spill cleanup, estimate impacts to marine resources from an oil spill, and to evaluate the potential environmental impacts caused by oil production (Jensen et al. 1990; Jensen et al. 1998; Kankara

et al 2016). Site-specific geographic information system (GIS)-based ESIs identifying the locations of sensitive resources and habitats have been published for much of the shoreline of the United States including the GoM (Knudsen and Druyor 2009; NOAA 2018). NOAA Office of Response and Restoration has published guidelines for creating shoreline ESIs with a composite index consisting of three components: shoreline classification, biological resources, and human-use resources (Peterson 2002; NOAA 2018). Shorelines are classified by type and ranked by their sensitivity, natural persistence of oil, and ease of cleanup (Peterson 2002). Shoreline sensitivity varies due to differences in tidal energy, shoreline slope, and substrate type with exposed rocky shorelines (Rank 1) ranked as least sensitive and marshes and mangroves (Rank 10) ranked as most sensitive in the NOAA criteria (Peterson 2002; Santos et al. 2012). Biological resources include areas with many distinct species, areas with large overall abundance of organisms, and areas where vulnerable species reside (e.g., seabirds, turtles, and other endangered species; Peterson 2002). These biological vulnerabilities may have a seasonal component as certain life stages are more vulnerable than others and may only present for part of the year (e.g., for breeding; Peterson 2002). Human-use components include historic sites and public use areas such as parks and recreational beaches. Both categorical and quantitative ESIs have been created for shoreline sensitivity to offshore spills specific to locations in the Mediterranean Sea (Adler and Inbar 2007; Castanedo et al. 2008; Fattal et al. 2010; Olita et al. 2012; Santos et al. 2013a; Santos et al. 2013b; Alves et al. 2014; Maitieg et al. 2018), GoM (Nelson et al. 2015; Nelson and Grubesic 2018), Brazil (Carmona et al. 2006; Szlafsztein and Sterr 2007; Romero et al. 2013), and Asia (Lan et al. 2015; Lee and Jung 2015). Environmental sensitivity is also regularly calculated using ESI methods by the Bureau of Ocean Energy Management (BOEM) for its Oil and Natural Gas Planning Program assessment (Niedoroda et

al. 2014; BOEM 2018a; Orr et al. 2018). However, these analyses may not be sufficiently spatially disaggregated to identify discrete, sensitive areas worthy of increased scrutiny. As well, they are difficult to compare across planning districts.

This study creates offshore ESIs to add to the existing suite of ESIs previously created and published for the coastal areas of the GoM. Offshore waters in the GoM contain heterogeneously distinct biological resources and human-use resources which can be threatened during large scale oil spills. Commercially important fish and shellfish species, ecologically important forage fish species, deep-sea corals, sea birds, and endangered mammal and turtle species are all found in offshore GoM waters (Felder et al. 2009; Sutton et al. 2017; Frasier et al. 2020; Perlin et al. 2020; Pulster et al. 2020). Up to half of known fish species in the GoM occur in mesopelagic deep waters and new species are being encountered there regularly as sampling effort expands (Sutton et al. 2020). These resources all have demonstrated lethal and sub-lethal effects from exposure to oil (Antonio et al. 2011; Carmichael et al. 2012; Schwacke et al. 2014; Tran et al. 2014; Etnoyer et al. 2016; Kinlan et al. 2016). Additionally, many economically important species of fish spawn in open waters (Chancellor 2015) and their larval life stages are particularly vulnerable to oil (Carls et al. 1999; Incardona et al. 2004; Hicken et al. 2011; Incardona et al. 2013). Primary production in offshore waters, although not as intense as in coastal waters nevertheless contributes to fishery production in the deep sea (Friedland et al. 2012). Human uses of resources in offshore waters include commercial and recreational fisheries, commercial shipping and cruise lines, military exercise areas, oil and natural gas extraction, renewable energy infrastructure, marine protected areas (MPAs) and other uses (Edgar et al. 2007; McCrea-Strub et al. 2011; BOEM 2018a, b).

The ESIs developed in this study combine quantitative spatial distributions of resources from disparate sources to create cumulative ESIs (C-ESIs). The spatial resolution relevant to the development of the C-ESI metrics and modeling of tradeoffs between extractive activities and resource conservation is necessarily a tradeoff of precision vs. the availability and usefulness of fine scale data. Too coarse a resolution (e.g., by BOEM planning districts) will not lead to the identification of significant ecological or economic "hot-spots" as candidates for special attention. Too fine a spatial scale is challenging to populate with data and may result in an intractably large optimization problem. For the purposes of this dissertation, I have chosen to summarize data by grid cells on the 0.5°x0.5° latitude/longitude resolution or 1°x1° latitude/longitude resolution scale which is a reasonable first pass compromise for the level of granularity to balance precision and access to data. This study takes a quantitative, cumulative approach to C-ESI formulation using a multi-attribute utility model (MAUM; Huber 1974) to quantify sensitivities of spatially explicit offshore areas across many resources without having to subjectively concatenate maps of the individual species or human-use components of the C-ESIs.

Each grid cell in the C-ESI is assigned a score via a MAUM equation. In an MAUM, the overall value, or utility, of a system is calculated by the weighted sum or product of the individual utility values for a set of separate and potentially contradictory attributes. The overall utility value is a score of how well the system meets multiple objectives or satisfies the needs of multiple stakeholders (Huber 1974). In the health industry, for example, MAUMs are used to assign patients an overall health index based on a suite of independent health attributes (e.g., vision, hearing, speech, ambulation, dexterity, emotion, cognition, and pain/discomfort). Individual patients are assigned a semi-quantitative value of 0 to 6 in each of the health attributes and these attribute scores are substituted into the utility function to give an overall health index

per patient (Feeny et al. 2002). MAUMs have also been used to appraise the overall sustainability of banks using a framework to assess a suite of attributes across multiple stakeholder priorities (e.g., regulators, shareholders, customers, employees; Rebai et al. 2012).

Similar to the human health and banking examples above, the environmental sensitivity of a marine geographic location can be estimated both by the biological attributes extant at that location and human dependence on the region that might be compromised by an oil well blowout or other significant event resulting in biological and/or economic loss. A preliminary model of this methodology was illustrated using three ecological variables and three economic (human-use) indicators in Chapter 2. This original MAUM focused on the diversity of larval fishes derived from abundance estimates from the Southeast Area Monitoring and Assessment Program (SEAMAP) described in Chancellor (2015) in both offshore and coastal areas and revenue estimates derived from vessel logbook data for coastal reef fisheries, highly migratory pelagic fisheries, and shrimp fisheries. Larval fish are highly sensitive to oil-related pollution as they are susceptible to physiological defects and mortality at exceedingly low concentrations of oil exposure (Carls et al. 1999; Incardona et al. 2004; Hicken et al. 2011; Incardona et al. 2013). Pollution from oil well blowouts would likely impact survival of a variety of species, varying seasonally (Chancellor 2015). Revenue estimates from various fisheries represent the quantified loss value of the human uses foregone in the event of an oil spill resulting in a fishery closure in a specified area.

The objectives of the present study are (1) to expand the list of spatially-distributed offshore resources developed in Chapter 2 to include the spatial probability distributions of selected species (fish, mammal, and turtle), spatial distributions of species richness based on a larger set of species' probability distributions, and the spatial distribution of presence/absence of

vulnerable deep-sea coral habitat, (2) to develop and demonstrate methodology for quantitatively and qualitatively comparing the spatial dissimilarity among these offshore resources, (3) to combine these spatially distributed resources into multiple cumulative ESIs (C-ESIs), (4) to evaluate individual resource components of the C-ESI to determine which resources are over- or under-represented in the C-ESI and to identify tradeoffs between resource components and provide potential guidance for applying weights to under-represented resource components, and (5) to develop methodology for adding optional weights to an individual resource component or a suite of resource components to create the C- ESIs and to test the sensitivity of the C-ESI to the addition of those weights.

While the weighting of attributes within the C-ESI lies outside of the scope of this dissertation and historically requires semi-quantitative approaches based on expert opinion, three weighted C-ESIs are created using three levels of weights as a demonstration of the sensitivity of the C-ESI to weighting. These weights are applied to a subset of species within the ESI identified as highly vulnerable by a preliminary vulnerability index being developed for fishes in the GoM (Woodyard et al. 2022). An additional C-ESI with the weighting of one species is created to confirm the weighting system performs as expected in prioritizing spatial units containing weighted resources.

The C-ESIs and the relative contributions of their individual components created from this study are used to identify "hot-spots" of resource sensitivity and to identify tradeoffs between resources. Spatial distributions of resources and cumulative C-ESIs serve as inputs for comparisons among oil spill scenarios (Chapter 4) and optimization network problems (Chapter 5).

3.2 Methods

Quantitative spatial distributions of offshore resources in the Gulf of Mexico were created for 13 fish species, six mammal species, four sea turtle species, three species richness groups, five commercial fisheries, ichthyoplankton total abundance, and deep-water coral reef presence/absence. These distributions were combined to create five unweighted C-ESIs and four weighted C-ESIs.

3.2.1 Species Selection (Fishes, Turtles, Mammals)

A total of 23 species were included in this study and are provided with their common and scientific names in Table 3.1. Twelve fish species were selected based on their abundance within the GoM and their commercial importance (Chen 2017). Selected commercially important fish species include Atlantic sailfish, Atlantic bluefin tuna, Atlantic blue marlin, Common dolphinfish, Greater amberjack, King mackerel, Red drum, Red grouper, Red snapper, Striped mullet, Atlantic swordfish, and Great northern tilefish. Warmingii's lanternfish was also added as a representative mesopelagic fish due to their relatively high abundance in the GoM and the importance of mesopelagic fishes generally as a prey species to many commercially important species, for a total of thirteen fish species. Six mammal species were selected based on their abundance within the GoM and the variation in their spatial distributions (Würsig 2017); Bottlenose dolphin, Pantropical spotted dolphin, Atlantic spotted dolphin, Sperm whale, Pygmy killer whale, and False killer whale. Five of the seven species of sea turtles found worldwide are found within the GoM (i.e., Kemp's Ridley, Hawksbill, Loggerhead, Leatherback, Green; Valverde and Holzwart 2017). I intended to include all five sea turtles found in the GoM but due to an incomplete probability of occurrence spatial distribution for Green turtles, this species was excluded from the creation of the C-ESIs.

3.2.2 Distributions of Probability of Species Presence

For the spatial distributions of species, I used probability of suitable habitat as a proxy for probability of species presence. Suitable habitat identified through presence data and environmental estimates can be used to develop species distribution models (SDMs; Elith and Leathwick 2009; Drexler and Ainsworth 2013). This study used the publicly available SDMs of suitable habitat developed by AquaMaps.org (Kaschner et al. 2010). AquaMaps is a joint project of FishBase and SealifeBase which creates global-wide probability of occurrence spatial distributions for species using occurrence data collected from multiple surveys combined with environmental parameters (i.e., an environmental envelope). AquaMaps provides a spatial probability distribution of the suitable habitat of a species for 1) the estimated native geographic range, 2) a predicted Year 2050 native range based on predicted environmental parameters in 2050, and 3) suitable habitat where the species could potentially live. Environmental factors included in the environmental envelope can include (1) Depth (m), (2) Temperature (°C), (3) Salinity (psu), (4) Primary Production ($mgC \cdot m^{-3} \cdot day^{-1}$), (5) Sea Ice Concentration (0-1 fraction) (not included in GoM), (6) Dissolved Bottom Oxygen ($mmol \cdot m^{-3}$), and (7) Distance to Land (km) depending on the species and geographic location. The estimated native geographic range, environmental parameters included in the species-specific envelope along with their acceptable ranges for inclusion in the species range, and occurrence cells (with environmental parameter measurements) are available for download as a .csv file for each species from AquaMaps.org. Estimated native range probability is published at the 0.5° latitude/longitude grid resolution with center points being located at X.25° and X.75° of latitude and longitude.

Estimated probability of occurrence for the native range was downloaded for all species in June 2020. Predicted occurrence records outside of latitude range [17°N to 32°N] and

longitude range [98°W to 80°W] for the Gulf of Mexico were removed. An intersection between the remaining points and the International Hydrographic Organization (IHO) shape file for the GoM (Figure 3.1; Flanders Marine Institute 2018) was performed in *QGIS* (QGIS Development Team, 2020) using the *Extract by Location* tool in *Vector Selection* menu of the *Processing Toolbox*. Two additional fields were created using the *field calculator* in *QGIS*:

1) **Overall_Probability>0.50**: Probabilities of less than 0.5 were converted to 0 as these were considered unlikely to indicate presence, while probabilities greater than or equal to 0.5 maintained their original values. The 0.5 distinction is recommended by AquaMaps as species are unlikely to occur in places where probability of suitable habitat is < 0.5. This 0.5 distinction is also used to determine which species are included in their published species richness estimations (See Section 3.2.4 below).

2) **Proportion_of_Probability: Overall_Probability>50** for each point divided by the total sum of the **Overall_Probability>50** for all points. **Proportion_of_Probability** was calculated since grid blocks with high probability of occurrence in a species with narrow spatial range are more important than grid blocks with high probability of species presence in a species with a wide spatial range.

These new fields were converted to a raster using the *Rasterize* tool in the *Processing Toolbox* of *ArcMap (*ArcMap 2016). For each species, two rasters were created: 1) a raster of the **Overall_Probability>50** and 2) a raster of **Proportion_of_Probability**. Two rasters were created for each of the 13 fish species, six mammal species, and four sea turtle species.

Created rastered resources were visually checked for accuracy with some fish and turtle species having an unexplained high probability value present at point [90.25°W, 25.75°N], while

displaying zero probability for surrounding points. AquaMaps owners were contacted and agreed that this point appeared to be in error. This point was removed using the *Serval* plugin in *QGIS*. This change was made to a total of eight fish species distributions and three turtle distributions (Red grouper, Greater amberjack, Golden tilefish, King mackerel, Red grouper, Red snapper, Spanish mackerel, Striped mullet, Kemp's Ridley, Hawksbill, Loggerhead). Final grids for all species probability of occurrence are found in Appendix B.

3.2.3 Dissimilarity in Species Distributions

Dissimilarity between species distributions was calculated as the mean average difference (MAD) between each species pair (Eq. 3.1). Since the grid cells of the distributions are probabilities of occurrence (ranged 0 to 1), as opposed to species counts, the MAD method was used as opposed to other measures of dissimilarity commonly used in biological datasets (e.g., Bray-Curtis). Pair-wise dissimilarity of the probability of occurrence values between mammal and fish species was calculated using the **Overall_Probability** rasters.

The dissimilarity score between each pair of species is defined as:

$$DissimilarityMAD = \frac{\sum_{k=1}^{n} \sqrt[2]{(OP_{ik} - OP_{jk})^2}\, abs[OverallProbability]}{n} \quad \text{Eq. 3.1}$$

where OP_{ik} is the **Overall_Probability** score of species *i* at grid cell *k*, O_{ik} is the **Overall_Probability** score of the compared species *j* at grid cell *k*, and *n* is the total number of grid cells in the distribution raster.

The dissimilarity score was found by creating a raster of the range for each pair of distributions (*r.series* function in *QGIS with GRASS* (GRASS Development Team, 2020), method = range) and then finding the mean of the values within the resulting raster within the GoM (*QGIS* using the *Zonal Statistics* tool in the *Raster Analysis* menu of the *Processing*

Toolbox, range as *raster layer*, IHO ocean (Fig3.1) as *Vector layer containing zones*, method = mean). Dissimilarity scores were calculated between all fishes and mammal species.

A cluster map was produced using the *seaborn* package (Waskom 2021) on the set of probability distribution rasters.

3.2.4 Spatial Distribution of Species Richness

This study created three rasters to spatially quantify species richness in the GoM. Species richness for three groups (1) bony fishes, 2) mammals, 3) elasmobranchs is available for download from AquaMaps at the 0.5°x0.5° latitude/longitude grid resolution. The species richness for each grid cell is calculated as number of species for which the probability of occurrence within that cell is > 0.5.

Species richness .csv files were accessed and downloaded from AquaMaps for all categories in June 2020. Species richness estimations from AquaMaps were based on suitable habitat and not sampling, so species accumulation curves were not created. Species richness point data inside latitude range [17°N to 32°N] and longitude range [98°W to 80°W] were converted to raster files. An intersection between the remaining points and the shape polygon for the GoM (Figure 3.1) was performed in *QGIS* using the *Extract by Location* tool in *Vector Selection* menu of the *Processing Toolbox*. Species richness values for bony fishes ranged between [2 and 1348], mammals ranged between [1 and 30], and Sharks/Rays ranging between [1 and 104]. For direct comparison between the three species richness groups, an additional field **SpeciesRichnessIndex** was created for each species richness group such that:

$$\mathbf{SpeciesRichnessIndex}_i = \mathbf{SpeciesRichness}_i / \max(\mathbf{SpeciesRichness}_{all}). \quad \text{Eq. 3.2}$$

where *i* represents the value at grid cell *i* and *all* represents the array of the **SpeciesRichness** values for all *i* values within the spatial domain.

The **SpeciesRichnessIndex** field then ranged from [0,1] for each species richness distribution. For each species, two rasters were created: 1) a raster of the **SpeciesRichness** and 2) a raster of **SpeciesRichnessIndex** using the *Rasterize* tool in the *Processing Toolbox* of *ArcMap*.

Since the species richness datasets downloaded from AquaMaps are created from the AquaMaps' individual species distributions, the **SpeciesRichness** bony fish raster exhibited the same data point anomaly at [90.25°W, 25.75°N], as did some of the individual bony fish probability distributions. I manually edited this raster value to the average of the surrounding raster values using the *Serval plugin* in *QGIS*. The mammals and elasmobranch species richness files were unaffected.

Finalized rasters for the three species richness distributions are found in Appendix B.

3.2.5 Spatial Distributions of Commercial Fisheries Economic Value

This study estimated measures of economic dependence for five fisheries at the 1°x1° latitude/longitude grid resolution: coastal species (reef fishes and small pelagic fishes), highly migratory species, white shrimp, pink shrimp, and brown shrimp. The National Marine Fisheries Service (NMFS) provided estimated revenue and landings at 1°x1° longitude/latitude resolution for coastal species (years 2013-2017) and the three shrimp fisheries (years 2011-2016) and estimated landings only for the highly migratory species (years 2013-2016).

The revenue and landing estimates for coastal reef fishes were aggregated by NMFS and provided for this study at 1°x1° longitude/latitude resolution. The estimations performed by

NMFS are detailed below and in Chancellor et al. (2020). Annual landings (pounds), reported to the Southeast Coastal Fisheries Logbook Program, and estimates of annual revenues for individual coastal species were assigned to each 1°x1° grid cell. Revenues were estimated by multiplying aggregated annual trip-level landings for each species by annual average ex-vessel prices from 2013-2017 (SAFE 2017). Ex-vessel prices represent the unit price paid at the time of landing by fish dealers to fishers for harvested but unprocessed catch (so-called first-sale value). Grids with less than three vessels reporting trip records were omitted to prevent identifying proprietary confidential information.

A total of 59 species were included in the coastal reef fisheries estimates provided by NMFS (Table 3.2). Estimated revenue was summed across each grid block for all species (distribution hereafter referred to as **CoastalSpeciesRevenue**). The sum of the total estimated coastal revenue for years 2013-2017 was $318M with the estimated revenue of the top three species summing to 71% of the total revenue (top 3 species: Red snapper (37%), Red grouper (26%), King mackerel (8%). The distribution of **CoastalSpeciesRevenue** by species and grid block is found in Figure 3.2. For comparison between fisheries, an additional indexed field named **CoastalSpeciesIndex** was created such that:

$$\mathbf{CoastalSpeciesIndex}_i = \mathbf{CoastalSpeciesRevenue}_i / \mathrm{sum}(\mathbf{CoastalSpeciesRevenue}_{all}) \quad \text{Eq. 3.3}$$

where *i* represents the value at grid cell *i* and *all* represents the array of the **CoastalSpeciesRevenue** values for all *i* values.

The **CoastalSpeciesIndex** point data were rasterized using the *Rasterize* tool in the *Processing Toolbox* of *ArcMap* and the sum of the values in the raster is 1. This raster can be found in Appendix B.

The landing estimates for the highly migratory species (HMS) were aggregated by NMFS and provided for this study at 1°x1° longitude/latitude resolution. The estimations performed by NMFS are detailed below and in Chancellor et al. (2020). Landings for eight highly migratory fish species (Table 3.2) were estimated by applying the proportion of numbers of individual species caught in each 1°x1° grid cell, as reported to the Atlantic Highly Migratory Species Fisheries Logbook Program, to total trip-level catch (pounds gutted weight). The resulting landings for each HMS were aggregated for each grid cell annually from 2013-2016. Landings were estimated for each grid cell in the same manner as described above for coastal species with similar considerations to protect confidential proprietary information. The distribution of landed pounds by species and grid cell can be found in Figure 3.3.

I estimated revenue for each grid cell from the provided landings by multiplying the landings for each species by the average price from NMFS commercial landings in the GoM for available years 2013 to 2016 (distribution hereafter referred to as **HighlyMigratoryRevenue**). For blue shark and porbeagle shark, the average price per pound for 'general sharks' was used, as no specific information was available for them. The top five ordered species ranked by the total pounds were 1) Yellowfin tuna, 2) Swordfish, 3) Albacore tuna 4) Bigeye tuna, 5) Bluefin tuna (from most to least). The addition of the price per pound changed the ranked order of the **HighlyMigratoryRevenue** to 1) Yellowfin tuna 2) Swordfish, 3) Bluefin tuna, 4) Bigeye tuna, 5) Albacore tuna (from most to least).

For comparison between fisheries, an additional indexed field named **HighlyMigratoryIndex (HMIndex)** was created such that:

$$\mathbf{HMIndex}_i = \mathbf{HighlyMigratoryRevenue}_i / \mathrm{sum}(\mathbf{HighlyMigratoryRevenue}_{all}) \quad \text{Eq. 3.4}$$

where *i* represents the value at grid cell *i* and *all* represents the array of the **HighlyMigratoryRevenue** values for all *i* values.

The **HighlyMigratoryIndex** point data was rasterized using the *Rasterize* tool in the *Processing Toolbox* of *ArcMap* and the sum of the values in the raster is 1. This raster can be found in Appendix B.

Shrimp fishery revenue estimates were aggregated by NMFS and provided for this study at the 1°x1° longitude/latitude resolution. The estimations performed by NMFS are detailed below and in Chancellor et al. 2020. Landings for the three dominant species of shrimp (white, brown, pink) were estimated from landings reported to the Gulf of Mexico Shrimp Permit Cellular Electronic Logbook program during years 2011-2016 and from price per pound reported by port agents and trip tickets (Species names in Table 3.2). Revenue was estimated as pounds landed multiplied by the price per pound and provided at the 1°x1° latitude/longitude grid resolution (referred to hereafter as **BrownShrimpRevenue, WhiteShrimpRevenue, PinkShrimpRevenue)**.

The combined estimated revenue for years 2011-2016 for all three species was $1.77 billion with brown shrimp summing to $999 million, white shrimp summing to $675 million, and pink shrimp summing to $100 million.

For comparison between fisheries, an additional indexed field for each species was created such that:

$$\mathbf{BrownShrimpIndex}_i = \mathbf{BrownShrimpRevenue}_i / \text{sum}(\mathbf{BrownShrimpRevenue}_{all}) \quad \text{Eq. 3.5}$$

$$\mathbf{WhiteShrimpIndex}_i = \mathbf{WhiteShrimpRevenue}_i / \text{sum}(\mathbf{WhiteShrimpRevenue}_{all}) \quad \text{Eq. 3.6}$$

$$\mathbf{PinkShrimpIndex}_i = \mathbf{PinkShrimpRevenue}_i/\text{sum}(\mathbf{PinkShrimpRevenue}_{all}) \quad \text{Eq. 3.7}$$

where *i* represents the value at grid cell *i* and *all* represents the array of the corresponding **ShrimpRevenue** values for all *i* values.

The **ShrimpIndex** point data was rasterized using the *Rasterize* tool in the *Processing Toolbox* of *ArcMap* and the sum of the values in the raster is 1. These rasters can be found in Appendix B.

3.2.6 Southeast Area Monitoring and Assessment Program (SEAMAP) Larval Abundance

This Gulf States Marine Fisheries Commission initiative is a 35+ year fisheries-independent ichthyoplankton dataset comprising of seasonal surveys in the northern GoM. Ichthyoplankton and egg counts per bongo or neuston tow are recorded along with location, depth, and total water filtered. Ichthyoplankton samples are identified to the lowest taxonomic level possible (Rester 2012; Lyczkowski-Shultz et al. 2013).

Ichthyoplankton counts and taxonomy were used to create an overlapping 1° latitude x 1° longitude grid of estimated abundance by species for the GoM. Samples included came from seasonal surveys from 2000 to 2015 collected via bongo nets. Standardized abundance was calculated for each sample as the estimated number of organisms under a 10 m^2 surface area. These standardized abundances were then aggregated across all years and all samples within each 1°x1° grid and divided by the total number of samples within that block. More information regarding the sampling techniques, species selection, and standardized abundance calculations from raw counts can be found in Chancellor (2015). A total of 58 species of larval fishes were included in the calculations (Table 3.3).

The distribution of the standardized abundance (**StanAbundance**) is heavily skewed left with few very high values and is distributed at the 1°x1° longitude/latitude resolution (Figure 3.4B) while the distributions of the **Proportion_of_Probability** rasters for the fish, mammal, and turtle species are skewed right and are created at the 0.5°x0.5° longitude/latitude grid resolution (Figure 3.4A).

To create a comparable presence/absence distribution for the larval fish which could then be combined with other rasters, I created a **LarvalPresence** field such that all values above or equal to the median **StanAbundance** were set to the median **StanAbundance** and all values less than the median conserved their values:

$$\mathbf{LarvalPresence_i} = \mathbf{StandAbun_i} \quad \text{when } StandAbun_i < median(StandAbun_{all})$$

and

$$\mathbf{LarvalPresence_i} = median(\mathbf{StandAbun_{all}}) \quad \text{when } StandAbun_i >= median(StandAbun_{all}) \quad \text{Eq. 3.8}$$

Then I created a **LarvalIndex** field such that:

$$\mathbf{LarvalIndex_i} = \mathbf{LarvalPresence_i}/sum(\mathbf{LarvalPresence_{all}}) \quad \text{Eq. 3.9}$$

where *i* represents the value at grid cell *i* and *all* represents the array of the corresponding **LarvalPresence** values for all *i* values. I converted the **LarvalIndex** from the 1°x1° latitude/longitude grid resolution to the 0.5°x0.5° latitude/longitude grid resolution by dividing the **LarvalIndex** value by four and assigning it to each of the four 0.5°x0.5° latitude/longitude grid resolution blocks within the original 1°x1° block. The final distribution of the **LarvalIndex** field is skewed right, sums to 1, and has a 0.5°x0.5° latitude/longitude grid resolution comparable to the proportion of suitable habitat of the individual species (Figures 3.4A, B)

The **LarvalIndex** field was converted to a raster using the *Rasterize* tool in the *Processing Toolbox* of *ArcMap* (Appendix B).

3.2.7 Deep-Sea Coral Habitat

Presence data for deep-sea soft and stony corals is publicly available for the Gulf of Mexico region via the NOAA Deep-Sea Coral Data Portal (NOAA 2020) which is funded in part by NOAA's Deep-Sea Coral Research and Technology Program (DSCRTP). The standard download file contains the following fields: catalog number, data provider, scientific name, vernacular name category, taxonomic rank, station, shallow flag, observation date, position (latitude, longitude), locality, location accuracy, depth, depth method, repository, identification qualifier, sampling equipment, record type, event ID, survey ID, dataset ID, and sample ID. The standard download file for the GoM was downloaded in April 2020. Catalog number records were identified as stony or soft based on their scientific name and vernacular name category. Records within the GoM study area were selected from the full data download in *QGIS* using the *Extract by Location* tool in *Vector Selection* menu of the *Processing Toolbox* with the IHO shape file for the GoM (Figure 3.1; Flanders Marine Institute 2018). These points were converted to a 0.5°x0.5° latitude/longitude raster with a value of 1 if at least one coral was present in the grid cells and 0 if not. This raster was created using the *Rasterize* tool in the *Processing toolbox* of *ArcMap* and was snapped to an existing 0.5°x0.5° raster for species distribution using the *Processing Extent* option. Lack of identified presence in a grid cell was treated as a confirmed absence, due to the relatively complete coverage of the surveys and the relatively large size of the grid cells. This raster was converted to a proportion of habitat raster by dividing the presence value of 1 by the total number of grid cells within the GoM study area where corals were identified (n=194). The scores for this new raster sum to 1 and are similarly comparable to the

spatial distributions of proportion of habitat for the individual species and larval fish. This raster can be found in Appendix B.

3.2.8 Creation of Cumulative Environmental Sensitivity Indices (C-ESIs)

This study created seven candidate Cumulative ESIs (C-ESIs) combined from the resource distribution rasters and a published Python script which can be used to generate additional C-ESIs from a set of input resource distribution rasters and a list of optional weights. The C-ESIs created in this study are:

1. Mammals C-ESI – unweighted
2. Turtles C-ESI – unweighted
3. Fish species C-ESI – unweighted
4. Fish species C-ESI – weighted (four levels)
5. Species Richness C-ESI – unweighted
6. Commercial Fisheries C-ESI – unweighted
7. Mammals, Turtles, Fish, Larval abundance, Corals C-ESI – unweighted

The Cumulative Sensitivity equation was modeled as a multi-attribute linear utility function (Huber 1974) combining the resource attributes such that the Cumulative Sensitivity (CS) at grid cell *j* is:

$$CS_j = \sum_{i=1}^{N} k_i * (VI_{ij}) \ / \text{N} \qquad \text{Eq. 3.10}$$

where *N* is the number of included sensitivity attributes, k_i is the optional weight coefficient assigned to the *i*th resource attribute, and VI_{ij} is the indexed score of the *i*th resource attribute at grid cell *j*. The resolution of the C-ESI raster is the same as the resolution of the input attribute rasters. For all of the C-ESIs except for the Species Richness C-ESI (ID 5), the value of each

grid cell in the C-ESI represents the proportion of the value of the C-ESI within that grid cell. The sum of the values of all the cells within each C-ESI sum to one.

For the Species Richness C-ESI, the Cumulative Sensitivity (Eq. 3.10) is a function of the three indices (each ranging [0,1]). The value of each grid cell in the Species Richness C-ESI theoretically ranges [0,1]. A grid cell with a $CS_j = 1$ would represent a grid cell with the maximum species richness for each included layer. The sum of the values of all the cells within the Species Richness C-ESI sum to 227.331.

The C-ESI rasters were created from the summation of the resource distribution rasters using the *r.series* command from the *GRASS* package in *QGIS*. The *r.series* (method: sum; weights: array of weights) command performs a selected calculation on a set of rasters with a set of optional provided weights.

3.2.9 Contribution of Individual Components and Identifying Tradeoffs

For each C-ESI, the score for each grid cell is a cumulative score from the resource rasters. I ranked the scores from the C-ESI for the grid cells from highest to lowest and graphed the resulting cumulative distribution to visually represent the degree of variation within the C-ESI scores (See Section 3.3.3 below). To identify which components are contributing the most (or least) to the final score, I graphed the cumulative distribution of each of the individual components (See Section 3.3.3 below). The graphing of the individual components was performed in Python using the *seaborn* package for each of the C-ESIs.

3.2.10 Weighted Fish Species ESIs and Exploration of Sensitivity

The CS function identified in Eq. 3.10 contains an optional weighting component that was set to one for all resources in the unweighted C-ESI scenarios. Four weighted C-ESIs were

created to demonstrate the functionality of the weighting component in the C-ESI creation process and explore the sensitivity of the C-ESI to the weighting of one or multiple resources.

Species-specific vulnerability to petrochemical exposure is not known for all species, but species-specific vulnerability can be estimated by using a trait-based framework to rank relative vulnerability and identify sensitive species (Polidoro et al. 2020; Schwing et al. 2020; Murawski et al. 2021; Sarrazin et al. 2021). Within the framework described in Polidoro et al. (2020), 18 species-specific traits in the categories of likelihood of exposure (due to habitat), individual species sensitivity (characteristics of the species), and population resistance (characteristics of the population), were identified and defined to categorize species vulnerabilities. This framework of identified traits was applied to GoM fishes in Woodyard et al. (2022). Vulnerability scores for the 13 selected fish species were provided by Polidoro and Woodyard in 2021 as part of a preliminary unpublished assessment for use in creating the weighted C-ESIs used in this study. For the purposes of the weighted C-ESIs, I divided the species into two categories based on their provided ranking (eight species defined as high vulnerability and five species defined as medium vulnerability).

The weighted C-ESIs were created with the same fish species and methodology as the unweighted C-ESIs. One C-ESI was created to establish the functionality of the weighting process and sensitivity of the addition of weight to one species. In this C-ESI, the lanternfish component was heavily weighted (weight of 10), and other fish species components maintained a weight of 1. Lanternfish may be an important indicator species for diel vertical migrating mesopelagic species that are likely quite vulnerable to oil spill effects (Romero et al. 2018) and were likely highly impacted by DWH (Sutton et al. 2020). I chose lanternfish as the single weighted species for the potential use of this C-ESI as indicator of the vulnerabilities of

mesopelagic species and because their distribution was the most unlike that of the other included fish species due to their deep-water presence and therefore a change in their weighting would be expected to have the largest noticeable impact on the final C-ESI.

Three additional C-ESIs were created to evaluate the sensitivity of the C-ESI to the weighting of a suite of species (fish species previously defined as high vulnerability). For these weighted C-ESIs, I used three levels of weighting for the highly vulnerable species (weight = 2, 4, and 8) and maintained the weight of 1 to the medium vulnerable species. These weights were applied as the k_i coefficients in Eq. 3.10.

3.2.11 Note for successfully running published scripts

This script and the other scripts published in this study were written in the *Python Console* plugin in QGIS Desktop 3.8.0 with GRASS 7.6.1. These scripts must be run in a Python environment and will not run in QGIS without GRASS enabled. In addition, the *pandas*, *numpy*, and *seaborn* dependencies were used in the scripts published in this study which must be loaded into any Python environment.

For this study I installed QGIS with GRASS using the OSGeo Installer (QGIS Installers, 2020). I installed third party package dependencies in the OSGeo4W Shell using the procedures found in Yusuf (2018).

3.3 Results

3.3.1 Spatial Distributions of Offshore Resources

A total of 33 resource raster distributions were created for use in combining ESIs (Table 3.4, Appendix B). Rasters created for larval abundance, deep-sea coral, and fish, mammal, and turtle species have values that sum to one over the entire distribution as the values represent proportion of suitable habitat. Rasters created for the three species richness categories and the

five economic fisheries have grid cells that range from 0 to 1, as they are calculated on a [0,1] index.

3.3.2 Dissimilarity in Species Distributions

A dissimilarity score was calculated using mean average difference (MAD) for each pair of probability of occurrence distributions for the fish and mammal species. This dissimilarity score represents the mean difference between two corresponding grid cells from a pair of probability distribution rasters (i.e., lower scores indicate higher similarity; Figure 3.5A). Pair-wise dissimilarity scores between species ranged from [0.03,0.8]. Species pairs with the lowest pair-wise dissimilarity scores (and therefore indicated higher similarity) were Red snapper and Greater amberjack (0.03), Pantropical spotted dolphin and False killer whale (0.05), King mackerel and Red snapper (0.07), Dolphinfish and Atlantic spotted dolphin (0.08), and King mackerel and Greater amberjack (0.08). Species pairs with the highest pair-wise dissimilarity scores were Sperm whale and Greater amberjack (0.8), Sperm whale and Red snapper (0.8), and Sperm whale and King mackerel (0.78).

The average pair-wise dissimilarity score was also calculated for each species with Sperm whale, Lanternfish, and Swordfish having the highest average dissimilarity scores respectively (Figure 3.5A). This average dissimilarity score provides a measure of how different these species distributions vary from the suite of other included species. Sperm whale and lanternfish had a pair-wise dissimilarity score of 0.13 showing that while they differed the most from the other included species, they were relatively close in similarity to each other.

The cluster map was created for the probability distributions of fish and mammal species as a more qualitative view of the dissimilarity between distributions (Figure 3.5B). The cluster map identifies in a hierarchical way the relationships of species (x-axis) and of site locations (y-

axis). For example, the three most similar pairs of species are Pantropical spotted dolphin/False killer whale, Swordfish/Bluefin tuna, and Red snapper/Greater amberjack respectively (Figure 3.5B). This cluster map has the advantage over the dissimilarity scores in indicating the complex relationships among all species and site groups. There are three major groupings of species in the hierarchy, corresponding to (1) deep water mammal species and lanternfishes, (2) large pelagic bony fishes and (3) coastal/continental shelf species.

3.3.3 Cumulative Environmental Sensitivity Indices (C-ESIs)

Six unweighted C-ESIs were created during this study from different sets of input rasters (Table 3.5). Each finalized C-ESI is a raster in the same resolution as the input rasters and can be found in Appendix B. The finalized C-ESIs varied both in the number of grid cells identified as "hot-spots" and the spatial distribution of the "hot-spots" with many C-ESIs showing "hot-spots" on the continental shelf.

The scores from the C-ESI grid cells were ordered from greatest to least and the cumulative sum of the scores was graphed for each C-ESI. The scores from the individual components were also graphed for each C-ESI. In a scenario where all the C-ESI scores for all grid cells were equal, this would result in an $y = x$ distribution line. The steepness of the slope of the initial line represents the variance in the C-ESI scores, with C-ESI scenarios with a very steep slope indicating the presence of very important grid cells (e.g., "hot-spots" of distribution), with a more flat line (x-y bisector) indicating more uniform distributions. Additionally, for each C-ESI, I also graphed the cumulative distribution of the individual components ordered by the scores of the total C-ESI. This graphing of the individual components serves as a visual representation of which components are best represented by the C-ESI. The steeper the slope of

the individual component, the more the distribution of that component is represented by the C-ESI.

The mammals C-ESI, which included probability of occurrence distributions for six species, had the highest C-ESI scores along the continental slope in the northern GoM as well as the continental slope on the western side off the Yucatan Peninsula (Figure 3.6). The cumulative sum of the individual components shows that the Pygmy killer whale, Pantropical spotted dolphin, and False killer whale were the best represented by this C-ESI as the cumulative distribution of these individual components had the steepest graphed slope (Figure 3.6). In a second group, Bottlenose dolphin and Atlantic spotted dolphin had the next steepest (and similar) slopes, followed by the Sperm whale. The Sperm whale has the distribution most unlike the other species, and the widest range, corresponding to a relatively low total C-ESI score.

For the Turtles C-ESI, the highest hotspot areas were located on the continental shelf to the slope break and occurred in areas shallower than as in the Mammals C-ESI (Figure 3.7). The slope of the cumulative sum was also steeper than that of the Mammals C-ESI. This steepness indicates that there is more variation within the Turtles C-ESI scores than the Mammals C-ESI. The corresponding individual component graph shows three species of turtles that are very similarly represented (Loggerhead, Kemp's Ridley, and Hawksbill) but with one species less well represented (Leatherback). Like the Mammals C-ESI example, these three species of turtles have more similar distributions in terms of overall size and location of range, while the Leatherback turtle has a wider range and is therefore less well represented in the C-ESI.

The Fish species C-ESI also identified "hot-spots" on the continental slope and on the shelf break but there was more variation between adjacent grid cells within these areas compared

to the Mammals and Turtles C-ESIs due to the increased number of species included (Figure 3.8).

The Fish Species C-ESI was chosen to demonstrate both the functionality of weighting different resource features and the sensitivity of the C-ESI to the addition of weights. In the initial cumulative distribution of the resource components for the Fish Species C-ESI, the lanternfish species was found to be the least represented with the shallowest slope (Figures 3.9 A). This species, like the sperm whale, is least represented because it has the distribution most unlike the other combined species and a large geographic range. To test the expected functionality of adding weights to the C-ESI, I weighted the lanternfish species at two levels (weight = 10, 20) while maintaining the weight of 1 for the other fish species. If the algorithm performed as expected, the resulting C-ESI with high lanternfish weights should favor the lanternfish distribution and prioritize offshore waters that indicate lanternfish presence. I expected that the individual component line for the lanternfish would be steeper than that of the other species. These expected results were realized as can be seen in the graph of the individual components for the Lanternfish weighted scenario vs the unweighted Fish Species scenario (Figure 3.8; Figure 3.9A). In the Lanternfish weighted scenario, grid cells containing both lanternfish and other species were prioritized first (e.g., Golden tilefish) but then cells containing only lanternfish were selected over grid cells containing other species which is demonstrated by the dramatic flattening of the component lines of the other fish species (Figure 3.9A). This effect was seen in both weighting scenarios (weight equal to 10 and 20) with the effect being more extreme in the weight = 20 scenario as expected.

Once the functionality of adding the weights was established, I then created three additional C-ESIs with varying weights applied to the suite of eight preselected “highly

vulnerable" species to observe the sensitivity of the C-ESIs to these weights (weights: 2, 4, and 8). As the weights of these eight species were increased, the C-ESI scores on the slope increased while the C-ESI scores for the grid cells on the shelf decreased (Figure 3.8). Resource components for species that were weighted in these scenarios were marked by a solid line, while resource components for species that remained unweighted were represented by a dashed line (Figure 3.9B). When the resource components were graphed, there was less noticeable movement between the resource component lines than with the weighted Lanternfish example. This was primarily due to the equal weighting of each of the vulnerable species and the conflicting spatial distributions between species that were similarly weighted. Some weighted species did see increases in their C-ESI representation (Golden tilefish, Warmingii's lanternfish, Atlantic blue marlin), while the representation of the other weighted species stayed about the same or decreased marginally (King mackerel, Greater amberjack, Red snapper). Some of the unweighted species did see decreases in their representation (Red drum, Striped mullet), while one unweighted species, Red grouper, increased their representation, probably as a byproduct of having a similar distribution to one or more weighted species. There were four species that had very straight slopes closest to $y = x$ due to their widespread distribution, two weighted (Common dolphinfish and Atlantic swordfish) and two unweighted (Atlantic sailfish and Atlantic bluefin tuna) and these remained mostly unchanged within all the weighting scenarios. I created another run with a weight of 25 which seemed virtually identical to the run with a weight of 8, indicating this was the convergent solution for the uniform weighting of this suite of species (Figure 3.9B).

The Species Richness C-ESI was comprised of the three species richness rasters for 1) ray finned fishes, 2) sharks and rays, and 3) mammals. The highest C-ESI areas traced the continental slope break which occurs as an overlap area for many species' distribution (Figure

3.10). The slopes of the cumulative sum of the individual resource components show that the Ray finned fishes were the most represented in the C-ESI followed by the Sharks and Rays, and then Mammals, but all three were well represented.

The Fisheries C-ESI (ID 6) differed from the other C-ESIs created in this study due to its 1.0°x1.0° resolution (versus the 0.5°x0.5° resolution of the other C-ESIs) and its spatial coverage. The spatial coverage of this C-ESI was only in the northern GoM (e.g., no current US fisheries in Mexico or Cuban waters and spatial data for fisheries landings unavailable for Mexico and Cuba). This C-ESI was created from five layers: coastal species fisheries, highly migratory species fisheries, and the brown shrimp, pink shrimp, and white shrimp fisheries. The three shrimp fisheries were created as separate layers due to their very different spatial distributions (Appendix B). These resources also differed in their absolute revenue levels, with estimated combined revenue between 2011-2016 for the brown, white, and pink shrimp landings equal to $999 million (M), $675M, and $100M respectively and coastal species fisheries estimated combined revenue from landings equal to $318M between 2013-2017. These fisheries resource layers were treated as unweighted using a relative index to avoid heavy bias towards the more valuable brown and white shrimp industries. The brown shrimp fishery occurs mostly in the western GoM with additional landings occurring in the central GoM. The majority of the white shrimp landings are from the central GoM. The majority of the pink shrimp landings were reported from one grid cell on the west Florida Shelf and this grid cell expectedly received the highest score in the combined C-ESI. The final Fisheries C-ESI has good coverage with visible "hot-spots" where all three of these shrimp fisheries primarily occur (Figure 3.11). We see the same results in the component graph, where the very first grid cell selected is the grid cell with

approximately 60% of the pink shrimp revenue. The other four resource layers are well represented with all slopes greater than 1.

An additional C-ESI (named "All Layers", ID 7) explored the incorporation of more features into the C-ESI and to test if these features could still be well represented. For this C-ESI, I combined rasters for all fish, mammal, and turtle species, and rasters of suitable habitat for the larval abundance of fishes and deep-sea corals for a total of twenty-five layers (Figure 3.12). Generally, the species that were well represented in their previous C-ESIs were still well represented even when combined with the additional layers. The sperm whale was the least well represented mammal species in the Mammals C-ESI and the least well represented species overall in the "All Layers" C-ESI. Tilefish were the most well represented species in the Fish Species C-ESI and the most well represented species overall in the "All Layers" C-ESI. Lanternfish were the least well represented species in the Fish Species C-ESI and were the least well represented fish species in the "All Layers" C-ESI. Leatherback sea turtles were the least well represented turtle species in the Turtles C-ESI and were still the least well represented turtle species in the "All Layers" C-ESI. In the two new layers that were created, larval fish were under-represented while deep-sea corals were well represented by the "All Layers" C-ESI.

3.4 Discussion

A variety of fishery-independent sampling data and fishery landings describe various aspects of biodiversity resources and can be combined to develop ESIs for the increasingly important deep-water areas of the GoM. The objective of this study was to demonstrate a methodology for converting disparate information sources for offshore resources into spatially-distributed grids (rasters) of the same resolution, standardizing the values within the grids to be quantifiably comparable, and then combining quantifiably comparable grids to create cumulative

ESIs (C-ESIs). These C-ESIs can then be used to identify "hot-spot" areas that may be especially vulnerable to deep-water oil spills. Such information can be used in initial determination of where and where not to site oil and gas facilities and to inform oil spill responders in the event of significant spills. The C-ESIs created in this study show vulnerability "hot-spots" in areas where deep sea oil drilling is taking place or proposed. C-ESIs created via this method can then be used as a potential decision-making tool when identifying areas and resources most at risk for an oil-well blowout or for special attention during oil spill responses. The C-ESIs created in this chapter also serve as necessary inputs for further analysis when comparing these resource layers to hypothetical oil spill scenarios (Chapter 4) and for optimization networks of areas potentially to be reserved from oil and gas development using the Marxan spatial planning tool (Chapter 5; Ball et al. 2009).

The majority of the C-ESIs created from this study are unweighted, but the addition of weights to some resources may be desirable and that functionality is demonstrated through the creation of several weighted C-ESIs. The weighting of one or multiple resources may be desirable due to either the increased vulnerability or importance of the specific resource(s) or because the resource(s) may be underrepresented within the C-ESI. In particular, offshore mesopelagic species, represented by a typical lanternfish species, may be particularly vulnerable to oil spills, with little resilience once polluted (Romero et al. 2018; Sutton et al. 2020). In this case, up weighting this species seems particularly important to the overall outcome especially since the majority of USA oil production in the GoM now comes from waters >1,500 m, which overlaps the distribution range of lanternfishes almost exactly (Murawski et al. 2020).

Species-specific vulnerability assessments often are scored as a combination of life history traits contributing to a species' individual vulnerability as well as a probability of

exposure score (Polidoro et al. 2021; Murawski et al. 2021). This study used preliminary vulnerability assessment scores based on previous frameworks (Woodyard et al. 2022) to weight a suite of GoM fishes by vulnerability score. The C-ESI created from weighting a suite of species was robust to changes in weights with the final C-ESI of the weighted fish species (ID 4) being comparable to the C-ESI for the unweighted fish species (ID 3), even at high levels of weighting (Figure 3.8, Figure 3.9 A, B). This is likely due to the number of weighted species (8 of 13) and the conflicting distribution ranges of the weighted species. A smaller number of weighted species, or weighted species with similar distribution ranges would likely result in a more significant change in the final C-ESI. Weighting an individual resource component may also be desirable if the resource component is more valuable than other resource components. For example, in the Fisheries C-ESI (ID 6) where the Brown Shrimp revenue is larger than the revenues of the other industries, a C-ESI looking at the total Revenue for fisheries in the GoM may want to weight these resources proportionally.

The weighting of individual resource components may also be desirable if a single resource component, or suite of resource components, is under-represented by the C-ESI. This can happen in situations where multiple resource components have similar distributions, leading to other resource components being under-represented. This study includes two tools that can be utilized in the potential determination of weighting an under-represented resource component. The first is to graph the individual components of the C-ESI and the second is to evaluate the dissimilarity between two or more resource components via a dissimilarity score or cluster map (e.g., Figure 3.5B) to interpret the individual component graph and make decisions regarding the weighting of individual resource components.

C-ESI scores for individual grid cells were ordered from greatest to least for each C-ESI. The cumulative sum was graphed for each C-ESI giving a measure of the variation of the C-ESI scores, as cumulative sum graphs with steeper slopes indicate more variation in the C-ESI scores. A uniform C-ESI would result in a slope of $y = x$ as all C-ESI scores would have the same value. The cumulative sum of the resource components was graphed as it accumulates within the ordered C-ESI grid cells. The graphing of the individual components serves as a visual representation of which components are under-represented by the C-ESI. The steeper the line of the individual component, the more the distribution of that component mimics the distribution of the C-ESI. Resource component lines with shallow slopes represent resources that are being under-selected for compared to other resources. Weighting of underrepresented resource components would increase the slope of that line (and representation in the C-ESI of that resource component) while flattening others. In the unweighted Turtles C-ESI (ID 2), three species of turtles have more similar native ranges (size and location), while the Leatherback turtle has a larger native range and is therefore less well represented. An increase in the weighting of the Leatherback turtle species (e.g., due to its highly endangered status) within this C-ESI would result in a more equitable representation of all four species within the C-ESI. This result was demonstrated within the Fish Species C-ESI (ID 3) by the creation of a C-ESI where Warmingii lanternfish were the only species weighted (Figure 3.9A). In the unweighted C-ESI, the Warmingii lanternfish component had the shallowest slope and was the least well represented. Changing the weight of the Warmingii lanternfish species to a weight of 10 increased the slope of that component so that it was the most well represented. A further increase in the weighting of Warmingii lanternfish to 20 further steepened this slope while flattening that of the other species.

The component graph along with the dissimilarity scores and cluster map can also be used to identify tradeoffs between species expected to occur if weights were added to one species, or group of species. Species with similar distributions (low pair-wise dissimilarity scores or clusters indicating high similarity) would be directionally impacted by the weighting of one or more species in that set. The contribution to the C-ESI of species outside of that group (and therefore their representation) would be lessened. In the Mammals C-ESI example, (ID 1, Figure 3.6) the Pygmy killer whale, Pantropical spotted dolphin, and False killer whale were the species most well represented by this C-ESI. This grouping is expected as Pygmy killer whale, Pantropical spotted dolphin, and False killer whale all have distributions with low dissimilarity scores and are clustered together indicating similarity in their distributions (Figures 3.5 A, B). Increasing the weight of Pygmy killer whale, Pantropical spotted dolphin, and/or False killer whale would result in a steeper component line (and more representation) for all three of these species while the contribution to the C-ESI of the other three species would lessen (and therefore their representation). Dissimilarity scores and cluster map were developed in this chapter to identify which species have similar distributions and therefore will respond to changes in weighting together. An application of weights and subsequent examination of this component graph could be used to identify weights such that all resource components were similarly well represented. An obvious extension to this work would be to compute the average sensitivities/resilience potential of the species components within the species clusters (Fig. 3.5B) to see if various species groups indeed are deserving of particular attention due to their lack of resilience potential. Thus, the "hot-spot" becomes a species group and not a single species.

The C-ESIs created via these methods demonstrates that C-ESIs with different suites of included resources (e.g., fishery components versus mammal distributions) result in spatially

different C-ESI distributions (e.g., Mammals C-ESI vs. Fisheries C-ESI (Figure 3.6, Figure 3.11)), different distributions of the same resources would also be likely to create spatially different C-ESIs. This study used probability of suitable habitat as a proxy for probability of occurrence, but this likely does not scale with abundance. For example, while AquaMaps reported red grouper occurrence data in the western GoM (Figure 3.13), other studies have shown that red grouper were not found there and were found in higher abundances on the west Florida shelf (Figure 3.14; Murawski et al. 2018). The included species, larval, and coral distributions treat all grid blocks with probability of occurrence = 1 as being equally important to a species, which makes these layers easily comparable. A similar C-ESI model which used standardized abundance estimates would potentially produce different results thus implying that there are other determinants of spatial distribution not included in the AquaMaps algorithm of habitat suitability.

The information created in this chapter is used in subsequent chapters to model the potential impacts on sensitive species to theoretical oil spills and to consider the selection of areas to reserve from future development activities owing to the occurrence of sensitive species (Chapters 4 and 5).

The methodology in this study is presented along with the published Python scripts for the creation of the C-ESIs and for the graphing of the component resources from a set of resource component rasters and optional weights.

3.5 Tables

Table 3.1 Common and scientific names for selected species whose individual probability of occurrence distributions were included in this study. Species abbreviations are used in subsequent Figures.

Category	Genus	Species	Common name	Abbreviations
Fish	*Ceratoscopelus*	*warmingii*	Warmingii's lanternfish	W.lantern
Fish	*Istiophorus*	*albicans*	Atlantic sailfish	A.sailfish
Fish	*Thunnus*	*thynnus*	Atlantic bluefin tuna	B.tuna
Fish	*Makaira*	*nigricans*	Atlantic blue marlin	B.marlin
Fish	*Coryphaena*	*hippurus*	Common dolphinfish	Mahi-mahi
Fish	*Seriola*	*dumerili*	Greater amberjack	G.amberjack
Fish	*Scomberomorus*	*cavalla*	King mackerel	K.mackerel
Fish	*Sciaenops*	*ocellatus*	Red drum	R. drum
Fish	*Epinephelus*	*morio*	Red grouper	R. grouper
Fish	*Lutjanus*	*campechanus*	Red snapper	R. snapper
Fish	*Mugil*	*cephalus*	Striped mullet	S. mullet
Fish	*Xiphias*	*gladius*	Atlantic swordfish	Swordfish
Fish	*Lopholatilus*	*chamaeleonticeps*	Great northern tilefish	Tilefish
Turtle	*Lepidochelys*	*kempii*	Kemp's Ridley	Kemps
Turtle	*Eretmochelys*	*imbricata*	Hawksbill	Hawksbill
Turtle	*Caretta*	*caretta*	Loggerhead	Logger
Turtle	*Dermochelys*	*coriacea*	Leatherback	Leather
Mammal	*Tursiops*	*truncates*	Bottlenose dolphin	Bottlenose
Mammal	*Stenella*	*attenuate*	Pantropical spotted dolphin	PS. dolphin
Mammal	*Stenella*	*frontalis*	Atlantic spotted dolphin	AS. dolphin
Mammal	*Physeter*	*macrocephalus*	Sperm whale	S. whale
Mammal	*Feresa*	*attenuate*	Pygmy killer whale	PK. whale
Mammal	*Pseudora*	*crassidens*	False killer whale	FK. whale

Table 3.2 Common and scientific names of species of fishes and shrimp used in developing indices for coastal reef fishes, coastal pelagic fishes, shrimp, and highly migratory fishes.

Grouping	Scientific name	Common name
Shrimp	Farfantepenaeus aztecus	Shrimp, brown
Shrimp	Litopenaeus setiferus	Shrimp, white
Shrimp	Penaeus duorarum	Shrimp, pink
Highly Migratory	Isurus oxyrinchus	Shark, mako
Highly Migratory	Katsuwonus pelamis	Tuna, skipjack
Highly Migratory	Lamna nasus	Shark, porbeagle
Highly Migratory	Prionace glauca	Shark, blue
Highly Migratory	Thunnus alalunga	Tuna, albacore
Highly Migratory	Thunnus albacares	Tuna, yellowfin
Highly Migratory	Thunnus obesus	Tuna, bigeye
Highly Migratory	Thunnus thynnus	Tuna, bluefin
Highly Migratory	Xiphias gladius	Swordfish
Coastal Species	Acanthocybium solandri	Wahoo
Coastal Species	Apsilus dentatus	Snapper, black
Coastal Species	Archosargus probatocephalus	Sheepshead, Atlantic
Coastal Species	Balistes capriscus	Triggerfish, gray
Coastal Species	Balistes vetula	Triggerfish, queen
Coastal Species	Calamus bajonado	Porgy, jolthead
Coastal Species	Calamus leucosteus	Porgy, whitebone
Coastal Species	Calamus nodosus	Porgy, knobbed
Coastal Species	Canthidermis sufflamen	Triggerfish, ocean
Coastal Species	Carangidae	Jacks, unc.
Coastal Species	Caulolatilus microps	Tilefish, blueline
Coastal Species	Centropristis striata	Sea bass, Atlantic, black, unc
Coastal Species	Coryphaena	Dolphinfish
Coastal Species	Ephippididae	Spadefish
Coastal Species	Epinephelus adscensionis	Hind, rock
Coastal Species	Epinephelus cruentatus	Graysby
Coastal Species	Epinephelus drummondhayi	Hind, speckled
Coastal Species	Epinephelus flavolimbatus	Grouper, yellowedge
Coastal Species	Epinephelus guttatus	Hind, red
Coastal Species	Epinephelus morio	Grouper, red
Coastal Species	Epinephelus mystacinus	Grouper, misty
Coastal Species	Epinephelus nigritus	Grouper, Warsaw
Coastal Species	Epinephelus niveatus	Grouper, snowy
Coastal Species	Etelis oculatus	Snapper, queen
Coastal Species	Euthynnus alletteratus	Tuna, little (tunny)
Coastal Species	Haemulidae	Grunts
Coastal Species	Haemulon album	Margate
Coastal Species	Haemulon plumieri	Grunt, white
Coastal Species	Lachnolaimus maximus	Hogfish
Coastal Species	Lopholatilus chamaeleonticeps	Tilefish
Coastal Species	Lutjanidae	Snappers, unc
Coastal Species	Lutjanus analis	Snapper, mutton
Coastal Species	Lutjanus apodus	Snapper, schoolmaster
Coastal Species	Lutjanus buccanella	Snapper, blackfin
Coastal Species	Lutjanus campechanus	Snapper, red
Coastal Species	Lutjanus cyanopterus	Snapper, cubera
Coastal Species	Lutjanus griseus	Snapper, mangrove
Coastal Species	Lutjanus jocu	Snapper, dog
Coastal Species	Lutjanus synagris	Snapper, lane
Coastal Species	Lutjanus vivanus	Snapper, silk
Coastal Species	Malacanthus plumieri	Tilefish, sand
Coastal Species	Mycteroperca bonaci	Grouper, black
Coastal Species	Mycteroperca microlepis	Grouper, gag
Coastal Species	Mycteroperca phenax	Scamp
Coastal Species	Mycteroperca venenosa	Grouper, yellowfin
Coastal Species	Ocyurus chrysurus	Snapper, yellowtail
Coastal Species	Pagrus pagrus	Porgy, red, unc
Coastal Species	Pomatomus saltatrix	Bluefish
Coastal Species	Pristipomoides aquilonaris	Wenchman
Coastal Species	Rachycentron canadum	Cobia
Coastal Species	Rhomboplites aurorubens	Snapper, vermilion
Coastal Species	Scomberomorus	Mackerel, king
Coastal Species	Scomberomorus maculatus	Mackerel, Spanish
Coastal Species	Seriola dumerili	Amberjack, greater
Coastal Species	Seriola fasciata	Amberjack, lesser
Coastal Species	Seriola rivoliana	Jack, Almaco
Coastal Species	Seriola zonata	Banded rudderfish
Coastal Species	Serranidae	Groupers
Coastal Species	Sparidae	Scups or porgies, unc

Table 3.3 Larval Species used in larval abundance raster
Scientific and common names of fish species used in developing the larval abundance resource. Data were collected on SEAMAP larval fish sampling cruises. More details on the species selection and calculation of standardized abundance can be found in Chancellor (2015).

Scientific Name	Common Name	Scientific Name	Common Name
Acanthocybium solandri	Wahoo	*Margrethia obtusirostra*	Bighead portholefish
Aplatophis chauliodus	Tusky eel	*Micropogonias undulatus*	Croaker, Atlantic
Bairdiella chrysoura	Silver perch	*Mugil cephalus*	Mullet, striped
Benthosema suborbitale	Lanternfish, smallfin	*Mugil curema*	Mullet, silver
Bonapartia pedaliota	Longray fangjaw	*Myrophis punctatus*	Speckled worm eel
Bregmaceros cantori	Striped codlet	*Nesiarchus nasutus*	Black gemfish
Carapus bermudensis	Atlantic pearlfish	*Notolychnus valdiviae*	Lanternfish, topside
Ceratoscopelus warmingii	Lanternfish, warming's	*Oligoplites saurus*	Leatherjack
Chlorophthalmus agassizi	Shortnose greeneye	*Ophichthus gomesii*	Shrimp eel
Chloroscombrus chrysurus	Atlantic bumper	*Ophichthus rex*	King snake eel
Cynoscion arenarius	Sea trout, white	*Opisthonema oglinum*	Herring, Atlantic thread
Cynoscion nebulosus	Sea trout, spotted	*Peprilus burti*	Butterfish, gulf
Decapterus punctatus	Scads, round	*Peprilus paru*	Harvestfish
Diogenichthys atlanticus	Lanternfish, longfin	*Pollichthys mauli*	Lightfish, stareye
Diplospinus multistriatus	Striped escolar	*Pomatomus saltatrix*	Bluefish
Engyophrys senta	Founder, spiny	*Pristipomoides aquilonaris*	Wenchman
Etrumeus teres	Herring, round	*Rachycentron canadum*	Cobia
Euthynnus alletteratus	Tuna, little (tunny)	*Rhomboplites aurorubens*	Snapper, vermilion
Gempylus serpens	Snake mackerel	*Sardinella aurita*	Sardine, Spanish
Harengula jaguana	Herring, scaled	*Sciaenops ocellatus*	Drum, red
Hygophum reinhardtii	Lanternfish, reinhardt's	*Scomber colias*	Mackerel, Atlantic chub
Katsuwonus pelamis	Tuna, skipjack	*Scomberomorus cavalla*	Mackerel, king
Lagodon rhomboides	Pinfish	*Scomberomorus maculatus*	Mackerel, Spanish
Larimus fasciatus	Drum, banded	*Selar crumenophthalmus*	Scads, bigeye
Leiostomus xanthurus	Spot	*Serraniculus pumilio*	Pygmy sea bass
Lobotes surinamensis	Atlantic tripletail	*Stellifer lanceolatus*	Drum, star
Lutjanus campechanus	Snapper, red	*Thunnus thynnus*	Tuna, bluefin
Lutjanus griseus	Snapper, mangrove	*Trachurus lathami*	Scads, rough
Luvarus imperialis	Louvar	*Xiphias gladius*	Swordfish

Table 3.4 List of Raster files with resolution level and ID number.

Type	Raster Layer	Resolution	ID Number
Fish	Warmingii's lanternfish	0.5 degree	1
Fish	Atlantic sailfish	0.5 degree	2
Fish	Atlantic bluefin tuna	0.5 degree	3
Fish	Atlantic blue marlin	0.5 degree	4
Fish	Common dolphinfish	0.5 degree	5
Fish	Greater amberjack	0.5 degree	6
Fish	King mackerel	0.5 degree	7
Fish	Red drum	0.5 degree	8
Fish	Red grouper	0.5 degree	9
Fish	Red snapper	0.5 degree	10
Fish	Striped mullet	0.5 degree	11
Fish	Atlantic swordfish	0.5 degree	12
Fish	Great northern tilefish	0.5 degree	13
Turtle	Kemp's Ridley	0.5 degree	14
Turtle	Hawksbill	0.5 degree	15
Turtle	Loggerhead	0.5 degree	16
Turtle	Leatherback	0.5 degree	17
Mammal	Bottlenose dolphin	0.5 degree	18
Mammal	Pantropical spotted dolphin	0.5 degree	19
Mammal	Atlantic spotted dolphin	0.5 degree	20
Mammal	Sperm whale	0.5 degree	21
Mammal	Pygmy killer whale	0.5 degree	22
Mammal	False killer whale	0.5 degree	23
Species Richness	Bony Fishes	0.5 degree	24
Species Richness	Elamobranchs	0.5 degree	25
Species Richness	Mammals	0.5 degree	26
Economic Fishery	Coastal Species	1 degree	27
Economic Fishery	Highly Migratory Species	1 degree	28
Economic Fishery	Brown shrimp	1 degree	29
Economic Fishery	White shrimp	1 degree	30
Economic Fishery	Pink shrimp	1 degree	31
Larval Fish	Abundance	0.5 degree	32
Benthic	Deep-sea coral	0.5 degree	33

Table 3.5 List of C-ESIs and contributing rasters IDs from Table 3.4.

ESI ID	Name of ESI	Raster ID numbers included in calculation
1	Mammals	18-23
2	Turtles	14-17
3	Fish Species – Unweighted	1-13
4	Fish Species – Weighted (Four Levels of Weights)	1-13 with weights
5	Species Richness	24-26
6	Commercial Fisheries	27-31
7	Mammals, Turtles, Fish, Larval Abundance, Deep-sea Coral habitat	1-23, 32, 33

3.6 Figures

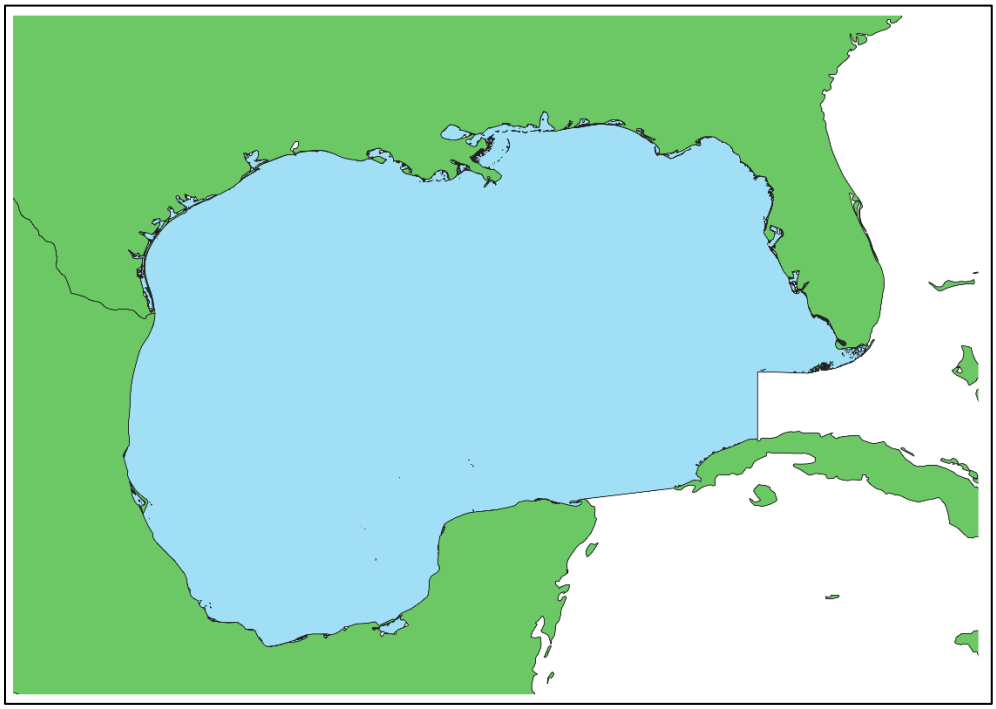

Figure 3.1 IHO Ocean shape file for the spatial extent of the GoM visualized in QGIS.
This shapefile was composed by the Flanders Marine Data and Information Centre using the publication 'Limits of Oceans & Seas, Special Publication No. 23' published by the International Hydrographic Organization (IHO) in 1953 (Flanders Marine Institute 2018).

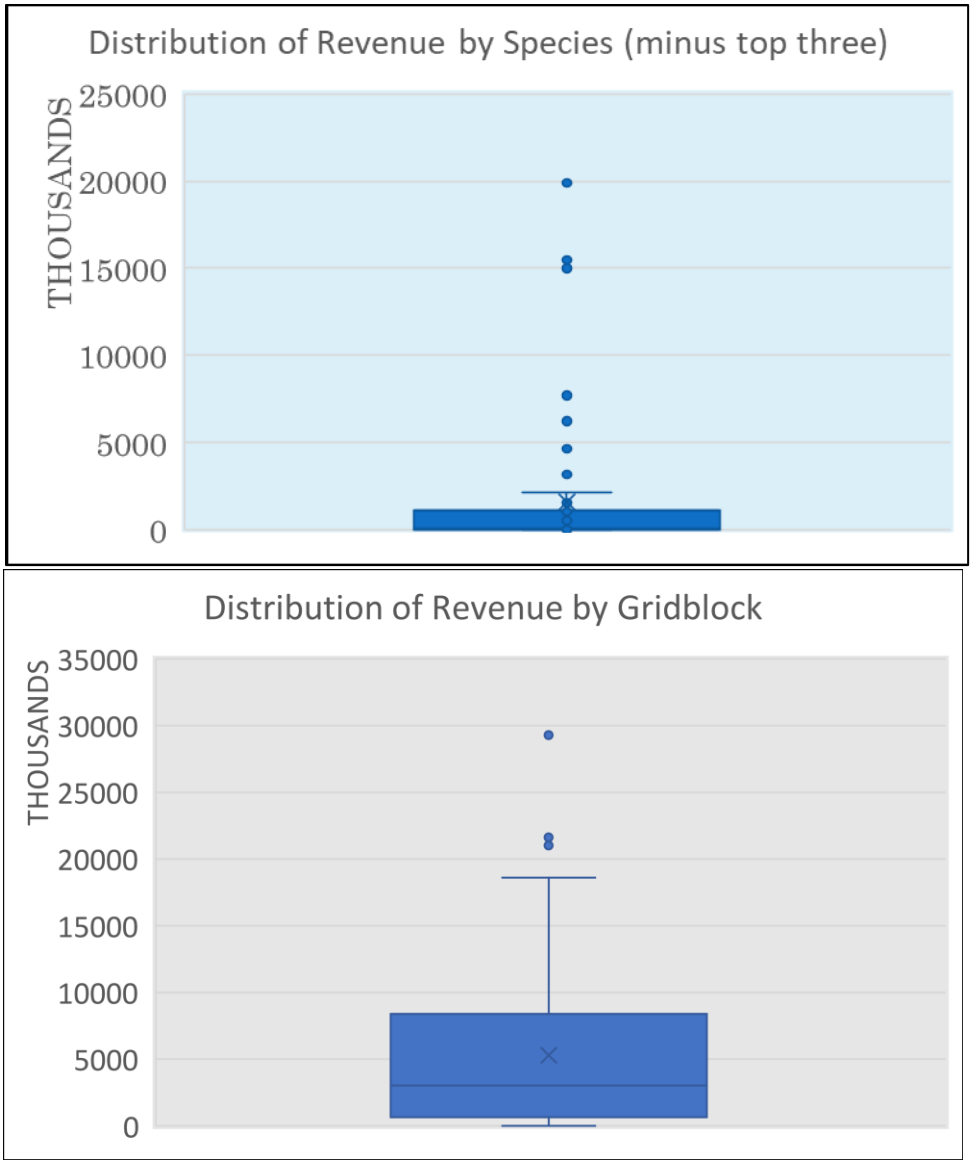

Figure 3.2 Coastal species revenue boxplots
Boxplots of distribution of Coastal Species Revenue (dollars in thousands, 2013-2017 combined) by species excluding top three species (top), and by grid block (bottom). The top and bottom of each box represent the 25th and 75th percentiles of the revenue estimates, respectively.

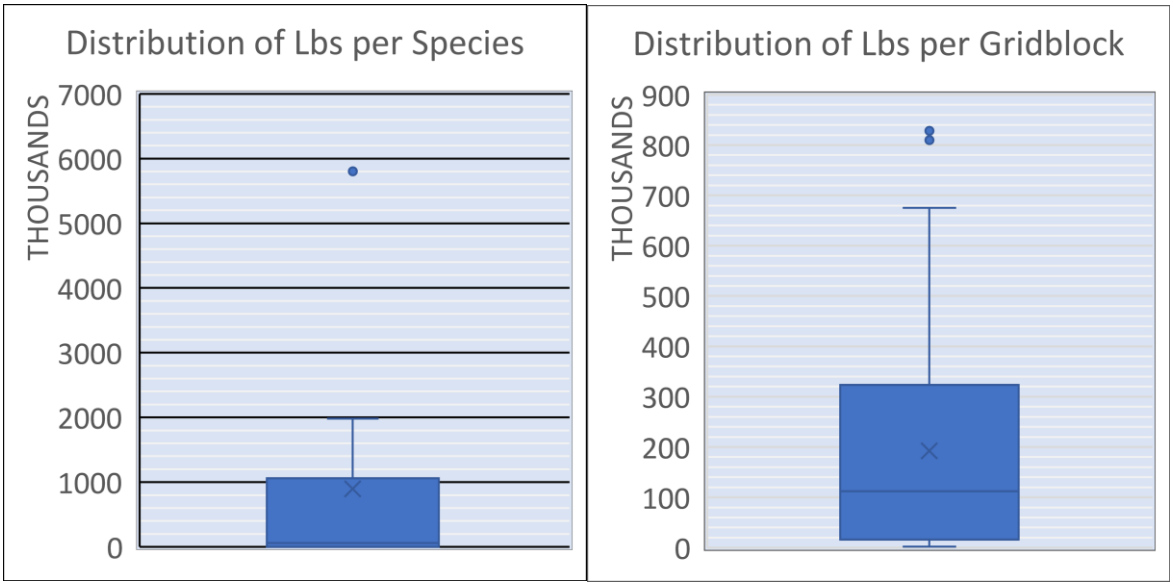

Figure 3.3 Highly migratory species landings boxplots
Boxplots of distribution of Highly Migratory Landings (thousands of lbs, 2013-2016 combined) by species (left), and by grid block (right). The top and bottom of each box represent the 25th and 75th percentiles of the landing estimates, respectively.

A

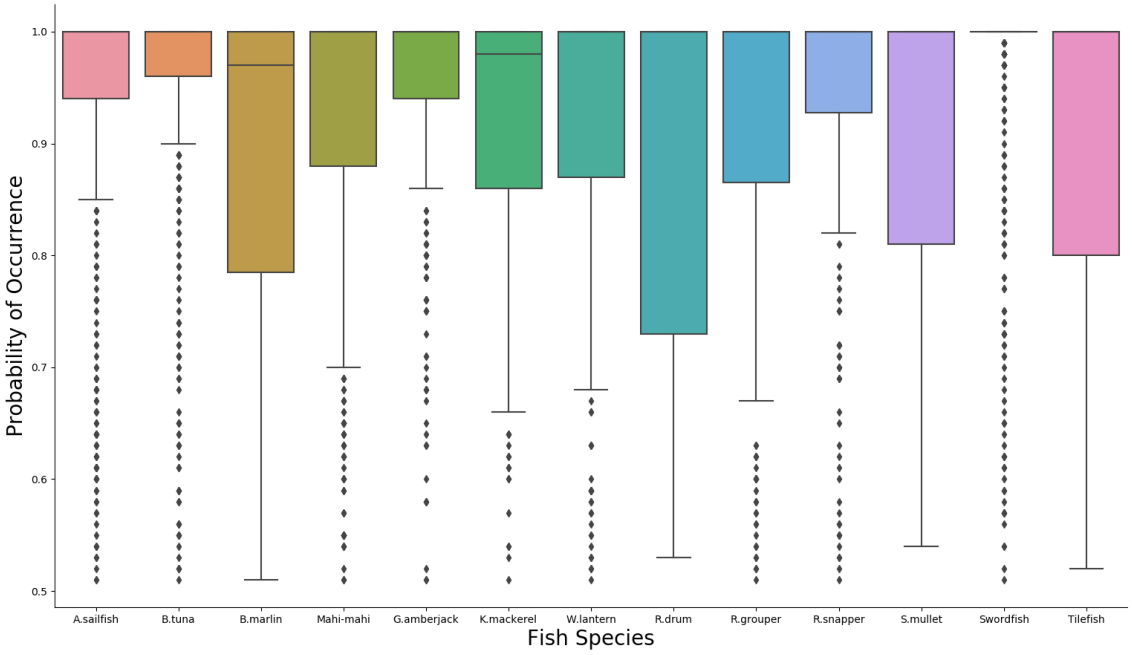

B

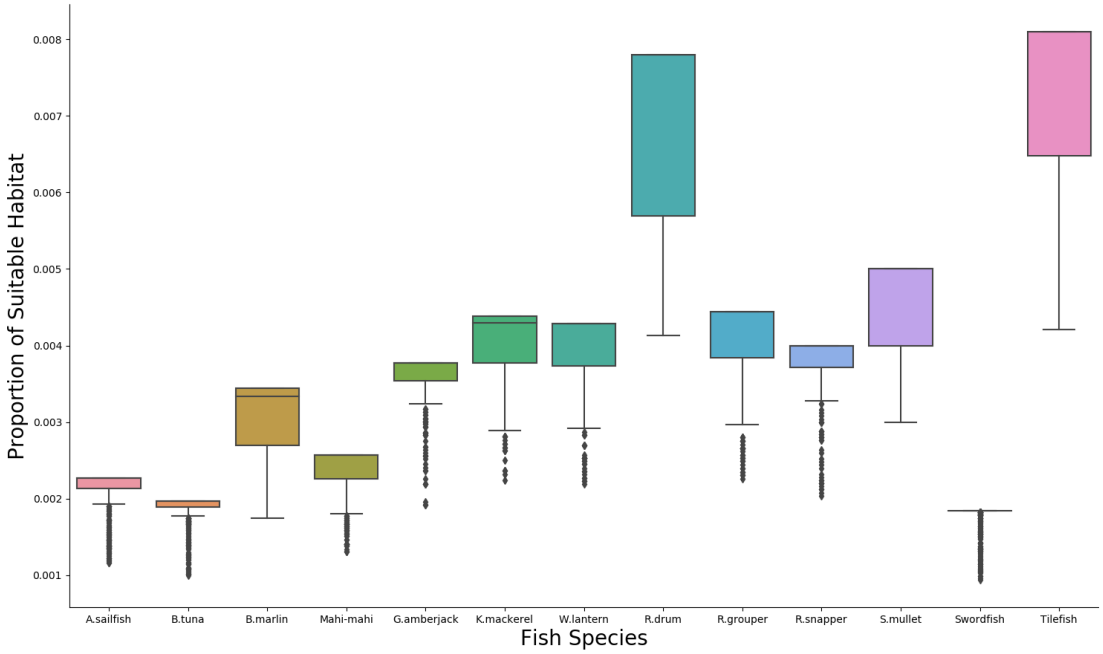

Figure 3.4A Distribution of probability of occurrence and proportion of suitable habitat for fish species

Distribution of Probability of Occurrence (A) and Proportion of Suitable Habitat (B) scores for fish species. Full name of fish species listed on x-axis labels can be found in Table 3.1.

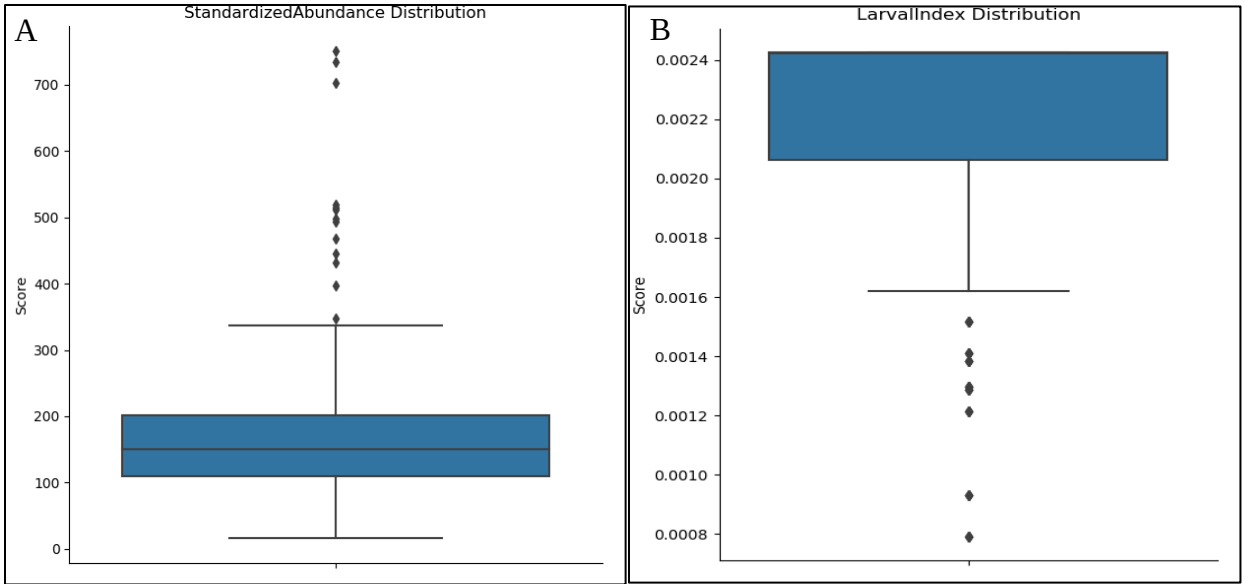

Figure 3.4B Distribution of proportion of suitable habitat for larval abundance
Distribution of Standardized Larval Abundance (before data transformation, (A)) and created variable Larval Index (after data transformation, (B)). Index was created for larval abundance layer to be comparable with proportion of suitable habitat layers shown in Figure 3.4A.

		Species column numbers correspond to labeled species row numbers																		Avg Score
		1	2	3	4	5	6	7	8	9	10	11	12	13	14	15	16	17	18	
1	Atlantic spotted dolphin	0																		0.32
2	Bottlenose dolphin	0.13	0																	0.31
3	False killer whale	0.41	0.41	0																0.40
4	Pantropical spotted dolphin	0.44	0.37	0.05	0															0.40
5	Pygmy killer whale	0.3	0.31	0.12	0.16	0														0.36
6	Sperm whale	0.58	0.64	0.26	0.31	0.36	0													0.54
7	Atlantic sailfish	0.12	0.25	0.48	0.54	0.38	0.46	0												0.37
8	Bluefin tuna	0.19	0.27	0.31	0.36	0.2	0.41	0.18	0											0.34
9	Dolphinfish	0.08	0.15	0.38	0.43	0.28	0.54	0.11	0.15	0										0.32
10	Greater amberjack	0.26	0.2	0.57	0.53	0.49	0.8	0.38	0.43	0.3	0									0.35
11	King mackerel	0.32	0.26	0.55	0.51	0.51	0.78	0.43	0.47	0.35	0.08	0								0.37
12	Lanternfish	0.49	0.56	0.21	0.25	0.27	0.13	0.37	0.32	0.45	0.72	0.72	0							0.48
13	Red drum	0.49	0.37	0.46	0.41	0.48	0.7	0.61	0.55	0.5	0.24	0.19	0.63	0						0.43
14	Red grouper	0.29	0.26	0.52	0.49	0.42	0.74	0.39	0.36	0.34	0.1	0.15	0.66	0.3	0					0.36
15	Red snapper	0.28	0.21	0.57	0.53	0.48	0.8	0.4	0.43	0.31	0.03	0.07	0.72	0.22	0.11	0				0.36
16	Striped mullet	0.39	0.27	0.52	0.47	0.5	0.76	0.51	0.51	0.4	0.13	0.09	0.7	0.11	0.22	0.13	0			0.39
17	Swordfish	0.23	0.34	0.6	0.65	0.5	0.38	0.12	0.3	0.22	0.48	0.55	0.42	0.71	0.51	0.5	0.6	0		0.46
18	Tilefish	0.44	0.34	0.36	0.33	0.3	0.61	0.55	0.38	0.45	0.24	0.26	0.52	0.3	0.18	0.23	0.28	0.67	0	0.38

Figure 3.5A Dissimilarity scores for mammals and fish
Dissimilarity scores calculated for included fish and mammal species. Scores are the average of the absolute value of the differences between the probabilities of occurrence across all grid cells. Higher scores correspond to higher dissimilarity. **Avg Score** is the average dissimilarity score between each species and the 17 other species.

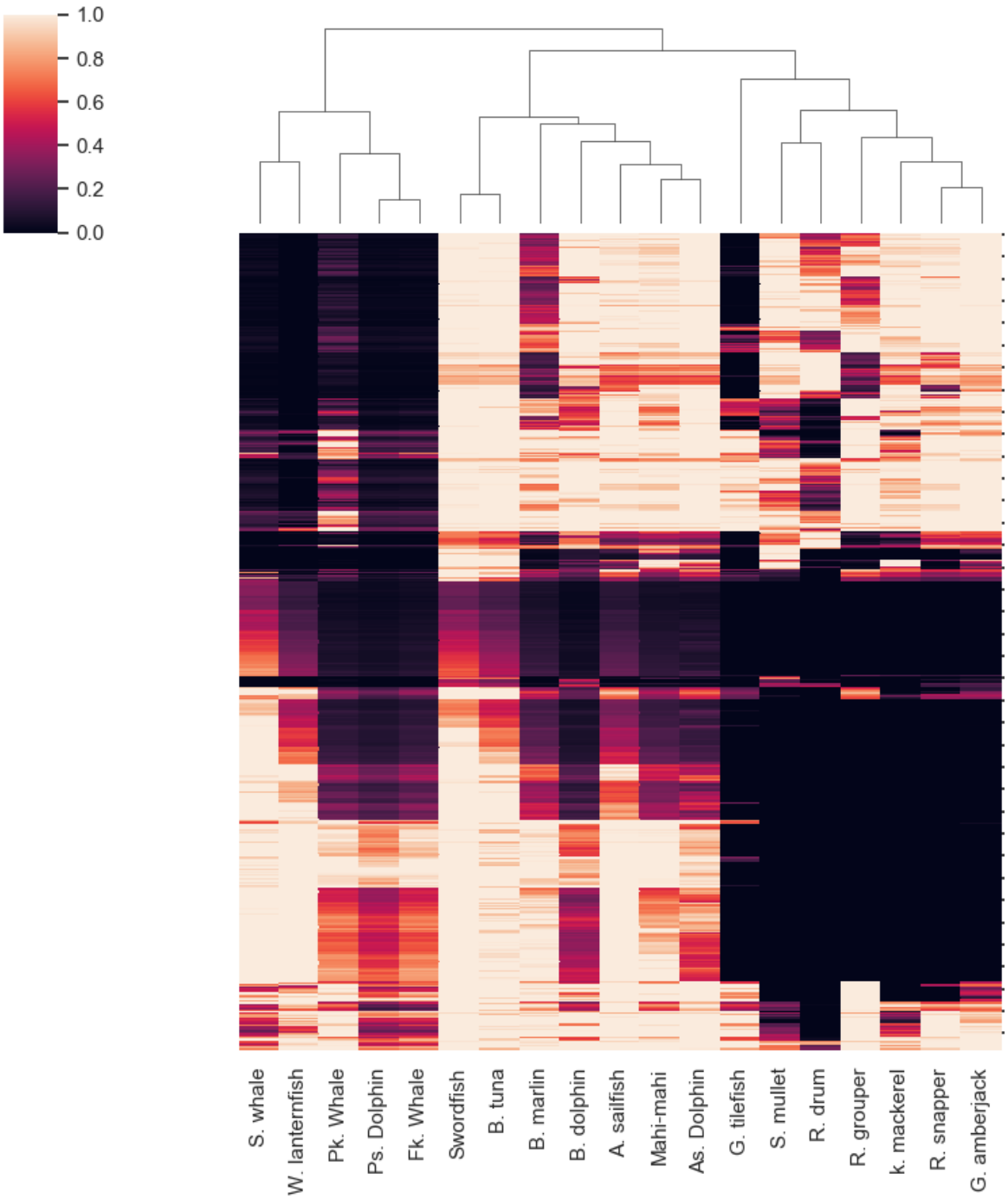

Figure 3.5B Cluster map for fish and mammal species
Cluster map created from the AquaMaps probability distributions for mammal and fish species using the *seaborn* package. Clusters for species are grouped on top x-axis, with the height of the cluster being proportional to the difference between the groups.

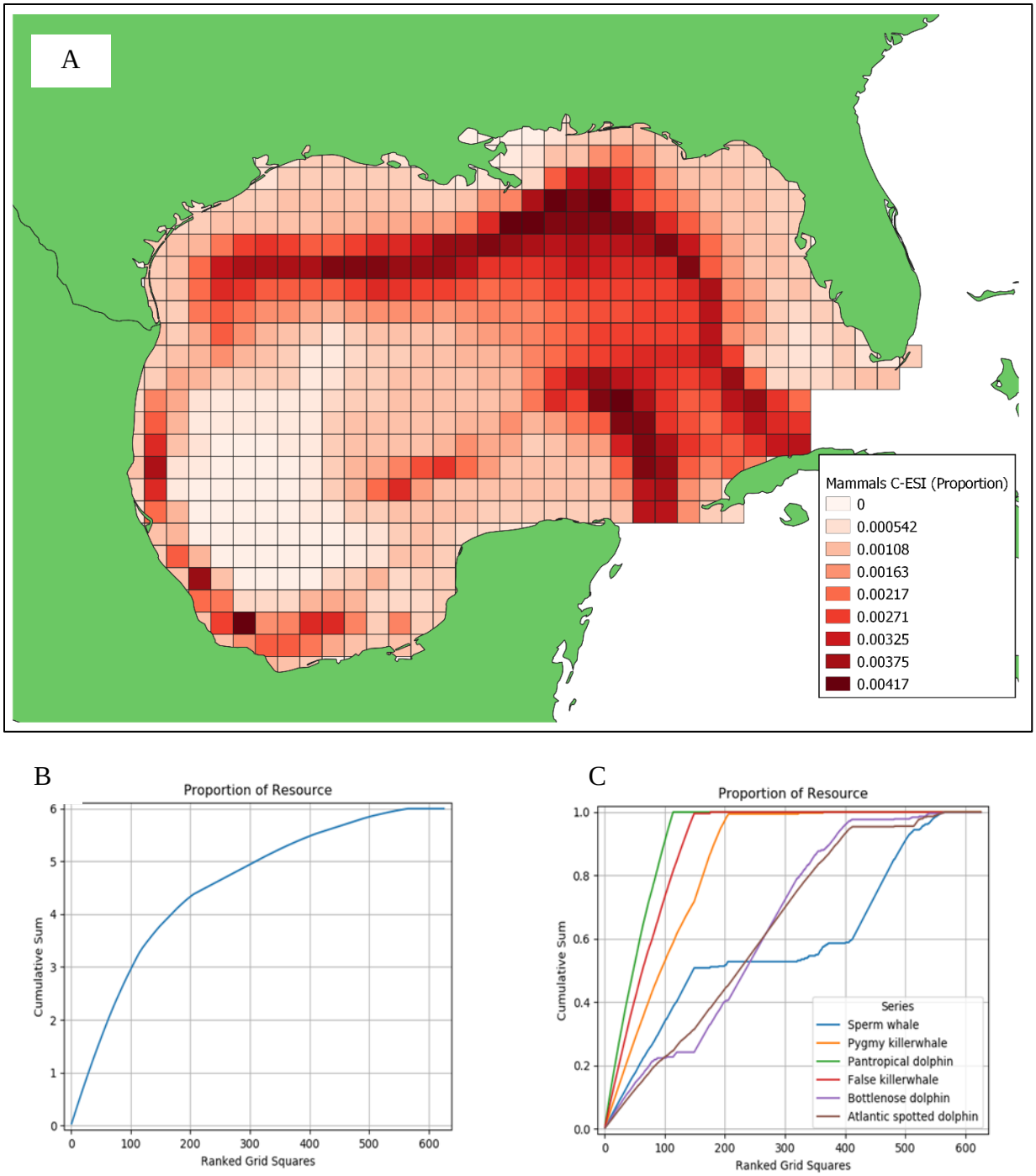

Figure 3.6 Mammals C-ESI (ID 1)
(A) Finalized raster of Cumulative Sensitivity for Mammals C-ESI ID 1 (Table 3.5). Proportion of resource by ranked grid square for Cumulative Sensitivity (B) and by individual component to the Cumulative Sensitivity (C).

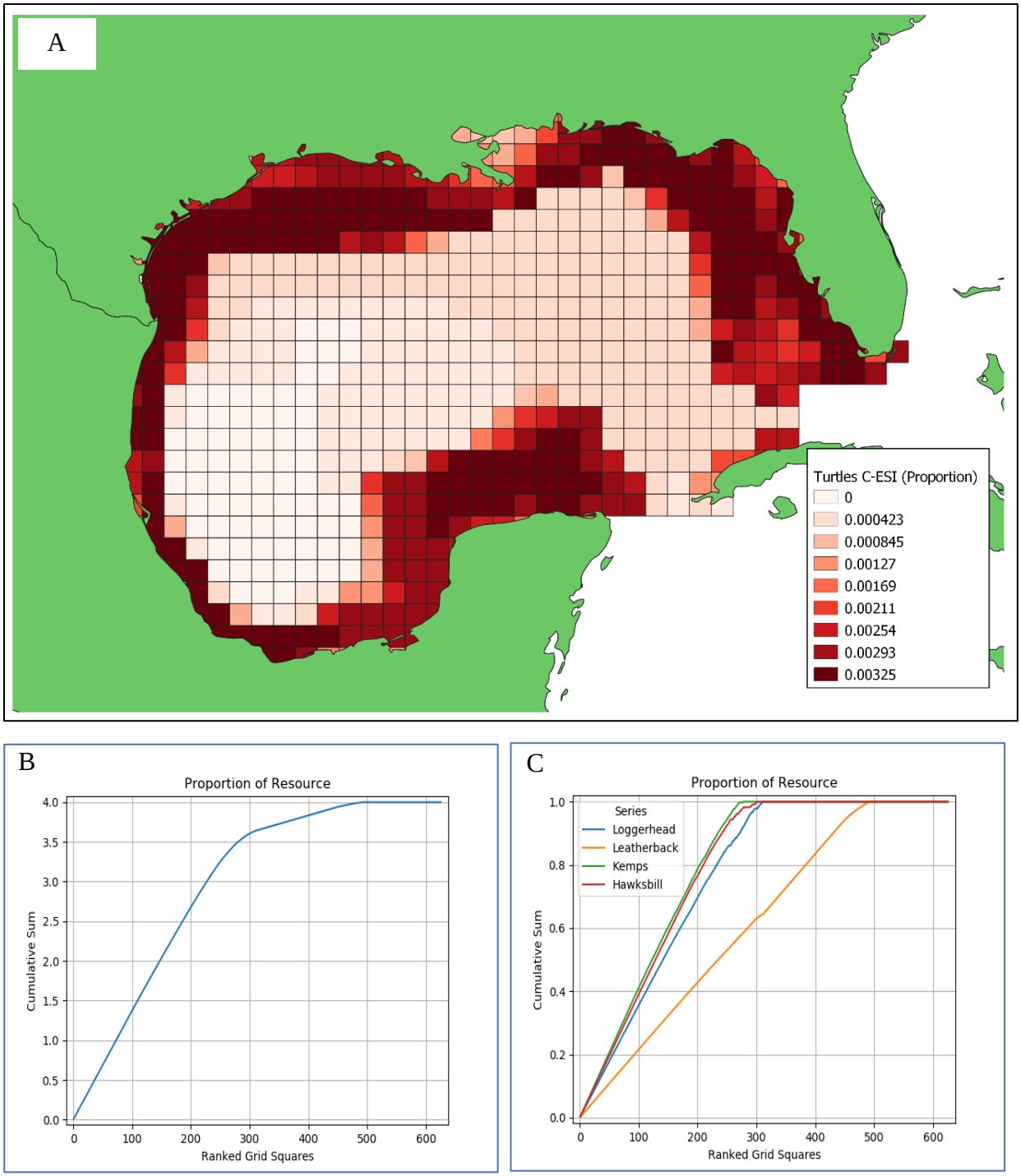

Figure 3.7 Turtles C-ESI (ID 2)
(A) Finalized raster of Cumulative Sensitivity for Sea turtles C-ESI ID 2 (Table 3.5). Proportion of resource by ranked grid square for Cumulative Sensitivity (B) and by individual component to the Cumulative Sensitivity (C).

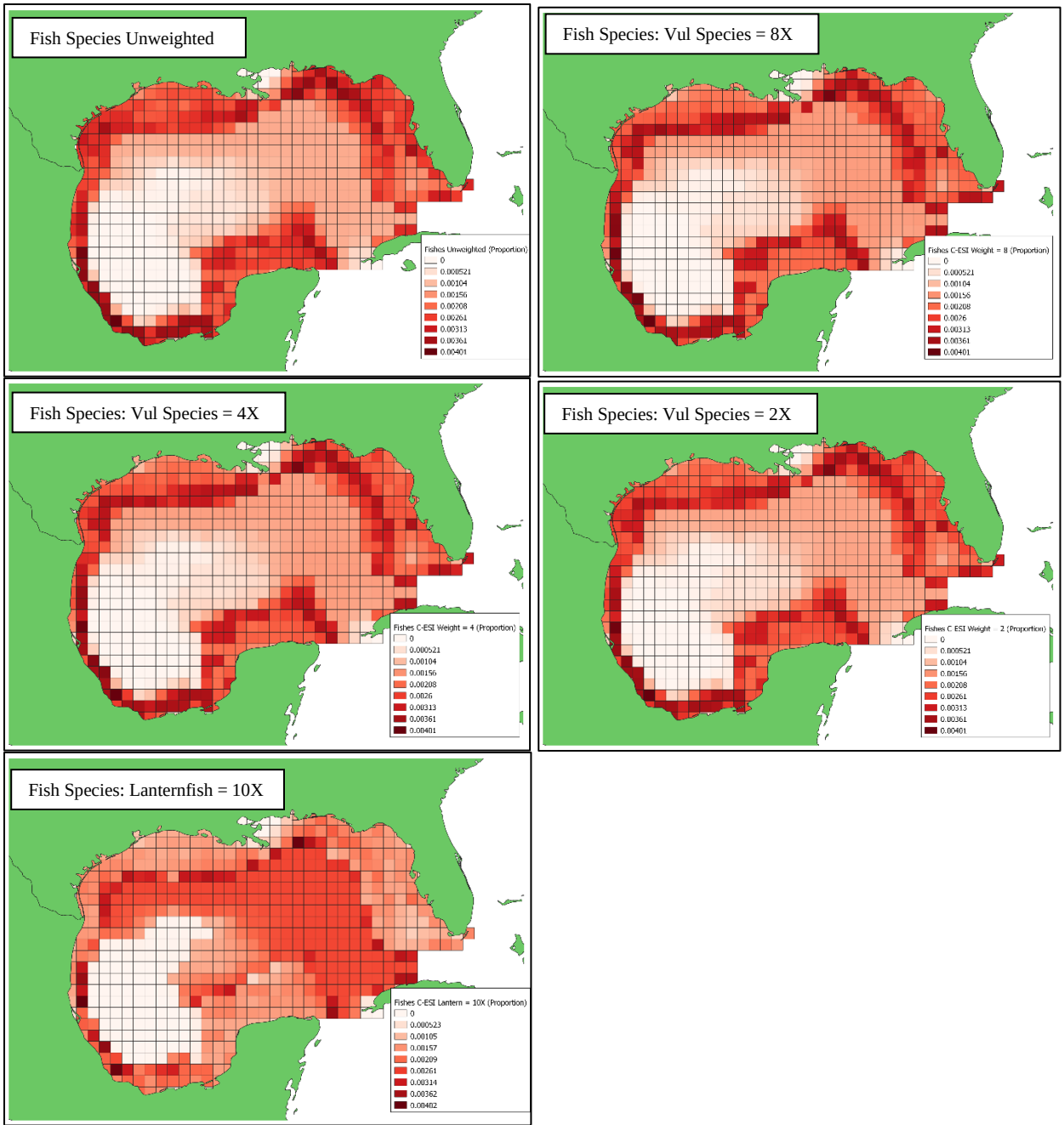

Figure 3.8 Fish species C-ESIs (ID 3 & 4)
Finalized raster of Cumulative Sensitivity for Unweighted Fish Species C-ESI and four weighted fish species C-ESIs ID 3 & 4 (Table 3.5). Weighted C-ESIs are for one species weighted (Warmingii lanternfish) and three levels of weighting (highly vulnerable species weighted at 2, 4, and 8 times that of the medium vulnerable species).

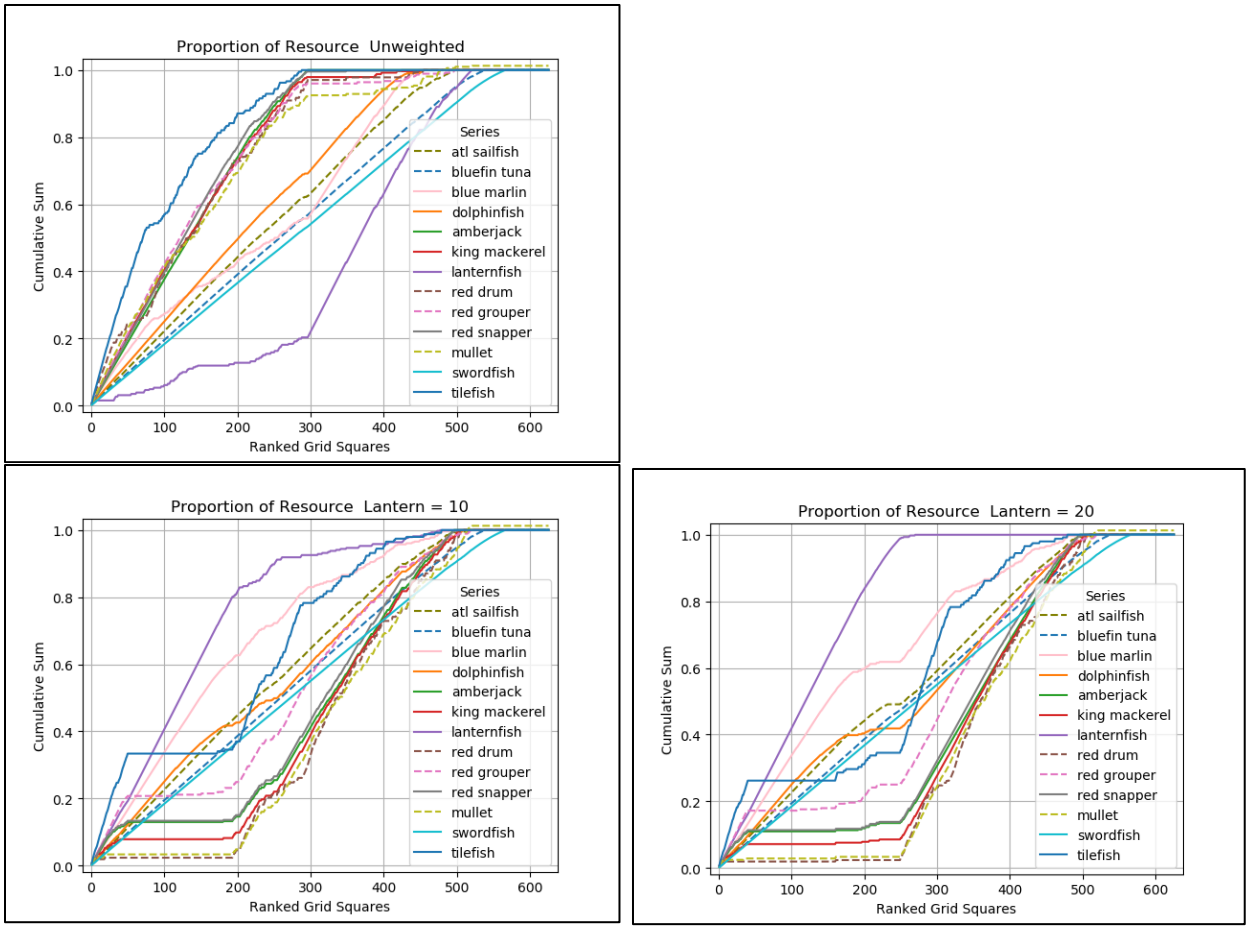

Figure 3.9A Cumulative sum by component for single weighted species
Proportion of resource by individual component to the Cumulative Sensitivity for fish species for the unweighted scenario and the weighting of one species (Warmingii lanternfish) at two levels (weight = 10, weight = 20)

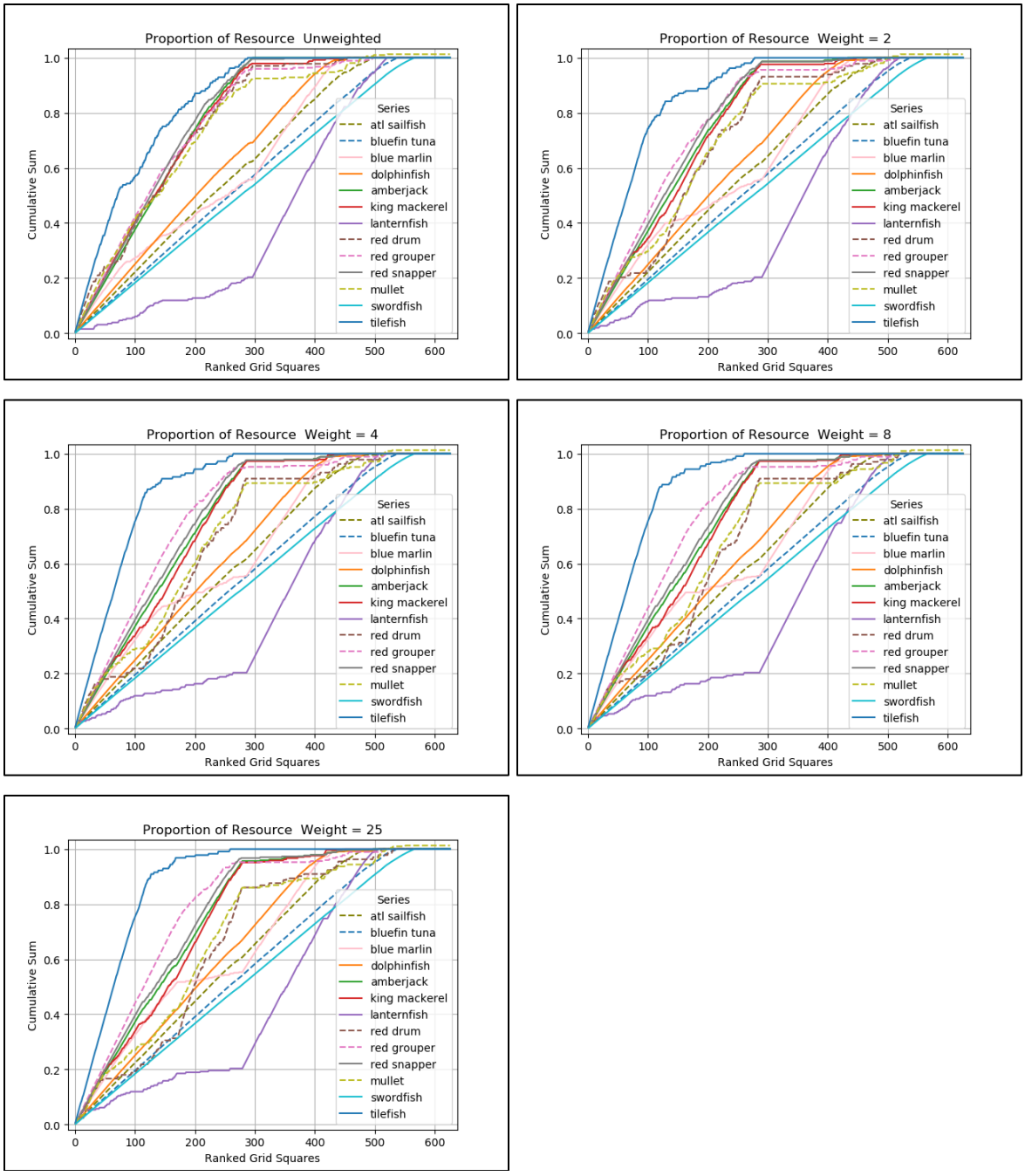

Figure 3.9B Cumulative sum by component for weighted suite of fish species
Proportion of resource by individual component to the Cumulative Sensitivity for the unweighted and weighted suite of species at 4 levels (2, 4, 8, 25). Species marked with a solid line were weighted in the group weighted scenarios.

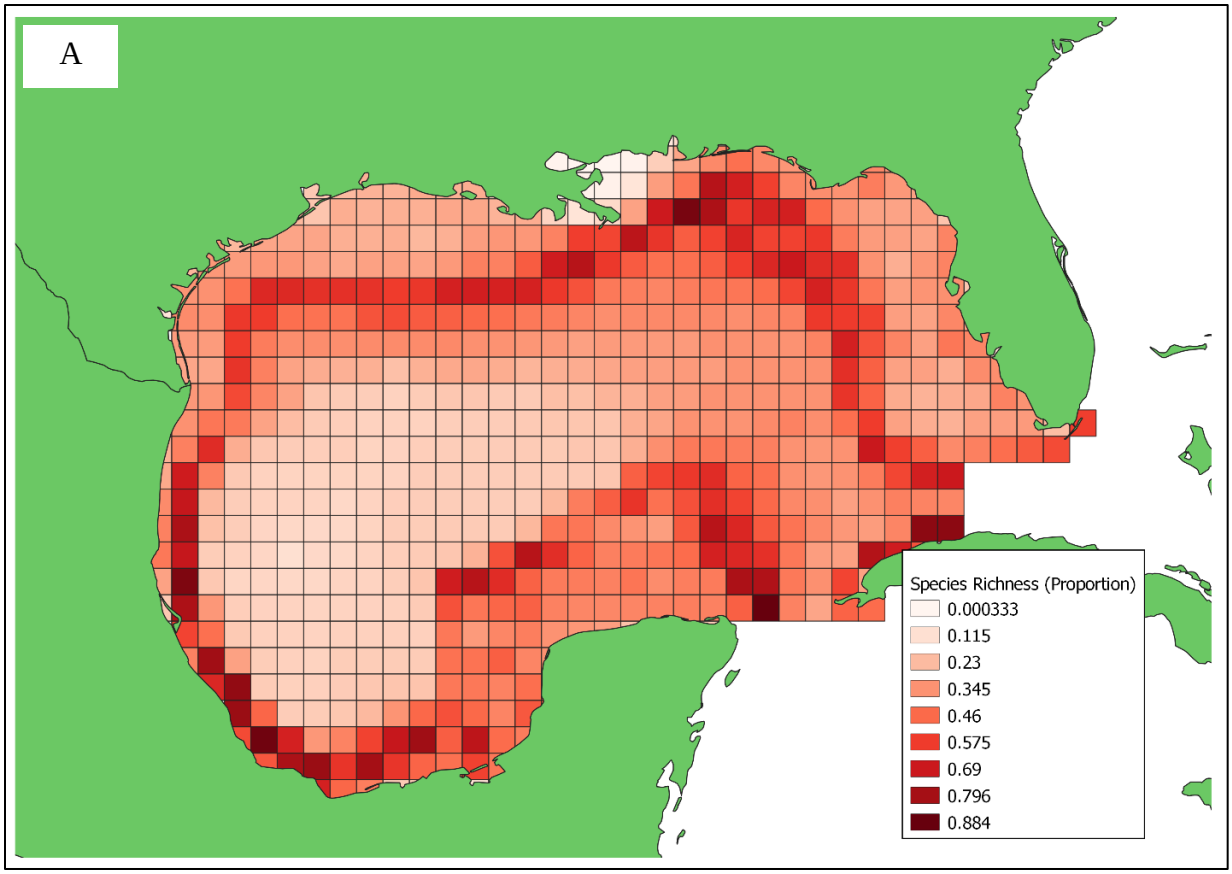

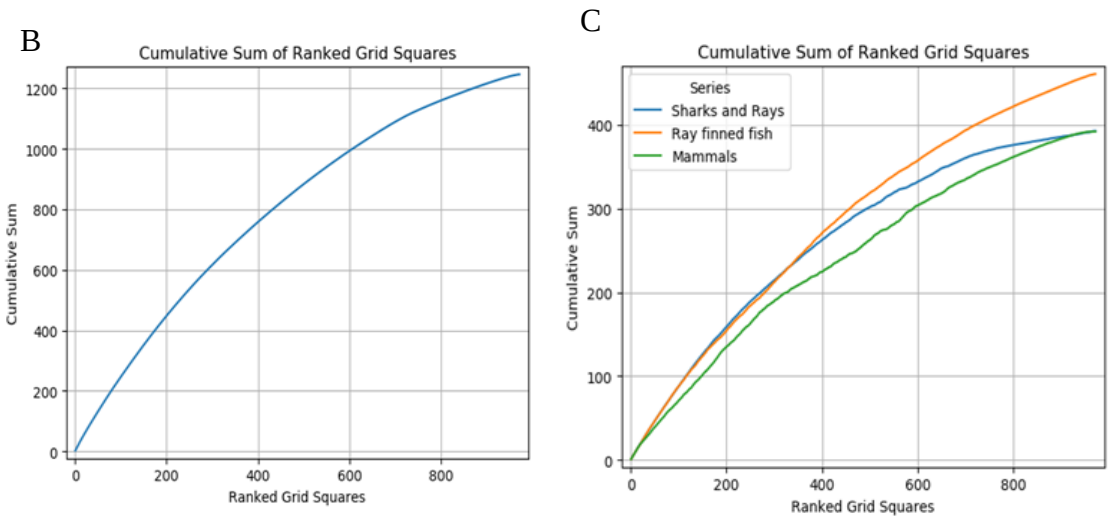

Figure 3.10 Species Richness C-ESI (ID 5)
(A) Finalized raster of Cumulative Sensitivity for Species Richness C-ESI ID 5 (Table 3.5). Proportion of resource by ranked grid square for Cumulative Sensitivity (B) and by individual component to the Cumulative Sensitivity (C).

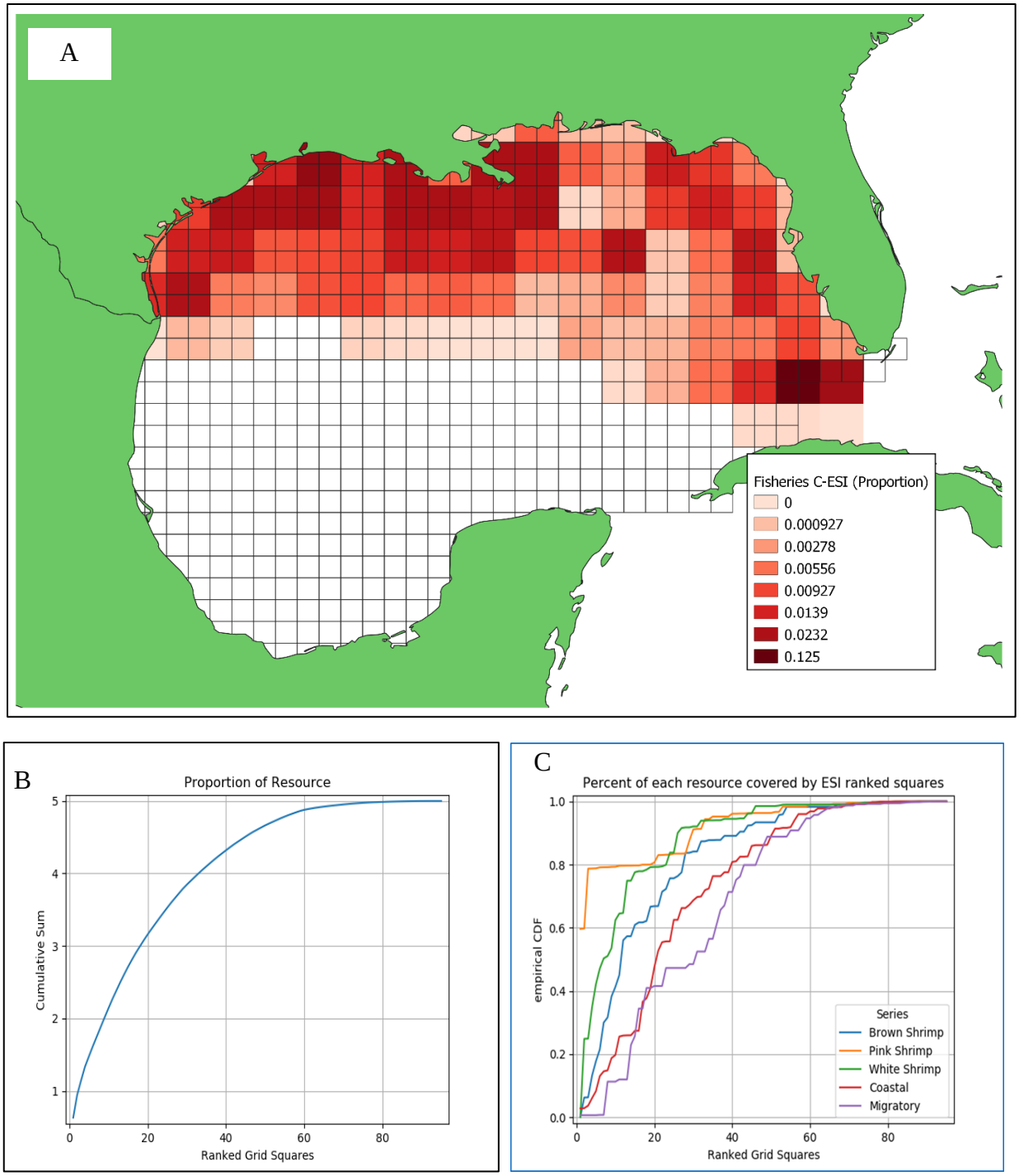

Figure 3.11 Commercial Fisheries C-ESI (ID 6)
(A) Finalized raster of Cumulative Sensitivity for Commercial fisheries C-ESI ID 6 (Table 3.5). Proportion of resource by ranked grid square for Cumulative Sensitivity (B) and by individual component to the Cumulative Sensitivity (C).

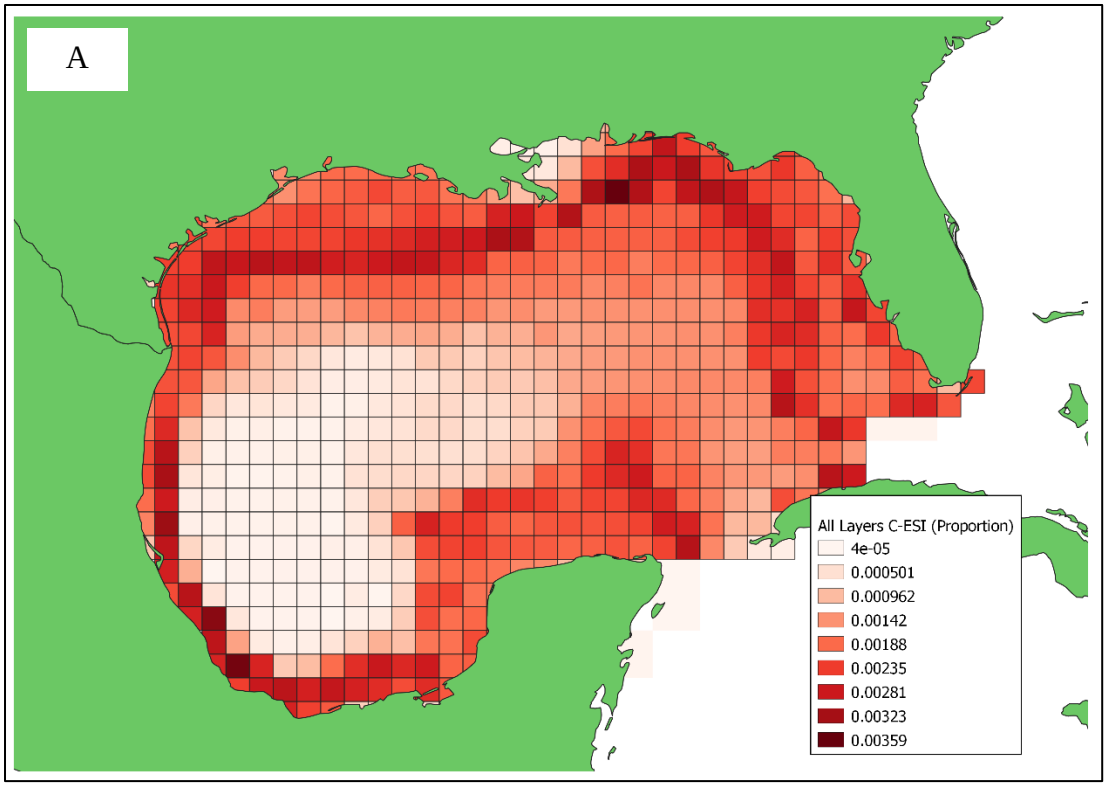

B

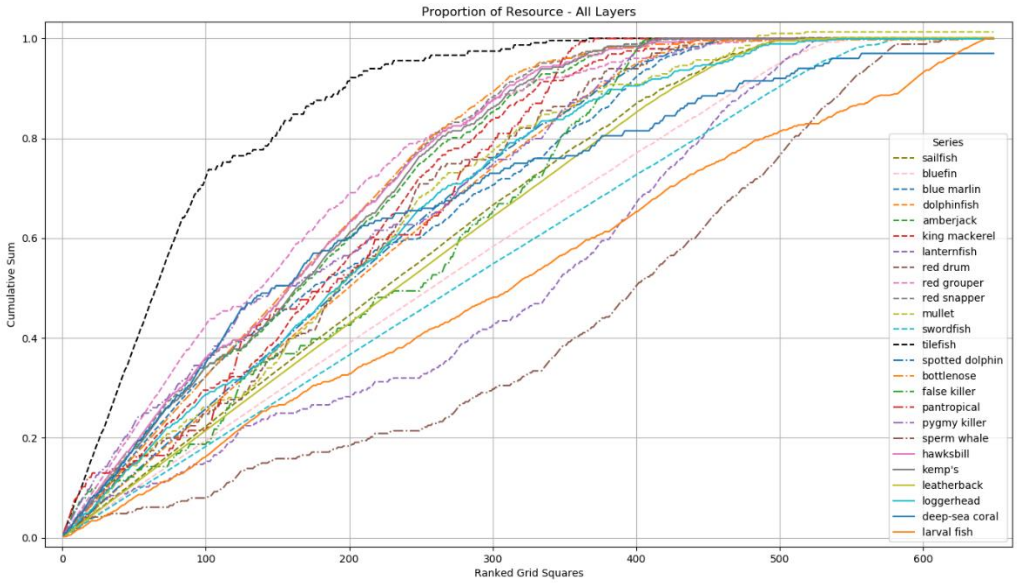

Figure 3.12 Cumulative All Layers C-ESI (ID 7)
(A) Finalized raster of Cumulative Sensitivity for All Layers C-ESI ID 7 (Table 3.5). Proportion of resource by individual component to the Cumulative Sensitivity (B).

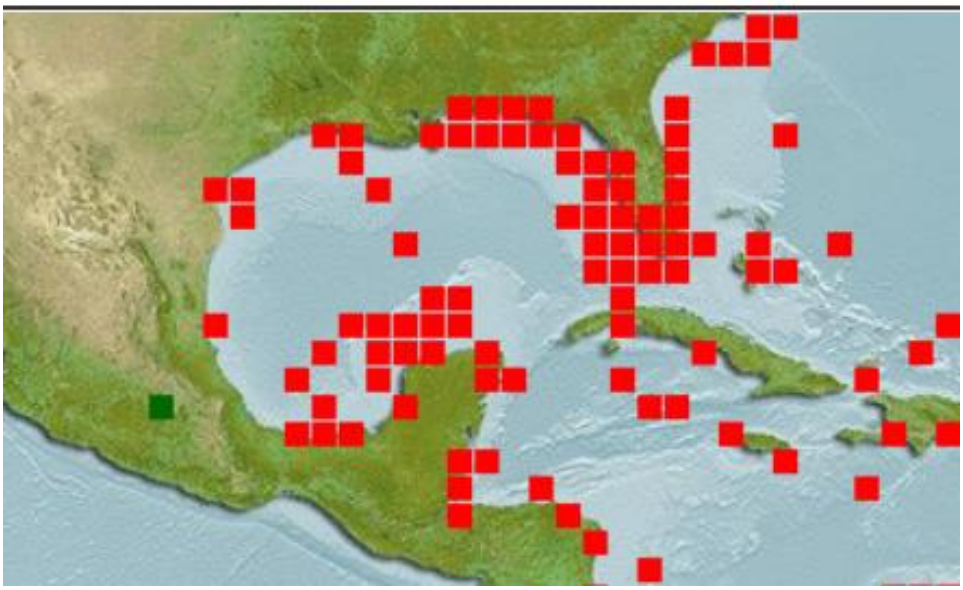

Figure 3.13 Red grouper point occurrence data used for creation of AquaMaps distribution. Graphic from http://www.obis.org.au/cgi-bin/cs_map.pl. This distribution includes the point at [90.25°W, 25.75°N] which was removed.

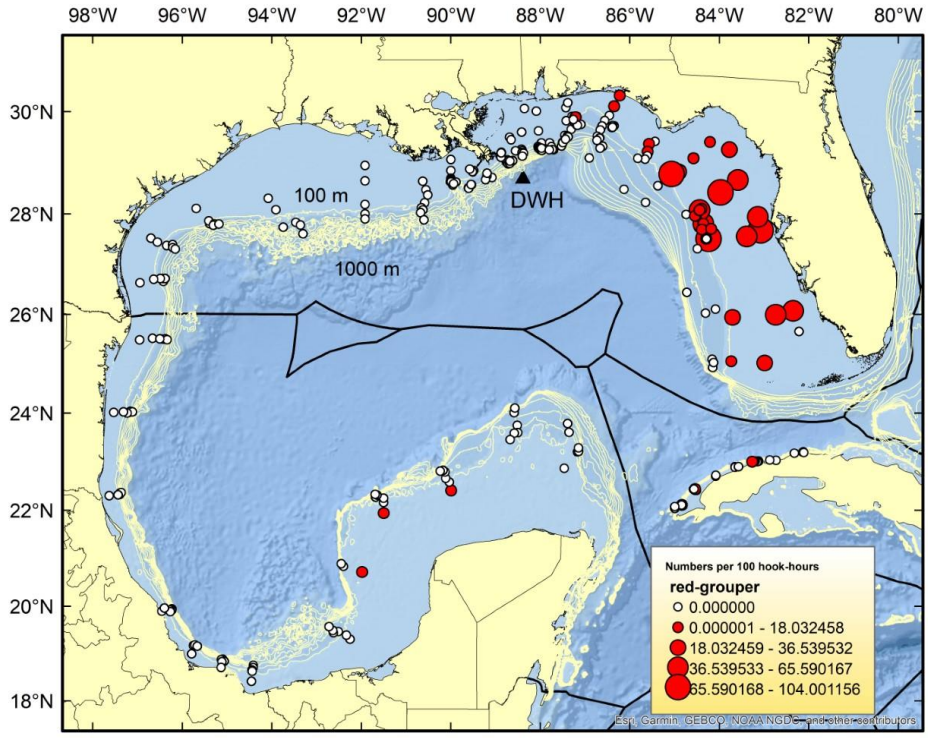

Figure 3.14 Red grouper catches from longline surveys in the GoM.
Graphic included with permission from data published in Murawski et al. (2018).

Chapter 4. Using Cumulative Environmental Sensitivity Indices (C-ESIs) to Identify Vulnerable Resource Impacts from Hypothetical Oil Well Blowouts

4.1 Introduction

Chapter 3 of this study focused on defining and demonstrating the methodology to create spatial distributions of offshore resources using disparate data sets of varying spatial resolution, and to combine these resource maps into Cumulative Environmental Sensitivity Indices (C-ESIs). Additionally, Chapter 3 outlined methodologies to weight these resource maps prioritizing specific resources (e.g., a higher revenue Shrimp species), resource specific vulnerabilities (e.g., weighting a suite of previously identified vulnerable species), or weighting of one or more resources to ensure substantial representation within the final C-ESI (e.g., weighting Warmingii lanternfish to prevent under representation). The resulting C-ESIs created in Chapter 3 identify "hot-spots" within the GoM which would be differentially susceptible to a significant oil well spill. In particular, the shelf slope region was a congregation area for many vulnerable species, which is also a region of intensive oil and gas development, especially recently (Murawski et al. 2020).

This chapter aims to demonstrate how the C-ESIs created in Chapter 3 can be used both to proactively identify offshore resources that may be potentially impacted due to hypothetical oil well blowouts, and as a reactive tool to identify potentially vulnerable offshore resources if an oil well blowout has occurred (e.g., as an aid to oil spill responders to prioritize response measures.)

This study uses distributions of surface oil for four hypothetical oil well blowout scenarios created using the Connectivity Modeling System (CMS) at the University of Miami (Paris et al. 2013; Berenshtein et al. 2020a). The origins of two of the simulations mimic the Deepwater Horizon (DWH) spill, but at two different times of year (spring and autumn). The other two simulations represent spring origin locations in the western GoM (where drilling is currently occurring) and the eastern GoM (currently withdrawn under 2021 Congressional Moratorium). These four location-specific scenarios with changes in origin location and time of year have previously been shown to have differing impacts on the suite of larval fish exposed to oil (Chancellor 2015). The oil well blowout scenarios will be used to demonstrate the utility of the C-ESIs (developed in Chapter 3) in evaluating of vulnerability of the suite of resources to the oil well blowouts and for identifying specific resources that may be differentially vulnerable in the event of these oil well blowout scenarios. The surface oil expressions from the modeled oil well blowouts are used to estimate which grid cells (rastered) are likely to encounter oil and at what concentrations of oil (relative to critical concentrations resulting in biological effects).

Marine organisms are exposed to oil through four major pathways: absorption of bioavailable hydrocarbon compounds into skin via direct contact with oil (e.g., sea turtles and mammals surfacing and diving), inhalation and aspiration (air-breathing animals may breathe in aerosol compounds), and ingestion (ingestion of water or sediments containing oil) (Westerholm and Rauch 2016). Polycyclic aromatic hydrocarbon (PAH) concentration levels and duration of exposure determine lethal and sublethal effects to biological resources through absorption. Toxicity tests are performed to identify critical thresholds (i.e., toxicity endpoints) in fish and invertebrate species to oil and dispersants used in oil cleanup. Toxicity endpoints calculated include EC50 (i.e., effect concentration at which 50% of the test population is affected), IC50

(i.e., inhibitory concentration) and LC50 (i.e., lethal concentration). EC50 or IC50 is primarily reported in chronic (i.e., days or weeks) toxicity tests and is the concentration at which 50% of the exposed organisms experience sublethal or lethal effects (positively correlated response = EC, negatively correlated response = IC) at a specified duration (e.g., 96-hour EC50). LC50 is primarily reported in acute (i.e., < 96 hours) toxicity tests and is the concentration where mortality in 50% of the exposed test organisms occurs (e.g., 24-hour LC50; Westerholm and Rauch 2016).

Fish eggs, larval fish, juveniles, and adult fish all can suffer lethal and/or sublethal effects from PAH exposure. Early life stages of fishes can suffer cardiac and morphological defects at levels as low as PAH = 0.5 µg/L ΣPAHs at the surface and PAH = 1 µg/L ΣPAHs at deeper waters (Carls et al. 1999; Incardona et al. 2004; Hicken et al. 2011; Incardona et al. 2013; Westerholm and Rauch 2016). Two cardiac effects, edema (pericardial fluid accumulation) and bradycardia (reduction in heart rate) were observed for three large pelagic species, Bluefin tuna, Yellowfin tuna, and amberjack using DWH MC252 oil at ΣPAH concentrations similar to those sampled during the spill (Incardona et al. 2014). The EC50 values for edema for Bluefin tuna, Yellowfin tuna, and amberjack, occurred at 0.8, 2.3, 12.4 µg/L ΣPAHs respectively. The thresholds for edema ranged from 0.3–0.6 µg/L, 0.5–1.3 µg/L, and 1.0–6.0 µg/L ΣPAHs for bluefin tuna, yellowfin tuna, and amberjack respectively, meaning that these effects begin to be observed in larvae at these lower concentrations (Incardona et al. 2014). The IC50 values for bradycardia (reduction in heart rate) occurred at 7.7, 6.1, and 18.2 µg L− 1 ΣPAH for bluefin, yellowfin tuna, and amberjack respectively while the exposure thresholds were in the range of 4.0–8.5 µg/L, 1.0–2.6 µg/L, 2.2–6.5 µg/L respectively. An estimated ~20% of water samples collected in the DWH sampling had concentrations higher than the edema thresholds and ~30%

had concentrations higher than the bradycardia thresholds (Incardona et al. 2014). Additionally, there is evidence to suggest that toxicity to eggs and larval fish increases when oil is weathered. In embryonic mahi-mahi, acute lethality (96 h LC50) occurred at 45.8 μg L− 1 ΣPAH (range 28.4–63.1) for wellhead oil collected at the source. When oil samples collected from the surface slick were used (representing the weathered oil), the acute lethality occurred at the significantly lower concentration of 8.8 μg L− 1 ΣPAH (range (7.4–10.3) for samples collected from the surface slick; Esbaugh et al. 2016). DWH occurred during the spawning seasons of these fish species and in concentrations above those thresholds listed here, therefore impacts to early life stage fishes may have been large and occurring over a large spatial extent.

The impacts caused by oil exposure to these early life stages can persist into adulthood for surviving larvae. In the laboratory, Mahi-mahi larvae/embryos that were exposed to 48 h exposure of 1.2 ± 0.6 μg L–1 ΣPAH and then raised for 25 days experienced acute sublethal impacts leading to a reduced critical swimming velocity of 37% (Mager et al. 2014). Juvenile and adult species also experience sublethal impacts when exposed to oil. Juvenile Mahi-mahi exposed to 24 h exposure of 30 ± 7 μg L–1 ΣPAH experienced acute sublethal impacts leading to a 22% decrease in critical swimming velocities (Mager et al. 2014). Adult red drum experienced 12.6% reduction in critical swimming velocity when exposed to 24-hour exposure of 4.1 μg L−1 ΣPAH and additional 18.4% reduction in aerobic scope at a higher exposure level of 12.1 μgL−1 ΣPAH (Esbaugh et al. 2016). Adult Mahi-mahi experience acute sublethal toxicity with significant reductions in critical swimming velocity (14%) and optimal swimming velocity (10%) and a 20% reduction in maximum metabolic rate at ΣPAH concentrations of 8.4 ± 0.6 μg L−1 (8.4 ppb) over a 24-hour exposure period (Stieglitz et al. 2016). Sublethal impacts in swimming characteristics are likely to have negative impacts on Mahi-mahi, Red

drum, and other large predatory species which rely on swimming performance to hunt and, in some highly migratory species, cover large migration distances (Stieglitz et al. 2016). Additionally, increased numbers of skin lesions were found on adult fishes in 2011 and 2012 after the DWH oil spill which impact species' health and fitness (Murawski et al. 2014).

Marine mammals are at risk of oil exposure through all four pathways since they breathe at the air/surface interface and can be exposed to oil through ingestion and respiration (Neff 1988; Marsili et al. 2001). Routine toxicological experimentation cannot generally be performed on mammals due to the Marine Mammal Protection Act (MMPA) and the Endangered Species Act, so toxicity data on marine mammals comes from the aftermath of accidental oil exposure in the case of a spill or historical studies. Bottlenose dolphins exposed to DWH oil experienced decreased immune function, higher rates of anemia, bacterial pneumonia, pulmonary abnormalities, and decreased reproductive success (Schwacke et al. 2014; Lane et al. 2015; De Guise et al. 2017; White et al. 2017; Ruberg et al. 2021). Increased dolphin strandings were also associated with exposure to DWH oil (Venn-Watson et al. 2015). According to a report published by the U.S. Fish and Wildlife Service (2011), 157 marine mammal deaths were attributed to the DWH oil spill, but this number is likely only a small percent of the true mortality due to the historical cetacean carcass-recovery proportion being around 2% (Williams et al. 2011). The combination of lethal and sublethal impacts observed in these studies likely negatively contributed to population levels for many marine mammals as eleven species of cetaceans were observed swimming through petroleum contaminated waters following DWH including five of the mammal species included in this study (i.e., Atlantic spotted dolphin, bottlenose dolphin, pantropical spotted dolphin, pygmy sperm whale, and sperm whale [Dias et al. 2017]).

The surface oil distributions from the four hypothetical oil well blowout scenarios were used to identify the maximum daily oil concentration (MDOCs) observed over the entire scenario time period for each 0.02°x0.02° latitude/longitude grid cell within the GoM study area (Figure 4.1). Minimum oil concentration threshold (MOCT) polygons of grid cells were created from the MDOC values and represent contiguous areas exposed to at least the MOCT for at least one day. These MOCT polygons, which represent critical toxicity thresholds throughout the range of observed oil concentrations, were then overlayed with the C-ESIs created in Chapter 3 to estimate the exposure of various resources to different oil concentration levels, using GIS methods.

The objectives of this chapter are therefore: (1) to demonstrate methodology to create MOCT polygons from modeled or actual surface oil expression, (2) compare the estimated impacts of the four oil well blowout scenarios using the C-ESIs and the MOCT polygons, (3) identify the most vulnerable resources to a given oil well blowout scenario using the C-ESIs and their components, and (4) provide open source scripting for the replication of this study. This available script can be used to create an MOCT polygon from any oil distribution, for any oil concentration level, and any duration of exposure and then find the intersection of this MOCT polygon with any resource or any suite of resources combined in a C-ESI.

4.2 Methods

4.2.1 Creation of Surface Oil Maximum Daily Oil Concentration (MDOC) Files

Four oil well blowouts were modeled using the open-source Connectivity Modeling System (CMS) adapted with an oil spill module (Paris et al. 2012; Paris et al. 2013; Berenshtein et al. 2020a). Origin locations for the scenarios were chosen at similar depths to the DWH blowout (e.g., an ultra-deep blowout) and to represent locations where drilling is currently

occurring or has previously been proposed. For each scenario, oil droplets were released for 87 days (as per DWH) and tracked for a total of 90 days. In each scenario, oil droplets were released at a depth of 1,222 m (slightly shallower than DWH at 1,500 m) in accordance with the conditions of the DWH oil well blowout (Berenshtein et al. 2020a). Total oil concentrations (ppb) are obtained by normalizing the total oil mass to the mass of water by 0.02°x0.02° latitude/longitude grid resolution in the upper 20m, and the daily averages are further determined from the 2-hourly output products (Berenshtein et al. 2020a). Note that the raster dimensions of the oil spill simulation are much smaller than the grids used to compile C-ESIs (Chapter 3).

The four simulated oil well blowout scenarios used in this study (i.e., Fig. 4.1) are:

(1) *Deepwater Horizon* control (DWH) – Located in the central GoM with a DWH origin point
Origin: 28.736 N, 88.365 W Start Date: April 20th, 2010

(2) *Deepwater Horizon* Fall (DWH Fall) – Located in the central GoM with a DWH origin point and a September start date
Origin: 28.736 N, 88.365 W Start Date: September 1st, 2010

(3) Western GoM – Located in the western GoM where drilling is currently active.
Origin: 27.000 N, 85.168 W Start Date: April 20th, 2010

(4) West Florida Slope (WFS) – Located in the eastern GoM on the continental slope where drilling has been prohibited until 2032.
Origin: 26.600 N, 93.190 W Start Date: April 20th, 2010

Daily oil concentrations (ppb) by 0.02°x0.02° latitude/longitude grid resolution in the upper 20m were provided for each of the oil spill scenarios. This study calculated the maximum daily oil concentration (MDOC; ppb) over the entire 90 days for each 0.02°x0.02° latitude/longitude grid cell. The distributions of the MDOC were mapped in QGIS (QGIS Development Team, 2020) for each oil well blowout scenario (Figure 4.1)

4.2.2 Creation of Minimum Oil Concentration Threshold (MOCT) Polygons

To create a boundary enclosing all the 0.02°x0.02° latitude/longitude grid cell where the MDOC was equal or greater to a predefined threshold, I used the *v.hull* command within the *GRASS* (GRASS Development Team, 2020) module in *QGIS* as described in van Breugel (2103). The *v.hull* command in *GRASS* builds a convex hull, or boundary, around a grouping of points and converts this boundary to a polygon (as .shp file). I chose twelve levels of minimum oil concentration thresholds (MOCT) (ppb) [X_c = 1, 5, 10, 25, 50, 100, 150, 200, 400, 800, 1500, 2000] as these concentrations cover the full range of the MDOC observed and created a polygon surrounding all the 0.02°x0.02° latitude/longitude points where the oil concentrations met or exceeded each X_c concentration. This set of nested polygons was created for each of the twelve X_c values for each of the four oil well blowout scenarios for a total of 48 polygons (Figures 4.2A, B).

4.2.3 Calculating Intersection of C-ESIs and MOCT Polygons

The *Zonal Statistics* tool within *QGIS' raster analysis* package calculates the intersection of a polygon (with at least one zone) with the mathematical expression (e.g., sum, max, average) of a value field in a raster. I used seven of the rastered C-ESIs (Table 4.1), 33 of the resource component rasters (Table 4.2) from Chapter 3, and the 48 MOCT polygons described above and calculated the intersection between each C-ESI raster and MOCT polygon for each oil well blowout scenario. The intersection between the MOCT polygon and the selected C-ESI (hereafter referred to as Cumulative Impact Proportion [CIP]) for each oil well blowout is then calculated as:

$$CIP_{kXc} = \sum_{i=1}^{n}(CS_{ij} * (D_{ij}))\ ) \qquad \text{Eq. 4.1}$$

where CIP_{kXc} is the CIP of oil well blowout k at MOCT level X_c, CS_{ij} is the Cumulative Sensitivity of the C-ESI (or individual raster) at grid cell (i, j), and D_{ij} is a dummy variable equaling 1 when grid cell (i, j) is within MOCT polygon kX_c and 0 when it is not. The CIS_{kXc} value then represents the proportion of the C-ESIs entire value which lies inside the MOCT polygon kX_c with an example value of 0.75 representing that 75% of the cumulative value of the selected C-ESI lies within the MOCT polygon created from oil well blowout k at MOCT level X_c.

Likewise, the intersection between the MOCT polygons and each resource component (hereafter referred to as Resource Impact Proportion [RIP]) for each oil well blowout was calculated by the same method (Eq. 4.1).

This study calculated an excess of 1500 intersections (48 MOCT shape files, 7 C-ESIs rasters, and 33 individual component rasters). I created a Python script to run these intersections, load the results into a data frame, and graph the results. This script is available as open source on https://github.com/echancellor/dissertation-scripts. It requires the *pandas* and *seaborn* dependencies to be installed in the Python environment and was run in the *Python Console* in *QGIS Desktop 3.8.0 with GRASS 7.6.1* (GRASS Development Team, 2020).

4.2.4 Toxicity Threshold Conversion to MOCT

In order to define the modeled intersections between the resource distributions and the MOCT polygons in terms of well-established toxicity thresholds, PAH thresholds (µg/L ΣPAHs) were converted to total petroleum hydrocarbons (TPH) values (ppb, µg/L) using the PAH-THP linear relationship described in Berenshtein et al. (2020a). Berenshtein et al. (2020a) identified two significant linear relationships, one for waters with depth ≤ 1 m ($p < 0.001$, $R2 = 0.9$, $n = 34$) and one for depths > 1 m ($p < 0.001$, $R2 = 0.3$, $n = 641$):

$$\log10(TPH+1) = 1.733 + 1.0074 \times \log10(PAH+1), \text{ for surface waters (depth} \leq 1m) \quad \text{Eq. 4.2}$$

$$\log10(TPH+1) = 1.58357 + 0.85257 \times \log10(PAH+1), \text{ for deeper waters (depth} > 1m) \quad \text{Eq. 4.3}$$

The toxicity amplification in Eq. 4.2 is due to the increased toxic effect of PAH combined with and UV radiation (Berenshtein et al. 2020a). PAH thresholds and their corresponding MOCT value (calculated as the TPH) are included in Table 4.5 for surface and deeper waters.

4.3 Results

4.3.1 Proportion of C-ESI within each MOCT Polygon

The Cumulative Impact Proportion (CIP) was calculated between the 48 MOCT polygons and the seven C-ESIs (Table 4.3). Summary statistics for the CIPs were calculated by oil well blowout scenario and C-ESI (Tables 4.4). The Resource Impact Proportion (RIP) was calculated between the MOCT polygons and the 33 resource components. The CIP or RIP between the C-ESI/resource component layer and the MOCT polygon represents the proportion of the C-ESI or resource component within the MOCT polygon respectively. Therefore, a CIP of 0.45 would represent that 45% of the resources included in that C-ESI were potentially exposed to oil at a concentration meeting or exceeding that of the MOCT polygon for at least one day.

4.3.2 Ranking Oil Well Blowout Scenarios by Resource Vulnerability

The CIP scores for the seven C-ESIs were used to create a “swarm” plot to rank the oil well blowout scenarios by their potential impact to the resources represented in the entire suite of created C-ESIs (Figures 4.3 A, B; generated from data from Table 4.3). The WGoM scenario had the lowest average CIP score with only one CIP score being larger than 0.34 and no CIP scores above 0.43. This is likely due in part to the smaller size of the MOCT polygons (i.e., the smaller overall footprint of the spill) generated in the WGoM scenario. The WGoM scenario

generated the smallest surface area of the MOCT polygons among the four scenarios, but had the largest high concentration MOCT polygons, indicating that the oil from the WGoM scenario may have been less dispersed, but with higher concentrations. The Fall and DWH scenarios had CIP scores that were distributed between 0 and 0.8, but still skewed left with more than two thirds of CIP scores below 0.5. Between the DWH and Fall scenarios, the Fall scenario indicated more vulnerability in the low MOCT ranges, with more CIP scores above 0.6 than the DWH scenario, but DWH indicated increased vulnerability at mid MOCT ranges, which are more likely to cause negative impacts to resources (e.g., toxicity to organisms, and fishery closures; Table 4.5; Berenshtein et al. 2020b). The WFS scenario had the highest average CIP score with most CIP scores falling between 0.2 and 0.6 for low to med MOCT ranges. These results indicate that the resources represented by this combined suite of C-ESI's would be most vulnerable to the WFS scenario, followed by DWH, Fall, and WGoM.

4.3.3 Resource Vulnerability to Oil Well Blowout Scenarios by C-ESI

The RIP scores for each resource included in each C-ESI were used to create a set of six plots for each of the six C-ESIs and each oil well blowout scenario (Figures 4.4-9). The weighted fish species C-ESIs were not included separately as the resource components for each of these C-ESIs are the same and would plot identically. Plots of the RIP scores for each of the individual resource components show the potential vulnerability of each resource component to the specified oil well blowout scenario. These graphs can help to identify resources that may be especially vulnerable within the C-ESI, and which contribute the most to the C-ESI CIP score listed in Table 4.3. Selected PAH concentrations of 0.5, 1.0, and 10.0 µg/L ΣPAHs were converted to MOCT µg/L concentrations using Eq. 4.3. PAH conversions are included in Table 4.5 along with PAH toxicity endpoints identified for fish species as previously described above

(Section 4.2.4). Vertical lines representing the estimated MOCT of these selected PAH concentrations were added to the plots of the RIP scores (Figures 4.4-8).

The Fisheries C-ESI graph of components (Figure 3.11) showed that one grid cell was responsible for ~60% of the Pink Shrimp fishery catch. This grid cell lies within the lowest MOCT polygon for two of the oil spill scenarios (DWH, and Fall) and within a moderate MOCT polygon for the WFS scenario (Figure 4.4). Mammals were the most impacted group within the Species Richness C-ESI across all four scenarios (Figure 4.5). For the Mammals C-ESI, in the DWH, Fall, and WFS scenarios, Pantropical spotted dolphin had the highest vulnerability scores while Atlantic spotted dolphin and Sperm whale had the lowest. In the WGoM scenario, Sperm whale was the most vulnerable and Common bottlenose dolphin the least (Figure 4.6). For the Turtles C-ESI, the order of most to least vulnerable was conserved in all four scenarios and though the entire concentration range, although the magnitude of the difference in the RIP scores varied (Figure 4.7). Leatherback sea turtle was identified as the most potentially vulnerable turtle species and Loggerhead sea turtle was the least vulnerable turtle species in all four scenarios (Figure 4.7). The Fish Species C-ESI had the most variation in the vulnerability rankings of the species between oil well blowout scenarios (Figure 4.8). When the resource layers for deep-sea corals and larval fish were added to the species layers for the Fish, Mammals, Turtles, Larval Fish, Deep Sea Corals C-ESI, the rankings of these layers were well conserved with deep sea corals being more vulnerable than larval fish for all four scenarios, but larval fish also being more vulnerable than other species (Figure 4.9).

4.4 Discussion

The objective of this study was to demonstrate the potential use of C-ESIs created in Chapter 3 to identify potentially vulnerable offshore resources which may be impacted by

simulated oil well blowouts in various origin locations across the northern Gulf of Mexico (USA waters). I used the seven C-ESIs created in Chapter 3 to analyze potential impacts of four modeled hypothetical oil well blowouts. The methodology presented in this chapter includes: 1) the creation of maximum daily oil concentration (MOCT) polygons from modeled oil blowout scenarios, 2) the calculation of cumulative impact proportion (CIP) scores between C-ESIs and MOCT polygons and individual resource impact proportion (RIP) scores between resource components and MOCT polygons and 3) the subsequent use of these scores in ranking oil well blowout scenarios in terms of potential vulnerability of various biological resources, and 4) identifying individual resources (e.g., species and fisheries) that are potentially vulnerable to specific oil well blowout scenarios. This methodology is designed to be replicable for virtually any oil well blowout scenario (hypothetical or actual) and can use existing and other candidate C-ESIs and associated resource components.

This study was designed to provide methodology to answer three major questions. 1) Are there significant differences between oil well blowout scenarios in terms of total potential impacts to the resources represented by the suite of C-ESIs? 2) Given a specific oil spill scenario, which suite of resources represented by individual C-ESIs are potentially the most vulnerable? and 3) Given a specific oil spill scenario and C-ESI, which resource components are potentially the most vulnerable and contributing the most to the CIP score?

This study illustrates that CIP scores from a suite of C-ESIs can give an overall estimate of vulnerability risk of an oil well blowout scenario (Figure 4.3A). For example, the WFS scenario was identified as potentially having the most impact on the suite of included C-ESIs (Table 4.3, Figure 4.3A).

When looking at a specific scenario, as would be the case in the event of an actual oil well blowout, the ability to analyze potential impacts to resources at two additional levels of detail is especially useful. Comparing individual CIPs within an oil well blowout scenario will give a medium level of detail regarding which resources may be vulnerable during that blowout scenario and an estimate of the magnitude of that potential vulnerability. For example, the Fisheries C-ESI shows the most potential vulnerability to the DWH scenario over the other C-ESIs (Figure 4.3B). The CIP score of 0.24 for the Fisheries C-ESI in the DWH Scenario at the 400 MOCT (ppb) level represents 24% of the total value of the resources represented in the Fisheries C-ESI was potentially exposed to at least 400 MOCT (ppb) for at least one day (Table 4.3). Individual RIPs within the Fisheries C-ESI for the DWH scenario at 400 MOCT (ppb) represent the fractions of the resources potentially exposed to at least 400 MOCT (ppb) for at least one day (i.e., ~50% of highly migratory species and ~20% of white shrimp; Figure 4.4).

While this study provides methodology to determine what proportion of resources were potentially exposed to oil at different MOCTs, the potential impacts of those exposures will differ based on resource sensitivity. Early life stages of fishes are especially vulnerable to oil exposure with cardiac deformities in embryonic Bluefin tuna at PAH concentrations as low as 0.3 µg/L (Incardona et al. 2014). While similar cardiac and morphological effects on larvae are observed to be consistent among fish species, the oil concentration level and duration of the exposure differs between species (Incardona et al. 2014). Larvae of Bluefin tuna, Yellowfin tuna, and Greater amberjack all develop edema with exposure to oil, but the E_{50} for these species was observed at 0.8, 2.3, and 12.4 µg/L ΣPAHs respectively and the threshold for edema was 0.3–0.6 µg/L, 0.5–1.3 µg/L, and 1.0–6.0 µg/L ΣPAHs respectively (Incardona et al. 2014; Table 4.5). These species would likely have differing degrees of impacts to their populations following

an oil well blowout, even if both species had equal densities of larvae present. Adult fish species also exhibited sublethal impacts from oil exposure on swimming performance, causing reductions in critical and optimal swimming speeds (Stieglitz et al. 2016; Esbaugh et al. 2016; Table 4.5). Reduced swimming performance could likely lead to losses in adult populations for some species as swimming performance can be crucial for predatory success, predation avoidance, and migration to spawning sites. Impacts to marine mammals are less precisely quantified as designed experiments are prohibited, but observations on marine mammals after a spill serve as useful starting points for estimating exposure (Schwacke et al. 2014; Takeshita et al. 2021). Eleven species of marine mammals were observed swimming through petroleum waters after the DWH event and 157 reported marine mammal deaths were attributed to the DWH event (U.S. Fish and Wildlife Service 2011; Dias et al. 2017). These deaths are likely underreported due to historical carcass recovery percentage estimates (about 2%) (Williams et al. 2011). For other human-use resources, important MOCT concentrations might be at what concentration a resource is closed (e.g., a shrimp fishery).

Due to the differing degrees of impacts to various resources the results generated from this methodology are most beneficial when combined with relevant toxicity thresholds. For biological resources such as Bluefin tuna or Bottlenose dolphin, the MOCT polygon giving the best estimate of impacts may vary with species sensitivity to oil and even the season. For example, if estimating impacts to Bluefin tuna in the event of an oil spill, an MOCT of 50 ppb might be the most useful for a spill occurring in April (like DWH) since Bluefin tuna primarily spawn during April to May and their larvae begin to experience cardiological defects at 0.3 μg L–1 ΣPAH (Incardona et al. 2014). If an oil spill occurred in September, e.g., the Fall scenario, an MOCT of 250 ppb might be more insightful, since adult Bluefin tuna emigrate from the Gulf

following spawning and adult fish of most species display reduced swimming and aerobic capabilities at higher PAH concentrations (Stieglitz et al. 2016; Esbaugh et al. 2016; Table 4.5).

Future Inclusion for Changes in Duration of Exposure

PAH toxicity in fish species is dependent upon both concentration and duration of oil exposure. For this study, the MDOC (ppb) was calculated as the maximum oil concentration identified for at least one day for each 0.02°x0.02° latitude/longitude grid block. A different exposure duration could be easily included by changing the input data creating the MOCT polygons. Oil distribution point data can be produced where the maximum oil concentration column is no longer representative of the one-day maximum, but, for example, the maximum concentration that is sustained for at least five days or "oil days" as per Murawski et al. (2014).

Model Elaboration for the Depth Distributions of Oil Concentrations and Resources

The distributions of oil concentrations used in this study represent the oil at the surface (0-20m) from the oil well blowout scenarios, but additional oil is found throughout the water column both in actual oil well blowouts (e.g., DWH and IXTOC-1) and accounted for in the simulated oil spills as modeled with the CMS. Vulnerable offshore resources are also distributed throughout the water column (Sutton et al. 2020) and in the benthos (Schwing et al. 2021). To identify additional potential vulnerabilities to resources found within the water column and the benthos, additional analysis could be completed using the methodology described in this study but with oil concentration files created for different depth ranges within the water column and spatial distributions of resources at corresponding depths.

While the resource components included in this study are not limited to the surface (e.g., deep-sea coral, tilefish, sperm whale), this study estimated impacts to these resources based on the surface expression of oil distribution. While some oil in surface waters may indeed descend

into deeper water and accumulate in the benthos via Marine Oil Snow Sedimentation and Flocculent Accumulation (MOSSFA, Schwing et al. 2021), the addition of resource distributions present at depth, and oil concentrations at depth may provide more accurate predictions of potential impact to those resources.

Limitations of Polygons created using the Convex Hull Algorithm

This study used the *convex hull* command within the *GRASS* module to create MOCT polygons. This method creates a polygon by drawing a boundary which meets a pre-defined set of requirements (i.e., MOCT level) and then encloses all points within the linear segments of that boundary. This method will therefore enclose any "holes" or "ribbons" within the oil distribution where the grid cell does not meet the MOCT threshold but is enclosed or surrounded by grid cells that do meet the MOCT threshold (e.g., voids). Therefore, this method will potentially result in a larger estimate of the areas exposed to a MOCT than the CMS model alone. While this conservative method has the advantage of more accurately predicting exposure to species who may move through these grid cells and allowing a buffer for the CMS model estimates, alternate less-conservative methods could be employed to create MOCT polygons that more accurately fit the CMS surface area model.

4.5 Tables

Table 4.1 List of C-ESIs and contributing resource raster IDs from Table 4.2.

ESI ID	Name of ESI	Raster ID numbers included in calculation
1	Mammals	18-23
2	Turtles	14-17
3	Fish Species – Unweighted	1-13
4	Fish Species – Weighted (Weight = 4)	1-13 with weights
5	Species Richness	24-26
6	Commercial Fisheries	27-31
7	Mammals, Turtles, Fish, Larval Abundance, Deep-sea Coral habitat	1-23, 32, 33

Table 4.2 List of Raster files with resolution level and ID number.

Type	Raster Layer	Resolution	ID Number
Fish	Warmingii's lanternfish	0.5 degree	1
Fish	Atlantic sailfish	0.5 degree	2
Fish	Atlantic bluefin tuna	0.5 degree	3
Fish	Atlantic blue marlin	0.5 degree	4
Fish	Common dolphinfish	0.5 degree	5
Fish	Greater amberjack	0.5 degree	6
Fish	King mackerel	0.5 degree	7
Fish	Red drum	0.5 degree	8
Fish	Red grouper	0.5 degree	9
Fish	Red snapper	0.5 degree	10
Fish	Striped mullet	0.5 degree	11
Fish	Atlantic swordfish	0.5 degree	12
Fish	Great northern tilefish	0.5 degree	13
Turtle	Kemp's Ridley	0.5 degree	14
Turtle	Hawksbill	0.5 degree	15
Turtle	Loggerhead	0.5 degree	16
Turtle	Leatherback	0.5 degree	17
Mammal	Bottlenose dolphin	0.5 degree	18
Mammal	Pantropical spotted dolphin	0.5 degree	19
Mammal	Atlantic spotted dolphin	0.5 degree	20
Mammal	Sperm whale	0.5 degree	21
Mammal	Pygmy killer whale	0.5 degree	22
Mammal	False killer whale	0.5 degree	23
Species Richness	Bony Fishes	0.5 degree	24
Species Richness	Elasmobranchs	0.5 degree	25
Species Richness	Mammals	0.5 degree	26
Economic Fishery	Coastal Species	1 degree	27
Economic Fishery	Highly Migratory Species	1 degree	28
Economic Fishery	Brown shrimp	1 degree	29
Economic Fishery	White shrimp	1 degree	30
Economic Fishery	Pink shrimp	1 degree	31
Larval Fish	Larval fish presence	0.5 degree	32
Benthic	Deep-sea coral presence	0.5 degree	33

Table 4.3 Cumulative Impact Proportion (CIP) Scores by C-ESI (columns) within each oil well blowout scenario at MOCT level (oil ppb). C-ESIs are color ranked by value within each row.

Scenario	oil ppb	Fisheries	FishWeighted	FishUnweighted	SpeciesRichness	Mammals	Turtles	Species,Larval,Coral
WFS	1	0.8545	0.5982	0.5839	0.6291	0.6650	0.5380	0.6074
WFS	5	0.6057	0.4748	0.4631	0.4970	0.5320	0.4133	0.4770
WFS	10	0.5726	0.4505	0.4390	0.4678	0.4987	0.3935	0.4509
WFS	25	0.5507	0.4152	0.4036	0.4333	0.4670	0.3585	0.4169
WFS	50	0.4539	0.3749	0.3631	0.3844	0.4163	0.3240	0.3741
WFS	100	0.4488	0.3531	0.3382	0.3658	0.4023	0.2985	0.3525
WFS	150	0.4430	0.3421	0.3274	0.3541	0.3908	0.2888	0.3418
WFS	200	0.4176	0.3305	0.3165	0.3433	0.3848	0.2770	0.3322
WFS	400	0.0790	0.1147	0.1068	0.1352	0.1510	0.0808	0.1172
WFS	800	0.0255	0.0351	0.0318	0.0443	0.0470	0.0235	0.0356
WFS	1500	0.0022	0.0043	0.0034	0.0060	0.0073	0.0010	0.0043
WFS	2000	0.0017	0.0039	0.0035	0.0052	0.0054	0.0022	0.0039
DWH	1	0.8545	0.5635	0.5557	0.5766	0.6103	0.5218	0.5746
DWH	5	0.8242	0.5134	0.5063	0.5124	0.5400	0.4790	0.5185
DWH	10	0.7322	0.3850	0.3719	0.3897	0.4295	0.3428	0.3903
DWH	25	0.4647	0.3210	0.3092	0.3381	0.3927	0.2653	0.3295
DWH	50	0.4396	0.2851	0.2746	0.3072	0.3635	0.2303	0.2955
DWH	100	0.2537	0.2185	0.2060	0.2575	0.3220	0.1500	0.2316
DWH	150	0.2535	0.1913	0.1797	0.2293	0.2857	0.1280	0.2039
DWH	200	0.2343	0.1494	0.1411	0.1829	0.2263	0.1030	0.1618
DWH	400	0.2144	0.1168	0.1111	0.1437	0.1788	0.0805	0.1281
DWH	800	0.0783	0.0540	0.0513	0.0715	0.0895	0.0383	0.0619
DWH	1500	0.0514	0.0124	0.0123	0.0164	0.0195	0.0125	0.0150
DWH	2000	0.0053	0.0045	0.0050	0.0048	0.0030	0.0060	0.0049
WGOM	1	0.4218	0.2711	0.2623	0.3172	0.3095	0.2405	0.2807
WGOM	5	0.3385	0.2289	0.2179	0.2633	0.2628	0.2023	0.2362
WGOM	10	0.3385	0.2030	0.1930	0.2342	0.2408	0.1770	0.2125
WGOM	25	0.2717	0.1739	0.1638	0.2047	0.2225	0.1425	0.1849
WGOM	50	0.2463	0.1543	0.1449	0.1826	0.1952	0.1278	0.1635
WGOM	100	0.1334	0.0965	0.0881	0.1323	0.1445	0.0703	0.1070
WGOM	150	0.1334	0.0918	0.0839	0.1239	0.1355	0.0678	0.1015
WGOM	200	0.1150	0.0870	0.0793	0.1165	0.1285	0.0635	0.0955
WGOM	400	0.0935	0.0743	0.0671	0.0970	0.1123	0.0508	0.0819
WGOM	800	0.0362	0.0312	0.0273	0.0500	0.0642	0.0130	0.0385
WGOM	1500	0.0053	0.0029	0.0026	0.0065	0.0073	0.0010	0.0045
WGOM	2000	0.0049	0.0028	0.0025	0.0057	0.0068	0.0010	0.0042
Fall	1	0.8216	0.7273	0.7103	0.8109	0.7938	0.6645	0.7313
Fall	5	0.7711	0.6074	0.5787	0.6797	0.7218	0.5080	0.6155
Fall	10	0.5943	0.4873	0.4590	0.5651	0.6443	0.3725	0.5025
Fall	25	0.3418	0.2378	0.2285	0.2777	0.3352	0.1735	0.2552
Fall	50	0.3032	0.1970	0.1897	0.2274	0.2735	0.1445	0.2103
Fall	100	0.2986	0.1623	0.1568	0.1866	0.2188	0.1288	0.1743
Fall	150	0.2956	0.1543	0.1490	0.1779	0.2085	0.1240	0.1661
Fall	200	0.2007	0.1132	0.1108	0.1316	0.1490	0.0960	0.1228
Fall	400	0.1383	0.0542	0.0552	0.0646	0.0755	0.0508	0.0621
Fall	800	0.0455	0.0119	0.0131	0.0150	0.0137	0.0160	0.0143
Fall	1500	0.0006	0.0001	0.0001	0.0001	0.0001	0.0002	0.0001
Fall	2000	0.0000	0.0000	0.0000	0.0000	0.0000	0.0000	0.0000

Table 4.4 Summary statistics of CIP by oil well blowout scenarios (A) and C-ESI (B)

A

Oil Scenario	mean	min	25%	50%	75%	max
DWH	0.26	0.00	0.09	0.23	0.39	0.85
Fall	0.25	0.00	0.05	0.17	0.35	0.82
WFS	0.30	0.00	0.07	0.35	0.45	0.85
WGoM	0.13	0.00	0.06	0.12	0.20	0.42

B

Cumulative ESI Name	mean	min	25%	50%	75%	max
Fish, Turtles, Mammals, Larval Fish, Coral	0.22	0.00	0.06	0.18	0.34	0.73
Fish Species - Unweighted	0.21	0.00	0.05	0.16	0.33	0.71
Fish Species - Weighted	0.22	0.00	0.05	0.17	0.34	0.73
Fisheries	0.31	0.00	0.08	0.26	0.45	0.85
Mammals	0.26	0.00	0.09	0.22	0.40	0.79
Species Richness	0.24	0.00	0.07	0.20	0.36	0.81
Turtles	0.18	0.00	0.05	0.13	0.29	0.66

Table 4.5 Published PAH µg L–1 ΣPAH toxicity thresholds converted to estimated MOCT ppb by use of three methods: two linear regression equations published in Berenshtein et al. 2020a., and a 1.5% estimator. Rows highlighted in yellow and bolded are graphed as vertical lines on Figures 4.4-4.8.

Toxicity threshold description	PAH µg L–1 ΣPAH	>1 m MDOC ppb	Surface MDOC ppb	PAH ~1.5% of TPH	Source of threshold
begin threshold edema bluefin tuna larvae	0.3	46.94	69.43	20.00	Incardona et al. 2014
larval fish toxicity at surface	**0.5**	**53.16**	**80.34**	**33.33**	**NRDAT**
E50 Edema in Bluefin tuna larvae	0.8	62.27	96.74	53.33	Incardona et al. 2014
larval fish toxicity deeper	**1.0**	**68.22**	**107.68**	**66.67**	**NRDAT**
Mahi-mahi larvae - reduced swim -37%	1.2	74.08	118.62	80.00	Mager et al. 2014
E50 Edema in Yellowfin tuna larvae	2.3	105.08	178.95	153.33	Incardona et al. 2014
Adult red drum - reduced swim -12.6%	4.1	152.75	277.95	273.33	Johansen and Esbaugh. 2017
I50 bradycardia Yellowfin tuna larvae	6.1	202.86	388.24	406.67	Incardona et al. 2014
I50 bradycardia Bluefin tuna larvae	7.7	241.42	476.63	513.33	Incardona et al. 2014
Adult mahi-mahi - reduced reduced swim -14%	8.4	257.96	515.34	560.00	Stieglitz et al. 2016
96 h LC50 Mahi-mahi larvae (surface slick)	8.8	267.32	537.47	586.67	Esbaugh et al. 2016
Conversion for vertical line on graph at 10 PAH	**10.0**	**295.09**	**603.90**	**666.67**	
Adult red drum - reduced aerobic scope -18.4%	12.1	342.65	720.26	806.67	Johansen and Esbaugh. 2017
E50 Edema in amberjack larve	12.4	349.35	736.89	826.67	Incardona et al. 2014
I50 bradycardia amberjack larvae	18.2	475.07	1058.95	1213.33	Incardona et al. 2014
Juvenile mahi-mahi - reduced swim -22%	30.0	715.24	1716.12	2000.00	Mager et al. 2014
96 h LC50 Mahi-mahi larvae (wellhead)	45.8	1016.59	2598.79	3053.33	Esbaugh et al. 2016

4.6 Figures

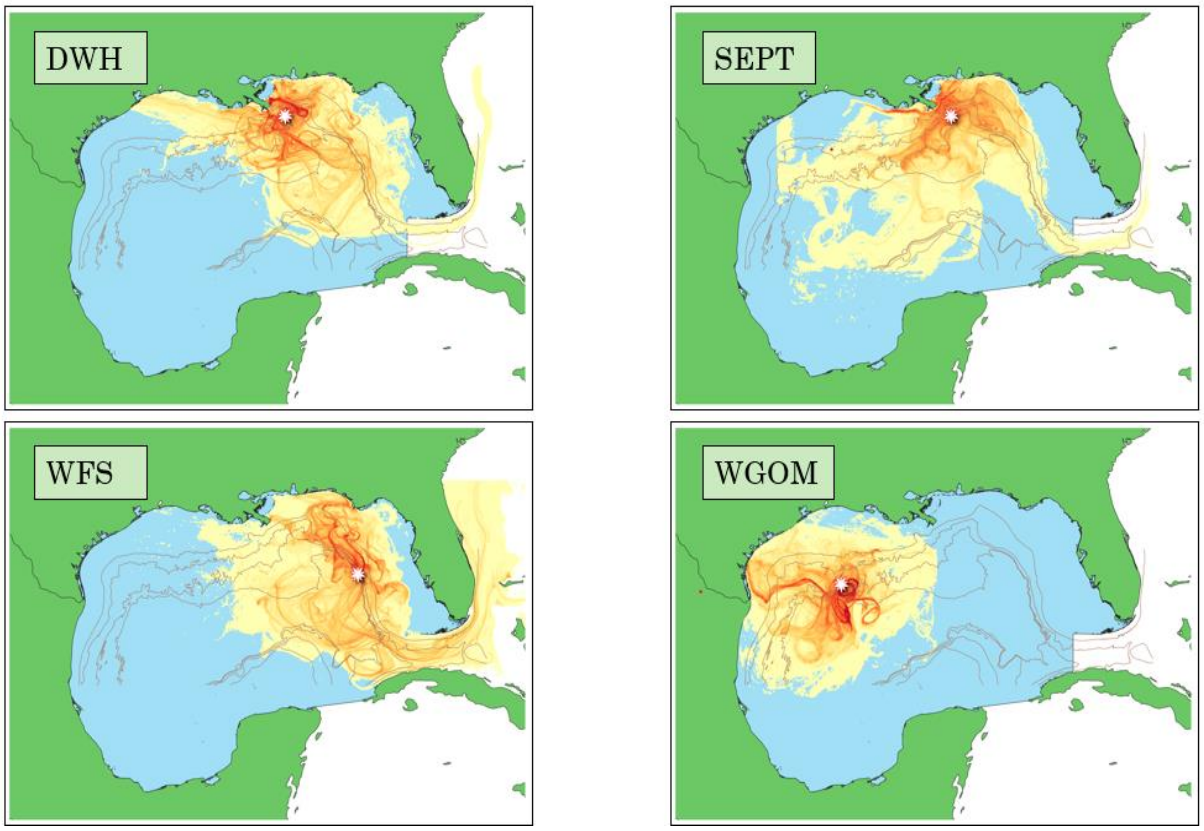

Figure 4.1 Surface distribution of the maximum daily oil concentration (ppb) for four oil well blowout scenarios visualized in QGIS.
DWH = Deepwater Horizon; SEPT = DWH occurring in September; WFS = West Florida Slope, WGoM = Western Gulf of Mexico. Origin of oil well blowout marked with white star

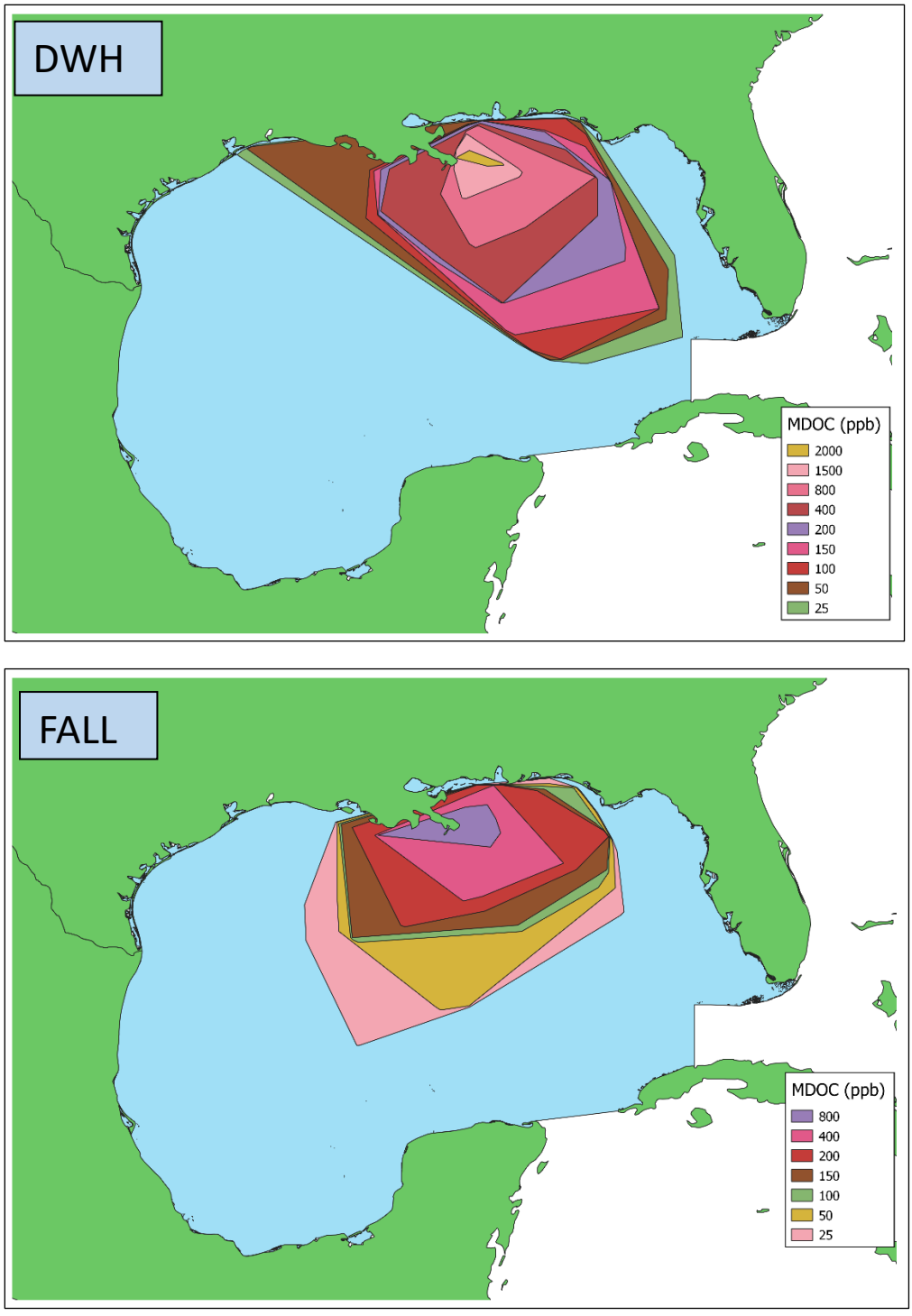

Figure 4.2A Convex hull minimum oil concentration threshold (MOCT) polygons created from the maximum daily oil concentration (MDOC) for DWH and FALL oil spill scenarios.
DWH = Deepwater Horizon; FALL = DWH occurring in September

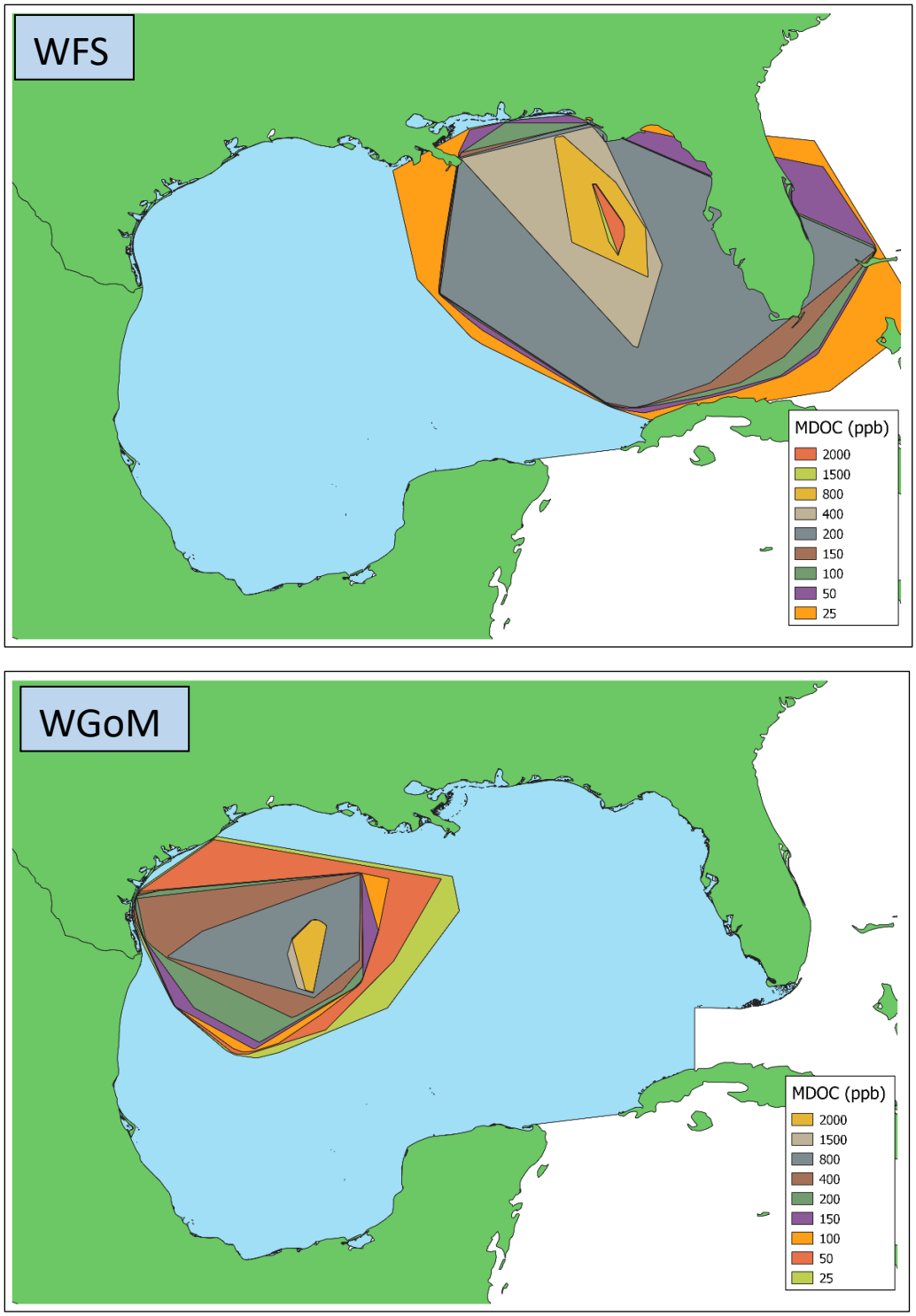

Figure 4.2B Convex hull minimum oil concentration threshold (MOCT) polygons created from the maximum daily oil concentration (MDOC) for WFS and WGoM spill scenarios.
WFS = West Florida Slope, WGoM = Western Gulf of Mexico.

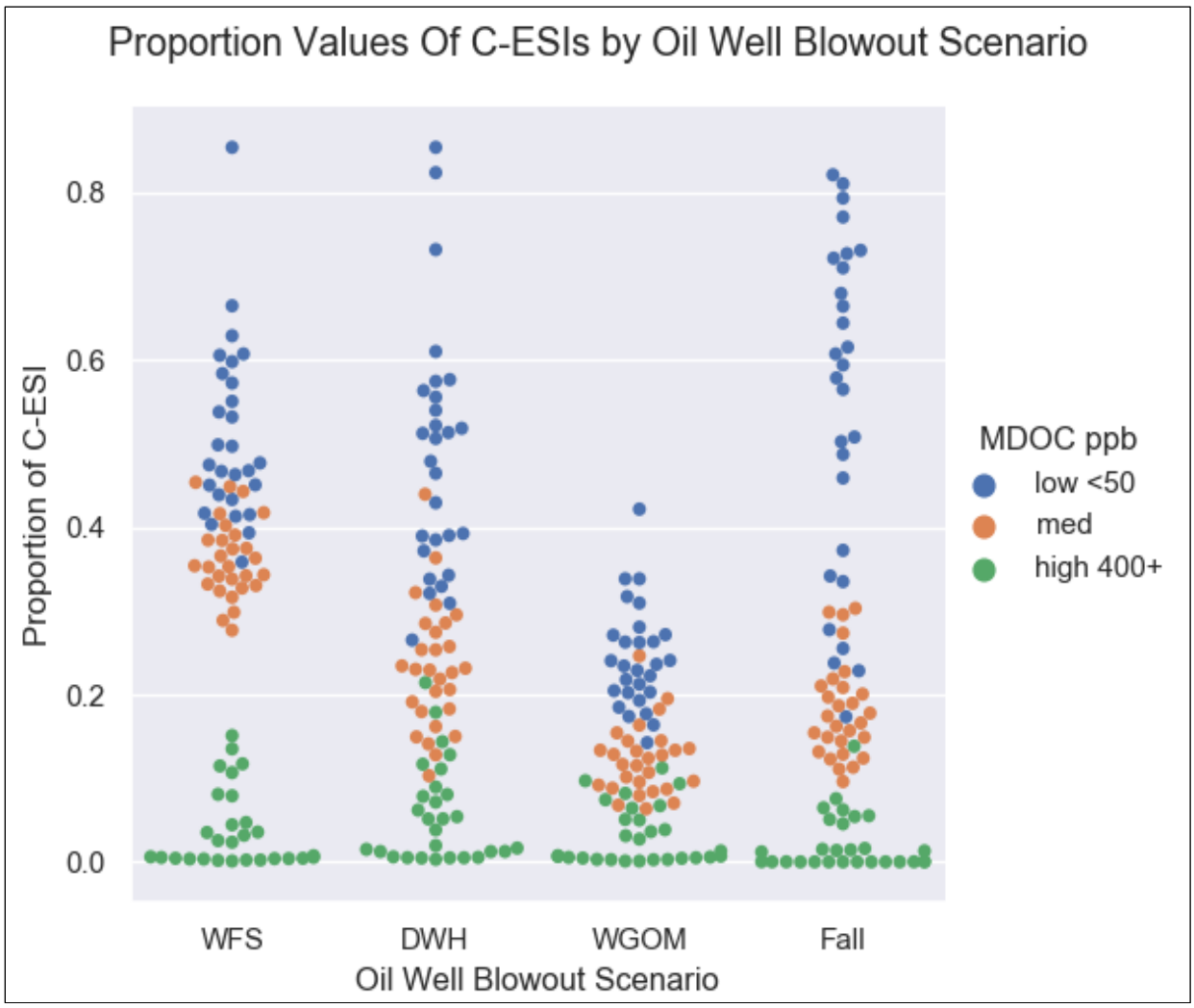

Figure 4.3A Comparison of CIP scores by oil well blowout scenario and MOCT level
Swarm plot of proportion of C-ESI (i.e., CIP) by oil well blowout scenario and MOCT level. WFS has highest CIP scores within the mid MOCT levels, while WGoM has the least.

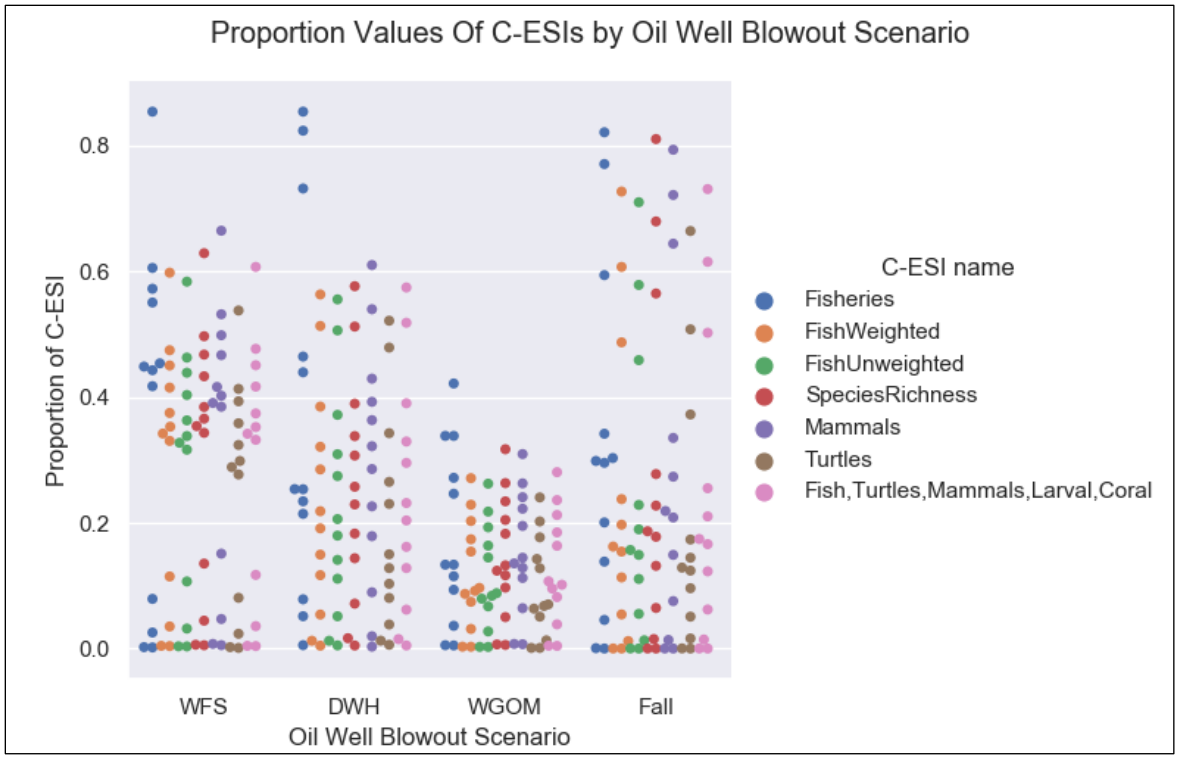

Figure 4.3B Comparison of CIP scores by oil well blowout scenario and C-ESI.
Swarm plot of proportion of C-ESI (i.e., CIP) by oil well blowout scenario and C-ESI. This graph is used to identify which C-ESI within each oil well blowout has the highest CIP values (e.g., The Fisheries C-ESI has the highest CIP values within the DWH scenario).

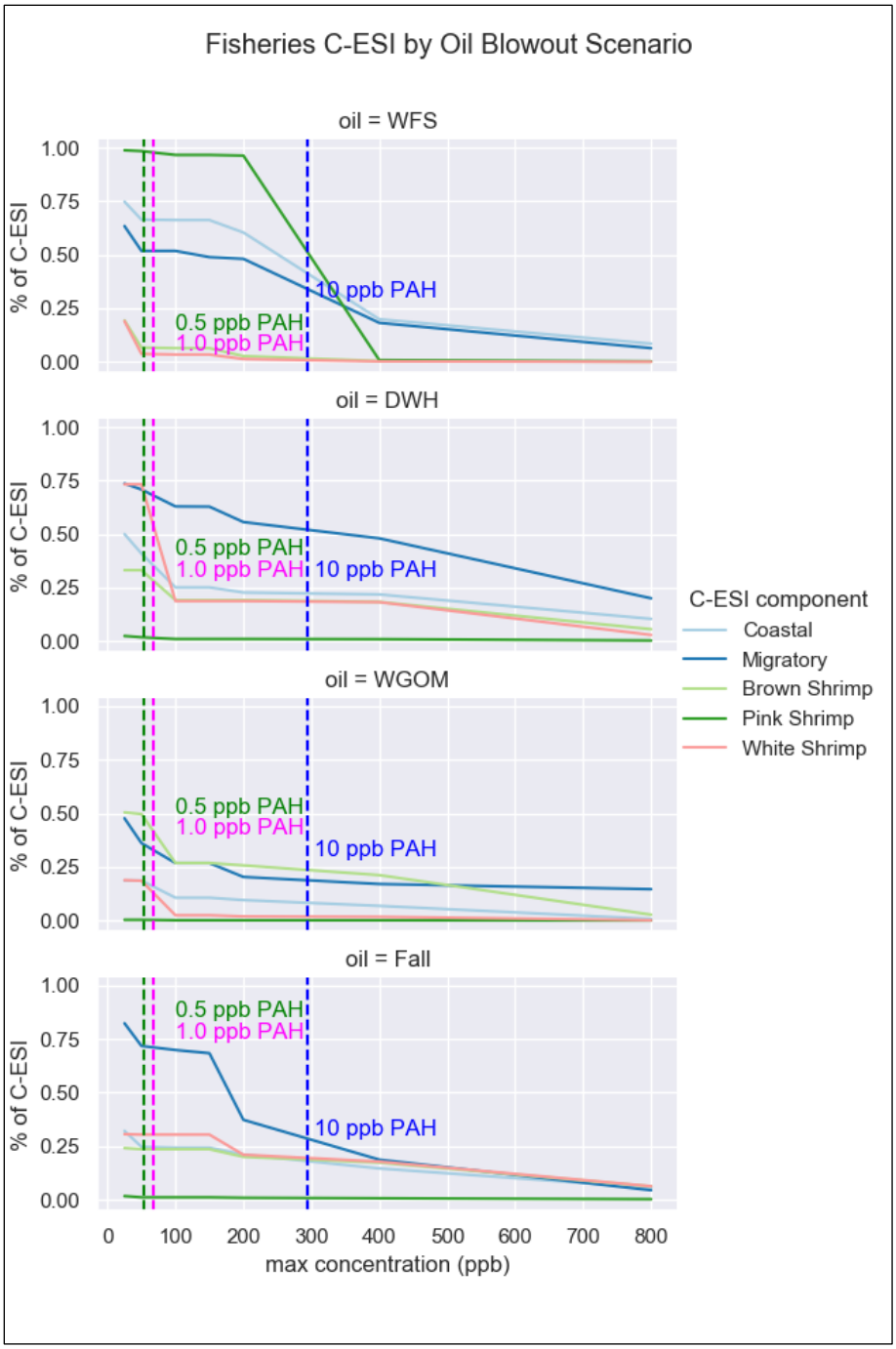

Figure 4.4 Fisheries C-ESI: Comparison of oil spill scenarios
Resource Impact Proportion (RIP) scores (y-axis) within each MOCT polygon (x-axis) by oil well blowout scenario. RIP score equals the proportion of the resource component value within the MOCT polygon, and therefore potentially exposed to at least that MOCT value.

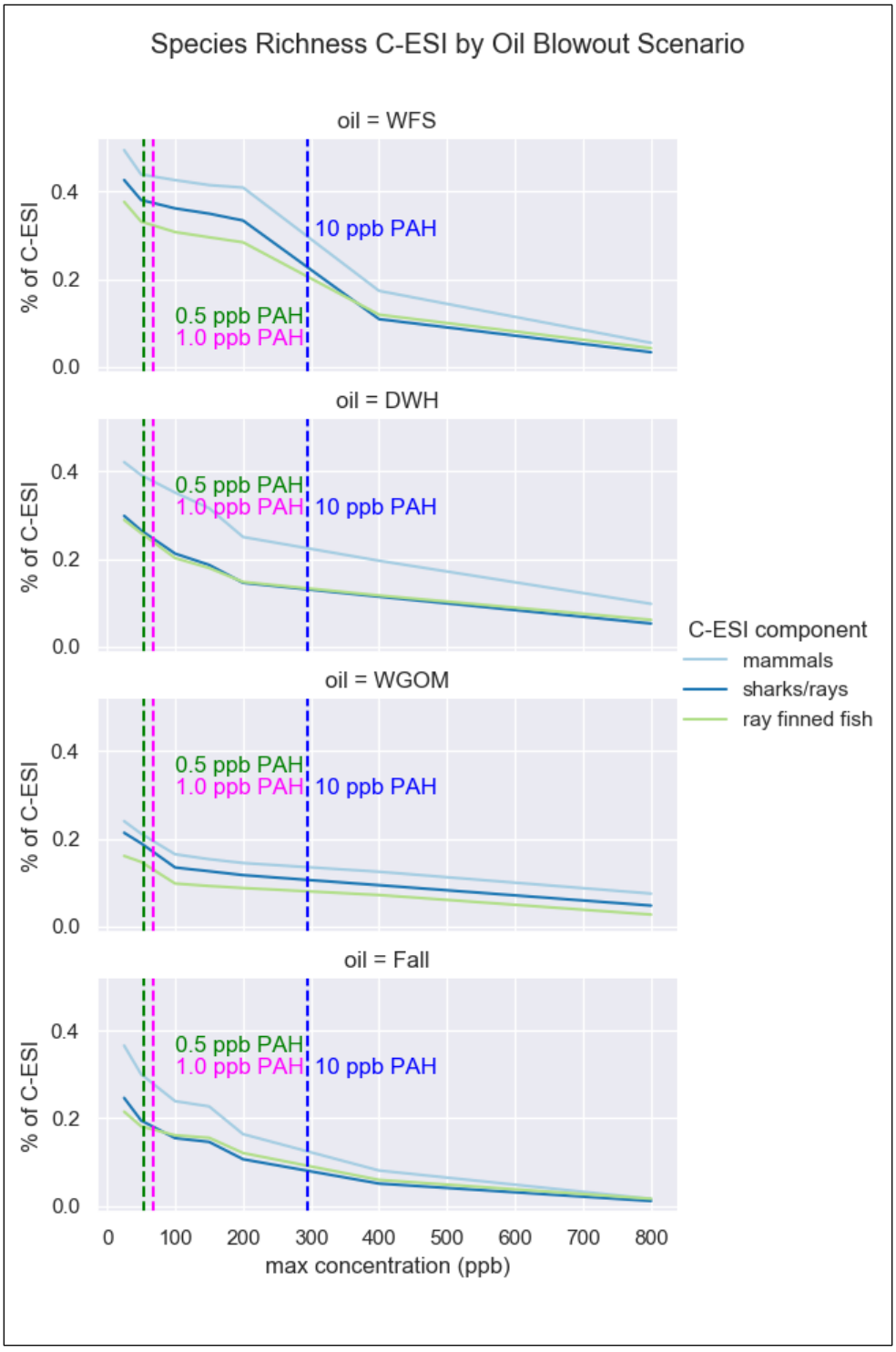

Figure 4.5 Species Richness C-ESI: Comparison of oil spill scenarios
Resource Impact Proportion (RIP) scores (y-axis) within each MOCT polygon (x-axis) by oil well blowout scenario. RIP score equals the proportion of the resource component value within the MOCT polygon, and therefore potentially exposed to at least that MOCT value.

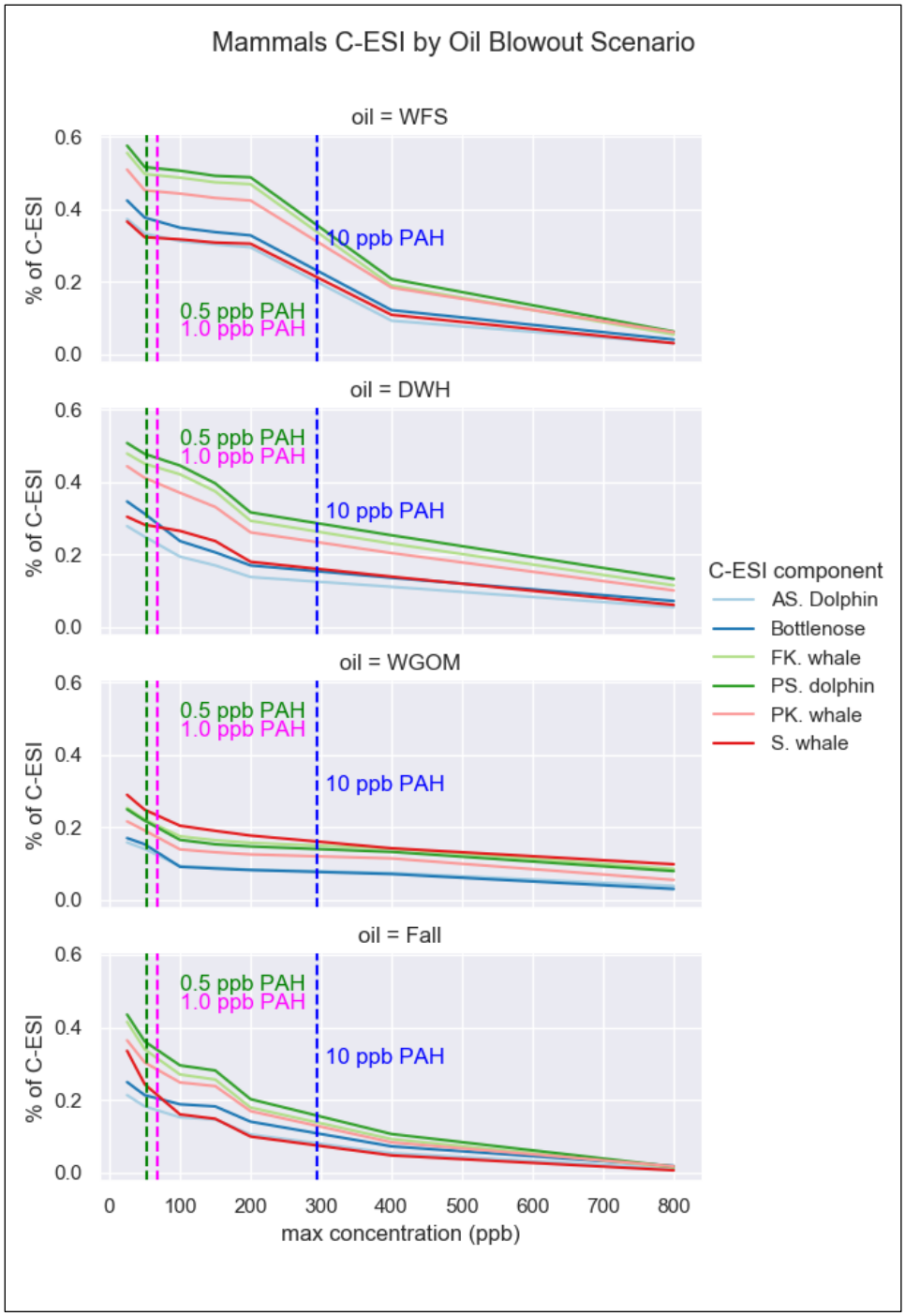

Figure 4.6 Mammals C-ESI: Comparison of oil spill scenarios
Resource Impact Proportion (RIP) scores (y-axis) within each MOCT polygon (x-axis) by oil well blowout scenario. RIP score equals the proportion of the resource component value within the MOCT polygon, and therefore potentially exposed to at least that MOCT value.

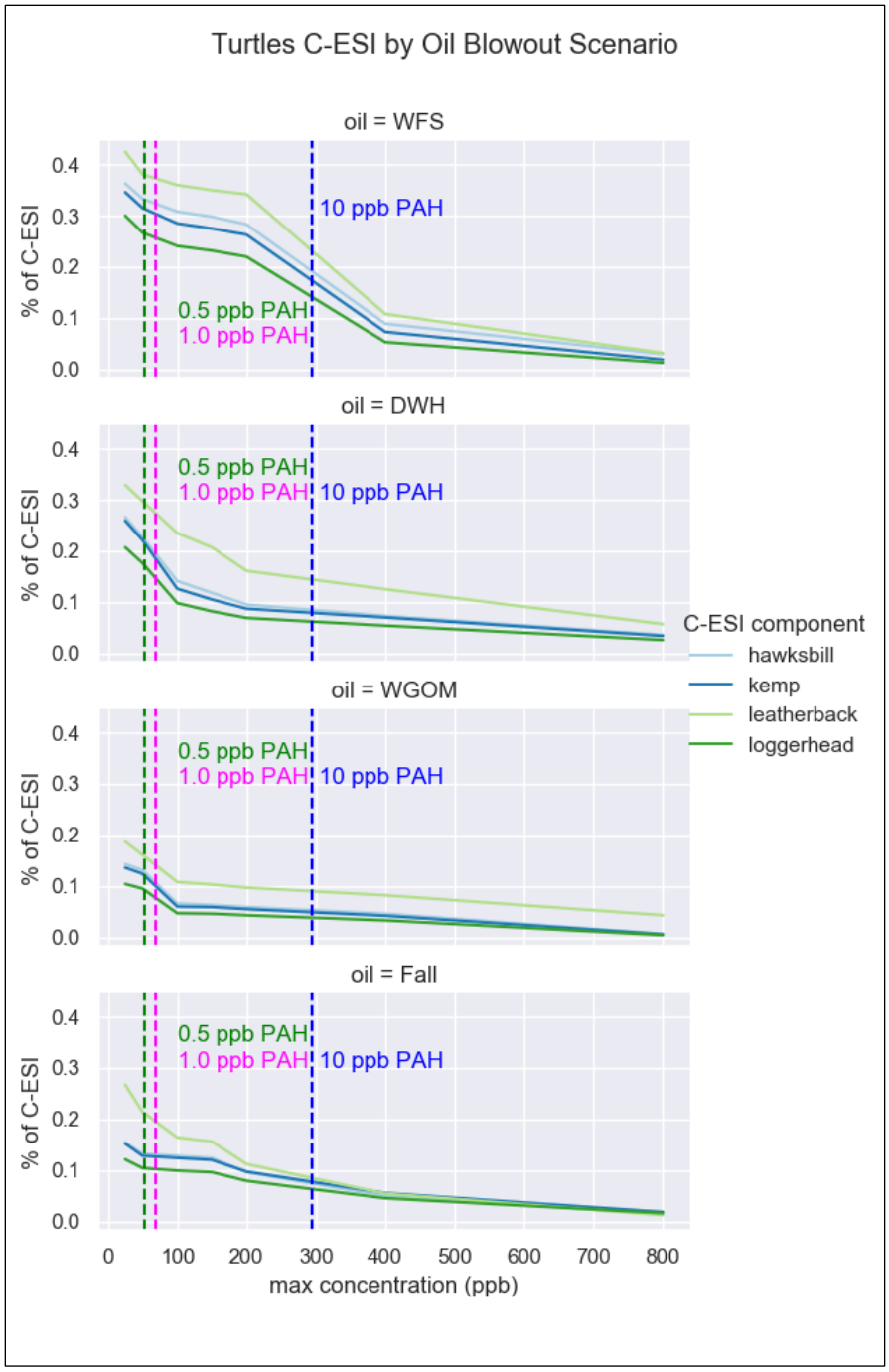

Figure 4.7 Turtles C-ESI: Comparison of oil spill scenarios
Resource Impact Proportion (RIP) scores (y-axis) within each MOCT polygon (x-axis) by oil well blowout scenario. RIP score equals the proportion of the resource component value within the MOCT polygon, and therefore potentially exposed to at least that MOCT value.

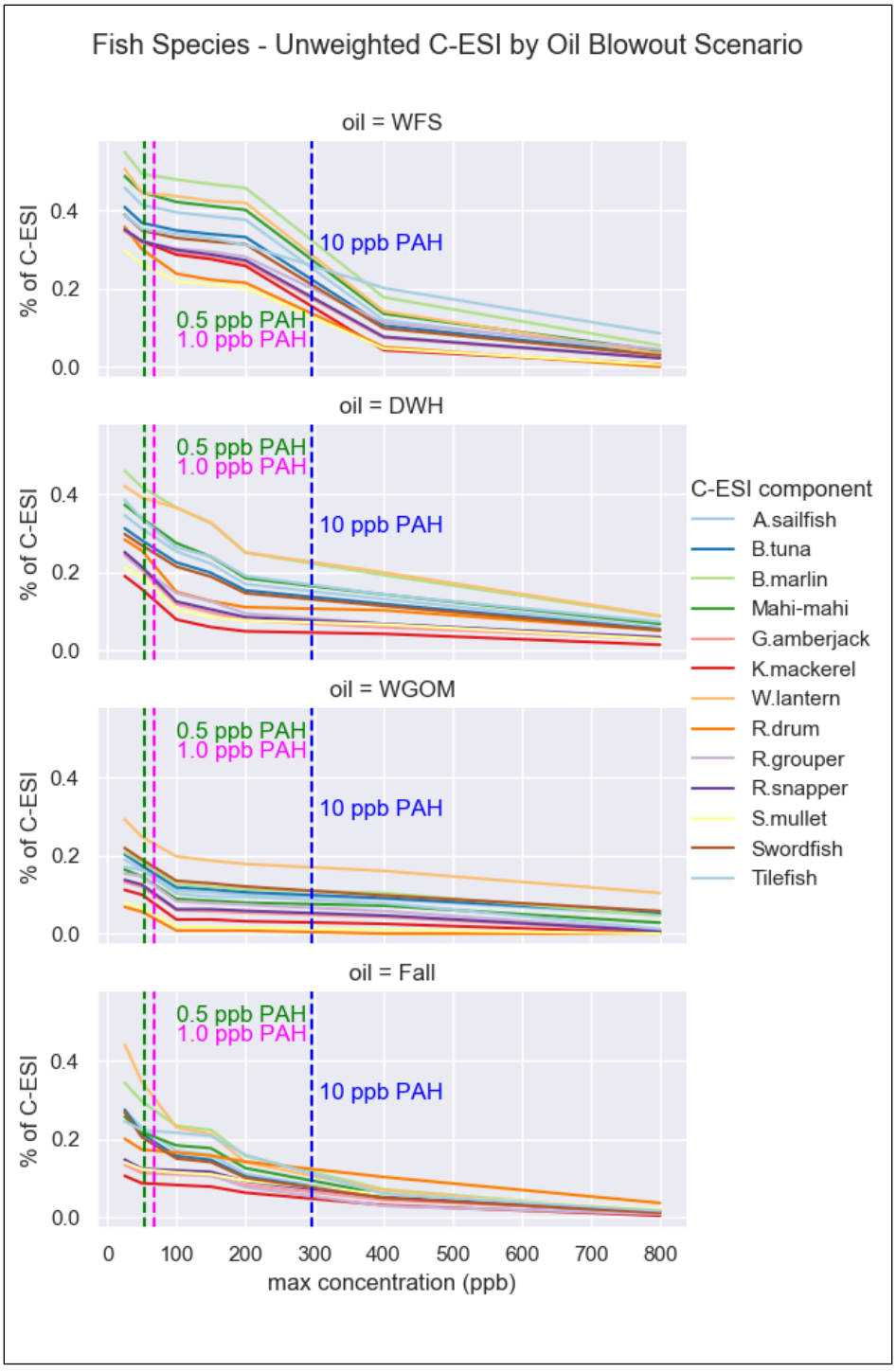

Figure 4.8 Fish Species C-ESI: Comparison of oil spill scenarios
Resource Impact Proportion (RIP) scores (y-axis) within each MOCT polygon (x-axis) by oil well blowout scenario. RIP score equals the proportion of the resource component value within the MOCT polygon, and therefore potentially exposed to at least that MOCT value.

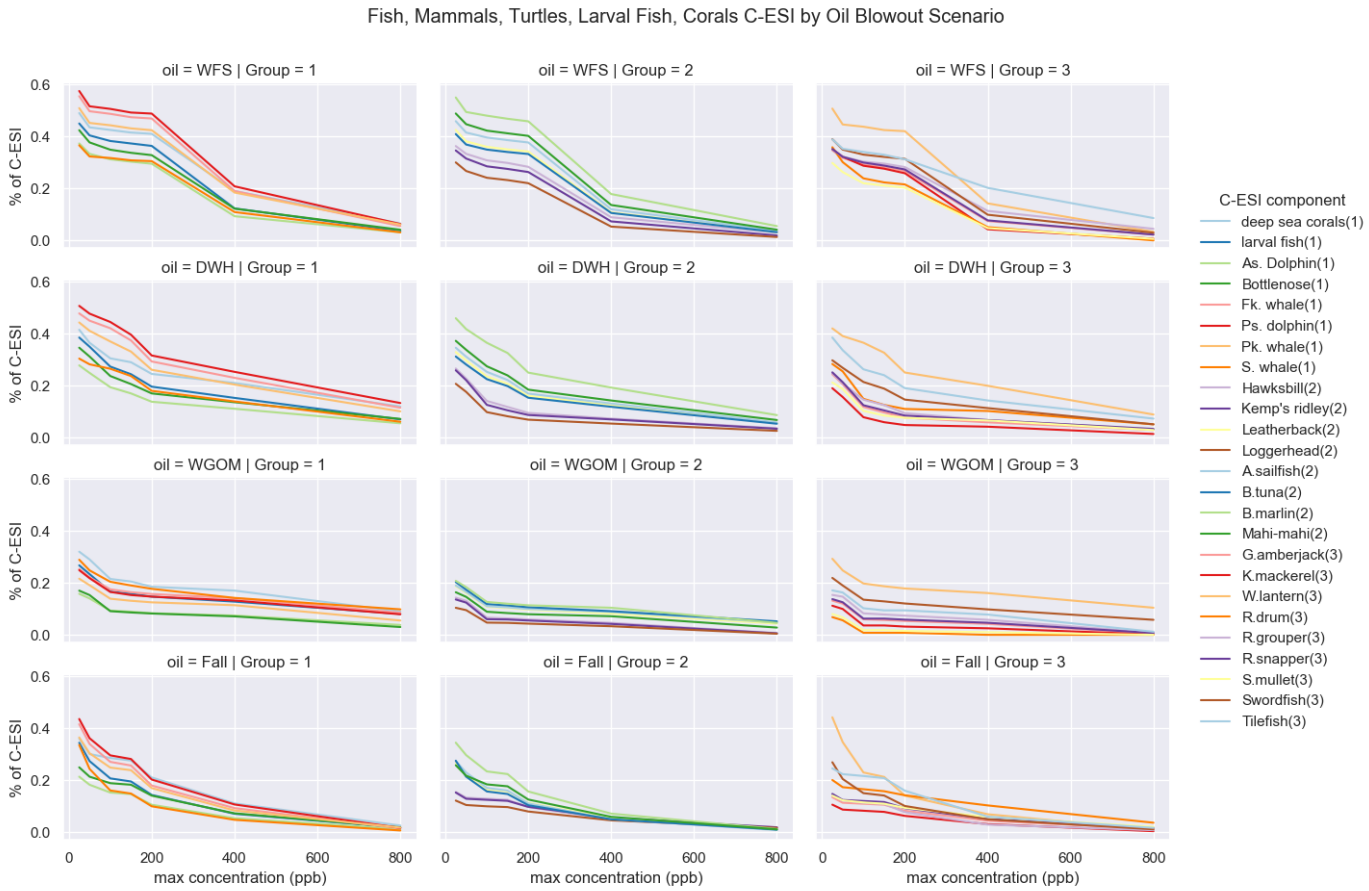

Figure 4.9 Fish, Mammals, Turtles, Larval Fish, Deep Sea Corals C-ESI: Comparison of oil spill scenarios
Resource Impact Proportion (RIP) scores (y-axis) within each MOCT polygon (x-axis) by oil well blowout scenario. RIP score equals the proportion of the resource component value within the MOCT polygon, and therefore potentially exposed to at least that MOCT value.

Chapter 5: Connecting Networks of Vulnerability "Hot-Spots" of Resources to Oil Spills with C-ESIs and the MARXAN Spatial Planning Solver

5.1 Introduction

Chapters 3 and 4 of this study combined spatial distributions of offshore living resources into Cumulative Environmental Sensitivity Indices (C-ESIs) and demonstrated the potential use of these C-ESIs to identify "hot-spots" within the GoM which could be susceptible to specific oil well blowout scenarios. This chapter demonstrates how C-ESIs developed in Chapter 3 might be used to identify regions for siting of oil production facilities by maximizing benefits to oil production while conserving vulnerable ecological resources. This study develops explicit tradeoff functions between oil production and spatial exclusion owing to the resources included in the C-ESIs. The utility of the tradeoff functions is demonstrated by using marine spatial planning (MSP) software, Marxan (Ball et al. 2009), to identify contiguous networks of ecological "hot-spots" with and without the inclusion of current oil production placement. "Hot-spot" networks identified without the inclusion of oil production represent the most ecologically important areas in a system in which no oil production occurs while "hot-spot" networks identified incorporating the tradeoff functions represent the most ecological areas to conserve given current oil production placement. The efficacy of the current Congressional Moratorium on oil/gas/mineral leasing off the gulf coast of Florida is then evaluated by calculating the proportion of the C-ESIs and Marxan "hot-spot" networks within the spatial boundaries of the

current Congressional Moratorium (Figure 5.1; Geospatial Services Division, Department of Interior - Bureau of Ocean Energy Management - Office of Strategic Resources, 2021).

Marine areas often have multiple sectors with demands for spatial allocation. These sectors may have mutually exclusive demands (cannot occur in the same place) or allow some degree of cooperation (can occur in the same place). Ecosystem based MSP aims to maximize the combined benefit from the ecosystem to all sectors. The MSP approach was mandated for marine resource management in the U.S. via executive order in 2005 (McLeod et al. 2005). Quantifying trade-offs between sectors requires an optimization approach often modeled as a Pareto horizon trade off analysis (White et al. 2012; Khiali-Miab et al. 2022). An example framework was demonstrated in White et al. 2012 via use of the proposed Cape Wind project and a set of three competing industries in this Nantucket area (Executive Office of Energy and Environmental Affairs (EEA) 2009). The sectors included in spatial planning for Cape Wind were the offshore wind development industry, and three competing sectors: the winter flounder fishery, the American lobster fishery, and the whale watching and conservation sector. White et al. (2012) compared the total ecosystem benefit of several wind energy siting plans created by single-sector management strategies (siting based solely on the value to one sector) and multi-sector management strategies (maximizing the benefit to all sectors). Sector tradeoffs were evaluated by plotting benefit values from sector A against benefit values for sector B such that each (X, Y) point represents a different theoretical management strategy that allocates X% of the area to sector A and Y% of the area to sector B. In their example in White et al. (2012), the wind energy sector and the flounder fishery sector were mutually exclusive, in that the industries could not occur in the same area, and both industries directly competed for the same grid cells. A development of the wind energy sector to its full capacity within a specified area would

necessarily require the flounder industry to be zero within the area occupied by the wind turbines and related buffer zones. This severe relationship is represented as the negatively sloped line by the tradeoff curve in Figure 5.2 (reproduced from White et al. 2012). The relationship between the wind energy sector and the lobster fishery sector as well as between the wind energy sector and the whale watching sector were less severe as these industries did not compete directly for the same habitat and thus could co-occur to a limited extent (Figure 5.2; White et al. 2012). Comparing a wind-siting plan developed by a single-sector management strategy with a plan developed by a multi-sector management strategy demonstrated the potential added value to the entire four sector system by incorporating a multi-sector planning approach (White et al. 2012).

This study uses a procedure similar to that employed in White et al. (2012) to parameterize pairwise tradeoffs between current oil production locations in the northern (USA) sector of the GoM and three C-ESIs created in Chapter 3 (i.e., Fisheries C-ESI, Mammals only C-ESI, and the Mammals, Fish, Turtles, Larvae, Coral (MFTLC) combined C-ESI.

The marine oil and gas industry in the GoM produces about 1.2 billion barrels of oil annually with oil production moving into deeper waters to meet demand (Murawski et al. 2020). Leases for oil drilling are sold by the U.S. Department of the Interior (DOI). The Bureau of Ocean Energy Management (BOEM) within the DOI produces and utilizes environmental impact assessment as part of their decision-making process on which areas to make available to oil drilling. Oil and natural gas leasing on new lands is highly contested. In January 2021, President Biden signed an executive order blocking all new oil and gas drilling, but a subsequent judgment in March 2021 negated this pause on an existing sale for 80 million acres in the Gulf of Mexico proposed in 2017 (Nilsen 2021). This ruling was reversed in January 2022 citing that the DOI's analysis of the climate impacts of the leases was incomplete (Nilsen 2022). The west

Florida shelf is also a major area of contention and has historically been included in potential plans for drilling (DOI 2018). The west Florida shelf is currently under a Congressional moratorium until 2032 via executive order issued by President Trump (Schwartz 2020; Figure 5.1).

While current oil production is not mutually exclusive with the existence of the resources represented in the C-ESIs, these resources are particularly at risk in the event of an oil well blowout (as detailed in Chapter 4) and so for the tradeoff curves created in this study, each 0.5°x0.5° latitude/longitude resolution grid cell will be allocated exclusively to either oil production or conservation of C-ESI resources. The importance of each grid cell varies by sector, with some grid cells being particularly important to oil production or particularly sensitive in the C-ESI (such as in the pink shrimp fishery where 60% of the value of the fishery is located within one grid cell). Like the wind energy/lobster fishery comparison (White et al. 2012), the tradeoff plots are generated with: (1) the oil production siting based on a single-sector approach (developing the highest producing sites first) and a multi-sector approach (including the net benefit to the C-ESI in the ranking of sites to develop). These tradeoff curves can identify sites that should potentially be reserved from oil production because they offer minimum benefit to the oil production sector and are identified by the C-ESI as being particularly sensitive. Importantly, not all the available locations within the spatial domain of the study are currently producing or have produced oil (more yet to be explored). However, quantifying the likely oil reserves is in unexplored lease blocks is highly speculative and is perhaps the topic for future research. Thus, in this example I used existing production data for the GoM.

"Hot-spot" areas in conservation are characterized as areas with high concentrations of endemic species and face threats of destruction (Myers. 1988, Myers. 1990). Identification and

protection of these “hot-spot” areas allows conservationists to focus their efforts on protecting areas which will provide the greatest pay-off (Myers. 1990). This study looks at identifying a minimum-set “hot-spot” network for two of the C-ESIs in both 1.) a pristine environment with no current oil production but where siting for oil production is being planned and 2.) the current oil production environment. These “hot-spot” networks are created through use of the Marxan spatial planning solver (Ball et al. 2009). Marxan is an optimization solver which can identify reasonably optimal network solutions to spatial network “knapsack” or “minimum-set” problems (Ball et al. 2009).

Linear multiple-choice knapsack problems (Kozanidis 2009) have been used for bi-objective decision-making problems looking to place multiple locations within an overall network. Knapsack problems aim to find an optimized solution of a set of elements to be included to maximize benefit while subject to a series of constraints. An example, and the origin of the name, is given by a hiker deciding what to pack in his knapsack to maximize comfort (benefit) while staying under a critical total weight for the bag (a constraint). In knapsack problems, each element is given cost and benefit values, and components are added until a constraint is met (Salkin and de Kluyver 1975; Martello and Toth 1990). Knapsack problems have been used by civil planning organizations to find optimized solutions to project selection when total budget and/or time are constrained (Brill 1979; Curtis and Molnar 1997; Ferreira 1997; Guikema and Milke 2003).

The “minimum-set problem” in conservation planning refers to finding a spatial planning solution with the least cost (e.g., area within no extraction zones, or cost to procure or manage a site) while meeting set conservation targets. In these types of problems, the region is divided into sites, and each site is associated with a cost of inclusion. The most basic formulation of this

problem includes minimizing the total cost of all sites included in the solution while meeting a minimum conservation goal for each species (Moilanen et al. 2009). An example of a minimum-set problem is the set-covering problem, which finds the minimum number of sites which cover at least one instance for all species (Possingham et al. 2000). Set-covering problems run the risk of not being effective for conservation since the solution may include only one site per organism which may not be enough sites to protect the species to a perturbation (Moilanen et al. 2009). Instead, a marine protected area (MPA) network is more likely to be modeled as a minimum-set problem, where conservation targets are set to a proportion of habitat or resource. These targets are then modeled as constraints (e.g., X% of coverage for each species, Y% of each habitat included) with the aim of minimizing the cost (i.e., the sum of the cost of the cells selected) of the MPA solution. These decision-making methods have been applied to a wide variety of environmental management problems (Possingham et al. 2000; Kobayashi and Polovina 2005; Sanchirico and Wilen 2005). Murawski et al. (2001) illustrated a similar optimization methodology for minimizing impacts on spatially disaggregated fishery catches while also maximizing the protection of species rarity (e.g., determining the boundaries of marine protected areas (MPAs) by selecting solutions sets of areas to be included in the MPAs).

Initial solutions to minimum-set problems included heuristic algorithms which rank sites on largest number of organisms not in the solution (greedy) or the largest number of rare species (rarity), add the highest ranked site, and then recalculate the rank for the remaining sites. Sites would be added until each species is represented (Possingham et al. 2000). These heuristic algorithms are not able to find an optimal solution and they only work for set-covering problems, as once a species is included in the solution, its abundance in other locations is no longer considered. The benefit to this approach is that a solution is quick to find.

As computing power has progressed, researchers have modeled minimum-set problems using linear integer programming (IP). In integer programming, one or more variables are restricted to being integers. Minimum-set problems in spatial planning are often modeled as binary IP problems because the decision to include or not include a site in the solution is a binary choice. The strength of linear IP to solve minimum set problems is the optimal solution can be found by using algorithms such as branch-and-bound (Possingham et al. 2000). It also allows for the addition of many different constraints that can be defined quantitatively. The weaknesses of a linear IP approach to solving a minimum set problem are the heavy computational requirements. These problems are difficult to solve with many sites (more than 20 or 30) (Possingham et al. 2000; Moilanen et al. 2009).

The two methods described above only solve for one solution and do not present alternatives which may be useful for decision makers to evaluate (e.g., their solutions may be inherently extreme, sparse, and ruthless, [Shepherd and Garrod 1981]). An alternative method is called simulated annealing. This minimization method works by calculating the "cost" of an initial random reserve solution, and then iteratively adding or subtracting sites from the solution set and recalculating the "cost" of this new solution. If the new solution is better (lower cost or more coverage), this change is made to the solution and the process continues until no other improvements can be made. The algorithm becomes more selective in terms of cost over coverage, which can help to prevent the solution at a local minimum where no single change can improve the solution, but a more optimal solution does exist elsewhere. The weakness of this method is that it is not necessarily able to identify an optimal solution to the minimum set problem, but it does outperform the previously explained heuristic methods. The benefits of this method are that it requires less computational power than linear IP (although more than the

heuristic methods mentioned) and can identify multiple solutions which can then be analyzed by the decision maker (Possingham et al. 2000).

The Marxan spatial planning solver uses simulated annealing to provide multiple minimum-set solutions and has been widely used to identify potential networks for marine protected areas with biodiversity management constraints. Marine spatial planning of aquaculture zones was designed using Marxan for regions off Portugal to minimize impacts to existing wild capture fisheries (Henriques et al. 2017). Marxan has also been used for rezoning of the Great Barrier Reef, designing a decision-making framework for assigning MPAs in the Caribbean, and is widely used in the US (Fernandes et al. 2005; Ball et al. 2009; Schill et al. 2015). Terrestrial and marine conservation planning efforts often uses total number of sites or total area as a proxy for cost. Including the actual cost of these plans is often beneficial and can create management plans that meet conservation goals at a fraction of the price compared to plans that only minimize total area included within exclusionary boundaries (Naidoo et al. 2006). Examples of costs that are not always directly proportional to total area include acquisition costs (purchase prices of areas to be included), management costs (cost to manage or oversee the area), and opportunity cost (i.e., value of an industry that is currently present that would be lost if it was removed; Naidoo et al. 2006). The Marxan spatial planning solver allows for the addition of these costs through use of a cost layer where each planning unit is assigned a cost and the total cost is minimized as opposed to the total area. The Marxan spatial planning solver requires a grid of selectable planning units with a cost per planning unit to minimize, and a set of feature files overlapping these planning units which are selected to meet constraints.

Given current oil production in the GoM, are there locations of resource concentration "hot-spots" that should be potentially reserved from development given their vulnerability to the

effects of oil spills? Are there differences in "hot-spot" networks created solely based on features in a "pristine" environment vs "hot-spot" networks created with the current *status quo* of oil production? What proportion of the resources represented in the C-ESIs are included within the existing Congressional moratorium? How does the spatial distribution of the existing Congressional moratorium compare to the "hot-spot" network identified by the Marxan solver? This study investigates these questions by developing tradeoff analyses for three C-ESIs created in Chapter 3 to quantifiably identify 0.5°x0.5° latitude/longitude resolution grid cells that should potentially be considered reserved from oil production and using the Marxan optimization framework to simulate two "hot-spot" networks, one created in a pristine environment versus one in the existing oil production environment.

5.2 Methods

5.2.1 Distribution of Current Oil and Natural Gas Production

Oil and natural gas production volume by well and lease number is public information made available by BOEM of the US Department of the Interior (DOI; BOEM 2018a, b) and was used in this study to model the spatial distribution of current oil and natural gas production. A total of 870 leases reported positive production in 2018 of which 226 leases produced natural gas only, eight leases produced oil only, and 636 leases produced both natural gas and oil (Figures 5.3, Figure 5.4). The total production of oil in 2018 in the GoM was reported as 612 MMbbl (million barrels) and the total production of natural gas was reported as 984 MMCF (million cubic feet). Maximum natural gas production by lease was 31 MMCF and maximum oil production by lease was 35 MMbbl. The maximum depth of the leases was 2936 m. The maximum depth for each lease was grouped into seven bins of 500 m width. Within each bin,

the count of leases, the distribution of lease production by type, and the total production by type was modeled in Figure 5.4.

Oil and natural gas production was also reported by well location in addition to by lease block. A total of 929 individual wells produced oil and/or natural gas in 2018: 629 produced oil and 836 produced natural gas. Oil and natural gas production by well number for the year 2018 was plotted as points and used to create a heat map for these resources in the GoM (Figure 5.3).

Oil and natural gas production by well was converted to oil and natural gas production by 0.5°x0.5° latitude/longitude resolution grid cells by summing up the total production within each grid cell and finding the proportion of the total production that occurred in each grid block.

5.2.2 Development of Single-Sector Tradeoff Curves

The single-sector management strategy for the oil and gas sector was designed as "retaining" each grid block in order from most to least productive. In Figure 5.2 (reproduced from White et al. 2012), the y-intercept is plotted at (0,1) and represents a solution where the wind energy is developed to the full capacity and therefore the sector represented on the x-axis is completely undeveloped (e.g., lobster fishery). The x-intercept represents the proportion of the second sector (e.g., lobster) when the first sector (i.e., wind energy) is completely undeveloped. To replicate this, the proportion of oil production per grid block was paired with the proportion of the C-ESI value within that grid block and graphed via a scatterplot (Figures 5.5 A-G). The grid blocks were then sorted in ascending order of oil or natural gas production and the cumulative proportion of the total oil or natural gas production was calculated for the addition of each ordered grid block (y-axis) (Figure 5.6). The proportion of the C-ESI that lies outside of the oil production area at point y was graphed on the x-axis such that every point (x,y) on this single-sector line represents a theoretical allocation where the proportion of the current oil

production lies on the y-axis (giving up lower oil producing cells first) and the x-axis represents the proportion of the C-ESI within the total oil production area which is NOT in the current theoretical allocation of oil. The point (0,1) represents the current oil and natural gas production (all of the area available to oil and natural gas production) and the point (1,0) represents zero oil development and therefore total reserve of the resources represented in the C-ESI as being unexposed to oil production and corresponding risks. These single-sector curves were created for oil production vs the Fisheries C-ESI, the Mammals C-ESI, and the Fish, Mammals, Turtles, Coral C-ESI (Figure 5.6).

I also modeled a theoretical opposite tradeoff scenario with the Mammals C-ESI, where I prioritized Mammal conservation by selecting a series of grid blocks to identify a theoretical mammal "hot-spot". Grid cells were sorted by their C-ESI value and graphed on the y-axis with oil production proportion graphed on the x-axis (Figure 5.7). The y-intercept of (0,1) then represents a solution with zero oil production and full mammal conservation from oil drilling exposure and the x-intercept of (1,0) then represents a solution with oil and natural gas production at the current production. Every point on this line therefore represents a theoretical allocation where Y% of Mammals C-ESI is reserved from oil production and X% of the current oil production is allocated for production.

5.2.3 Development of Multi-Sector Tradeoff Curves

For the multi-sector tradeoff curves, instead of sorting the grid blocks by the single component (e.g., oil production or mammal reservation from oil production, etc.), I created a third value which combined the proportion of the primary component and subtracted the proportion of the secondary component:

$$\text{Multi-Sector Value}_{jk} = P_{jk} + (1 - S_{jk}) * W \qquad \text{Eq. 5.1}$$

such that P_{jk} is the proportion of the primary component at grid block (j, k), S_{jk} is the proportion of the secondary component at grid block (j, k) and W is a fractional weight applied to S_{jk} such that the secondary component does not dominate the first. The mutually beneficial multi-sector value described in Eq. 5.1 gives the desired result of prioritizing grid blocks with a high proportion of the primary component (e.g., oil production) and a low proportion of the secondary component (e.g., mammal C-ESI) over grid blocks with high proportions of the primary component and the secondary component (e.g., high oil production/high mammal sensitivity). The mutually beneficial multi-sector value also penalizes the selection of cells with high proportions of the secondary components and low proportions of the primary component (e.g., penalizes selecting low oil productivity/high mammal sensitivity sites). The degree of the weight applied will determine the degree of this incentive/penalty. This creation of a weighted mutual benefit equation is described in White et al. (2012) although the exact equation is not provided (e.g., Eq. 5.1).

The grid blocks were then sorted by this multi-sector value and then the same (x, y) points were graphed (Proportion of Y within the area vs, proportion of X outside of the area). The multi-sector value is not graphed and is only created for the modified sort. The multi-sector tradeoff curves were graphed on the same plots as the single-sector curves to compare the two methods.

Multi-sector tradeoff curves were created for Oil Production vs Mammals C-ESI, Fisheries C-ESI, and the combined Fish, Mammals, Turtles, Larvae, Coral C-ESI. An additional tradeoff curve was created for the theoretical example of siting mammal reserves around the oil production sites (Figure 5.6, Figure 5.7).

5.2.4 Use of Marxan to Identify Minimum-Set Conservation Networks

Marxan "hot-spot" network solutions select a network of planning units from an overall set of possible planning units to optimize the minimum-set solution. Running a Marxan scenario requires the Marxan.exe file and a set of well-defined input files. Marxan.exe does not contain a user interface to either create these input files or visualize the solutions and so another visualization program must be used. Both *ArcMap* (ArcMap 2016) and *QGIS* (QGIS Development Team, 2020) have published packages to help create input files and can be used to visualize solutions. *Zonae Cogito* is an additional package that provides a user interface to visualize Marxan solutions and edit and calibrate input parameters (Segan et al. 2011). The *Zonae Cogito* user interface allows the user to explore how changing of certain parameters in Marxan impacts the solution. The input files for all scenarios in this study were created using the *QMarxan Toolbox* plug-in in *QGIS*. Methods for creating these files are described in the Marxan training handbook (Serra-Sogas and Lieverknecht 2019) created by Pacific Marine Analysis and Research Association (PacMARA) and taught during an *Introduction to Marxan* course by PacMARA in Victoria, BC in August of 2019. Exploration and calibration of solutions were performed in *Zonae Cogito*. Final solutions with calibrated parameters were visualized in *QGIS*.

5.2.5 Development of Marxan Scenarios

This study used Marxan spatial planning software to illustrate differences between networks of "hot-spots" assuming a pristine environment with no oil production (single-sector approach) and networks of "hot-spots" including current oil production (multi-sector approach). Two scenarios (Fisheries and Mammals) were chosen to simulate siting reserves based only on the resource layers included and ignoring the lost opportunity cost of oil production. These two scenarios used a uniform cost layer in Marxan representing area. The second two scenarios simulated multi-sector planning and included oil production in the cost file, such that the cost of

each grid cell was equal to the proportion of production plus 0.001 and all other grid cell costs were set to 0.001. Oil production is treated as the cost to minimize to create the tradeoff between the C-ESI and the oil production as seen in Figure 5.6. This cost file therefore ensured that the solution would still minimize area and boundary length, while adding additional cost to selecting cells that were particularly valuable to oil. The list of scenarios created for this study with their included rasters from Chapter 3 are given in Table 5.1 and Table 5.2).

5.2.6 Creation of Input Files for Scenarios

In this study, a 0.5°x0.5° latitude/longitude resolution planning unit grid was created in *QGIS* (named: pulayer.shp) and used for all scenarios (Figure 5.8). Each scenario required a unique set of six additional input files. The cost file (pu.dat) assigns a cost value to each planning unit in pulayer.shp. This cost file will be minimized by the solver. I created two cost files for the Marxan runs: (1) a uniform cost file where each planning unit had the same cost to represent the single-sector management strategy of selecting cells based solely on the features being protected (2) a cost file where each planning unit had a cost representative of the proportion of the 2018 oil production within that grid cell representing a multi-sector strategy of selecting cells based on the lost opportunity cost of oil production.

Feature files represent the spatial distribution of a feature to conserve (i.e., habitat or species distribution). The puvsp.dat and puvsporder.dat files assign a proportion of each feature present to each planning unit. Following methodology published by PacMARA (Serra-Sogas and Lieverknecht 2019), this was done by using the *Raster Analysis* tool in *QGIS* and finding the proportion of intersection between each planning unit and the presence/absence feature. The feature value of each planning unit therefore ranges between 0 and 1, with zero representing the feature is not found in the planning unit and one representing the feature covers the entire

planning unit. The species feature files used in this study are rastered probability of occurrence with values [0,0.5-1], and the economic fishery files are rastered index with values [0,1] and therefore must be calculated differently than in Serra-Sogas and Lieverknecht (2019). This study therefore used the *Zonal Statistics* tool within *QGIS* which calculates the expression (e.g., sum, mean, max) of a raster within a .shp file (in this case, the pulayer.shp file). This study used the maximum expression with *Zonal Statistics*, so each planning unit was assigned the corresponding probability or proportion value from the feature raster. The maximum expression was used instead of the sum or average expression for cases in which the resolution of the feature raster does not match the resolution of the 0.5°x0.5° latitude/longitude grid resolution planning unit file (e.g. Fisheries resources are aggregated at 1°x1° latitude/longitude grid resolution), using the average expression (or maximum) over the sum ensures that the resulting smaller planning units will maintain the same probability of occurrence as the larger raster from which they were calculated. A boundary file (bound.dat) was auto generated with the *QMarxan Toolbox* based off the planning units. A species file (spec.dat) was also created giving the desired target proportion of each feature to be maintained (i.e., 30%). Scenarios in this study used 30% as a target proportion goal which serves as a common starting point for analysis for conservation goals in Marxan (Watts et al. 2009) and was used in exploratory scenarios described in Serra-Sogas and Lieverknecht (2019). The 30% conservation goal is also addressed in both President Biden's 2021"Conserving and Restoring America the Beautiful" report which details the Presidents goal of conserving 30% of America's lands and waters by 2030 (Jenkins and Naftel 2022) and The United Nations Convention on Biological Diversity 2021 meeting with their proposed "30X30" target to conserve 30% of the global ocean by 2030 (Kubiak 2020). The Species Penalty Factor (SPF) is included to increase the penalty for not meeting the conservation

targets and was created with a default value of 1 and calibrated in later steps (for scenarios where necessary).

5.2.7 Running Marxan and Generating Output Files

The initial set of Marxan solutions are created by running a copy of the Marxan.exe application within a folder which contains of a set of correctly named folders and input files (generated above 5.2.6). The solver runs in the command prompt and produces a set of output files. The number of minimum-set solutions provided by Marxan can be set in the input files and was set to 10 for this study. Therefore, each scenario run resulted in 10 minimum-set network solutions.

The set of output files produced from a successful Marxan run (e.g., named *scenario X)* include (1) a summary file (named *scenario_sum*) which compares the cost, number of planning units, boundary length, and penalty of the 10 identified minimum-set network solutions, (2) a frequency of solutions file (named *scenario_ssoln*) listing each planning unit and the number of solutions it was included in (0 to 10), (3) a solution set file (named *scenario_r00001-n*) for each of the *n=10* identified solutions which displays the planning unit ID and a value 1 if the planning unit is included in the solution and a 0 if it is not (used for visualizing the solution via GIS methods), and (4) a solution detail file (named *scenario_mv00001-n*) for each of the *n=10* identified solutions detailing the proportion of each feature that was selected in each solution and which features (if any) did not meet the target (i.e., 30%).

5.2.8 Calibration of Boundary Length Modifier (BLM) and Species Penalty Factor (SPF) in Zonae Cogito

Zonae Cogito was used to visualize the minimum-set network solutions and frequency of solutions for each scenario. *Zonae Cogito* also allows for calibration of parameters within the

user interface and will modify the input files. Therefore, this study followed best practices described in Serra-Sogas and Lieverknecht (2019) and made a new copy of each scenario before exploring parameter sensitivity, as the original input files will be written over during calibration. This study used *Zonae Cogito* to analyze and calibrate two parameters: Boundary Length Modifier (BLM) and Species Penalty Factor (SPF).

The default BLM for each scenario was set to 0. Increasing the BLM adds cost to the boundary portion of the Marxan optimization equation. As BLM is increased, the total cost of the solution increases while the total boundary length of the solution decreases (Marxan chooses a more compact solution). When calibrating BLM in *Zonae Cogito*, BLM is varied over a defined set of values and the total cost is calculated for the resulting solutions. Graphs of *cost* vs. *total boundary length* were created in *Zonae Cogito* and a value was selected which adds a small percentage of cost and a large decrease in total boundary length per Marxan best practices (Serra-Sogas and Lieverknecht 2019).

The SPF for each scenario was set to the default value of 1. Under the default SPF, some solutions will not meet conservation targets for each feature. Increasing the SPF increases the cost of failing to meet the target requirement in the Marxan optimization equation. During calibration, the SPF is varied over a defined set of values and the resulting missing values score is calculated for the resulting solution. Graphs of SPF vs Missing Values were created in *Zonae Cogito* and a new SPF value was chosen as the lowest SPF value where the missing values approach zero per Marxan best practices (Serra-Sogas and Lieverknecht 2019).

The BLM and SPF calibration was performed on the initial solution for all scenarios. Where a new BLM and/or SPF value was identified, the Marxan scenario was rerun with the new

parameter(s). The best solution and frequency of solution from the rerun scenario are referred to as the final best solution and final frequency of solution.

5.3 Results

5.3.1 Scatterplots of C-ESI Proportions vs. Oil and Gas Production

The proportion of the total GoM C-ESI that lies within the current US oil and natural gas production area was ~40%, ~20%, and ~18% for the Fisheries C-ESI, Mammals C-ESI, and the Mammals, Fish, Turtles, Larvae, Coral (MFTLC) C-ESI respectively. Scatterplots of the proportion of oil and gas production versus the proportion of the C-ESI within the current production area were created for the Mammals C-ESI, the Fisheries C-ESI, and the MFTLC C-ESI (Figures 5.5A-F). These plots serve as an initial classification of grid cells into four quadrants: (Q1) high productivity-high sensitivity, (Q2) high productivity-low sensitivity (Q3), low productivity-low sensitivity and (Q4) low productivity-high sensitivity. Much of the potential benefit of implementing multi-sector marine spatial planning comes from prioritizing high productivity-low sensitivity (Q2) grid cells over high productivity-high sensitivity (Q1) grid cells and potentially avoiding low productivity-high sensitivity (Q4) grid cells completely. The scatter plots do not have a high proportion of points in both Q1 and Q2. In some cases, there are points in Q2 but not in Q1, indicating that most of the high oil productivity grid cells are of low sensitivity in the C-ESI (and therefore no way to optimize) or there are points in Q1 but not in Q2, representing that most of the high productivity cells are also high sensitivity and therefore important to the C-ESI, but there are no high productivity-low sensitivity cells (from Q2) to prioritize over them.

As a means of comparison, I also created a scatterplot of the Mammals C-ESI proportions from the entire GoM vs oil production (Figure 5.5G). In this scatterplot, there are many points in

Q1 and Q2 which indicates that there are many high sensitivity points both within and outside of the high oil productivity areas indicating potential benefit from multi-sector MSP.

In scatterplots from Figures 5.5 A-F, points that lie in Q4 (low production-high sensitivity) would be the first grid cells to consider reserving from oil production as they do not add much value to the oil production sector and are of high value to the C-ESI. In Figure 5.5G, points that lie in Q4 (low sensitivity-high productivity) would be the most valuable grid cells to include for the siting of oil production facilities. The tradeoff between including or excluding each additional grid cell is made quantifiably explicit through the development of the tradeoff curves.

5.3.2 Single-sector and Multi-sector Tradeoff Curves

Single-sector and multi-sector tradeoff curves were developed for oil production versus the three C-ESIs. As anticipated from the scatter plots there was not much space between the two lines which represents the additional improvement possible to the system of area closures by implementing a multi-sector MSP strategy. Nevertheless, the tradeoff functions are still useful in identifying specific grid cells to be potentially removed from production. At the top left side of the curve in Figure 5.5A (Oil production versus Mammals C-ESI), the oil production ranges from (0,1) to ~(0.4,0.98). These two points represent potential reservation proportions such that all the grid cells included to the left of X=0.4 effectively decrease the oil production by ~2% while adding ~40% of the benefit to the Mammals C-ESI. The grid cells making up this part of the tradeoff curve are therefore likely points with low production of oil and relatively high sensitivity levels to the C-ESI. These grid cells might be worth reserving from oil production entirely since the lost benefit to the whole production industry is low and the benefit to the resources represented by the C-ESI is high.

For comparison, I also ran the single-sector and multi-sector tradeoff curves on the hypothetical mammal reserve scenario. As expected, these plots look more similar to the plots from White et al. (2012) and indicates the multi-sector scenario may offer considerable benefit to both sectors accruing from an optimized system of closures where marine spatial planning might be useful (Figure 5.7). When comparing the single-sector plot to the multi-sector plot, the value of the benefit to the whole system can be easily compared by comparing two points on the same horizontal line or vertical line. For example, on the single-sector tradeoff function, there exists a point at ~(0.4,0.91) where 60% of the oil production is reserved and 91% of the mammals C-ESI is reserved. On the multi-sector line, there also exists a point at ~(0.4,0.98) which adds benefit to mammals at no cost to oil production (no change in X, positive change in Y), a point at ~(0.93, 0.91) which adds benefit to oil production at no additional cost to mammals (positive change in X, no change in Y), and a point at ~(0.92,0.93) which increases the benefit to both sectors (positive change in X and Y). The y-axis on this plot ends at 0.8 since only 20% of the mammal's C-ESI overlaps with the oil production sector. Similar to the top left of the Oil Production with Mammals C-ESI graphed in Figure 5.5A and discussed above, the bottom right of this plot also represents the set of grid blocks with high importance to the mammals C-ESI and low importance to the oil production sector.

5.3.3 Scenario 1: Fisheries Marxan Solution – uniform cost, single sector

A Fisheries Marxan scenario was run to identify a network of planning units which would minimize cost (area) and conserve 30% of each of the five fishing industry distributions created in Chapter 3 (i.e., brown shrimp, white shrimp, pink shrimp, coastal species, highly migratory species). For the scenario, a uniform cost layer was used with the cost of each planning unit corresponding to estimated square meters within the block. The same indexed files for each of

the fisheries used in the creation of the C-ESI were used as the feature files. Based on best practices described by in Serra-Sogas and Lieverknecht (2019), these feature file proportions were multiplied by the number of the kilometers in each planning unit (3086 square kilometers in a 0.5°x0.5° latitude/longitude grid square). In the reference models in Serra-Sogas and Lieverknecht (2019), the cost per planning unit was about half of the value of the area per planning unit, so this study used a uniform value of 1500 for each planning unit in the pu.dat input file. The boundary length value in bound.dat was the length (in kms) of one of the planning units, or 55.56. The same planning unit shapefile was used for all four scenarios (Figure 5.8).

The Fisheries scenario was run to find 10 solutions with initial parameters BLM = 0 and SPF = 1. All 10 solutions were very similar in cost with 34 planning units selected in each solution and total scores ranging from [55,963.94, 56,163.98] and the selected initial best solution was run 9 (Appendix C). The initial best solution (set of chosen planning units) and frequency of solution (number of times each planning unit was part of one of the ten solutions) were visualized in *QGIS* (Figure 5.9). In all 10 solutions, four out of five solutions met their target, with the *highly migratory species* feature target not being met in any of the 10 runs (Appendix C).

The default BLM value was 0 and this was calibrated in *Zonae Cogito* by looking at a range of BLM values from 0 to 100 and, after identifying an inflection point at 22, from 0 to 22. BLM modifier of 7.33 was chosen as the inflection point as it added a 13% increase in cost and a 23% reduction in Total Boundary Length (Appendix C).

The default SPF was set to 1 and the Marxan solution at this SPF value did not meet all species targets. This value was calibrated in *Zonae Cogito* by graphing the Missing Values on

the y axis versus a range of SPF values [1,10] on the x axis and identifying the SPF value where the Missing Values approaches 0 (Appendix C). The selected SPF value was identified as 9.44.

Marxan was rerun with the same input files but with BLM = 7.33 and SPF = 9.44 and the results were visualized in QGIS (Figure 5.9). The total scores of the new set of solutions ranged from [73104, 76620], the number of selected planning units in the solution ranged from 40 to 42, all targets were met, the solution was more compact, and the final best solution was run 9 (Appendix C).

5.3.4 Scenario 2: Mammals Marxan Solution

Similar methodology applied in *Scenario 1: Fisheries* in 5.3.3 was applied in *Scenario 2: Mammals*. For this scenario, the same cost file was used as for *Scenario 1: Fisheries*, with uniform cost distribution of 1500 and the feature files being created from the six mammal species probability distributions as created in Chapter 3 (Table 5.1 and 5.2).

All 10 solutions were again very similar in cost and number of planning units selected (124-126 planning units) and the selected initial best solution was run 9 (Appendix C). The initial best solution (set of chosen planning units) and frequency of solution (number of times each planning unit was part of one of the ten solutions) were visualized in *QGIS* (Figure 5.10). In all 10 solutions all targets were met.

The default BLM value was 0 and this was calibrated in *Zonae Cogito* by looking at a range of BLM values. A BLM modifier of 4.44 was identified from the large reduction in Total Boundary Length (-63%) and the negligible increase in Total Cost (Appendix C).

The default SPF was set to 1 and all targets were met at this level of SPF, so this parameter was not calibrated. Marxan.exe was rerun with the same input files and BLM = 4.44

and SPF = 1 and the results were visualized in *QGIS* (Figure 5.11). The number of planning units in the final solution as well as the total cost remained relatively unchanged, but the connectivity score decreased from 16296 to 5992 (Appendix C).

5.3.5 Scenario 3: Fisheries with Oil Production as Cost

The *Scenario 3: Fisheries with Oil Production as Cost* was modeled with the same input files as Scenario 1, except the cost file was edited to be the proportion of the oil production per grid cell plus 0.001 (to give each grid cell a non-zero cost). This cost file was multiplied by 1,500,000 to bring the cost file into similar range of the cost file for Scenario 1 (cost in Scenario 1 was 1500 for all planning units and minimum cost in Scenario 3 was 1500). This scenario used the same bound.dat, and pu.dat, and planning unit file as the previous two scenarios. The best solution and frequency of solution was visualized in QGIS (Figure 5.12).

5.3.6 Scenario 4: Mammal Species with Oil Production as Cost

The *Scenario 4: Mammal Species with Oil Production as Cost* was modeled with the same input files as Scenario 2, except the cost file was the same oil production cost file that was used in Scenario 3. The best solution and frequency of solution was visualized in QGIS (Figure 5.13).

5.3.7 Evaluation of 2032 Congressional Moratorium

The spatial boundaries of the Congressional Moratorium were mapped from the shape file provided by the Department of the Interior (Geospatial Services Division, Department of Interior - Bureau of Ocean Energy Management - Office of Strategic Resources, 2021). The intersection between the Congressional Moratorium area and each of the C-ESIs created in Chapter 3 was found using the *Zonal Statistics* tool within *QGIS*. The Moratorium area covers

20.3% of the study area (132 of 650 0.5°x0.5° latitude/longitude resolution grid cells) and contains between 17.5% and 20.7% of the value of each C-ESI (Table 5.3, Figure 5.14).

In the Marxan Scenario 2, the mammal "hot-spot" networks identified without the inclusion of current oil production consisted of 124 0.5°x0.5° latitude/longitude resolution grid cells of which 49 (39.5%) were located within the boundaries of the Congressional Moratorium. In Marxan Scenario 4, where the tradeoff function was used to identify the mammal "hot-spot" network, the network consisted of 137 0.5°x0.5° latitude/longitude resolution grid cells of which 73 (53.2%) were located within the moratorium area (Figures 5.15 A, B).

5.4 Discussion

The C-ESIs created in Chapter 3 of this study and current or proposed marine oil production can be used to create explicit tradeoffs between the resources represented by the C-ESIs and oil production on a grid cell level. These tradeoffs combined with MSP software can then be used to create "hot-spot" networks which maximize the system-wide benefit to both sectors by maximizing oil production while protecting sensitive "hot-spot" areas. Both tradeoff functions and "hot-spot" networks created in this study or in this manner could serve as additional tools in the decision making of areas to be made available for, or reserved from, offshore oil production.

This chapter developed tradeoff curves between C-ESIs and oil production to identify the quantifiably explicit tradeoff value for each grid cell where oil production was reported in BOEM Offshore Statistics by Water Depth for 2018 (BOEM 2018b). The (x, y) points on the tradeoff curves represent theoretical allocations of grid cells to oil production or reservation from oil production such that Y% of the oil production is conserved and X% of the resource value in the C-ESI is conserved. These curves then allow for quantifiably explicit comparisons between

theoretical allocations. These tradeoff curves also identify grid cells with low oil production and high resource sensitivity which should potentially be reserved from oil production as their exclusion from oil production would have minimal negative impact on the oil production industry as a whole and are identified as ecologically important by the C-ESI. These tradeoff functions and subsequently identified grid cells can act as an additional decision-making tool as part of an environmental assessment when looking at sites to be included or excluded from future or current oil exploration.

While the tradeoff functions described above identify the tradeoff between the two sectors of environmental sensitivity and oil production at the grid cell level, it is often impractical to assign individual grid cells to a specific sector. MSP selects groups of grid cells using the same tradeoff values to develop a solution consisting of one or more contiguous areas. This study used Marxan MSP software to identify a minimum-set "hot-spot" network for the resources represented in the Fisheries C-ESI and the Mammals C-ESI both in a hypothetical pristine system with no oil drilling yet occurring and the current state of oil production as of 2018. These minimum-set "hot-spot" networks represent groupings of grid cells that are potentially most important to protect in a hypothetical environment where drilling is not currently occurring, but production sites are being planned, as well as the most important grid cells to protect in a system which has already allocated grid cells to oil production. For both scenarios, the addition of the reported 2018 oil production as cost resulted in an increased number and frequency of selected grid cells in the WFS in the minimum-set "hot-spot" network. This result indicates that in a hypothetical reserve created to protect a significant proportion of offshore marine resources and sited around existing oil production, the grid cells on the WFS would be most valuable to that solution.

The two mammal "hot-spot" network solutions were compared to the area currently protected and withdrawn from oil production under the Congressional Moratorium. The areas withdrawn under the moratorium are fairly aligned with the "hot-spot" networks identified in this study with 39.5% of the "hot-spot" network identified in Scenario 2 being located within the withdrawn areas. In Scenario 4, where the mammal reserve is sited around current oil production, the overlap is even larger with 53.2% of the "hot-spot" network being located within the withdrawn areas. The "hot-spot" networks identified in this study can potentially be utilized in the decision-making process supporting the continued closure of these withdrawn areas.

Evaluation of the Best Solution for Marxan Scenarios

The final minimum-set network solutions created for the four Marxan scenarios differed from one another in size (number of planning units selected in the solution), location within the Gulf of Mexico, and the frequency of selection within the solutions due to the differences in the distributions of the included features and the differences in the cost files.

For each of the four scenarios, the number of planning units included in each of the 10 best solutions was relatively constant (+/- 2 planning units selected between solutions within each scenario), showing that while the individual planning units chosen to make up the solution varied between runs in the Scenarios, the Marxan process was consistent in minimizing the total number of planning units required to meet the criteria.

The location within the Gulf of Mexico of the network solution also varied between the scenarios. For *Scenario 1: Fisheries – Pristine System*, the identified solution consisted of four to five small networks spanning across the northern GoM. This is an expected result since the fisheries making up these features are diverse and do not extensively overlap. This solution was able to therefore identify and include grid cells important for each fishery resource. For *Scenario*

2: Mammals, the final minimum-set network solution consisted of two reserve areas with the larger area covering much of the continental slope and an additional smaller area off the coast of Mexico in the eastern GoM. For *Scenario 3: Fisheries – Oil Production as Cost*, the network solution grid included more cells on the WFS and WGoM. In *Scenario 4: Mammals – Oil Production as Cost*, the two reserves created from Scenario 1: Mammals -Pristine System were replaced by a single reserve covering much of the eastern Gulf of Mexico (much of which is currently in the Congressional moratorium region).

Evaluation of the Frequency of Solutions for Marxan Scenarios

Each Marxan scenario performed in this study consists of ten solutions from separate runs. The two files visualized in *QGIS* and included in this study are a "best solution" and a "frequency of solutions". The "best solution" will be a network of planning units where each planning unit is either selected (value of 1) or unselected (a value of 0). The best solution is picked from the 10 solutions based on the Total Score of the ten solutions. The "frequency of solutions" represents the number of times (up to the total number of runs) the planning unit was chosen as part of the solution network. While the "best solution" is useful in a situation where one is identifying and/or designing a reserve area where only one solution can be implemented, the "frequency of solutions" gives insight into how interchangeable and robust the solutions are. Planning units that are selected in all 10 solutions are vital to the solution, planning units that are selected in some runs are important, but have characteristics that are similar to other areas, and planning units that are not selected in any runs are of the lowest priority to the solution.

Areas for Future Study

This study identifies grid cells with low oil production and high sensitivity as most desirable to remove from oil production, but it is likely that the probability of an oil well blowout

occurring in one of these grid cells is substantially lower than in grid cells where more oil is being produced and there are likely increased numbers of wells.

Additionally, the tradeoff curves and minimum-set "hot-spot" networks developed in this chapter treat the consequences of oil production as potentially occurring on a grid cell by cell basis. Oil spills originating in a particular grid cell may have spatial footprints far beyond the source grid, as illustrated in the CMS oil spill simulations (Chapter 4; Figure 4.1). Thus, if there are larger scale regions that encompass these trajectories it may provide a more realistic view of inherent tradeoffs. While the BLM was used in the Marxan minimum-set networks to group grid cells together, this BLM could be further revised to better represent expected oil spill coverage based on the origin point of the spill.

5.5 Tables

Table 5.1 List of Raster files included in this chapter with resolution level and ID number. Reproduced as a subset from Chapter 4 Table 4.2

Type	Raster Layer	Resolution	ID Number
Mammal	Bottlenose dolphin	0.5 degree	18
Mammal	Pantropical spotted dolphin	0.5 degree	19
Mammal	Atlantic spotted dolphin	0.5 degree	20
Mammal	Sperm whale	0.5 degree	21
Mammal	Pygmy killer whale	0.5 degree	22
Mammal	False killer whale	0.5 degree	23
Economic Fishery	Coastal Species	1 degree	27
Economic Fishery	Highly Migratory Species	1 degree	28
Economic Fishery	Brown shrimp	1 degree	29
Economic Fishery	White shrimp	1 degree	30
Economic Fishery	Pink shrimp	1 degree	31

Table 5.2 List of Marxan Scenarios and contributing raster IDs from Table 5.1

Scenario ID	Name of ESI	Raster ID numbers included in calculation
1	Commercial Fisheries with uniform cost	27-31
2	Mammals with uniform cost	18-23
3	Fisheries with oil production use as cost	27-31
4	Mammals with oil production used as cost	18-23

Table 5.3 Proportion of the value of each C-ESI within the Congressional Moratorium area.

C-ESI	Proportion(C-ESI) within Moratorium
Turtles	0.197
Mammals	0.178
Fishes Unweighted	0.200
Fishes Weight = 2	0.203
Fishes Weight = 4	0.206
Fishes Weight = 8	0.207
Fishes Lanternfish = 10	0.175
Fisheries	0.194
All Layers	0.198
Species Richness	0.177

5.6 Figures

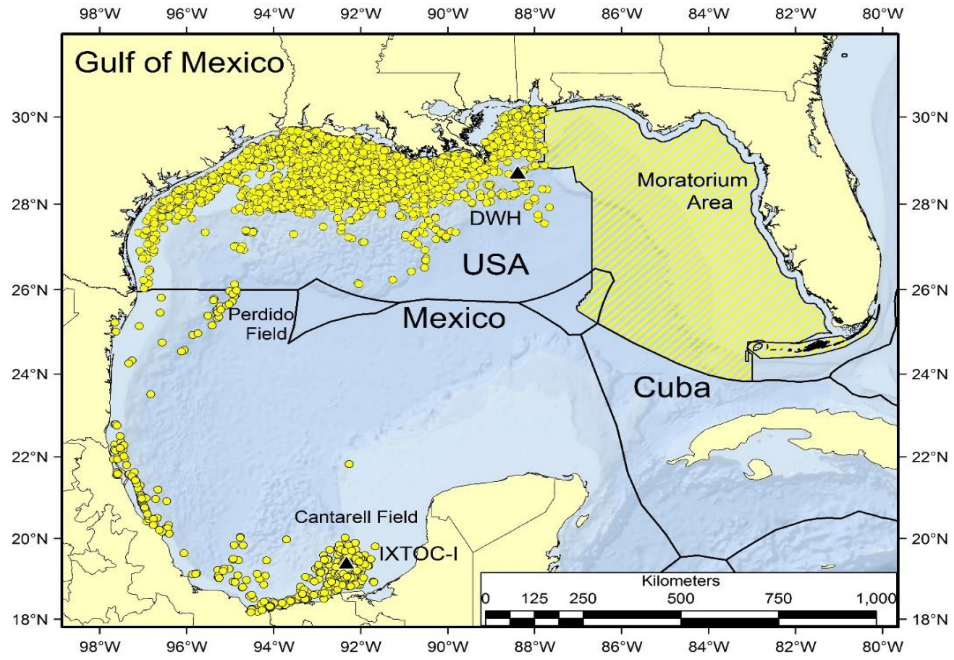

Figure 5.1 Boundaries for areas withdrawn from oil/gas/mineral leasing off the gulf coast of Florida under the Congressional Moratorium and extended by Presidential proclamation until June 30, 2032

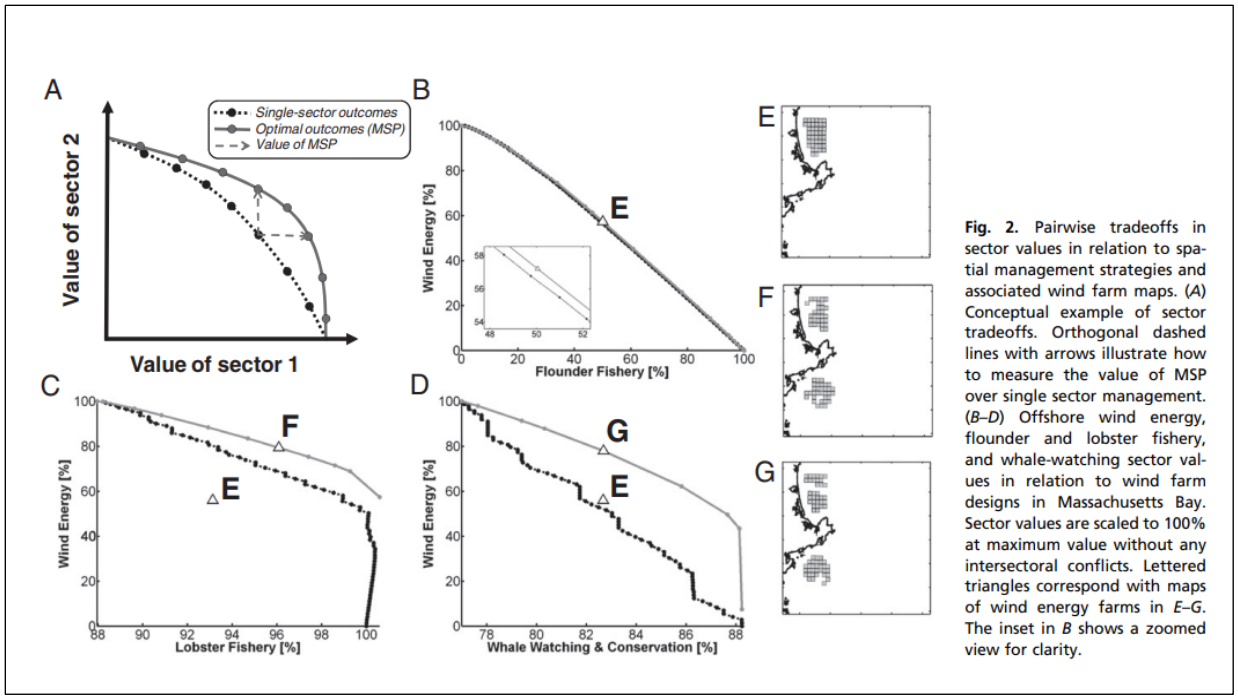

Fig. 2. Pairwise tradeoffs in sector values in relation to spatial management strategies and associated wind farm maps. (*A*) Conceptual example of sector tradeoffs. Orthogonal dashed lines with arrows illustrate how to measure the value of MSP over single sector management. (*B–D*) Offshore wind energy, flounder and lobster fishery, and whale-watching sector values in relation to wind farm designs in Massachusetts Bay. Sector values are scaled to 100% at maximum value without any intersectoral conflicts. Lettered triangles correspond with maps of wind energy farms in *E–G*. The inset in *B* shows a zoomed view for clarity.

Figure 5.2 Pairwise tradeoffs in sector values for Nantucket Cape Wind proposal.
Figure is reproduced from White et al. 2012 to illustrate the pairwise tradeoff functions between the wind energy sector and three other sectors (i.e., flounder fishery, lobster fishery, whale watching and conservation).

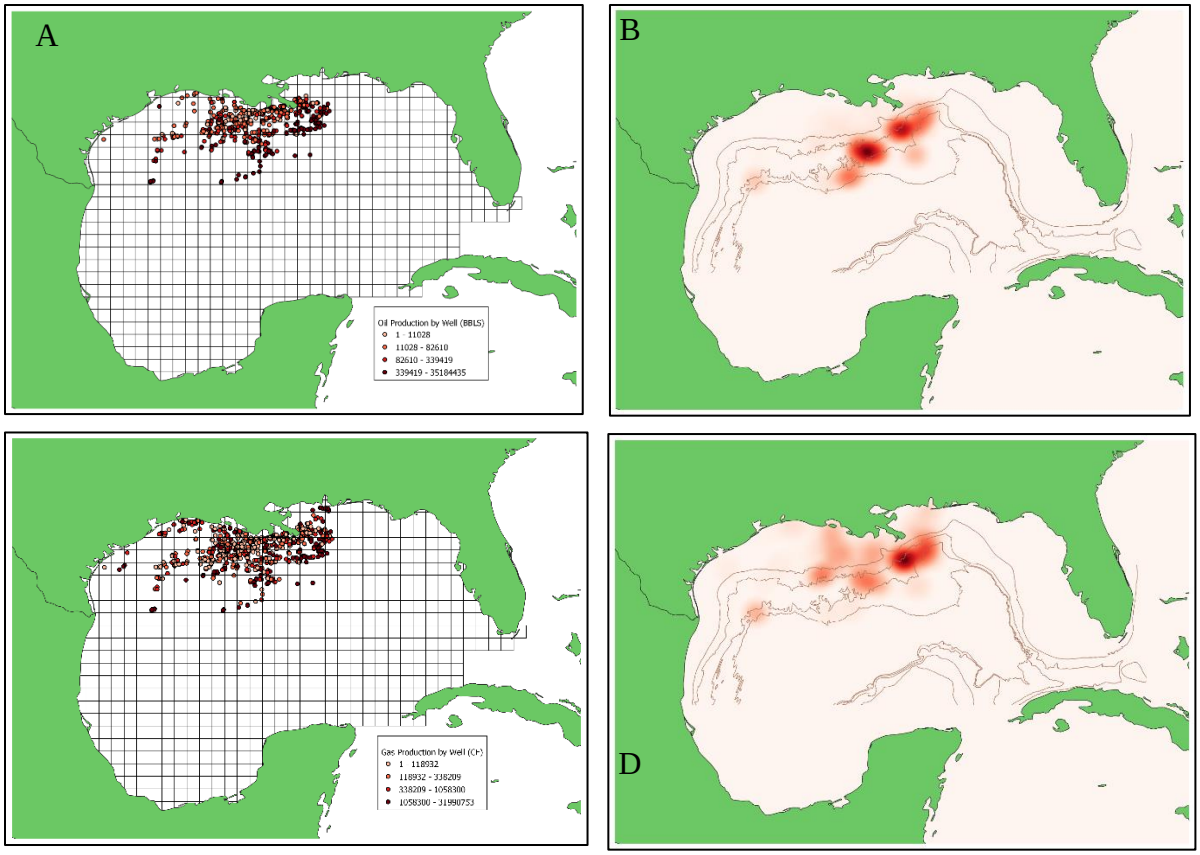

Figure 5.3 Oil and natural gas production in the Gulf of Mexico
Oil production in barrels (bbls) by well location (A) and heatmap (B) and natural gas production in cubic feet (CF) by well location (C) and heatmap (D) produced from publicly available production data from Bureau of Ocean Energy Management Offshore Statistics by Water Depth (BOEM. 2018b) https://www.data.boem.gov/.

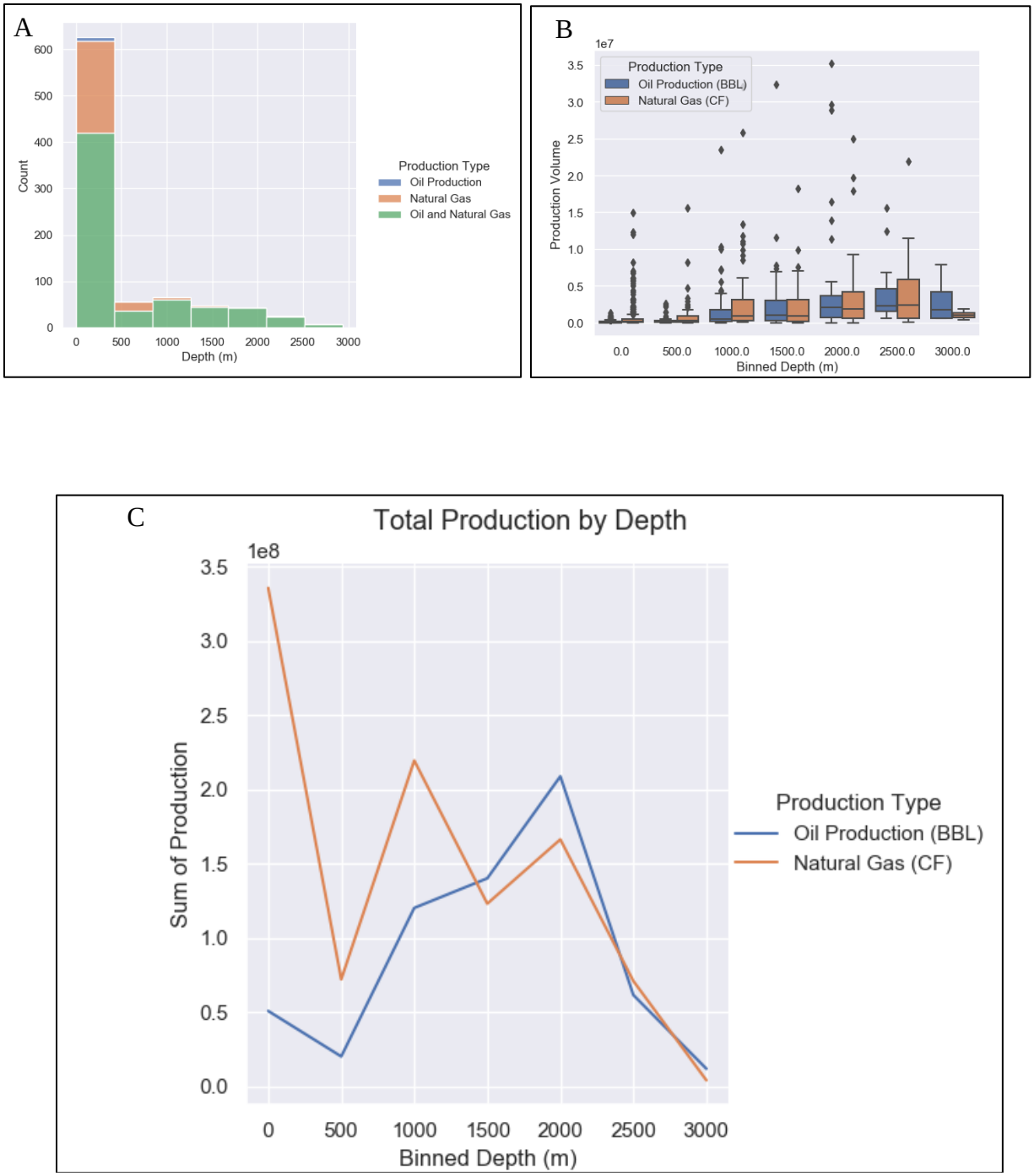

Figure 5.4 Count and mean production of leases of oil and natural gas production in the Gulf of Mexico by depth.
A total of 870 leases with positive production in 2018 were binned by depth in 500m increments. A total of 226 leases produced natural gas, 8 leases produced oil only with 636 leases producing both oil and natural gas (A). The distribution of the producing leases by each time displayed as a box plot (B). The total sum of production by type for each depth bin (C).

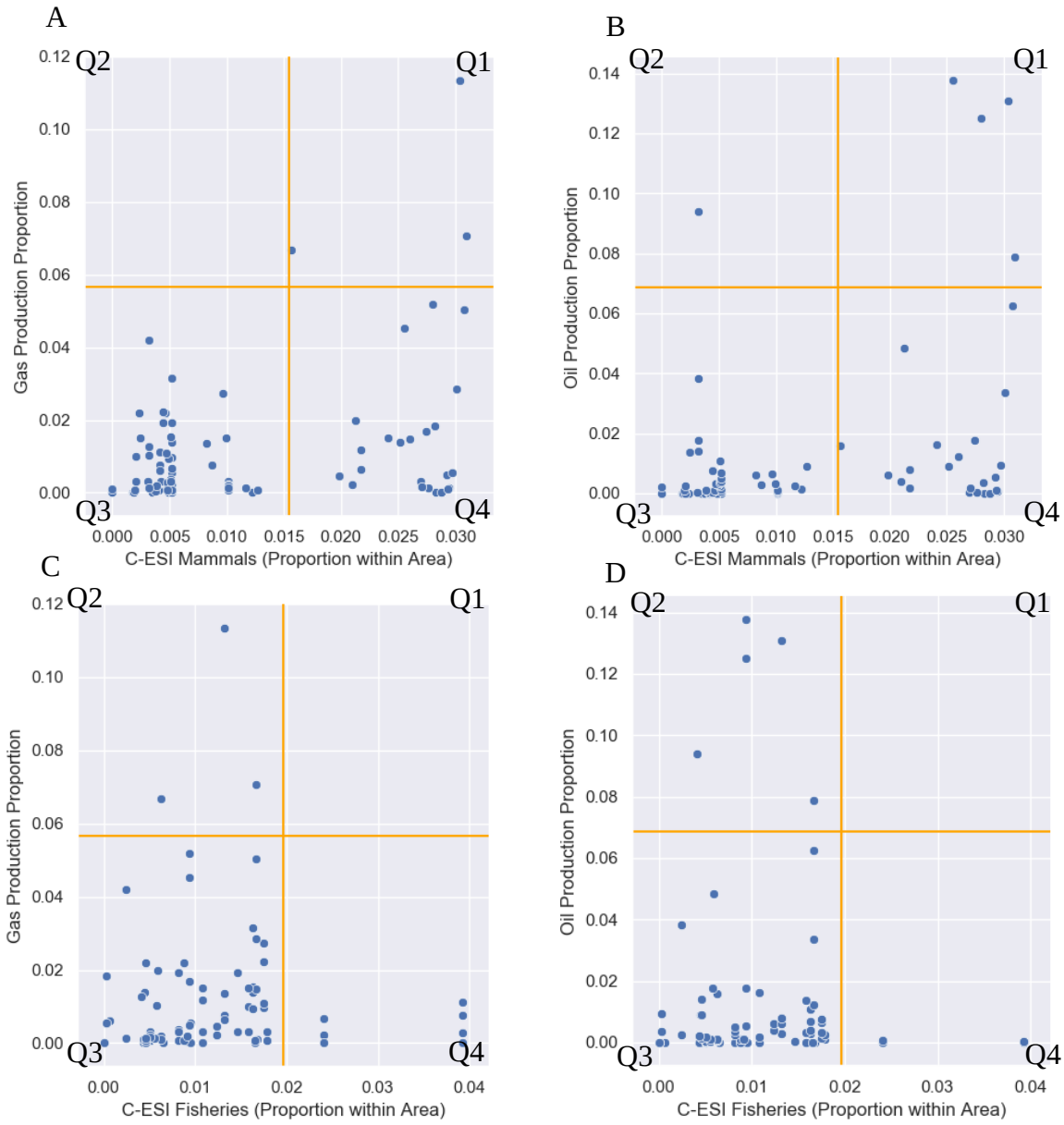

Figure 5.5A-D Scatterplots of C-ESI proportions by natural gas and oil production proportions. Scatterplots of the proportion of the natural gas production (A, C) or oil production (B, D) versus the proportion of the selected C-ESI within the oil and natural gas production area. Bisecting lines (orange) represent the approximate midpoints of the range of x and y.
Q1 = High Production, High Sensitivity Q2 = High Production, Low Sensitivity
Q3 = Low Production, Low Sensitivity Q4 = Low Production, High Sensitivity

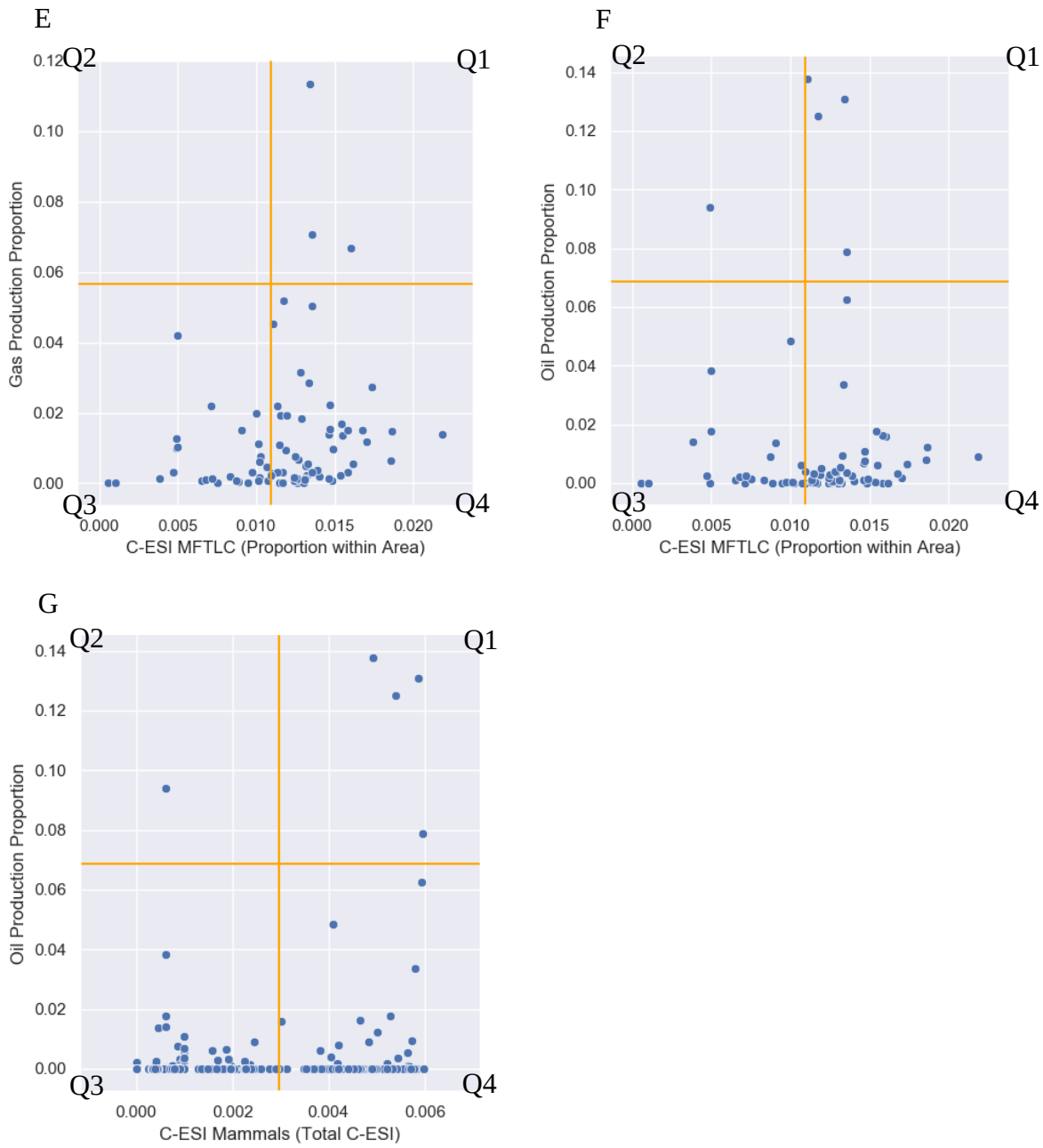

Figure 5.5E-G Scatterplots of C-ESI proportions by oil or natural gas proportions.
Scatterplots represent the proportion of the natural gas production (E) or oil production (F) versus the proportion of the MFTLC C-ESI within the oil and natural gas production area.
Scatterplot (G) is the proportion of the Mammals C-ESI (all grid blocks included) versus the proportion of the oil production per grid block.
Bisecting lines (orange) represent the approximate midpoints of the range of x and y.

Q1 = High Production, High Sensitivity Q2 = High Production, Low Sensitivity
Q3 = Low Production, Low Sensitivity Q4 = Low Production, Low Sensitivity

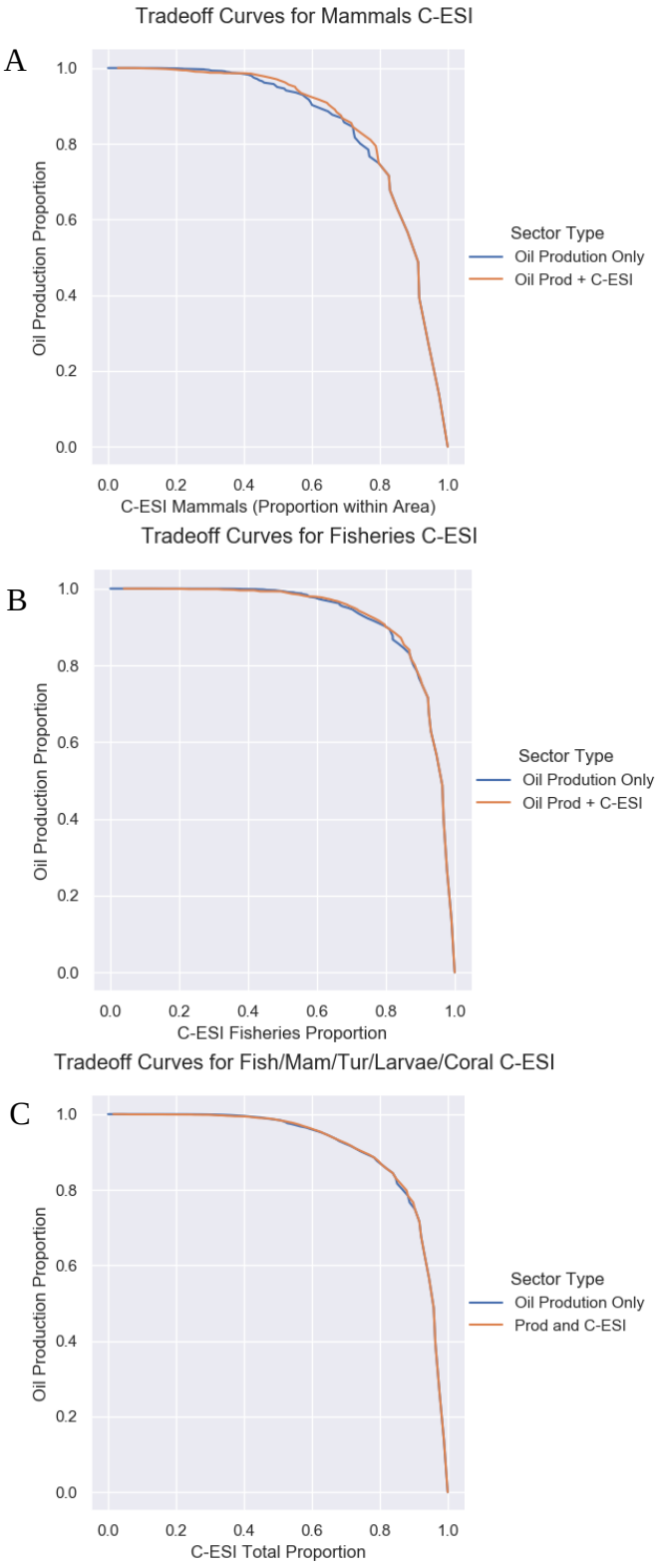

Figure 5.6 Single- vs. Multi-Sector tradeoff curves for oil production sector vs ESI.
Tradeoff curves between proportion of oil production (y-axis) and proportion of C-ESI (x-axis).

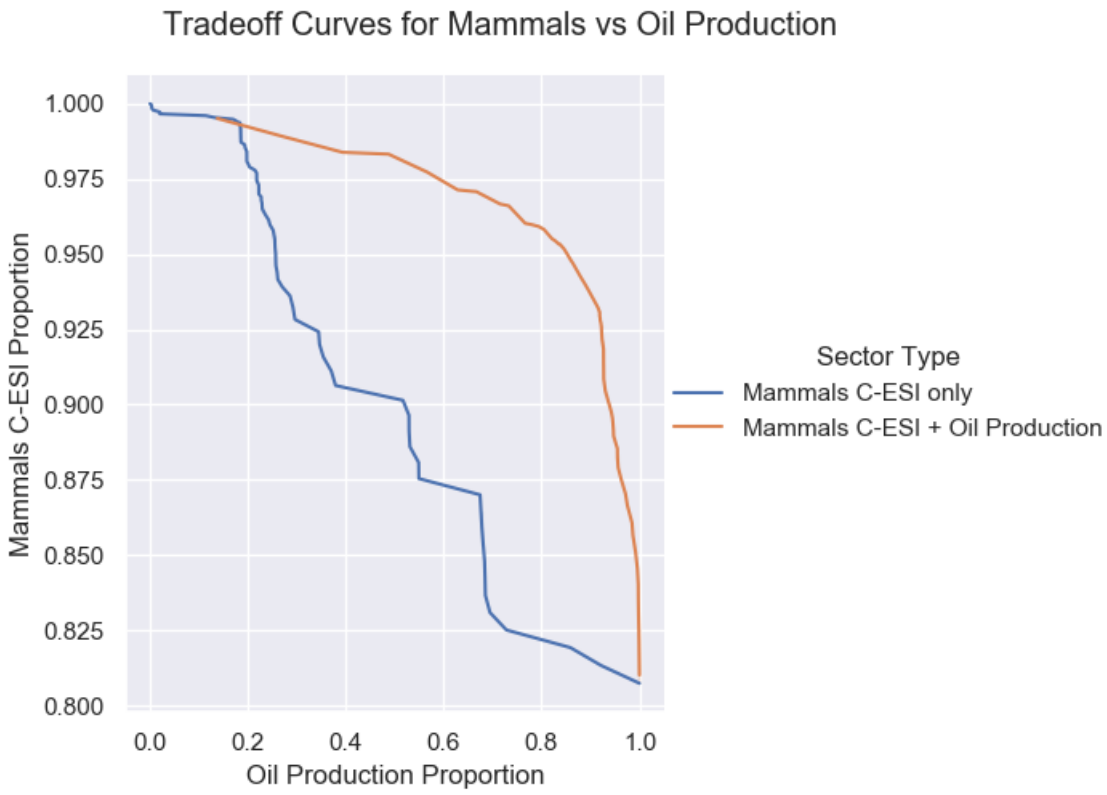

Figure 5.7 Single- vs. Multi-Sector tradeoff curves for a hypothetical mammal reservation. Tradeoff curves of a single-sector siting strategy (blue line) and a multi-sector siting strategy including lost opportunity to the Oil Production sector (orange line)

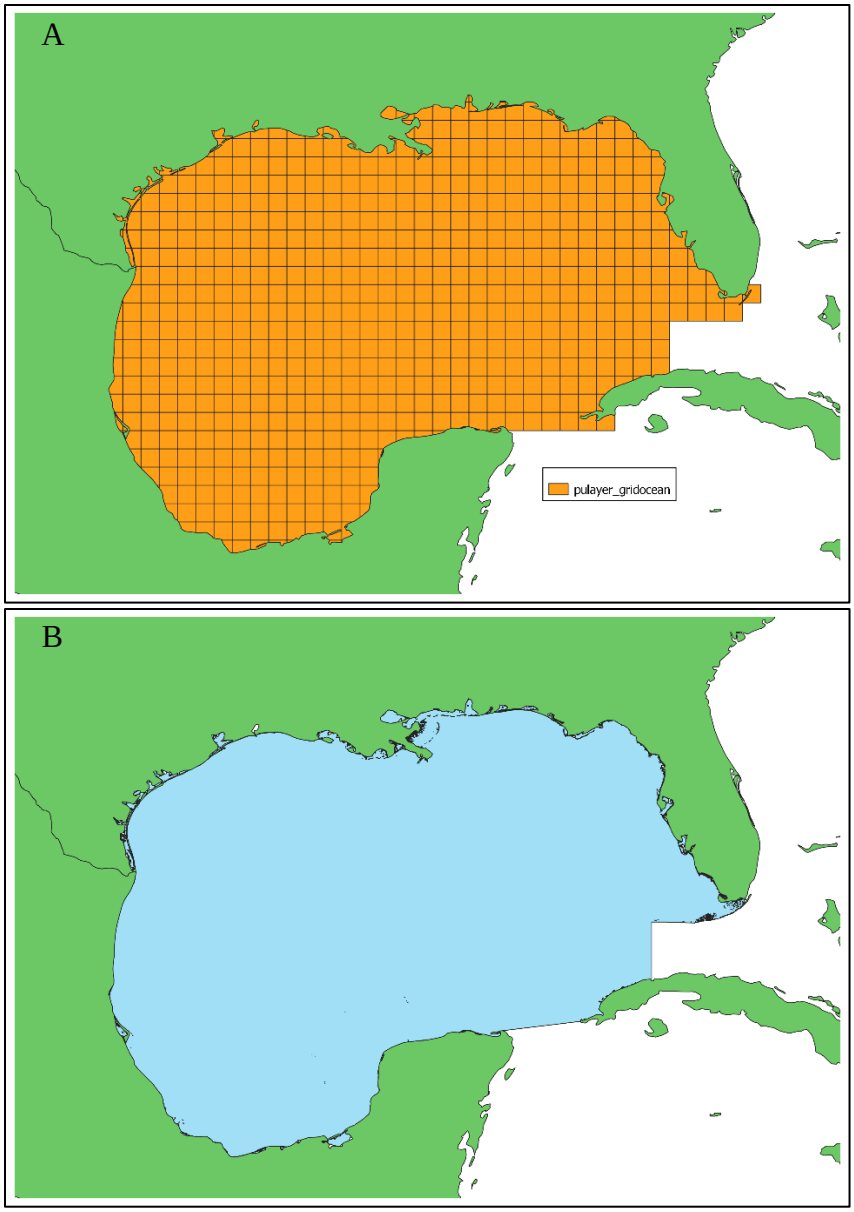

Figure 5.8 Planning unit shapefile.
Planning unit shapefile (A) used for all Marxan scenarios created as an intersection of a 0.5°x0.5° latitude/longitude resolution grid and the IHO ocean shape file (Flanders Marine Institute 2018) (B). Planning unit shapefile created from methods described in Serra-Sogas and Lieverknecht (2019).

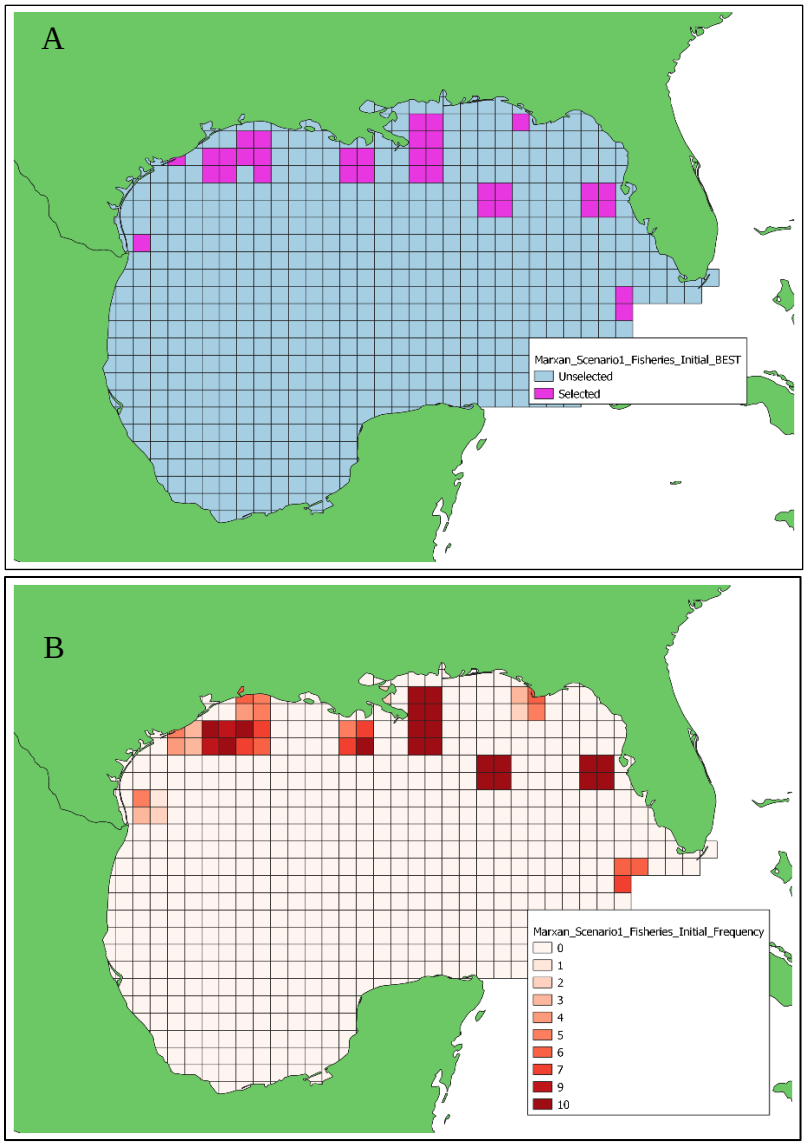

Figure 5.9 Best and Frequency for Scenario 1: Fisheries – Pristine System.
Initial *Best Solution* for Marxan Scenario 1 before calibration of Boundary Length Modifier (BLM) and Species Penalty Factor (SPF) (A). Initial *Frequency of Solution* for Marxan Scenario 1 before calibration of BLM and SPF (B). Results visualized in QGIS.

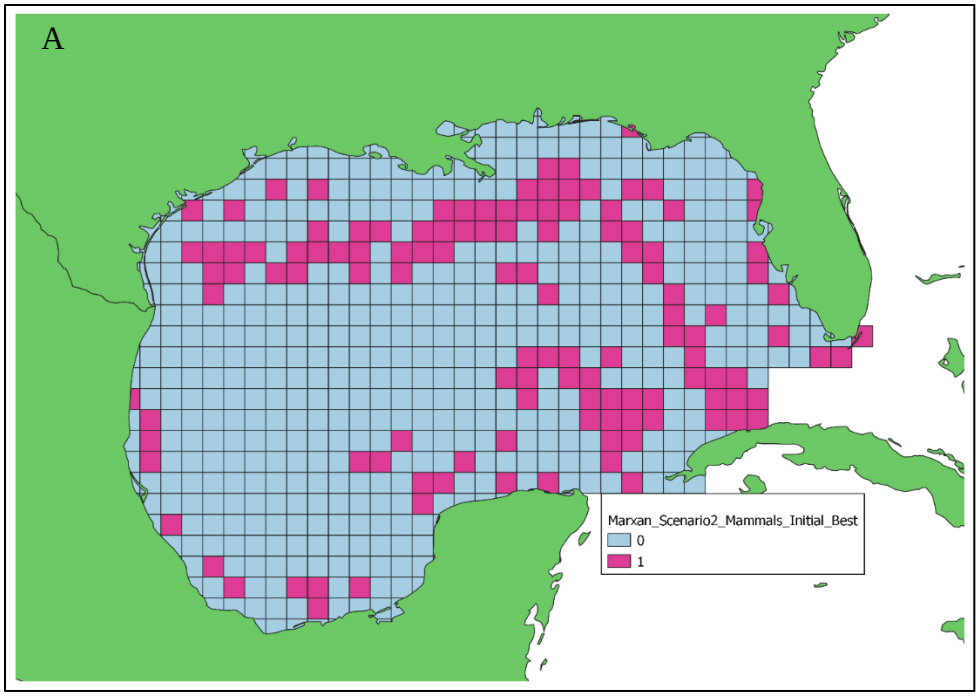

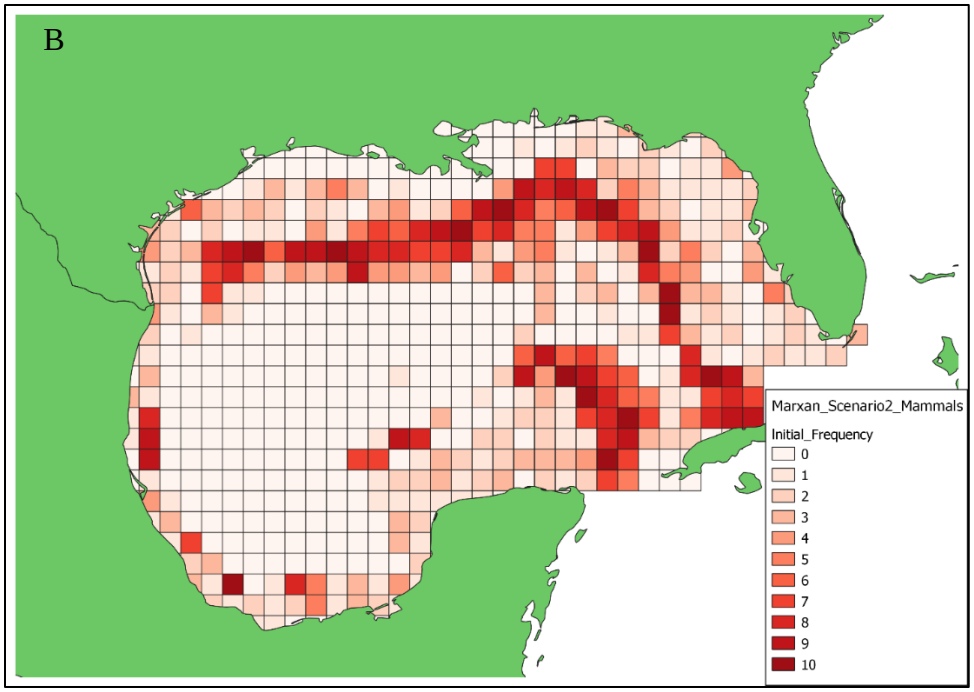

Figure 5.10 Initial Best and Frequency for Scenario 2: Mammals – Pristine System. Initial *Best Solution* for Marxan Scenario 1 before calibration, Boundary Length Modifier (BLM)=0 and Species Penalty Factor (SPF)=1 (top). Initial *Frequency of Solution* for Marxan Scenario 1 before calibration, BLM=0 and SPF=1 (bottom). Results visualized in QGIS.

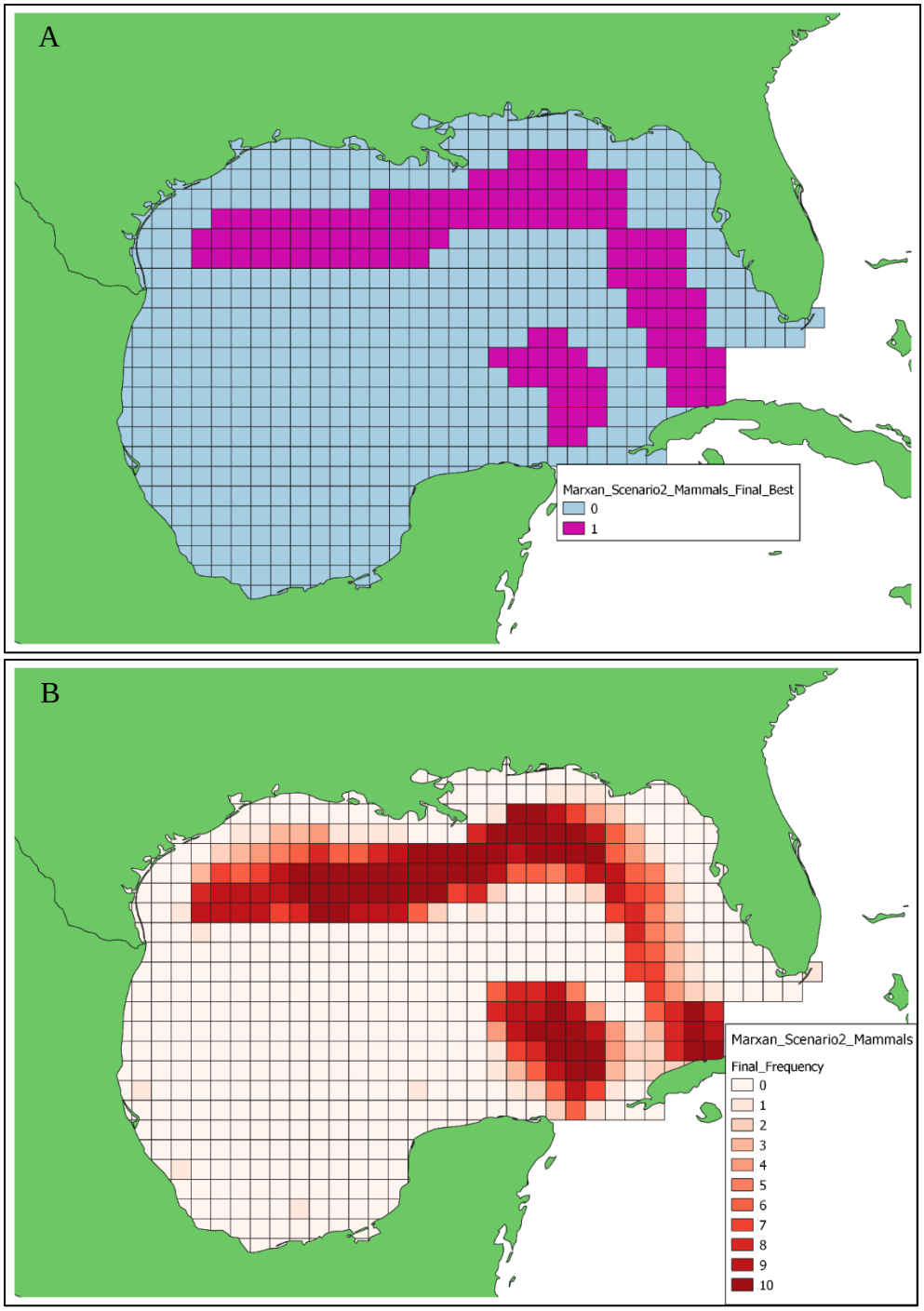

Figure 5.11 Final Best and Frequency Scenario 2: Mammals - Pristine System.
Final *Best Solution* for Marxan Scenario 2 with Boundary Length Modifier (BLM) = 4.44 and Species Penalty Factor (SPF) = 1 (A).
Final *Frequency of Solution* for Marxan Scenario 1 with BLM = 4.44 and SPF = 1 (B).
Results visualized in QGIS.

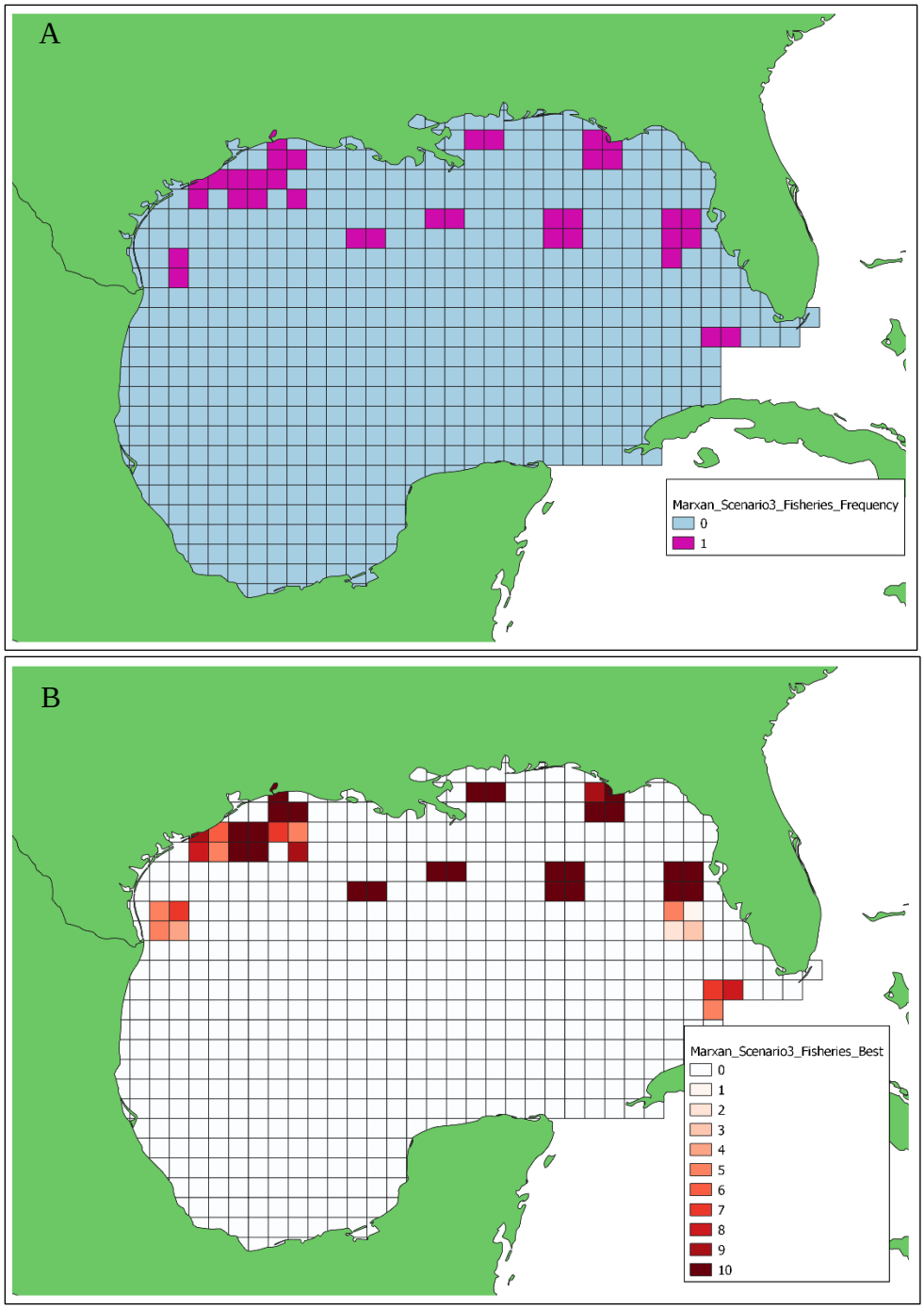

Figure 5.12 Final Best and Frequency Scenario 3: Fisheries – Oil Production as Cost.
Final *Best Solution* for Marxan Scenario 3 using a weighted cost layer representing oil production (A).
Final *Frequency of Solution* for Marxan Scenario 3 (B).
Results visualized in QGIS.

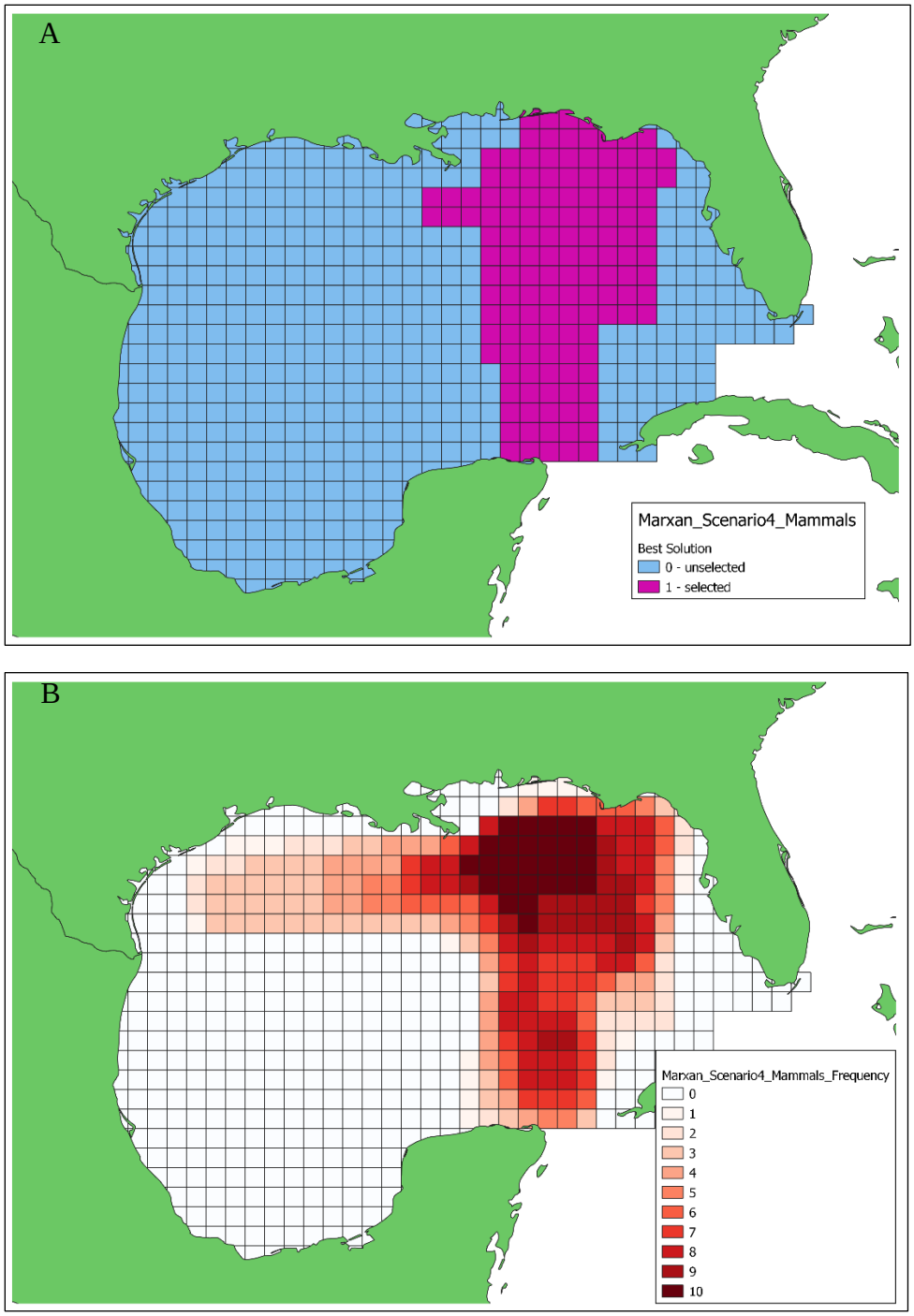

Figure 5.13 Final Best Solution and Frequency Scenario 4: Mammals - Oil Production as Cost.
Final *Best Solution* for Marxan Scenario 4 using a weighted cost layer representing oil production (A).
Final *Frequency of Solution* for Marxan Scenario 4 (B). Results visualized in QGIS.

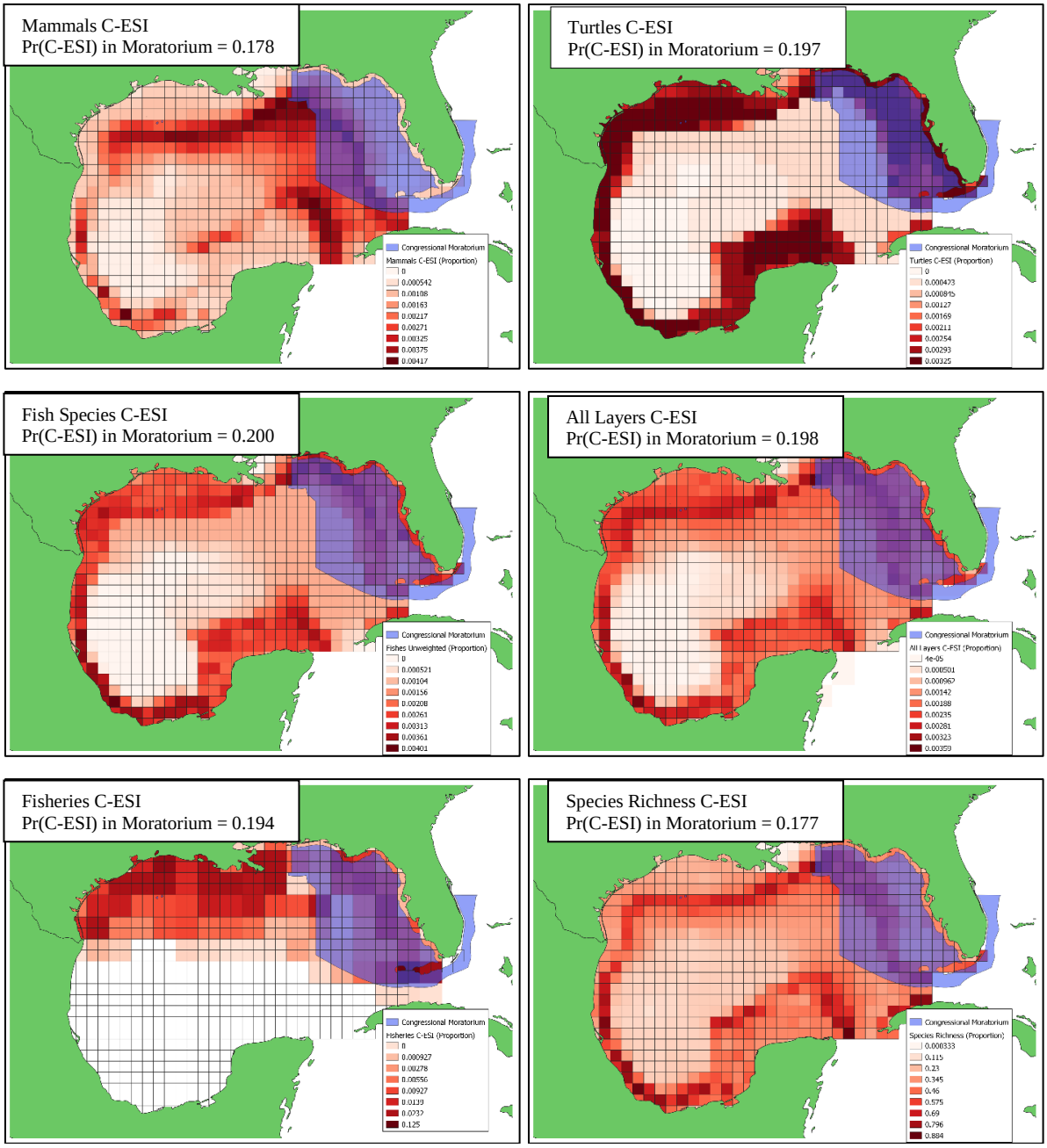

Figure 5.14 C-ESIs mapped with the Congressional Moratorium
Proportion of the total value of the C-ESI within the current boundary for the Congressional Moratorium (Geospatial Services Division, Department of Interior - Bureau of Ocean Energy Management - Office of Strategic Resources, 2021).

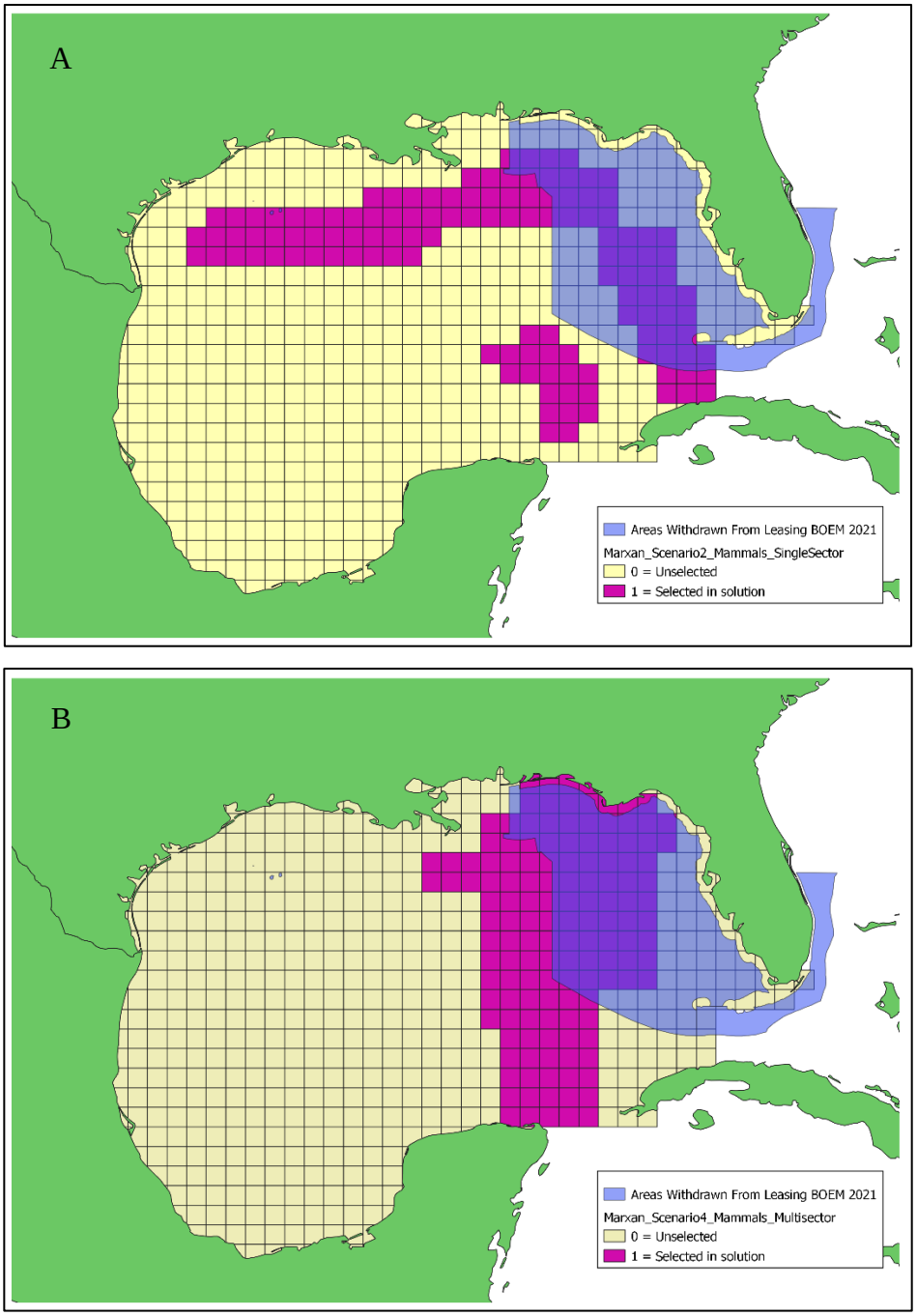

Figure 5.15 Mammal Scenario 4 solution mapped with the Congressional Moratorium Boundaries for the Congressional Moratorium on oil/gas/mineral leasing off the gulf coast of Florida extended by Presidential proclamation until June 30, 2032
Boundary for the Congressional Moratorium (Geospatial Services Division, Department of Interior - Bureau of Ocean Energy Management - Office of Strategic Resources, 2021) mapped with mammal "hot-spot" networks identified in Scenarios 2 (A) and 4 (B).

Chapter 6: Conclusions

The main objectives of this study are to spatially quantify offshore marine resources and to explore the utility of these spatial distributions in identifying individual locations and/or networks of "hot-spot" locations which are particularly vulnerable to negative effects of oil exposure in the event of an oil spill. The identified locations can be used in the decision-making process in prioritizing areas for oil spill response, for the initial siting process for oil production facilities (e.g., reserving highly sensitive areas), and for justification to open or maintain current areas withdrawn from oil production (e.g., areas withdrawn from oil/gas/mineral leasing off the gulf coast of Florida under Congressional Moratorium until 2032).

In Chapter 3, spatial distributions of marine resources from multiple sources with different resolutions, scales, and measurements were scaled and/or transformed to an index to represent gridded proportions of the occurrence of each resource. These gridded resource maps were then concatenated to create multiple Cumulative Environmental Sensitivity Indices (C-ESIs). This chapter demonstrated the methodology for adding weights to certain resources (e.g., species or fisheries of special concern) within the C-ESI based on species-specific vulnerability provided by a separate vulnerability index (Polidoro et al. 2021; Woodyard et al. 2022). This chapter also illustrated the use of dissimilarity measures and clustering to provide input on which pairs or groups of resources might be spatially correlated. Hot-spot areas of combined sensitivity were identified by the C-ESIs particularly along the continental slope.

In Chapter 4, the maximum daily oil concentration (MDOC) was calculated for each cell in the 0.02°x0.02° latitude/longitude grid in the upper 20 m of the water column for four hypothetical oil well blowout scenarios in the Gulf of Mexico. The four oil well blowout scenarios were modelled using the Connectivity Modeling System (CMS; Paris et al. 2013) with two start dates and three origin locations and with depth and duration of oil release comparable to the DWH event. As PAH toxicity to biological resources and fishery closures are generally defined by exceeding a set threshold, GIS polygons were drawn around all grid cells with MDOC values equal to or exceeding a defined minimum oil concentration threshold (MOCT). These MOCT polygons represent contiguous areas which were likely exposed to at least the MOCT for at least one day and covered a range of oil concentrations. Intersections were then calculated between each MOCT polygon and C-ESI to find the Cumulative Impact Value (CIP). Intersections were also calculated between each MOCT polygon and resource layer to find the Resource Impact Value (RIP). These intersections represent the proportion of the C-ESI value or resource value exposed to at least the MOCT for at least one day. The results from Chapter 4 suggest that of the four modeled oil well blowouts included in this study, the blowout occurring on the West Florida Shelf would have had the largest impact on the suite of C-ESIs. The modeled oil spill scenarios indicated that while a spill off the continental shelf near Texas would have the smallest overall footprint, it would affect fisheries more severely than two simulated spills near DWH (spring and autumn) and a spill in the eastern Gulf.

Marine organisms experience lethal and sublethal impacts from oil exposure over a wide spectrum of oil concentrations. Species-specific toxicity endpoints are determined through toxicity experiments and are generally defined by both the concentration and duration of the exposure. For protected species, toxicity experiments generally cannot be performed and must

be estimated from observations after an oil spill. While the MOCT polygons are based on a one-day duration and cover a wide range of oil concentrations, polygons could be customized for target species by changing both the MOCT concentration and the duration of the exposure used to make the polygon. If estimating impacts to Bluefin tuna in the event of an oil spill, an MOCT of 50 ppb might be the most useful for a spill occurring in April (like DWH) since Bluefin tuna primarily spawn during April to May and their larvae begin to experience cardiological defects at 0.3 μg L–1 ΣPAH (Incardona et al. 2014). If an oil spill occurred in September, like the Fall scenario, an MOCT of 250 ppb might be more useful, as Bluefin tuna larvae would likely not be present and adult fish species begin to display reduced swimming and aerobic capabilities only at these higher PAH concentrations (Stieglitz et al. 2016; Esbaugh et al. 2016; Table 4.5).

Chapter 5 demonstrated how the C-ESIs developed in Chapter 3 might be used to identify siting opportunities that would maximize benefit to both the oil production sector and the conservation of resources through the development of quantifiably explicit tradeoff functions between oil production and the resources included in the C-ESIs. Oil and natural gas production for 2018 by oil well and location was used to create a 0.5°x0.5° latitude/longitude resolution grid of the 2018 oil production (BOEM Offshore Statistics by Water Depth; BOEM. 2018b). The oil production grid was converted to proportion of oil production and directly compared at the grid cell level to the resource layers and C-ESIs. The value of each grid cell to each sector could then be explicitly compared. A multi-sector marine spatial planning approach was used to rank grid cells based on their total benefit to the system consisting of two sectors: oil production and resource conservation. The ranked grid cells are then mapped to create tradeoff curves. The (x, y) points on the tradeoff curves then represent theoretical allocations of grid cells to oil production or reservation from oil production such that Y% of the oil production is conserved

and X% of the resource value in the C-ESI is conserved. These tradeoff curves were able to identify grid cells with low oil production and high resource sensitivity that should potentially be reserved from oil production as their exclusion from oil production would have a minimal negative impact on the oil production sector as a whole and are identified as important to resources by the C-ESI. Chapter 5 also demonstrated the use of the C-ESIs created in Chapter 3 to build a minimum set "hot-spot" network using the marine spatial planning (MSP) software, Marxan. The Marxan solver creates a minimum-set solution of grid cells by minimizing the cost (defined by a cost layer) while conserving a set percentage of each included resource (called features). By using the resource layers created in Chapter 3 as the feature files and the oil production grid created in Chapter 5 as an optional cost layer, this study created two "hot-spot" networks for both the Fisheries C-ESI and the Mammals C-ESI representing a hypothetical pristine environment for which oil production is being considered (grid cell cost is uniform) and for the current production environment (grid cell cost is based on the 2018 oil production grid). The pristine network represents groupings of grid cells that are potentially most important to protect in a hypothetical environment where no drilling is currently occurring and siting facilities are being considered, while the current production network represents the most important grid cells to protect in a system which has already allocated some grid cells to oil production. For both scenarios, the current production "hot-spot" network resulted in increased number and frequency of grid cells in the WFS that were selected as part of the minimum-set "hot-spot" network. These WFS grid cells identified as part of the "hot-spot" network overlap with the areas currently protected and withdrawn from oil leasing/production under the 2021 Congressional Moratorium with 39.5% of the pristine mammal "hot-spot" network and 53.2% of the current production mammal "hot-spot" network being located within the withdrawn areas.

This overlap indicates that these WFS grid cells are important to include in a hypothetical reserve created to conserve environmental sensitivity in a hypothetical pristine GoM where oil production siting is being considered. The importance of these WFS grid cells increases when considering a hypothetical reserve created to conserve environmental sensitivity in a GoM where some areas are already set aside for oil production (i.e., the current environment). Therefore, in the current oil production environment, the current areas withdrawn under the 2021 Congressional moratorium serve as a reserve to conserve this environmental sensitivity. The "hot-spot" networks identified in this study can potentially be utilized in the decision-making regarding the continued closure of these withdrawn areas.

The integrated collection of methods presented here are designed to add to the crucial knowledge base for planning and prioritizing oil spill response, predicting impacts from an oil spill to individual resources and groups of resources, and to assist in the decision-making process for making new and existing sites available to oil production.

References

Adler, E., Inbar, M., 2007. Shoreline sensitivity to oil spills, the Mediterranean coast of Israel: Assessment and analysis. Ocean & Coastal Management 50, 24–34. https://doi.org/10.1016/j.ocecoaman.2006.08.016

Alves, T.M., Kokinou, E., Zodiatis, G., 2014. A three-step model to assess shoreline and offshore susceptibility to oil spills: The South Aegean (Crete) as an analogue for confined marine basins. Marine Pollution Bulletin 86, 443–457. https://doi.org/10.1016/j.marpolbul.2014.06.034

Antonio, F.J., Mendes, R.S., Thomaz, S.M., 2011. Identifying and modeling patterns of tetrapod vertebrate mortality rates in the Gulf of Mexico oil spill. Aquatic Toxicology 105, 177–179. https://doi.org/10.1016/j.aquatox.2011.05.022

ArcMap (version 10.5. 1), 2016. Software. Redlands, CA: Esri Inc, 2016.

Ball, I.R., Possingham, H.P., Watts, M., 2009. Marxan and Relatives: Software for Spatial Conservation Prioritization. Oxford University Press.

Bejarano, A.C., Barron, M.G., 2014. Development and practical application of petroleum and dispersant interspecies correlation models for aquatic species. Environmental science & technology 48, 4564–4572.

Bejarano, A.C., Barron, M.G., 2016. Aqueous and tissue residue-based interspecies correlation estimation models provide conservative hazard estimates for aromatic compounds. Environmental Toxicology and Chemistry 35, 56–64.

Bejarano, A.C., Mearns, A.J., 2015. Improving environmental assessments by integrating Species Sensitivity Distributions into environmental modeling: Examples with two hypothetical oil spills. Marine Pollution Bulletin 93, 172–182.

Bejarano, A.C., Wheeler, J.R., 2020. Scientific basis for expanding the use of Interspecies Correlation Estimation models. Integrated Environmental Assessment and Management 16, 528–530.

Berenshtein, I., Perlin, N., Ainsworth, C.H., Ortega-Ortiz, J.G., Vaz, A.C., Paris, C.B., 2020a. Comparison of the Spatial Extent, Impacts to Shorelines, and Ecosystem and Four-Dimensional Characteristics of Simulated Oil Spills, in: Murawski, S.A., Ainsworth, C.H., Gilbert, S., Hollander, D.J., Paris, C.B., Schlüter, M., Wetzel, D.L. (Eds.), Scenarios and Responses to Future Deep Oil Spills: Fighting the Next War. Springer International Publishing, Cham, pp. 340–354. https://doi.org/10.1007/978-3-030-12963-7_20

Berenshtein, I., Perlin, N., Murawski, S.A., Joye, S.B., Paris, C.B., 2020b. Evaluating the Effectiveness of Fishery Closures for Deep Oil Spills Using a Four-Dimensional Model, in: Murawski, S.A., Ainsworth, C.H., Gilbert, S., Hollander, D.J., Paris, C.B., Schlüter, M., Wetzel, D.L. (Eds.), Scenarios and Responses to Future Deep Oil Spills: Fighting the Next War. Springer International Publishing, Cham, pp. 390–402. https://doi.org/10.1007/978-3-030-12963-7_23

Bureau of Ocean Energy Management (BOEM). 2018a. 2019-2024 National Outer Continental Shelf Oil and Gas Leasing Draft Proposed Program. Available online: https://www.boem.gov/NP-Draft-Proposed-Program-2019-2024 380 pp.
Bureau of Ocean Energy Management (BOEM). 2018b. Bureau of Ocean Energy Management Offshore Statistics by Water Depth. Available online: https://www.data.bsee.gov/Leasing/OffshoreStatsbyWD/Default.aspx
Bureau of Ocean Energy Management (BOEM). 2021. Gulf of Mexico Energy Security Act (GOMESA) Available online: https://www.boem.gov/oil-gas-energy/energy-economics/gulf-mexico-energy-security-act-gomesa (accessed 7.16.22).
Brill, E.D., 1979. The Use of Optimization Models in Public-Sector Planning. Management Science 25, 413–422. https://doi.org/10.1287/mnsc.25.5.413
Carls, M.G., Rice, S.D., Hose, J.E., 1999. Sensitivity of fish embryos to weathered crude oil: Part I. Low-level exposure during incubation causes malformations, genetic damage, and mortality in larval pacific herring (Clupea pallasi). Environmental Toxicology and Chemistry 18, 481–493. https://doi.org/10.1002/etc.5620180317
Carmichael, R.H., Graham, W.M., Aven, A., Worthy, G., Howden, S., 2012. Were Multiple Stressors a 'Perfect Storm' for Northern Gulf of Mexico Bottlenose Dolphins (Tursiops truncatus) in 2011? PLOS ONE 7, e41155. https://doi.org/10.1371/journal.pone.0041155
Carmona, S.L., Gherardi, D.F.M., Tessler, M.G., 2006. Environment Sensitivity Mapping and Vulnerability Modeling for Oil Spill Response along the São Paulo State Coastline. Journal of Coastal Research 1455–1458.
Castanedo, S., Pombo, C., Fernandez, F., Medina, R., Puente, A., Juanes, J.A., 2008. Oil spill vulnerability atlas for the Cantabrian Coast (Bay of Biscay, Spain). International Oil Spill Conference Proceedings 2008, 137–144. https://doi.org/10.7901/2169-3358-2008-1-137
Chancellor, E., 2015. Vulnerability of larval fish populations to oil well blowouts in the Northern Gulf of Mexico. (Unpublished master's thesis). College of Marine Science, University of South Florida, Saint Petersburg, FL
Chancellor, E., Murawski, S.A., Paris, C.B., Perruso, L., Perlin, N., 2020. Comparative environmental sensitivity of offshore Gulf of Mexico waters potentially impacted by ultra-deep oil well blowouts, in: Scenarios and Responses to Future Deep Oil Spills. Springer, pp. 443–466.
Chen, Y., 2017. Fish resources of the Gulf of Mexico, in: Habitats and Biota of the Gulf of Mexico: Before the Deepwater Horizon Oil Spill. Springer, pp. 869–1038.
Computer generated distribution maps for *Caretta caretta* (Loggerhead sea turtle), with modelled year 2050 native range map based on IPCC RCP8.5 emissions scenario. www.aquamaps.org, version 10/2019 preliminary version. Accessed 10 Jun. 2020.
Computer generated distribution maps for *Ceratoscopelus warmingii* (Warmingii's lanternfish), with modelled year 2050 native range map based on IPCC RCP8.5 emissions scenario. www.aquamaps.org, version 10/2019 preliminary version. Accessed 9 Jun. 2020
Computer generated distribution maps for *Coryphaena hippurus* (Common dolphinfish), with modelled year 2050 native range map based on IPCC RCP8.5 emissions scenario. www.aquamaps.org, version 10/2019 preliminary version. Accessed 16 Jun. 2020
Computer generated distribution maps for *Dermochelys coriacea* (Leatherback sea turtle), with modelled year 2050 native range map based on IPCC RCP8.5 emissions scenario. www.aquamaps.org, version 10/2019 preliminary version. Accessed 10 Jun. 2020.

Computer generated distribution maps for *Epinephelus morio* (Red grouper), with modelled year 2050 native range map based on IPCC RCP8.5 emissions scenario. www.aquamaps.org, version 10/2019 preliminary version. Accessed 9 Jun. 2020

Computer generated distribution maps for *Eretmochelys imbricata* (Hawksbill sea turtle), with modelled year 2050 native range map based on IPCC RCP8.5 emissions scenario. www.aquamaps.org, version 10/2019 preliminary version. Accessed 10 Jun. 2020.

Computer generated distribution maps for *Feresa attenuate* (Pygmy killer whale), with modelled year 2050 native range map based on IPCC RCP8.5 emissions scenario. www.aquamaps.org, version 10/2019 preliminary version. Accessed 9 Jun. 2020.

Computer generated distribution maps for *Istiophorus albicans* (Atlantic sailfish), with modelled year 2050 native range map based on IPCC RCP8.5 emissions scenario. www.aquamaps.org, version 10/2019 preliminary version. Accessed 9 Jun. 2020

Computer generated distribution maps for *Lepidochelys kempii* (Kemp's Ridley sea turtle), with modelled year 2050 native range map based on IPCC RCP8.5 emissions scenario. www.aquamaps.org, version 10/2019 preliminary version. Accessed 10 Jun. 2020.

Computer generated distribution maps for *Lopholatilus chamaeleonticeps* (Great northern tilefish), with modelled year 2050 native range map based on IPCC RCP8.5 emissions scenario. www.aquamaps.org, version 10/2019 preliminary version. Accessed 10 Jun. 2020.

Computer generated distribution maps for *Lutjanus campechanus* (Red snapper), with modelled year 2050 native range map based on IPCC RCP8.5 emissions scenario. www.aquamaps.org, version 10/2019 preliminary version. Accessed 9 Jun. 2020

Computer generated distribution maps for *Makaira nigricans* (Blue marlin), with modelled year 2050 native range map based on IPCC RCP8.5 emissions scenario. www.aquamaps.org, version 10/2019 preliminary version. Accessed 9 Jun. 2020.

Computer generated distribution maps for *Mugil cephalus* (Striped mullet), with modelled year 2050 native range map based on IPCC RCP8.5 emissions scenario. www.aquamaps.org, version 10/2019 preliminary version. Accessed 9 Jun. 2020

Computer generated distribution maps for *Physeter macrocephalus* (Sperm whale), with modelled year 2050 native range map based on IPCC RCP8.5 emissions scenario. www.aquamaps.org, version 10/2019 preliminary version. Accessed 9 Jun. 2020.

Computer generated distribution maps for *Pseudora crassidens* (False killer whale), with modelled year 2050 native range map based on IPCC RCP8.5 emissions scenario. www.aquamaps.org, version 10/2019 preliminary version. Accessed 9 Jun. 2020.

Computer generated distribution maps for *Sciaenops ocellatus* (Red drum), with modelled year 2050 native range map based on IPCC RCP8.5 emissions scenario. www.aquamaps.org, version 10/2019 preliminary version. Accessed 10 Jun. 2020.

Computer generated distribution maps for *Scomberomorus cavalla* (King mackerel), with modelled year 2050 native range map based on IPCC RCP8.5 emissions scenario. www.aquamaps.org, version 10/2019 preliminary version. Accessed 10 Jun. 2020.

Computer generated distribution maps for *Seriola dumerili* (Greater amberjack), with modelled year 2050 native range map based on IPCC RCP8.5 emissions scenario. www.aquamaps.org, version 10/2019 preliminary version. Accessed 16 Jun. 2020.

Computer generated distribution maps for *Stenella attenuate* (Pantropical spotted dolphin), with modelled year 2050 native range map based on IPCC RCP8.5 emissions scenario. www.aquamaps.org, version 10/2019 preliminary version. Accessed 9 Jun. 2020.

Computer generated distribution maps for *Stenella frontalis* (Atlantic spotted dolphin), with modelled year 2050 native range map based on IPCC RCP8.5 emissions scenario. www.aquamaps.org, version 10/2019 preliminary version. Accessed 9 Jun. 2020.
Computer generated distribution maps for *Thunnus thynnus* (Atlantic bluefin tuna), with modelled year 2050 native range map based on IPCC RCP8.5 emissions scenario. www.aquamaps.org, version 10/2019 preliminary version. Accessed 9 Jun. 2020
Computer generated distribution maps for *Tursiops truncates* (Bottlenose dolphin), with modelled year 2050 native range map based on IPCC RCP8.5 emissions scenario. www.aquamaps.org, version 10/2019 preliminary version. Accessed 9 Jun. 2020.
Computer generated distribution maps for *Xiphias gladius* (Atlantic swordfish), with modelled year 2050 native range map based on IPCC RCP8.5 emissions scenario. www.aquamaps.org, version 10/2019 preliminary version. Accessed 9 Jun. 2020
Computer Generated Richness Map for Actinopterygii. www.aquamaps.org, version Oct. 2019. Web. Accessed 17 Jul. 2020.
Map generated 2020-07-13.
Computer Generated Richness Map for Elasmobranchii. www.aquamaps.org, version Oct. 2019. Web. Accessed 17 Jul. 2020.
Map generated 2020-07-13
Computer Generated Richness Map for Mammalia. www.aquamaps.org, version Oct. 2019. Web. Accessed 17 Jul. 2020.
Map generated 2020-07-13.
Curtis, F.A., Molnar, G.S., 1997. A municipal infrastructure management systems model. Canadian Journal of Civil Engineering 24, 1040.
De Guise, S., Levin, M., Gebhard, E., Jasperse, L., Hart, L.B., Smith, C.R., Venn-Watson, S., Townsend, F., Wells, R., Balmer, B., 2017. Changes in immune functions in bottlenose dolphins in the northern Gulf of Mexico associated with the Deepwater Horizon oil spill. Endangered Species Research 33, 291–303.
Dias, L.A., Litz, J., Garrison, L., Martinez, A., Barry, K., Speakman, T., 2017. Exposure of cetaceans to petroleum products following the Deepwater Horizon oil spill in the Gulf of Mexico. Endangered Species Research 33, 119–125.
DOI, 2018. Secretary Zinke Announces Plan for Unleashing America's Offshore Oil and Gas Potential [WWW Document]. URL https://www.doi.gov/pressreleases/secretary-zinke-announces-plan-unleashing-americas-offshore-oil-and-gas-potential (accessed 10.1.18).
Drexler, M., Ainsworth, C.H., 2013. Generalized Additive Models Used to Predict Species Abundance in the Gulf of Mexico: An Ecosystem Modeling Tool. PLOS ONE 8, e64458. https://doi.org/10.1371/journal.pone.0064458
Edgar, G.J., Russ, G.R., Babcock, R.C., 2007. Marine protected areas. Marine ecology 27, 533–555.
Elith, J., Leathwick, J.R., 2009. Species distribution models: ecological explanation and prediction across space and time. Annual review of ecology, evolution, and systematics 40, 677–697.
Energy Information Administration (EIA). 2018. Energy Information Administration Gulf of Mexico Fact Sheet. Available online: https://www.eia.gov/special/gulf_of_mexico/ (accessed on October 2018).

Energy Information Administration (EIA). 2021. Energy Information Administration Gulf of Mexico Fact Sheet. Available online: https://www.eia.gov/energyexplained/oil-and-petroleum-products/offshore-oil-and-gas-in-depth.php (accessed on June 2022).
Esbaugh, A.J., Mager, E.M., Stieglitz, J.D., Hoenig, R., Brown, T.L., French, B.L., Linbo, T.L., Lay, C., Forth, H., Scholz, N.L., 2016. The effects of weathering and chemical dispersion on Deepwater Horizon crude oil toxicity to mahi-mahi (Coryphaena hippurus) early life stages. Science of the Total Environment 543, 644–651.
Etnoyer, P.J., Wickes, L.N., Silva, M., Dubick, J.D., Balthis, L., Salgado, E., MacDonald, I.R., 2016. Decline in condition of gorgonian octocorals on mesophotic reefs in the northern Gulf of Mexico: before and after the Deepwater Horizon oil spill. Coral Reefs 35, 77–90.
Executive Office of Energy and Environmental Affairs (EEA). 2009. Draft Massachusetts Ocean Management Plan (Executive Office of Energy and Environmental Affairs, Commonwealth of Massachusetts, Boston) Vol 1, pp 1–140.
Fattal, P., Maanan, M., Tillier, I., Rollo, N., Robin, M., Pottier, P., 2010. Coastal vulnerability to oil spill pollution: the case of Noirmoutier Island (France). Journal of Coastal Research 26, 879–887.
Feeny, D., Furlong, W., Torrance, G.W., Goldsmith, C.H., Zhu, Z., DePauw, S., Denton, M., Boyle, M., 2002. Multiattribute and single-attribute utility functions for the health utilities index mark 3 system. Medical care 40, 113–128.
Felder, D.L., Camp, D.K., Tunnell Jr, J.W., 2009. An introduction to Gulf of Mexico biodiversity assessment. Gulf of Mexico origin, waters, and biota 1, 1–13.
Fernandes, L., Day, J.O.N., Lewis, A., Slegers, S., Kerrigan, B., Breen, D.A.N., Cameron, D., Jago, B., Hall, J., Lowe, D., 2005. Establishing representative no-take areas in the Great Barrier Reef: large-scale implementation of theory on marine protected areas. Conservation biology 19, 1733–1744.
Ferreira, L., 1997. Planning Australian freight rail operations: an overview. Transportation Research part A: Policy and practice 31, 335–348.
Flanders Marine Institute (2018). IHO Sea Areas, version 3. Available online at https://www.marineregions.org/ https://doi.org/10.14284/323
Frasier, K.E., 2020. Evaluating Impacts of Deep Oil Spills on Oceanic Marine Mammals, in: Murawski, S.A., Ainsworth, C.H., Gilbert, S., Hollander, D.J., Paris, C.B., Schlüter, M., Wetzel, D.L. (Eds.), Scenarios and Responses to Future Deep Oil Spills: Fighting the Next War. Springer International Publishing, Cham, pp. 419–441. https://doi.org/10.1007/978-3-030-12963-7_25
Friedland, K.D., Stock, C., Drinkwater, K.F., Link, J.S., Leaf, R.T., Shank, B.V., Rose, J.M., Pilskaln, C.H., Fogarty, M.J., 2012. Pathways between primary production and fisheries yields of large marine ecosystems. PloS one 7, e28945.
Geospatial Services Division, Department of Interior - Bureau of Ocean Energy Management - Office of Strategic Resources, Office Chief, 2021. BOEM Outer Continental Shelf Areas Withdrawn from Leasing [WWW Document]. URL https://metadata.boem.gov/geospatial/BOEM_OCS_Areas_Withdrawn_from_leasing_2021.xml
GRASS Development Team, 2020. Geographic Resources Analysis Support System (GRASS) Software, Version 7.6.1
Guikema, S.D., Milke, M.W., 2003. Sensitivity analysis for multi-attribute project selection problems. Civil Engineering and Environmental Systems 20, 143–162.

Henriques, N.S., Monteiro, P., Bentes, L., Oliveira, F., Afonso, C.M., Gonçalves, J.M., 2017. Marxan as a zoning tool for development and economic purposed areas-Aquaculture Management Areas (AMAs). Ocean & Coastal Management 141, 90–97.
Hicken, C.E., Linbo, T.L., Baldwin, D.H., Willis, M.L., Myers, M.S., Holland, L., Larsen, M., Stekoll, M.S., Rice, S.D., Collier, T.K., 2011. Sublethal exposure to crude oil during embryonic development alters cardiac morphology and reduces aerobic capacity in adult fish. Proceedings of the National Academy of Sciences 108, 7086–7090.
Huber, G.P., 1974. Multi-attribute utility models: A review of field and field-like studies. Management science 20, 1393–1402.
Incardona, J.P., Collier, T.K., Scholz, N.L., 2004. Defects in cardiac function precede morphological abnormalities in fish embryos exposed to polycyclic aromatic hydrocarbons. Toxicology and applied pharmacology 196, 191–205.
Incardona, J.P., Gardner, L.D., Linbo, T.L., Brown, T.L., Esbaugh, A.J., Mager, E.M., Stieglitz, J.D., French, B.L., Labenia, J.S., Laetz, C.A., 2014. Deepwater Horizon crude oil impacts the developing hearts of large predatory pelagic fish. Proceedings of the National Academy of Sciences 111, E1510–E1518.
Incardona, J.P., Swarts, T.L., Edmunds, R.C., Linbo, T.L., Aquilina-Beck, A., Sloan, C.A., Gardner, L.D., Block, B.A., Scholz, N.L., 2013. Exxon Valdez to Deepwater Horizon: comparable toxicity of both crude oils to fish early life stages. Aquatic toxicology 142, 303–316.
Jenkins, M.E., Naftel, H., 2022. Public Interest Comment: Interagency Efforts to Develop the American Conservation and Stewardship Atlas. The Center for Growth and Opportunity.
Jensen, J.R., Halls, J.N., Michel, J., 1998. A systems approach to Environmental Sensitivity Index (ESI) mapping for oil spill contingency planning and response. Photogrammetric Engineering and Remote Sensing 64, 1003–1014.
Jensen, J.R., RAMSEY III, E.W., Holmes, J.M., Michel, J.E., Savitsky, B., Davis, B.A., 1990. Environmental sensitivity index (ESI) mapping for oil spills using remote sensing and geographic information system technology. International Journal of Geographical Information System 4, 181–201.
Kankara, R.S., Subramanian, B.R., 2007. Oil Spill Sensitivity Analysis and Risk Assessment for Gulf of Kachchh, India, using Integrated Modeling. coas 23, 1251–1258. https://doi.org/10.2112/04-0362.1
Kankara, R.S., Arockiaraj, S., Prabhu, K., 2016. Environmental sensitivity mapping and risk assessment for oil spill along the Chennai Coast in India. Marine Pollution Bulletin 106, 95–103. https://doi.org/10.1016/j.marpolbul.2016.03.022
Kaschner, K., Kesner-Reyes, K., Garilao, C., Rius-Barile, J., Rees, T., Froese, R., 2010. Predicted range maps for aquatic species.
Kassomenos, P.A., 2004. Risk analysis for environmental hazards: the case of oil spills, in Crete. Global Nest: the International Journal 6, 39–51.
Kazanis, E., Maclay, D., Shepard, N., 2015. Estimated oil and gas reserves Gulf of Mexico OCS region December 31, 2013. Bureau of Ocean Energy Management (BOEM) report.
Khiali-Miab, A., Grêt-Regamey, A., Axhausen, K.W., van Strien, M.J., 2022. A network optimisation approach to identify trade-offs between socio-economic and ecological objectives for regional integrated planning. City and Environment Interactions 13, 100078. https://doi.org/10.1016/j.cacint.2021.100078

Kinlan, B.P., Winship, A.J., White, T.P., Christensen, J., 2016. Modeling at-sea occurrence and abundance of marine birds to support Atlantic marine renewable energy planning: Phase I report.
Knudsen R, Druyor R (2009) USCG Sector St Petersburg - Digital Area Contingency Plan for Oil Spill Response. C. f. S. Analysis. St Petersburg, Florida, Florida Fish and Wildlife Conservation Commission - Fish and Wildlife Research Institute.
Kobayashi, D.R., Polovina, J.J., 2005. Evaluation of time-area closures to reduce incidental sea turtle take in the Hawaii-based longline fishery: generalized additive model (GAM) development and retrospective examination.
Kozanidis, G., 2009. Solving the linear multiple choice knapsack problem with two objectives: profit and equity. Computational Optimization and Applications 43, 261–294.
Kubiak, L. 2020. Why the world must commit to protecting 30 percent of the planet by 2030 (30X30). *Natl. Resour. Def. Counc (NRDC)*.
Lan, D., Liang, B., Bao, C., Ma, M., Xu, Y., Yu, C., 2015. Marine oil spill risk mapping for accidental pollution and its application in a coastal city. Marine pollution bulletin 96, 220–225.
Lane, S.M., Smith, C.R., Mitchell, J., Balmer, B.C., Barry, K.P., McDonald, T., Mori, C.S., Rosel, P.E., Rowles, T.K., Speakman, T.R., 2015. Reproductive outcome and survival of common bottlenose dolphins sampled in Barataria Bay, Louisiana, USA, following the Deepwater Horizon oil spill. Proceedings of the Royal Society B: Biological Sciences 282, 20151944.
Lee, M., Jung, J.-Y., 2015. Pollution risk assessment of oil spill accidents in Garorim Bay of Korea. Marine Pollution Bulletin 100, 297–303.
Lyczkowski-Shultz, J., Hanisko, D.S., Sulak, K.J., Konieczna, M., Bond, P.J., 2013. Characterization of ichthyoplankton in the northeastern Gulf of Mexico from SEAMAP plankton surveys, 1982-1999. Gulf and Caribbean Research 25, 43–98.
Mager, E.M., Esbaugh, A.J., Stieglitz, J.D., Hoenig, R., Bodinier, C., Incardona, J.P., Scholz, N.L., Benetti, D.D., Grosell, M., 2014. Acute embryonic or juvenile exposure to Deepwater Horizon crude oil impairs the swimming performance of mahi-mahi (Coryphaena hippurus). Environmental science & technology 48, 7053–7061.
Maitieg, A., Lynch, K., Johnson, M., 2018. Coastal resources spatial planning and potential oil risk analysis: case study of Misratah's coastal resources, Libya, in: 19th International Conference on Geography and Environmental Studies. Https://Www. Researchgate. Net/Publication/323445887_Coastal_Resources_Spatial_Planning_and_Potential_Oil_Risk_Analysis_Case_Study_of_Misratah% 27s_Coastal_Resources_Libya.
Marsili, L., Caruso, A., Fossi, M.C., Zanardelli, M., Politi, E., Focardi, S., 2001. Polycyclic aromatic hydrocarbons (PAHs) in subcutaneous biopsies of Mediterranean cetaceans. Chemosphere 44, 147–154.
Martello, S., Toth, P., 1990. Knapsack problems: algorithms and computer implementations. John Wiley & Sons, Inc.
Matisziw, T.C., Grubesic, T.H., 2013. Geographic perspectives on vulnerability analysis. GeoJournal 78, 205–207. https://doi.org/10.1007/s10708-011-9420-z
Mccrea-Strub, A., Kleisner, K., Sumaila, U.R., Swartz, W., Watson, R., Zeller, D., Pauly, D., 2011. Potential impact of the Deepwater Horizon oil spill on commercial fisheries in the Gulf of Mexico. Fisheries 36, 332–336.

McLeod, K. L., J. Lubchenco, S. R. Palumbi, and A. A. Rosenberg. 2005. Scientific Consensus Statement on Marine Ecosystem-Based Management. Signed by 217 academic scientists and policy experts with relevant expertise and published by the Communication Partnership for Science and the Sea at http://compassonline.org/?q=EBM.

Moilanen, A., Wilson, K., Possingham, H., 2009. Spatial conservation prioritization: quantitative methods and computational tools. Oxford University Press.

Murawski, S.A., Fogarty, M., Rago, P., Brodziak, J., 2001. Quantitative methods for MPA design, with application to the NE USA. Marine protected areas: design and implementation for conservation and fisheries restoration. Woods Hole Oceanographic Institution 27–29.

Murawski, S.A., Hogarth, W.T., Peebles, E.B., Barbeiri, L., 2014. Prevalence of external skin lesions and polycyclic aromatic hydrocarbon concentrations in Gulf of Mexico fishes, post-Deepwater Horizon. Transactions of the American Fisheries Society 143, 1084–1097.

Murawski, S.A., Hollander, D.J., Gilbert, S., Gracia, A., 2020. Deepwater oil and gas production in the Gulf of Mexico and related global trends, in: Scenarios and Responses to Future Deep Oil Spills. Springer, pp. 16–32.

Murawski, S.A., Kilborn, J.P., Bejarano, A.C., Chagaris, D., Donaldson, D., Hernandez Jr, F.J., MacDonald, T.C., Newton, C., Peebles, E., Robinson, K.L., 2021. A synthesis of Deepwater Horizon impacts on coastal and nearshore living marine resources. Frontiers in Marine Science 7, 1212.

Murawski, S.A., Peebles, E.B., Gracia, A., Tunnell Jr, J.W., Armenteros, M., 2018. Comparative abundance, species composition, and demographics of continental shelf fish assemblages throughout the Gulf of Mexico. Marine and Coastal Fisheries 10, 325–346.

Myers, N., 1988. Threatened biotas:" hot spots" in tropical forests. Environmentalist 8, 187–208.

Myers, N., 1990. The biodiversity challenge: expanded hot-spots analysis. Environmentalist 10, 243–256.

Naidoo, R., Balmford, A., Ferraro, P.J., Polasky, S., Ricketts, T.H., Rouget, M., 2006. Integrating economic costs into conservation planning. Trends in ecology & evolution 21, 681–687.

Neff, J.M., 1988. Composition and fate of petroleum and spill-treating agents in the marine environment. Synthesis of effects of oil on marine mammals.

Nelson, J.R., Grubesic, T.H., 2018. The implications of oil exploration off the Gulf Coast of Florida. Journal of Marine Science and Engineering 6, 30.

Nelson, J.R., Grubesic, T.H., Sim, L., Rose, K., Graham, J., 2015. Approach for assessing coastal vulnerability to oil spills for prevention and readiness using GIS and the Blowout and Spill Occurrence Model. Ocean & Coastal Management 112, 1–11.

Niedoroda A, Davis S, Bowen M, Nestler E, Rowe J, Balouskus R, Schroeder M, Gallaway B, Fechhelm R (2014) A Method for the Evaluation of the Relative Environmental Sensitivity and Marine Productivity of the Outer Continental Shelf. Prepared by URS Group, Inc., Normandeau Associates, Inc., RPS ASA, and LGL Ecological Research Associates, Inc. for the U.S. Department of the Interior, Bureau of Ocean Energy Management. Herndon, VA OCS Study BOEM 616. 80 pp. + appendices

Nilsen, E., 2021. Biden administration reopens oil and gas leasing in the Gulf of Mexico - CNNPolitics [WWW Document]. URL https://www.cnn.com/2021/11/17/politics/biden-oil-gas-leasing-gulf-of-mexico-climate/index.html (accessed 5.22.22a).

Nilsen, E., 2022. Federal judge cancel oil and gas leases in Gulf of Mexico citing climate crisis - CNNPolitics [WWW Document]. URL https://www.cnn.com/2022/01/27/politics/judge-cancels-oil-gas-leases-gulf-of-mexico-climate/index.html (accessed 5.22.22b).

NOAA, 2020. National Database for Deep-Sea Corals and Sponges (version 02005120). https://deepseacoraldata.noaa.gov/; NOAA Deep Sea Coral Research & Technology Program.

NOAA, 2018. Office of Response and Restoration. Environmental Sensitivity Index (ESI) Maps https://response.restoration.noaa.gov/maps-and-spatial-data/environmental-sensitivity-index-esi-maps.html. Accessed October 2018

Olita, A., Cucco, A., Simeone, S., Ribotti, A., Fazioli, L., Sorgente, B., Sorgente, R., 2012. Oil spill hazard and risk assessment for the shorelines of a Mediterranean coastal archipelago. Ocean & Coastal Management 57, 44–52.

Orr, R., Hammerle, K., Frye, M., 2018. Development of the 2019-2024 National Oil and Gas Leasing Program on the United States Outer Continental Shelf. Presented at the 2018 AAPG International Conference and Exhibition.

Paris, C.B., Helgers, J., Van Sebille, E., Srinivasan, A., 2013. Connectivity Modeling System: A probabilistic modeling tool for the multi-scale tracking of biotic and abiotic variability in the ocean. Environmental Modelling & Software 42, 47–54.

Paris, C.B., Hénaff, M.L., Aman, Z.M., Subramaniam, A., Helgers, J., Wang, D.-P., Kourafalou, V.H., Srinivasan, A., 2012. Evolution of the Macondo well blowout: simulating the effects of the circulation and synthetic dispersants on the subsea oil transport. Environmental science & technology 46, 13293–13302.

Perlin, N., Paris, C.B., Berenshtein, I., Vaz, A.C., Faillettaz, R., Aman, Z.M., Schwing, P.T., Romero, I.C., Schlüter, M., Liese, A., 2020. Far-field modeling of a deep-sea blowout: sensitivity studies of initial conditions, biodegradation, sedimentation, and subsurface dispersant injection on surface slicks and oil plume concentrations, in: Deep Oil Spills. Springer, pp. 170–192.

Peterson, J., 2002. Environmental sensitivity index guidelines: Version 3.0.

Polidoro, B., Matson, C.W., Ottinger, M.A., Renegar, D.A., Romero, I.C., Schlenk, D., Wise Sr, J.P., González, J.B., Bruns, P., Carpenter, K., 2021. A multi-taxonomic framework for assessing relative petrochemical vulnerability of marine biodiversity in the Gulf of Mexico. Science of The Total Environment 763, 142986.

Possingham, H., Ball, I., Andelman, S., 2000. Mathematical methods for identifying representative reserve networks, in: Quantitative Methods for Conservation Biology. Springer, pp. 291–306.

Pulster, E.L., Gracia, A., Snyder, S.M., Romero, I.C., Carr, B., Toro-Farmer, G., Murawski, S.A., 2020. Polycyclic Aromatic Hydrocarbon Baselines in Gulf of Mexico Fishes, in: Murawski, S.A., Ainsworth, C.H., Gilbert, S., Hollander, D.J., Paris, C.B., Schlüter, M., Wetzel, D.L. (Eds.), Scenarios and Responses to Future Deep Oil Spills: Fighting the Next War. Springer International Publishing, Cham, pp. 253–271. https://doi.org/10.1007/978-3-030-12963-7_15

QGIS Development Team, 2020. QGIS Geographic Information System. Open Source Geospatial Foundation. URL http://qgis.org

QGIS Installers, 2020. URL https://www.qgis.org/en/site/forusers/alldownloads.html

Rebai, S., Azaiez, M.N., Saidane, D., 2012. Sustainable Performance Evaluation of Banks using a Multi-attribute Utility Model: An Application to French Banks. Procedia Economics and Finance, 2nd Annual International Conference on Accounting and Finance (AF 2012) and Qualitative and Quantitative Economics Research (QQE 2012) 2, 363–372. https://doi.org/10.1016/S2212-5671(12)00098-6

Rester, J.K., 2012. SEAMAP Environmental and Biological Atlas of the Gulf of Mexico, 2012. Gulf States Marine Fisheries Commission No. 206.

Romero, A.F., Abessa, D.M.S., Fontes, R.F.C., Silva, G.H., 2013. Integrated assessment for establishing an oil environmental vulnerability map: Case study for the Santos Basin region, Brazil. Marine Pollution Bulletin 74, 156–164. https://doi.org/10.1016/j.marpolbul.2013.07.012

Romero, I., Sutton, T., Carr, B., Quintana-Rizzo, E., Ross, S., Hollander, D., Torres, J., 2018. Decadal Assessment of Polycyclic Aromatic Hydrocarbons in Mesopelagic Fishes from the Gulf of Mexico Reveals Exposure to Oil-Derived Sources. Environmental Science & Technology 52, 10985–10996. https://doi.org/10.1021/acs.est.8b02243

Ruberg, E.J., Elliott, J.E., Williams, T.D., 2021. Review of petroleum toxicity and identifying common endpoints for future research on diluted bitumen toxicity in marine mammals. Ecotoxicology 30, 537–551. https://doi.org/10.1007/s10646-021-02373-x

Salkin, H.M., De Kluyver, C.A., 1975. The knapsack problem: A survey. Naval Research Logistics Quarterly 22, 127–144. https://doi.org/10.1002/nav.3800220110

Sanchirico, J.N., Wilen, J.E., 2005. Optimal spatial management of renewable resources: matching policy scope to ecosystem scale. Journal of Environmental Economics and Management 50, 23–46. https://doi.org/10.1016/j.jeem.2004.11.001

Santos, C., Carvalho, R., Andrade, F., 2013a. Quantitative assessment of the differential coastal vulnerability associated to oil spills. Journal of Coastal Conservation 17, 25–36. https://doi.org/10.1007/s11852-012-0215-2

Santos, C., Michel, J., Neves, M., Janeiro, J., Andrade, F., Orbach, M., 2013b. Marine spatial planning and oil spill risk analysis: Finding common grounds. Marine pollution bulletin 74. https://doi.org/10.1016/j.marpolbul.2013.07.029

Sarrazin, V., Kuhs, V., Kullmann, B., Kreutle, A., Pusch, C., Thiel, R., 2021. A sensitivity-based procedure to select representative fish species for the Marine Strategy Framework Directive indicator development, applied to the Greater North Sea. Ecological Indicators 131, 108161. https://doi.org/10.1016/j.ecolind.2021.108161

Schill, S.R., Raber, G.T., Roberts, J.J., Treml, E.A., Brenner, J., Halpin, P.N., 2015. No Reef Is an Island: Integrating Coral Reef Connectivity Data into the Design of Regional-Scale Marine Protected Area Networks. PLOS ONE 10, e0144199. https://doi.org/10.1371/journal.pone.0144199

Schwacke, L.H., Smith, C.R., Townsend, F.I., Wells, R.S., Hart, L.B., Balmer, B.C., Collier, T.K., De Guise, S., Fry, M.M., Guillette, L.J., Lamb, S.V., Lane, S.M., McFee, W.E., Place, N.J., Tumlin, M.C., Ylitalo, G.M., Zolman, E.S., Rowles, T.K., 2014. Health of common bottlenose dolphins (Tursiops truncatus) in Barataria Bay, Louisiana, following the deepwater horizon oil spill. Environ Sci Technol 48, 93–103. https://doi.org/10.1021/es403610f

Schwartz, M.S., 2020. As Election Nears, Trump Expands Moratorium On Exploratory Drilling In Atlantic. NPR.

Schwing, P.T., Machain-Castillo, M.L., Brooks, G.R., Larson, R.A., Fillingham, J.N., Sanchez-Cabeza, J.A., Ruiz-Fernández, A.C., Hollander, D.J., 2021. Multi-proxy assessment of recent regional-scale events recorded in Southern Gulf of Mexico sediments. Marine Geology 434, 106434. https://doi.org/10.1016/j.margeo.2021.106434

Schwing, P.T., Montagna, P.A., Joye, S.B., Paris, C.B., Cordes, E.E., McClain, C.R., Kilborn, J.P., Murawski, S.A., 2020. A Synthesis of Deep Benthic Faunal Impacts and Resilience Following the Deepwater Horizon Oil Spill. Frontiers in Marine Science 7.

Segan, D.B., Game, E.T., Watts, M.E., Stewart, R.R., Possingham, H.P., 2011. An interoperable decision support tool for conservation planning. Environmental Modelling & Software 26, 1434–1441. https://doi.org/10.1016/j.envsoft.2011.08.002

Serra-Sogas, N., Lieverknecht, L. 2019. Introduction to Marxan. Training Handbook. Pacific Marine Analysis and Research Association. Victoria, Canada

Shepherd, J.G., Garrod, D.J., 1981. Modelling the response of a fishing fleet to changing circumstances, using cautious non-linear optimization. ICES Journal of Marine Science 39, 231–238. https://doi.org/10.1093/icesjms/39.3.231

Sim, L.H., 2013. Blowout and spill occurrence model.

Stieglitz, J.D., Mager, E.M., Hoenig, R.H., Benetti, D.D., Grosell, M., 2016. Impacts of Deepwater Horizon crude oil exposure on adult mahi-mahi (Coryphaena hippurus) swim performance. Environ Toxicol Chem 35, 2613–2622. https://doi.org/10.1002/etc.3436

Sutton, T., Cook, A., Moore, J., Frank, T., Judkins, H., Vecchione, M., Nizinski, M., Youngbluth, M., 2017. Inventory of Gulf oceanic fauna data including species, weight, and measurements. Meg Skansi cruises from Jan. 25 - Sept. 30, 2011 in the Northern Gulf of Mexico. Gulf of Mexico Research Initiative Information and Data Cooperative (GRIIDC). https://doi.org/10.7266/N7VX0DK2

Sutton, T.T., Frank, T., Judkins, H., Romero, I.C., 2020. As Gulf Oil Extraction Goes Deeper, Who Is at Risk? Community Structure, Distribution, and Connectivity of the Deep-Pelagic Fauna, in: Murawski, S.A., Ainsworth, C.H., Gilbert, S., Hollander, D.J., Paris, C.B., Schlüter, M., Wetzel, D.L. (Eds.), Scenarios and Responses to Future Deep Oil Spills: Fighting the Next War. Springer International Publishing, Cham, pp. 403–418. https://doi.org/10.1007/978-3-030-12963-7_24

Szlafsztein, C., Sterr, H., 2007. A GIS-based vulnerability assessment of coastal natural hazards, state of Pará, Brazil. J Coast Conserv 11, 53–66. https://doi.org/10.1007/s11852-007-0003-6

Takeshita, R., Bursian, S.J., Colegrove, K.M., Collier, T.K., Deak, K., Dean, K.M., De Guise, S., DiPinto, L.M., Elferink, C.J., Esbaugh, A.J., Griffitt, R.J., Grosell, M., Harr, K.E., Incardona, J.P., Kwok, R.K., Lipton, J., Mitchelmore, C.L., Morris, J.M., Peters, E.S., Roberts, A.P., Rowles, T.K., Rusiecki, J.A., Schwacke, L.H., Smith, C.R., Wetzel, D.L., Ziccardi, M.H., Hall, A.J., 2021. A review of the toxicology of oil in vertebrates: what we have learned following the Deepwater Horizon oil spill. Journal of Toxicology and Environmental Health, Part B 24, 355–394. https://doi.org/10.1080/10937404.2021.1975182

Tran, T., Yazdanparast, A., Suess, E.A., 2014. Effect of Oil Spill on Birds: A Graphical Assay of the Deepwater Horizon Oil Spill's Impact on Birds. Comput Stat 29, 133–140. https://doi.org/10.1007/s00180-013-0472-z

U.S. Fish and Wildlife Service (2011) Deepwater Horizon Response Consolidated Fish and Wildlife Collection Report. USFWS and NOAA.

Valverde, R.A., Holzwart, K.R., 2017. Sea Turtles of the Gulf of Mexico, in: Ward, C.H. (Ed.), Habitats and Biota of the Gulf of Mexico: Before the Deepwater Horizon Oil Spill: Volume 2: Fish Resources, Fisheries, Sea Turtles, Avian Resources, Marine Mammals, Diseases and Mortalities. Springer, New York, NY, pp. 1189–1351. https://doi.org/10.1007/978-1-4939-3456-0_3

van Breugel, P., 2013. Point coordinates to polygon – part I . Ecostudies - Using Open Source in Ecology and Biodiversity Research [WWW Document]. ECODIV.EARTH. URL https://pvanb.wordpress.com/2013/01/17/point-to-polygon-part-i/

Venn-Watson, S., Colegrove, K.M., Litz, J., Kinsel, M., Terio, K., Saliki, J., Fire, S., Carmichael, R., Chevis, C., Hatchett, W., Pitchford, J., Tumlin, M., Field, C., Smith, S., Ewing, R., Fauquier, D., Lovewell, G., Whitehead, H., Rotstein, D., McFee, W., Fougeres, E., Rowles, T., 2015. Adrenal Gland and Lung Lesions in Gulf of Mexico Common Bottlenose Dolphins (Tursiops truncatus) Found Dead following the Deepwater Horizon Oil Spill. PLOS ONE 10, e0126538. https://doi.org/10.1371/journal.pone.0126538

Waskom, M.L., 2021. seaborn: statistical data visualization. Journal of Open Source Software 6, 3021. https://doi.org/10.21105/joss.03021

Watts, M.E., Ball, I.R., Stewart, R.S., Klein, C.J., Wilson, K., Steinback, C., Lourival, R., Kircher, L., Possingham, H.P., 2009. Marxan with Zones: Software for optimal conservation based land- and sea-use zoning. Environmental Modelling & Software, Special issue on simulation and modelling in the Asia-Pacific region 24, 1513–1521. https://doi.org/10.1016/j.envsoft.2009.06.005

Westerholm, D. A., Rauch III, S. D., 2016. Deepwater Horizon oil spill: Final programmatic damage assessment and restoration plan and final programmatic environmental impact statement.

White, C., Halpern, B., Kappel, C., 2012. Ecosystem service tradeoff analysis reveals the value of marine spatial planning for multiple ocean uses. Proceedings of the National Academy of Sciences of the United States of America 109, 4696–701. https://doi.org/10.1073/pnas.1114215109

White, N.D., Godard-Codding, C., Webb, S.J., Bossart, G.D., Fair, P.A., 2017. Immunotoxic effects of in vitro exposure of dolphin lymphocytes to Louisiana sweet crude oil and Corexit™. Journal of Applied Toxicology 37, 676–682. https://doi.org/10.1002/jat.3414

Williams, R., Gero, S., Bejder, L., Calambokidis, J., Kraus, S.D., Lusseau, D., Read, A.J., Robbins, J., 2011. Underestimating the damage: interpreting cetacean carcass recoveries in the context of the Deepwater Horizon/BP incident. Conservation Letters 4, 228–233. https://doi.org/10.1111/j.1755-263X.2011.00168.x

Woodyard, M., Polidoro, B.A., Matson, C.W., McManamay, R.A., Saul, S., Carpenter, K.E., Collier, T.K., Di Giulio, R., Grubbs, R.D., Linardich, C., Moore, J.A., Romero, I.C., Schlenk, D., Strongin, K., 2022. A comprehensive petrochemical vulnerability index for marine fishes in the Gulf of Mexico. Science of The Total Environment 820, 152892. https://doi.org/10.1016/j.scitotenv.2021.152892

Würsig, B., 2017. Marine Mammals of the Gulf of Mexico, in: Ward, C.H. (Ed.), Habitats and Biota of the Gulf of Mexico: Before the Deepwater Horizon Oil Spill: Volume 2: Fish Resources, Fisheries, Sea Turtles, Avian Resources, Marine Mammals, Diseases and Mortalities. Springer, New York, NY, pp. 1489–1587. https://doi.org/10.1007/978-1-4939-3456-0_5

Yusuf, U., 2018. How to Install Third-party Python Modules in QGIS 3.x [WWW Document]. URL https://youtu.be/94W51WuDKzA

Appendix A: Published Chapter

Comparative environmental sensitivity of offshore Gulf of Mexico waters potentially impacted by ultra-deep oil well blowouts

Chancellor, E., Murawski, S.A., Paris, C.B., Perruso, L., Perlin, N., 2020. Comparative environmental sensitivity of offshore Gulf of Mexico waters potentially impacted by ultra-deep oil well blowouts, in: Scenarios and Responses to Future Deep Oil Spills. Springer, pp. 443–466.

Chapter 26
Comparative Environmental Sensitivity of Offshore Gulf of Mexico Waters Potentially Impacted by Ultra-Deep Oil Well Blowouts

Emily Chancellor, Steven A. Murawski, Claire B. Paris, Larry Perruso, and Natalie Perlin

Abstract Environmental sensitivity indices (ESIs) have long been used to identify coastal and shoreline resources particularly vulnerable to oil spills and ensuing mitigation measures. In the Gulf of Mexico, oil production by the United States and Mexico has increasingly focused on deepwater sources. As oil exploration and production continue further offshore, deepwater and open ocean pelagic resources increasingly become the focus of susceptibility to oil well blowouts. Methodologies are proposed to spatially quantify ESIs specifically for offshore living marine resources. A multi-attribute utility model is proposed to integrate biological resource sensitivity measures and measures of potential economic losses to define spatially explicit environmental sensitivity. Model sensitivity is examined using three weighting schemes for various environmental attributes. The relative environmental sensitivities of four simulated deepwater blowouts in the Gulf of Mexico were analyzed and compared. While differences were found between four oil well blowout scenarios in terms of the overall sensitivity and to the individual attributes, results were relatively insensitive to the weights assigned to various attributes. The uses of ESIs in optimizing oil production locations to minimize potential impacts on sensitive ecological resources and economic uses are discussed.

E. Chancellor (✉) · S. A. Murawski
University of South Florida, College of Marine Science, St. Petersburg, FL, USA
e-mail: echancellor@mail.usf.edu; smurawski@usf.edu

C. B. Paris · N. Perlin
University of Miami, Department of Ocean Sciences, Rosenstiel School of Marine and Atmospheric Science, Miami, FL, USA
e-mail: cparis@rsmas.miami.edu; nperlin@rsmas.miami.edu

L. Perruso
National Marine Fisheries Service, Southeast Fisheries Science Center, Miami, FL, USA
e-mail: larry.perruso@noaa.gov

S. A. Murawski et al. (eds.), *Scenarios and Responses to Future Deep Oil Spills*,
https://doi.org/10.1007/978-3-030-12963-7_26

Keywords Environmental sensitivity indices · ESI · Multi-attribute utility theory · Gulf of Mexico

26.1 Introduction

The Gulf of Mexico (GoM) provides almost all of the offshore oil production in the United States (~97%; EIA 2018) with estimated oil reserves of over 3.67 billion barrels (Kazanis et al. 2015). In the GoM, US and Mexico oil production has increasingly focused on deepwater sources to maintain and increase volumes as these deepwater sources are more productive than shallower fields (i.e., depth has a positive logarithmic relationship with production, Murawski et al. 2020, Fig. 2.5). Additionally, deepwater areas in the eastern GoM that are currently under moratorium for drilling under the GoM Energy Security Act of 2007 (Sissine 2007) have been included in future proposals for oil exploration and production (DOI Press 2018). The significant offshore movement of marine oil and gas production challenges traditional paradigms for habitat and species sensitivity considerations as being purely coastal issues. As oil production drilling continues to move further offshore, offshore marine resources become increasingly susceptible to oil well blowouts.

Potential biological and human use resource losses to coastal areas and shorelines have been estimated by various methods including the use of environmental sensitivity indices (ESIs; Jensen et al. 1990). ESIs for the offshore areas can estimate the potential losses of these offshore marine resources and can serve as valuable input for resource planning for offshore drilling (identification of particularly sensitive areas) and for prioritization of response efforts in the event of future deepwater oil well blowouts.

In this chapter, we explore methodologies to spatially quantify the relative sensitivity of offshore marine resources in the northern GoM using ESIs and illustrate this methodology using a subset of relevant ecological and economic data. A multi-attribute utility model (Huber 1974) is proposed to integrate biological resource sensitivity and economic loss potential to define overall spatial and temporal sensitivity. This chapter outlines methodologies for ESIs, creates a preliminary ESI matrix for the northern GoM based on several biological and economic datasets, and uses these ESIs to compare sensitivities for four simulated deepwater oil well blowouts in the GoM. We outline additional relative ecological datasets and propose optimization modeling approaches to quantify trade-offs between production and environmental protection that may be useful in the oil well siting process.

26.2 History of Environmental Sensitivity Indices in Oil Spill Response

Historically, ESIs have been created to identify environmentally sensitive coastal areas for the prioritization of oil spill cleanup (Jensen et al. 1990, 1998). The National Oceanic and Atmospheric Administration (NOAA) has published guidelines for

creating shoreline ESIs consisting of an index with three components; shoreline type, biological resources, and human uses of resources (Petersen et al. 2002; NOAA Response and Restoration 2018). The shoreline type is classified into one of eight categories based on published NOAA criteria. Biological components include areas with many distinct species, areas of large overall abundance of biological organisms, and areas where vulnerable species are present (e.g., seabirds, turtles, and other endangered species). Human use components include historical sites and public use areas such as parks and recreational beaches. ESIs created under these guidelines are graphical and largely qualitative, as areas are marked as sensitive or not, and can be marked sensitive due to meeting only one of the three above criteria. Sensitive areas defined under this process are not quantitative in the relative sense or necessarily comparable across landscapes.

Site-specific geographic information system (GIS)-based ESIs have been published for much of the shoreline of the United States including the GoM (Knudsen and Druyor 2009; NOAA ORR 2018). Categorical and quantitative ESIs have been created for shoreline sensitivity to offshore spills in many areas and for marine spatial planning specific to locations in the Mediterranean Sea (Kassomenos 2004; Adler and Inbar 2007; Castañedo et al. 2008; Fattal et al. 2010; Santos et al. 2013; Olita et al. 2012; Alves et al. 2014; Maitieg et al. 2018) GoM (Nelson et al. 2015; Nelson and Grubesic 2018), Brazil (Carmona et al. 2004; Szlafsztein and Sterr 2007; Romero et al. 2013), and Asia (Lan et al. 2015; Lee and Jung 2015; Kankara et al. 2016). Environmental sensitivity is also regularly calculated using ESI methods by the Bureau of Ocean Energy Management (BOEM) for Oil and Natural Gas Planning Program Assessment (BOEM 2018; Niedoroda et al. 2014). However, these analyses may not be spatially disaggregated enough to identify discrete, sensitive areas worthy of increased scrutiny. This chapter differs from the previous research by moving the focus from exclusively shoreline areas to deeper regions and resources and developing the ESIs at a finer spatial scale of resolution: 1° latitude × 1° longitude resolution for offshore areas of the northern GoM.

26.3 The Need for an Offshore ESI

Like the coastal areas, offshore waters contain biological resources and human use patterns threatened during an oil well blowout. The offshore waters of the GoM are biologically important as they are home to multiple species of economically important fish and shellfish (Pulster et al. 2020; Sutton et al. 2020; Perlin et al. 2020). As well, offshore areas support ecologically important forage species and other animals of concern including mammals, turtles, seabirds, and deep-sea corals which all experience lethal and sublethal effects from exposure to oil (Antonio et al. 2011; Carmichael et al. 2012; Schwacke et al. 2013; Tran et al. 2014; Haney et al. 2014; Etnoyer et al. 2016; Frasier 2020). Many economically important fish species spawn

in open waters, and their larval life stages are particularly vulnerable to oil. Up to half of known fish species in the GoM occur in mesopelagic deep waters, and new species are being encountered there (Sutton et al. 2017, 2020). Human uses of resources in offshore waters include commercial and recreational fisheries, commercial shipping and cruise lines, military exercise areas, oil and gas leases, renewable energy infrastructure, and other uses (McCrea-Strub et al. 2011; BOEM Offshore Statistics by Water Depth 2018).

This chapter defines quantitative ESI scores via a multi-attribute utility model (MAUM; Huber 1974). In a MAUM, the overall value, or utility, is calculated by the weighted sum or product of the individual utility values of a set of attributes. The definition of this overall utility then allows for comparisons to be made between different sets of attributes, particularly focusing on the sensitivity of the relative weights assigned to each attribute. In the health industry, for example, MUAMs are used to assign patients an overall health index based on several independent health attributes, e.g., vision, hearing, speech, ambulation, dexterity, emotion, cognition, and pain/discomfort. Coefficients for the attributes are calculated from surveys of the importance of the listed attributes. Individual patients are then assigned a semi-quantitative value of 0–6 in each of the health attributes, and these attribute scores are then substituted into the utility function in order to give an overall health index per patient (Feeny et al. 2002). We develop a similar methodology for the creation of the ESIs for the offshore areas in the GoM.

Similar to the human health example above, the environmental sensitivity of a marine geographic location can be determined both by the biological attributes extant at that location and human dependence on the region that might be compromised by an oil well blow out or other significant events resulting in biological and/or economic losses. To illustrate these issues, we develop a MAUM based on three ecological variables and three economic (human use) indicators. Using results from the systematic SEAMAP larval sampling program (Chancellor 2015), we focus on the diversity of larval fishes in both offshore and coastal areas. Larval fish are highly sensitive to oil-related pollution as they are susceptible to physiological defects and mortality at exceedingly low concentrations of oil exposure (Carls et al. 1999; Incardona et al. 2004, 2013; Hicken et al. 2011). Pollution from oil well blowouts would likely impact survival of a variety of species, varying seasonally (Chancellor 2015). We gridded the results of the larval diversity, estimated species richness, and overall abundance data into 1° latitude × 1° longitude rectangles for the northern GoM (Figs. 26.1 and 26.2). In addition to larval measures, we computed measures of economic dependence assigned to the same 1° grid rectangles using estimated offshore (pelagic) ex-vessel revenues and species composition based on vessel logbook information made available from the National Marine Fisheries Service. These data are compared with similar revenue estimates derived from vessel logbook data for coastal reef fishes, coastal migratory pelagic species, and shrimp fisheries.

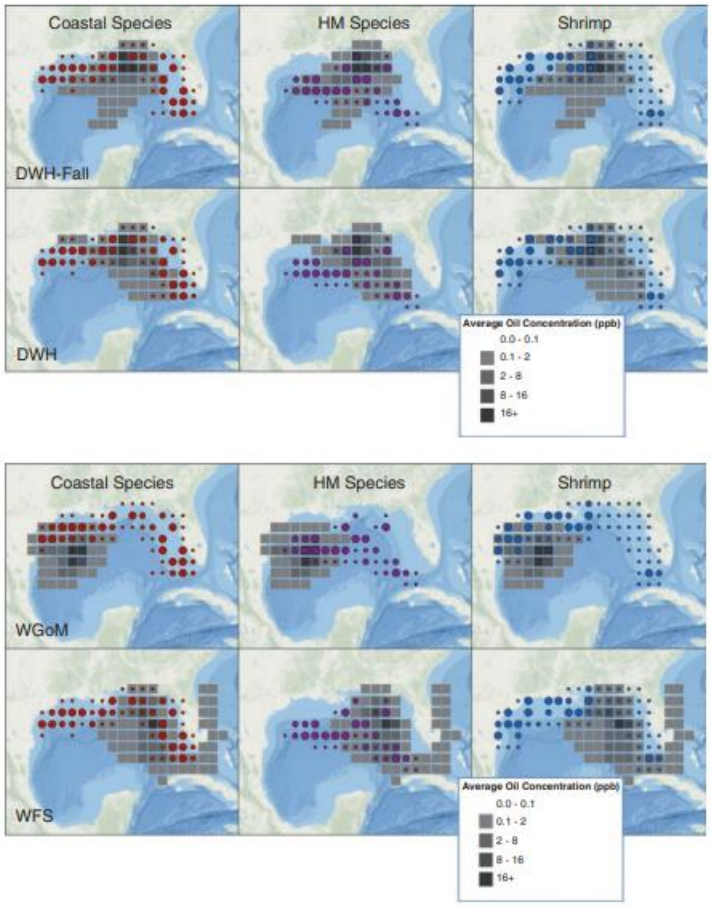

Fig. 26.1 (**upper**) Indexed values for the sensitivity attributes of coastal species fishery catches, HMS fishery catches, and shrimp fishery catches (left to right) spatially mapped against two simulated blowouts (top to bottom), DWH-Fall = the *Deepwater Horizon* spill but starting in September (vs. April) and DWH = the *Deepwater Horizon* scenario. (**lower**) Indexed values for the sensitivity attributes of coastal species fishery catches, HMS fishery catches, and shrimp fishery catches (left to right) spatially mapped against two simulated blowouts (top to bottom), WGoM Western Gulf of Mexico, WFS West Florida Slope

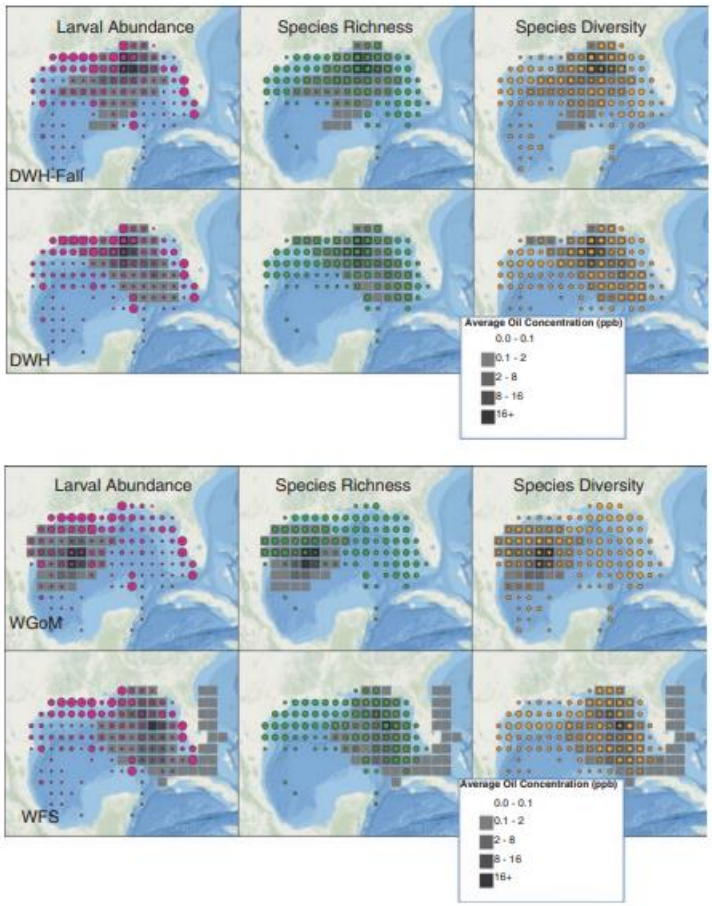

Fig. 26.2 (**upper**) Indexed values for the sensitivity attributes of larval abundance, estimated species richness, and Shannon diversity index (left to right) spatially mapped against two simulated blowouts (top to bottom), DWH-Fall = the *Deepwater Horizon* spill but starting in the Fall (September vs. April) and DWH = the *Deepwater Horizon* scenario. (**lower**) Indexed values for the sensitivity attributes of larval abundance, estimated species richness, and Shannon diversity index (left to right) spatially mapped against two simulated blowouts (top to bottom), WGoM Western Gulf of Mexico, WFS West Florida Slope

26.4 Description of Ecological and Economic Datasets

Southeast Area Monitoring and Assessment Program (SEAMAP) Ichthyoplankton counts and taxonomy were used to create a 1° latitude × 1° longitude grid of estimated abundance by species for the GoM. Samples included came from seasonal surveys from 2000 to 2015 collected via bongo nets. Standardized abundance was calculated for each sample by the estimated number of organisms under a 10 m^2 surface area. These standardized abundances were then calculated across all years and all samples within each 1° × 1° grid and divided by the total number of samples within that block. More information regarding the sampling techniques, species selection, and standardized abundance calculations from raw counts can be found in Chancellor (2015). A total of 58 species of larval fishes were included (Table 26.1).

Coastal Reef Fish and Coastal Migratory Pelagics Annual landings (pounds), reported to the Southeast Coastal Fisheries Logbook Program, and estimates of annual revenues for individual coastal species were assigned to each 1° × 1° grid rectangle. Estimated revenue per grid rectangle is a function of annual trip-level landings and ex-vessel prices aggregated and provided by National Marine Fisheries Service (NMFS)/Southeast Fisheries Science Center (SEFSC) (Overstreet & Liese 2018). Ex-vessel prices represent the unit price paid at the time of landing by fish dealers to fishers for harvested but unprocessed catch. Grids with less than three vessels reporting trip records were omitted to prevent identifying confidential proprietary information. Fifty-nine species were included in the coastal reef fisheries data (Table 26.2).

Highly Migratory Species (HMS) Landings for eight HMS (Table 26.2) were provided by NMFS/SEFSC for each 1° × 1° grid rectangle and were estimated by applying the proportion of numbers of individual species caught in each grid rectangle, as reported to the Atlantic Highly Migratory Species Fisheries Logbook Program, to total trip-level catch (pounds gutted weight). The resulting pounds for each HMS were aggregated for each grid cell annually from 2013 to 2016. Revenue for the HMS pounds was estimated for all species using the average price from NMFS' commercial landings in the GoM for available years 2013–2016 (Personal communication from the National Marine Fisheries Service, Fisheries Statistics Division. [September 2018]). For blue shark and porbeagle shark, the average price per pound for "general sharks" was used, as no specific information was available for them.

Shrimp Revenue estimates for the three dominant species of shrimp (white, brown, pink) were provided by NMFS/SEFSC for each 1° × 1° grid rectangle and were estimated from aggregated landings reported to the Gulf of Mexico Shrimp Permit Cellular Electronic Logbook program during years 2011–2016 and from price per pound reported by port agents and trip tickets (Table 26.2). All three data groupings used to estimate revenues adhere to confidentiality standards and are not adjusted for inflation.

Table 26.1 Scientific and common names of larval species used in developing environmental sensitivity indices herein. Data were collected on SEAMAP larval fish sampling cruises (Chancellor 2015)

Scientific name	Common name	Scientific name	Common name
Acanthocybium solandri	Wahoo	*Margrethia obtusirostra*	Bighead portholefish
Aplatophis chauliodus	Tusky eel	*Micropogonias undulatus*	Croaker, Atlantic
Bairdiella chrysoura	Silver perch	*Mugil cephalus*	Mullet, striped
Benthosema suborbitale	Lanternfish, smallfin	*Mugil curema*	Mullet, silver
Bonapartia pedaliota	Longray fangjaw	*Myrophis punctatus*	Speckled worm eel
Bregmaceros cantori	Striped codlet	*Nesiarchus nasutus*	Black gemfish
Carapus bermudensis	Atlantic pearlfish	*Notolychnus valdiviae*	Lanternfish, topside
Ceratoscopelus warmingii	Lanternfish, Warming's	*Oligoplites saurus*	Leather jack
Chlorophthalmus agassizi	Shortnose greeneye	*Ophichthus gomesii*	Shrimp eel
Chloroscombrus chrysurus	Atlantic bumper	*Ophichthus rex*	King snake eel
Cynoscion arenarius	Sea trout, white	*Opisthonema oglinum*	Herring, Atlantic thread
Cynoscion nebulosus	Sea trout, spotted	*Peprilus burti*	Butterfish, gulf
Decapterus punctatus	Scads, round	*Peprilus paru*	Harvestfish
Diogenichthys atlanticus	Lanternfish, longfin	*Pollichthys mauli*	Lightfish, stareye
Diplospinus multistriatus	Striped escolar	*Pomatomus saltatrix*	Bluefish
Engyophrys senta	Founder, spiny	*Pristipomoides aquilonaris*	Wenchman
Etrumeus teres	Herring, round	*Rachycentron canadum*	Cobia
Euthynnus alletteratus	Tuna, little (tunny)	*Rhomboplites aurorubens*	Snapper, vermilion
Gempylus serpens	Snake mackerel	*Sardinella aurita*	Sardine, Spanish
Harengula jaguana	Herring, scaled	*Sciaenops ocellatus*	Drum, red
Hygophum reinhardtii	Lanternfish, Reinhardt's	*Scomber colias*	Mackerel, Atlantic chub
Katsuwonus pelamis	Tuna, skipjack	*Scomberomorus cavalla*	Mackerel, king
Lagodon rhomboides	Pinfish	*Scomberomorus maculatus*	Mackerel, Spanish
Larimus fasciatus	Drum, banded	*Selar crumenophthalmus*	Scads, bigeye
Leiostomus xanthurus	Spot	*Serraniculus pumilio*	Pygmy sea bass
Lobotes surinamensis	Atlantic tripletail	*Stellifer lanceolatus*	Drum, star
Lutjanus campechanus	Snapper, red	*Thunnus thynnus*	Tuna, bluefin
Lutjanus griseus	Snapper, mangrove	*Trachurus lathami*	Scads, rough
Luvarus imperialis	Louvar	*Xiphias gladius*	Swordfish

Table 26.2 Common and scientific names of species and families of fish and shrimp used in developing coastal reef fish, coastal migratory pelagics, and shrimp and highly migratory species fisheries' landings and revenue data

Coastal species		Highly migratory species		Shrimp species	
Scientific name	Common name	Scientific name	Common name	Scientific name	Common name
Acanthocybium solandri	Wahoo	*Isurus oxyrinchus*	Shark, mako	*Farfantepenaeus aztecus*	Shrimp, brown
Apsilus dentatus	Snapper, black	*Katsuwonus pelamis*	Tuna, skipjack	*Litopenaeus setiferus*	Shrimp, white
Archosargus probatocephalus	Sheepshead, Atlantic	*Lamna nasus*	Shark, porbeagle	*Penaeus duorarum*	Shrimp, pink
Balistes capriscus	Triggerfish, gray	*Prionace glauca*	Shark, blue		
Balistes vetula	Triggerfish, queen	*Thunnus alalunga*	Tuna, albacore		
Calamus bajonado	Porgy, jolthead	*Thunnus albacares*	Tuna, yellowfin		
Calamus leucosteus	Porgy, whitebone	*Thunnus obesus*	Tuna, bigeye		
Calamus nodosus	Porgy, knobbed	*Thunnus thynnus*	Tuna, bluefin		
Canthidermis sufflamen	Triggerfish, ocean	*Xiphias gladius*	Swordfish		
Carangidae	Jacks				
Caulolatilus microps	Tilefish, blueline				
Centropristis striata	Sea bass, Atlantic, black				
Coryphaena	Dolphinfish				
Ephippididae	Spadefish				
Epinephelus adscensionis	Hind, rock				
Epinephelus cruentatus	Graysby				
Epinephelus drummondhayi	Hind, speckled				
Epinephelus flavolimbatus	Grouper, yellowedge				
Epinephelus guttatus	Hind, red				
Epinephelus morio	Grouper, red				
Epinephelus mystacinus	Grouper, misty				
Epinephelus nigritus	Grouper, Warsaw				

(continued)

Table 26.2 (continued)

Coastal species		Highly migratory species		Shrimp species	
Scientific name	Common name	Scientific name	Common name	Scientific name	Common name
Epinephelus niveatus	Grouper, snowy				
Etelis oculatus	Snapper, queen				
Euthynnus alletteratus	Tuna, little (tunny)				
Haemulidae	Grunts				
Haemulon album	Margate				
Haemulon plumieri	Grunt, white				
Lachnolaimus maximus	Hogfish				
Lopholatilus chamaeleonticeps	Tilefish				
Lutjanidae	Snappers				
Lutjanus analis	Snapper, mutton				
Lutjanus apodus	Snapper, schoolmaster				
Lutjanus buccanella	Snapper, blackfin				
Lutjanus campechanus	Snapper, red				
Lutjanus cyanopterus	Snapper, cubera				
Lutjanus griseus	Snapper, mangrove				
Lutjanus jocu	Snapper, dog				
Lutjanus synagris	Snapper, lane				
Lutjanus vivanus	Snapper, silk				
Malacanthus plumieri	Tilefish, sand				
Mycteroperca bonaci	Grouper, black				
Mycteroperca microlepis	Grouper, gag				
Mycteroperca phenax	Scamp				
Mycteroperca venenosa	Grouper, yellowfin				
Ocyurus chrysurus	Snapper, yellowtail				
Pagrus pagrus	Porgy, red				

(continued)

Table 26.2 (continued)

Coastal species		Highly migratory species		Shrimp species	
Scientific name	Common name	Scientific name	Common name	Scientific name	Common name
Pomatomus saltatrix	Bluefish				
Pristipomoides aquilonaris	Wenchman				
Rachycentron canadum	Cobia				
Rhomboplites aurorubens	Snapper, vermilion				
Scomberomorus cavalla	Mackerel, king				
Scomberomorus maculatus	Mackerel, Spanish				
Seriola dumerili	Amberjack, greater				
Seriola fasciata	Amberjack, lesser				
Seriola rivoliana	Jack, Almaco				
Seriola zonata	Banded rudderfish				
Serranidae	Groupers				
Sparidae	Scups or porgies				

26.5 Calculation of Sensitivity Attributes

Six sensitivity attributes were created forming our trial ESIs. These were the following:

Biological All SEAMAP samples were assigned to the same 1° grid rectangle block system as for fishery landings. The following three attributes were calculated for SEAMAP larval samples within each grid rectangle:

1. *Species richness of larval fish species* – Larval species richness was estimated using the *specpool* function from the *vegan* package in *R*. This function computes the asymptotes of the rarefaction curves to estimate the total species richness per grid rectangle and allows comparisons among grid rectangles with different sampling frequencies (Gotelli and Cowell 2001; Cowell et al. 2004). Grid rectangles with less than five samples were excluded from this calculation.

We used the first-order jackknife method to estimate the number of missing species, $\hat{f}_0$, (Oksanen 2018):

$$\hat{f}_0 = f_1 \frac{N}{N-1} \tag{26.1}$$

where f_1 is the number of species found in only one site and N is the total number of sites. The jackknife estimator operates under the assumption that we miss about as many species as we only see once (Smith and van Belle 1984). The estimated species richness , Sp, is the sum of the species observed, So, plus the estimated number of missing species, $\hat{f}_0$:

$$\mathrm{Sp} = \mathrm{So} + \hat{f}_0 \tag{26.2}$$

2. *Shannon-Wiener diversity of larval fish species* – The Shannon-Wiener diversity index (Hill 1973) was calculated for each grid rectangle using the *diversity* function in the *vegan* package. The Shannon-Wiener diversity calculation used in this chapter is (Oksanen 2018):

$$H = -\sum_{i=1}^{S} p_i \ln p_i \tag{26.3}$$

where p_i is the proportion of species i and S is the number of species such that the $\sum p_i = 1$.

3. *Overall abundance of larval fish species* – Larval abundance was calculated for each grid rectangle by summing the total abundance for all species within the block and dividing by the number of samples.

$$Abundance = \left(\sum_{i=1}^{m} x_i\right) / n \tag{26.4}$$

where x_i is the standardized abundance for each species, i within the grid rectangle, m is the number of species, and n is the number of samples within the grid rectangle.

Economic Data:

4. *Revenue value of coastal species* – Coastal species revenue (CRev) was calculated as the sum of revenue from all coastal species within each grid rectangle.
5. *Revenue value of HMS* – HMS revenue (HMRev) was calculated as the sum of revenue from all HMS within each grid rectangle.
6. *Revenue value of shrimp species* – Shrimp revenue (SRev) was calculated as the sum of revenue from all shrimp species within each grid rectangle.

26.6 Creation of the ESIs

Each attribute was normalized to a relative (0–1) by finding the proportion of the total within each grid rectangle.

$$vI_j = v_j / (\sum_{j=1}^{n} v_j) \tag{26.5}$$

where v_j is the value of the attribute v for grid rectangle, j and n is the total number of grid rectangles, and vI_j is the indexed value.

The cumulative sensitivity equation was modeled as a multi-attribute linear utility function combining the sensitivity attributes such that the cumulative sensitivity (CS) at grid rectangle j is:

$$CS_j = \sum_{i=1}^{N} k_i * (vI_{ij}) \tag{26.6}$$

where N is the number of included sensitivity attributes, k_i is the coefficient assigned to the ith attribute, and VI_{ij} is the indexed score of the ith sensitivity attribute at grid rectangle j.

The CS variable is then mapped onto the 1° × 1° grid resulting in a spatial distribution of the environmental sensitivity index. The sensitivity of the coefficients (k) was analyzed by creating the CS variable map under three different methods for weighting k: all coefficients having equal weights ($k = 1$), economic sensitivity coefficients weighted more heavily ($k_1 = 1.3$, $k_2 = 0.7$), and environmental sensitivity coefficients weighted more heavily ($k_1 = 0.7$, $k_2 = 1.3$).

26.7 Comparison with Modeled Oil Well Blowouts

To demonstrate the utility of the proposed ESIs, four oil well blowouts were modeled using the open-source Connectivity Modeling System (CMS) adapted with an oil module (Paris et al. 2012, 2013; Berenshtein et al. 2020a). Origin locations for the scenarios were chosen at locations with similar depths to the DWH blowout and to represent locations where drilling is currently occurring or proposed. For each scenario, oil droplets were released during 87 days (similar to DWH) and tracked for a total of 90 days. In each scenario, oil droplets were released at a depth of 1222 m in accordance to the conditions of the DWH oil well blowout. Total petroleum hydrocarbon (TPH) concentrations (ppb) are obtained by normalizing the total oil mass to the mass of water in 0.02° grid boxes in the upper 20 m, and the daily averages are further determined from the 2 hourly output products.

The simulated oil well blowouts scenarios are:

1. *Deepwater Horizon* control (DWH) – Located in the central GoM with a DWH origin point
   Origin: 28.736 N, 88.365 W Start Date: April 20, 2010

2. *Deepwater Horizon* September (DWH Sept) – Located in the central GoM with a DWH origin point and a September start date
   Origin: 28.736 N, 88.365 W Start Date: September 1, 2010
3. Western GoM – Located in the western GoM where drilling is currently active.
   Origin: 27.000 N, 85.168 W Start Date: April 20, 2010
4. West Florida Slope (WFS) – Located in the eastern GoM on the continental slope where drilling has been prohibited at least until 2022.
   Origin: 26.600 N, 93.190 W Start Date: April 20, 2010

We use the ESIs summed over all grid rectangles to compare and rank the sensitivity to these four blowout scenarios.

TPH concentrations per day were obtained by normalizing the total oil mass to the mass of water in 0.02° grid boxes in the upper 20 m. The average oil concentration (in ppb) for each 1° × 1° grid was further calculated by the summation of the simulated oil concentration per grid per day and then finding the average oil concentration over all 90 days. This was calculated for each oil well blowout scenario:

$$OC_{sj} = \left(\sum_{i=1}^{90}\left(\sum_{k=1}^{n} o_{ki}\right)\right) / 90 \tag{26.7}$$

where OC_{sj} is the oil concentration for scenario s at 1° × 1° grid rectangle j, o_{ki} is the kth oil concentration in grid rectangle j during day i, and n is the total number of oil concentration measurements within block j during day i. The six ecological and economic attributes are mapped with the average oil concentration for each scenario (Figs. 26.1 and 26.2).

The distribution of values of OC_{sj} (Fig. 26.3, left) shows a highly skewed distribution with a few, 1° × 1° grid rectangles near the well blowout origins having very high oil concentrations (Figs. 26.1 and 26.2). Because these oil concentrations are averaged over 90 days, there were likely areas and days where episodic higher oil exposures within blocks occurred. The OC_{sj} values were transformed into a piecewise root function where any oil concentration between 0 and 1 average ppb was assigned a value of 1 and OC_{sj} values greater than one were transformed by the square root function:

$$OI_{sj} = \begin{cases} 1 & when\, OI_{sj} > 0\, and < 1 \\ OC_{sj}^{\left(\frac{1}{2}\right)} & when\, OI_{sj} \geq 1 \end{cases} \tag{26.8}$$

This transformation emphasizes the importance of moderate oil concentrations that may affect larval fish and contamination levels that would result in fishery closures (Berenshtein et al. 2020b) while reducing the multiplication factor of the most heavily oiled areas to a maximum of 5.47. The distributions of the original OC_{sj} and OI_{sj} values are plotted in Fig. 26.3.

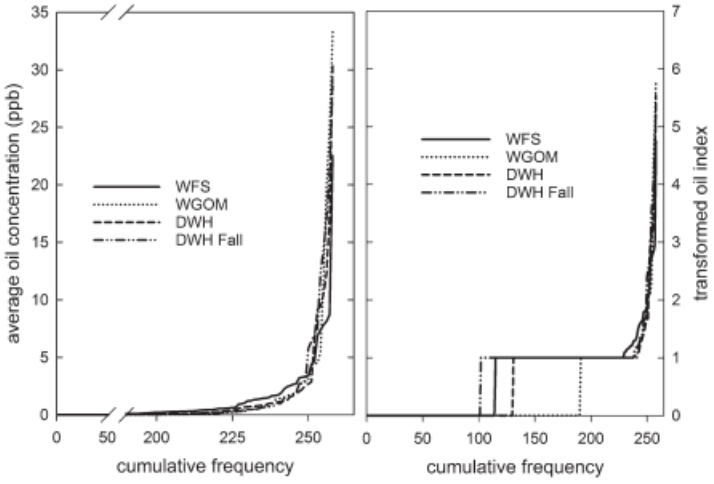

Fig. 26.3 Sorted distribution by 1° grid rectangle of the average oil concentration (OC) distribution for all four scenarios (left) and transformed oil concentration index (OI) for all scenarios (right). The OI is a square root transformation of the OC with values between 0 and 1 rounded to 1

The overall sensitivity for each oil well blowout was then calculated as:

$$ES_k = \sum_{i=1}^{n} (CS_{ij} * (OI_{ijk})) \tag{26.9}$$

where ES_k is the overall environmental sensitivity of oil well blowout k, CS_{ij} is the cumulative sensitivity at point (i j), OI_{ij} is the oil index score at point (i, j) for spill k, and n is the number of 1° × 1° grid rectangles.

26.8 Results

Overall sensitivity was calculated for each oil scenario and attribute pair for a total of 24 measures (Fig. 26.4; Table 26.4). Coastal species' revenue had relatively similar sensitivity scores for all scenarios except for the Western GoM blowout where the corresponding score was lower than for any other oil scenario – attribute pair.

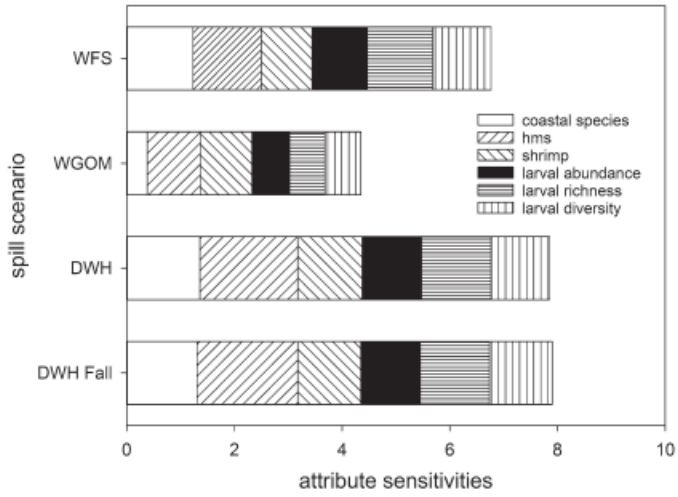

Fig. 26.4 Summed relative attribute sensitivities for ecological (larval abundance, richness, diversity) and economic impacts (on fisheries for coastal species, highly migratory species, and shrimps) of four simulated deepwater oil blowouts in the Gulf of Mexico. Weighting is equal for all attributes

Both of the *Deepwater Horizon* simulations were especially problematic for highly migratory species as most of the reported fishing activity took place within this region. Shrimp fisheries were impacted almost evenly for all four scenarios. For all six attributes, the Western GoM spill had the lowest overall sensitivity score. DWH and DWH Sept had similar impact scores for all scenarios. For this study, the larval sensitivity and economic resource attributes were aggregated over all seasons. However, larvae demonstrate significant seasonality with some species occurring during the spring (swordfish, bluefin tuna, round herring), summer (cobia, Spanish mackerel, king mackerel, spotted sea trout, little tunny), or fall (scaled herring, vermilion snapper, red drum, Chancellor 2015, Table 26.3). In real-world spills such as the DWH oil well blowout, season will thus be a major factor in determining fish species sensitivity and impacts.

The summation of the sensitivity indices for all six attributes (ES_k) was initially calculated with equally weighting coefficients for each term: $k = 1$ (Table 26.4). Under this first weighting scheme model, DWH and DWH Sept had the highest overall sensitivity followed by the WFS and then Western GoM.

The impacts of differential weighting of the relative importance of ecological and economic measures were simulated by varying the coefficients, k_i, for each of the six attributes. For the second weighting scheme model, k for larval measures

Table 26.3 Proportions of total catch for selected species from SEAMAP larval surveys, by month (Chancellor 2015)

	Month											
Species	1	2	3	4	5	6	7	8	9	10	11	12
Swordfish	0.31	0.00	0.00	0.33	0.15	0.11	0.00	0.04	0.05	0.00	0.00	0.00
Herring, round	0.10	0.10	0.62	0.03	0.01	0.00	0.00	0.00	0.00	0.00	0.04	0.09
Lanternfish, smallfin	0.15	0.18	0.12	0.16	0.16	0.03	0.01	0.03	0.02	0.01	0.02	0.11
Tuna, bluefin	0.00	0.00	0.00	0.22	0.78	0.00	0.00	0.00	0.00	0.00	0.00	0.00
Sea trout, white	0.01	0.09	0.43	0.02	0.00	0.04	0.24	0.03	0.07	0.05	0.02	0.01
Lanternfish, longfin	0.09	0.11	0.11	0.18	0.23	0.03	0.01	0.05	0.02	0.02	0.03	0.12
Lanternfish, Warming's	0.07	0.08	0.08	0.24	0.24	0.04	0.01	0.04	0.03	0.04	0.05	0.09
Tuna, skipjack	0.00	0.02	0.04	0.22	0.35	0.10	0.01	0.14	0.08	0.03	0.01	0.00
Wahoo	0.00	0.00	0.00	0.18	0.28	0.09	0.10	0.22	0.13	0.00	0.00	0.00
Cobia	0.00	0.00	0.00	0.28	0.09	0.16	0.26	0.07	0.06	0.00	0.00	0.08
Sea trout, spotted	0.00	0.00	0.03	0.00	0.01	0.11	0.65	0.07	0.09	0.04	0.00	0.00
Tuna, little (tunny)	0.00	0.00	0.00	0.06	0.03	0.17	0.31	0.31	0.11	0.00	0.00	0.00
Mackerel, Spanish	0.00	0.00	0.00	0.00	0.01	0.29	0.38	0.17	0.15	0.00	0.00	0.00
Snapper, red	0.00	0.00	0.00	0.00	0.01	0.27	0.35	0.15	0.16	0.05	0.01	0.00
Mackerel, king	0.00	0.00	0.00	0.00	0.01	0.22	0.18	0.28	0.25	0.05	0.00	0.00
Sardine, Spanish	0.00	0.02	0.00	0.11	0.04	0.14	0.06	0.14	0.27	0.22	0.01	0.00
Herring, Atlantic thread	0.02	0.00	0.01	0.00	0.00	0.11	0.36	0.23	0.17	0.01	0.05	0.03
Herring, scaled	0.00	0.00	0.00	0.00	0.01	0.40	0.16	0.15	0.04	0.00	0.23	0.00
Snapper, vermilion	0.00	0.00	0.00	0.02	0.02	0.10	0.13	0.21	0.31	0.17	0.03	0.00
Drum, red	0.00	0.00	0.00	0.00	0.00	0.00	0.01	0.01	0.44	0.52	0.00	0.00

Catches from all samples were aggregated by month and divided by the total number of samples collected during that month. Proportions were calculated as the proportion of standardized abundance each month aggregating to the total. Shading indicates months of higher proportion of total spawning activity

was increased by 30% (×1.3), and *k* for the economic measures was reduced by 30% (×0.7). This change maintained the same relative ranking of overall sensitivity as the equally weighted method. For the third weighting scheme model, *k* for the larval measures was reduced by 30% (0.7), and *k* for the economic measures was increased by 30% (1.3). This change also maintained the relative rankings of the spills.

Table 26.4 Relative cumulative sensitivity of each of four deepwater oil spill scenarios with respect to three economic environmental sensitivity indices and three environmental sensitivity indices

ESI attribute	Spill scenario			
	DWH Sept	DWH	WGoM	WFS
Coastal species revenue	1.31	1.36	0.38	1.23
HMS revenue	1.87	1.82	0.99	1.27
Shrimp revenue	1.17	1.20	0.95	0.95
Larval abundance	0.96	0.98	0.57	0.94
Larval species richness	1.29	1.29	0.66	1.21
Larval Shannon diversity	1.01	1.00	0.56	1.00
Weighting Scheme				
Larval k = 1, economic k = 1	1.27	1.27	0.68	1.10
Larval k = 1.3, economic k = 0.7	1.21	1.22	0.66	1.08
Larval k = 0.7, economic k = 1.3	1.28	1.28	0.77	1.07

The bottom three rows test the overall result as functions of different weighting coefficients (k) for economic and environmental attributes. Relative impact by scenario for each individual attribute (top six rows) and combined for all six attributes for three k weighting schemes (bottom three rows)

26.9 Discussion

Quantitative approaches to ESI formulation using multi-attribute utility models and their application to simulated oil spills demonstrate the potential to (1) quantify sensitivities of spatially explicit offshore areas to local oil spills across many metrics without having to subjectively concatenate maps and to (2) compare potential sensitivities of different oil spill scenarios ranging widely over the GoM. The latter is particularly important as a potential tool for identifying specific locations (at varying spatial scales) that may be too environmentally or economically sensitive to allow oil development. In this sense, such a planning tool could conceivably be brought into the oil facility siting process.

While we demonstrate the MAUM method for assessing oil spill sensitivity across six metrics, there are many more data sets that can be incorporated into such an analysis. These include abundance and distribution data for marine mammals and sea turtles (Frasier 2020), seabirds, deepwater corals, noncommercial fishes (including mesopelagic communities; Sutton et al. 2020), and areas where primary production is high. Potential additional economic attributes include the spatial distributions of recreational fishing, commercial and cruise ship activity, locations of renewable energy infrastructure, and military preparedness, as well as other human-centric uses and invaluable archeological sites including shipwrecks in the Gulf (e.g., lost ships of Cortez).

The weighting coefficients in this chapter are varied to show the sensitivity of the overall estimated impact of an oil well blowout to the individual attributes. In future

applications, these coefficients can be varied to (1) add or subtract weight from an attribute due to oil well blow out characteristics (e.g., increasing the weight of k for spills where dispersants are used to account for organisms that are potentially harmed by dispersants) or (2) to add or subtract weight from an attribute where one is deemed "more important" than another (e.g., prioritizing endangered organisms, fisheries with higher revenue values, etc.).

The ESIs described in this chapter also have applications for the development of quantitative models for optimizing the conflicting objectives of maximizing energy production while minimizing potential impacts on species and other economic uses. There is a rich body of literature using linear programming models, GAMS, and other optimization tools for such analyses (e.g., Sanchirico and Wilen 2005; Kobayashi and Polovina 2005). Drilling plans in the GoM have multiple potentially conflicting objectives, including:

1. Maximizing oil production P_j
2. Minimizing the costs of exploration (costs associated with new wells) k_iC_j
3. Minimizing the biological resources at risk in the case of an oil well blowout ES_j
4. Minimizing impacts on human use activities at risk in the case of an oil well blowout HU_j

Murawski et al. (2001) illustrated a similar optimization methodology for minimizing impacts on spatially disaggregated fishery catches while also maximizing the protection of species rarity (e.g., determining the boundaries of marine protected areas). A similar optimization approach could be applied to oil production planning for offshore areas. For example, one might consider the objective function:

$$\max a1 * \sum_j D_j * \left(P_j - \left(k_i C_j\right)\right) + a2 \sum_j \left(D_j - 1\right) * \mathrm{ES}_j + a3 \sum_j \left(D_j - 1\right) * \mathrm{HU}_j \qquad (26.10)$$

where D_j is an element of the design vector with values of 0 and 1 indicating if site j is included in the selected drilling plan, P_j is the potential(or actual) oil/gas production potential at spatial block j, C_j is a variable with values of 0 and 1 indicating if a site is currently being drilled, k_i is the cost of exploration and drilling at a new site, ES_j is the sum of the biological resource ESI values, HU_j is the sum of the human use ESIs at site j, and a1, a2, and a3 are weighted coefficients. Oil production for unexplored blocks, although uncertain, can be quantified for the purposes of such modeling in a number of potential ways: (1) using the average water depth of the block with the regression model fitted to existing block productivity to forecast production potential, (2) using geostatistical methods and existing well production data to forecast production of unexplored blocks, (3) using exploration data (e.g., seismic) compiled by the oil companies to predict resource potential (Murawski et al. 2020, Fig. 2.6), or (4) compiling spatial data from within known geological plays (BOEM 2018; Locker and Hine 2020).

The goal of such modeling is to understand the potential trade-offs of environmental protection vs. potential foregone economic opportunities or negative impacts

of various spatial regulatory schemes. Presumably, the models could be elaborated by incorporating a number of other considerations such as trans-boundary impacts (across national boundaries) as a penalty function (actions to be avoided). As well, if accident potentials vary spatially, such data could be incorporated. A key feature to be considered in such analyses is the spatial block size being analyzed. In our example (Figs. 26.1 and 26.2), we used a 1° × 1° block size which is a reasonable trade-off of spatial granularity for the purposes of illustration but is far larger than typical lease blocks offered in the US GoM. Certainly more precise block-by-block analyses could be undertaken, subject to the availability of the required data sets at this resolution. The other consideration in spatial scaling of such optimization methods is the likely spatial extent of deep blowouts. For spills similar in volume and distribution to DWH, about 12 1° × 1° blocks were significantly impacted, but this varied by season and spill location (Figs. 26.1 and 26.2).

While spatial optimization methods cannot be the only decision support tool for informing drilling plans, the applications are useful as input into the process of determining oil and gas development planning with a focus on protecting valuable economic and ecological resources. Using such tools can help visualize and quantify the inherent trade-offs that must be considered in balancing energy production with resource protection.

Acknowledgments This research was made possible by a grant from the Gulf of Mexico Research Initiative, CIMAGE II/III. Data for this chapter were collected under the Southeast Area Monitoring and Assessment Program (SEAMAP) or provided by National Marine Fisheries Service (NMFS). The authors would like to thank Allison Shideler for providing HMS landings data and Jo Williams and James Primrose for providing shrimp landings and revenue estimates. The scientific results and conclusions, as well as any views or opinions expressed herein, are those of the authors and do not necessarily reflect those of NOAA or the Department of Commerce.

References

Adler E, Inbar M (2007) Shoreline sensitivity to oil spills, the Mediterranean coast of Israel. Assessment analysis. Ocean Coast Manag 50:24–34

Alves TM, Kokinou E, Zodiatis G (2014) A three-step model to assess shoreline and offshore susceptibility to oil spills: the South Aegean (Crete) as an analogue for confined marine basins. Mar Pollut Bull 86:443–457

Antonio F, Mendes R, Thomaz S (2011) Identifying and modeling patterns of tetrapod vertebrate mortality rates in the Gulf of Mexico oil spill. Aquat Toxicol 105:177–179

Berenshtein I, Perlin N, Ainsworth CH, Ortega-Ortiz JG, Vaz AC, Paris CB (2020a) Comparison of the spatial extent, impacts to shorelines, and ecosystem and 4-dimensional characteristics of simulated oil spills (Chap. 20). In: Murawski SA, Ainsworth C, Gilbert S, Hollander D, Paris CB, Schlüter M, Wetzel D (eds) Scenarios and responses to future deep oil spills – fighting the next war. Springer, Cham

Berenshtein I, Perlin N, Murawski SA, Graber H, Samantha Joye S, Paris CB (2020b) Evaluating the effectiveness of fishery closures for deep oil spills using a 4-dimensional model (Chap. 23). In: Murawski SA, Ainsworth C, Gilbert S, Hollander D, Paris CB, Schlüter M, Wetzel D (eds) Scenarios and responses to future deep oil spills – fighting the next war. Springer, Cham

BOEM Offshore Statistics by Water Depth (2018) Available online: https://www.data.boem.gov/Leasing/OffshoreStatsbyWD/Default.aspx

Carls MG, Rice SD, Hose JE (1999) Sensitivity of fish embryos to weathered crude oil: Part I. Low-level exposure during incubation causes malformations, genetic damage, and mortality in larval pacific herring (*Clupea pallasii*). Environ Toxicol Chem 18:481–493

Carmichael RH, Graham WM, Aven A, Worthy G, Howden S (2012) Were multiple stressors a "perfect storm" for northern Gulf of Mexico bottlenose dolphins (*Tursiops truncatus*) in 2011? PLoS One 7:e41155

Carmona S, Gherardi D, Tessler M (2004) Environment sensitivity mapping and vulnerability modeling for oil spill response along the São Paulo State coastline. J Coast Res 39:1455–1458

Castañedo S, Pombo C, Fernandez F, Medina R, Puente A, Juanes J (2008) Oil spill vulnerability atlas for the Cantabrian Coast Bay of Biscay, Spain. Int Oil Spill Conf Proc:137–144. https://doi.org/10.7901/2169-3358-2008-1-137

Chancellor E (2015) Vulnerability of larval fish populations to oil well blowouts in the northern Gulf of Mexico. (Unpublished master's thesis), College of Marine Science, University of South Florida, Saint Petersburg, FL

Cowell RK, Mao XC, Chang J (2004) Interpolating, extrapolating, and comparing incidence-based species accumulation curves. Ecology 85:2717–2727

DOI Secretary Zinke Announces Plan for Unleashing America's Offshore Oil and Gas Potential (2018) Available online: https://www.doi.gov/pressreleases/secretary-zinke-announces-plan-unleashing-americas-offshore-oil-and-gas-potential. Accessed on Oct 2018

Energy Information Administration (EIA) (2018) Energy Information Administration Gulf of Mexico fact sheet. Available online: https://www.eia.gov/special/gulf_of_mexico/. Accessed on Oct 2018

Etnoyer PJ, Wickes LN, Silva M, Dubick JD, Balthis L, Salgado E, MacDonald IR (2016) Decline in condition of gorgonian octocorals on mesophotic reefs in the northern Gulf of Mexico: before and after the Deepwater Horizon oil spill. Coral Reefs 35:77–90

Fattal P, Maanan M, Tillier I, Rollo N, Robin M, Pottier P (2010) Coastal vulnerability to oil spill pollution: the case of Noirmoutier Island (France). J Coast Res 25(5):879–887

Feeny D, Furlong W, Torrance G, Goldsmith C, Zhu Z, DePauw S, Denton M, Boyle M (2002) Multiattribute and single-attribute utility functions for the health utilities index Mark 3 System. Med Care 40:113–128. http://www.jstor.org/stable/3767552

Frasier K (2020) Evaluating impacts of deep oil spills on oceanic marine mammals (Chap. 25). In: Murawski SA, Ainsworth C, Gilbert S, Hollander D, Paris CB, Schlüter M, Wetzel D (eds) Scenarios and responses to future deep oil spills – fighting the next war. Springer, Cham

Gotelli NJ, Cowell RK (2001) Quantifying biodiversity: procedures and pitfalls in the measurement and comparison of species richness. Ecol Lett 4:379–391

Haney JC, Geiger HJ, Short JW (2014) Bird mortality from the Deepwater Horizon oil spill. II. Carcass sampling and exposure probability in the coastal Gulf of Mexico. Mar Ecol Prog Ser 513:239–252

Hicken CE, Linbo TL, Baldwin DH, Willis ML, Myers MS, Holland L, Larsen M, Stekoll MS, Rice SD, Collier TK, Scholz NL, Incardona JP (2011) Sublethal exposure to crude oil during embryonic development alters cardiac morphology and reduces aerobic capacity in adult fish. Proc Natl Acad Sci U S A 108(17):7086–7090

Hill MO (1973) Diversity and evenness: a unifying notation and its consequences. Ecology 54:427–473

Huber GP (1974) Multi-attribute utility models: a review of field and field-like studies. Manag Sci 20:1393–1402

Incardona JP, Collier TK, Scholz NL (2004) Defects in cardiac function precede morphological abnormalities in fish embryos exposed to polycyclic aromatic hydrocarbons. Toxicol Appl Pharmacol 196:191–205

Incardona JP, Swarts TL, Edmunds RC, Linbo TL, Aquilina-Beck A, Sloan CA, Gardner LD, Block BA, Scholz NL (2013) Exxon Valdez to *Deepwater Horizon*: comparable toxicity of both crude oils to fish early life stages. Aquat Toxicol 142–143:303–316

Jensen JR, Ramsey EW, Holmes JM, Michel JE, Savitsky B, Davis BA (1990) Environmental sensitivity index (ESI) mapping for oil spills using remote sensing and geographic information system technology. Int J Geogr Inf Syst 4:181–201

Jensen JR, Halls JN, Michel J, Carolina S (1998) A systems approach to environmental sensitivity index (ESI) mapping for oil spill contingency planning and response. Photogramm Eng Remote Sens 64:1003–1014

Kankara RS, Arockiaraj S, Prabhu K (2016) Environmental sensitivity mapping and risk assessment for oil spill along the Chennai Coast in India. Mar Pollut Bull 106:95–103

Kassomenos PA (2004) Risk analysis for environmental hazards: the case of oil spills, in Crete. Global Nest 6:39–51

Kazanis E, Maclay D, Shepard N (2015) Estimated oil and gas reserves Gulf of Mexico OCS region December 31, 2013; Bureau of Ocean Energy Management (BOEM) report; BOEM: New Orleans, LA, USA

Knudsen RR, Druyor RD (2009) USCG Sector St Petersburg – digital area contingency plan for oil spill response. C. f. S. analysis. St Petersburg, Florida, Florida Fish and Wildlife Conservation Commission – Fish and Wildlife Research Institute

Kobayashi DR, Polovina JJ (2005) Evaluation of time-area closures to reduce incidental sea turtle take in the Hawaii-based longline fishery: Generalized Additive Model (GAM) development and retrospective examination. NOAA Technical Memorandum NMFS-PIFSC-4, 39 pp

Lan D, Liang B, Bao C, Ma M, Xu Y, Yu C (2015) Marine oil spill risk mapping for accidental pollution and its application in a coastal city. Mar Pollut Bull 96:220–225

Lee M, Jung J-Y (2015) Pollution risk assessment of oil spill accidents in Garorim Bay of Korea. Mar Pollut Bull 100:297–303

Locker S, Hine AC (2020) An overview of the geologic origins of hydrocarbons and production trends in the Gulf of Mexico (Chap. 4). In: Murawski SA, Ainsworth C, Gilbert S, Hollander D, Paris CB, Schlüter M, Wetzel D (eds) Scenarios and responses to future deep oil spills – fighting the next war. Springer, Cham

Maitieg A, Lynch K, Johnson M (2018) Coastal resources spatial planning and potential oil risk analysis: case study of Misratah's coastal resources, Libya. In: 19th International conference on geography and environmental studies. https://www.researchgate.net/publication/323445887_Coastal_Resources_Spatial_Planning_and_Potential_Oil_Risk_Analysis_Case_Study_of_Misratah%27s_Coastal_Resources_Libya

McCrea-Strub A, Kleisner K, Sumaila UR, Swartz W, Watson R, Zeller D, Pauly D (2011) Potential impact of the Deepwater Horizon oil spill on commercial fisheries in the Gulf of Mexico. Fisheries (Bethesda) 36:332–336

Murawski S, Fogarty M, Rago P, Brodziak J (2001) Quantitative methods for MPA design, with application to the NE USA. Marine protected areas: design and implementation for conservation and fisheries restoration. Woods Hole Oceanographic Institution, 27–29 August 2001

Murawski SA, Hollander DJ, Gilbert S, Gracia A (2020) Deep-water oil and gas production in the Gulf of Mexico, and related global trends (Chap. 2). In: Murawski SA, Ainsworth C, Gilbert S, Hollander D, Paris CB, Schlüter M, Wetzel D (eds) Scenarios and responses to future deep oil spills – fighting the next war. Springer, Cham

Nelson JR, Grubesic TH (2018) The implications of oil exploration off the Gulf Coast of Florida. J Mar Sci Eng 6. https://doi.org/10.3390/jmse6020030

Nelson J, Grubesic T, Sim L, Rose K, Graham J (2015) Approach for assessing coastal vulnerability to oil spills for prevention and readiness using GIS and the Blowout and Spill Occurrence Model. Ocean Coast Manag 112:1–11

Niedoroda A, Davis S, Bowen M, Nestler E, Rowe J, Balouskus R, Schroeder M, Gallaway B, Fechhelm R (2014) A method for the evaluation of the relative environmental sensitivity and marine productivity of the outer continental shelf. Prepared by URS Group, Inc., Normandeau Associates, Inc., RPS ASA, and LGL Ecological Research Associates, Inc. for

the U.S. Department of the Interior, Bureau of Ocean Energy Management. Herndon, VA OCS Study BOEM 616, 80 pp. + appendices

NOAA Office of Response and Restoration (2018) Environmental Sensitivity Index (ESI) maps https://response.restoration.noaa.gov/resources/environmental-sensitivity-index-esi-maps

Oksanen J (2018) Vegan: ecological diversity. https://CRAN.R-project.org/package=vegan

Olita A, Cucco A, Simeone S, Ribotti A, Fazioli L, Sorgente B, Sorgente R (2012) Oil spill hazard and risk assessment for the shorelines of a Mediterranean coastal archipelago. Ocean Coast Manag 57:44–52

Overstreet E, Liese C (2018) Economics of the Gulf of Mexico reef fish fishery-2015. NOAA technical memorandum NMFS-SEFSC-724. 78 p.

Paris CB, Hénaff ML, Aman ZM, Subramaniam A, Helgers J, Wang DP, Kourafalou VH, Srinivasan A (2012) Evolution of the Macondo well blowout: simulating the effects of the circulation and synthetic dispersants on the subsea oil transport. Environ Sci Technol 46:13293–13302

Paris CB, Helgers J, Van Sebille E, Srinivasan A (2013) Connectivity Modeling System (CMS): a multi-scale tool for the tracking of biotic and abiotic variability in the ocean. Environ Model Softw 42:47–54

Perlin N, Berenshtein I, Vaz A, Faillettaz R, Schwing P, Romero I, Schlüter M, Liese A, Viamonte J, Noirungsee N, Gros J, Paris C (2020) Far-field modeling of deep-sea blowout: sensitivity studies of initial conditions, biodegradation, sedimentation and SSDI on surface slicks and oil plume concentrations. In: Murawski SA, Ainsworth C, Gilbert S, Hollander D, Paris CB, Schlüter M, Wetzel D (eds) Deep oil spills: facts, fate and effects. Springer, Cham

Petersen J, Michel J, Zengel S, White M, Lord C, Plank C (2002) Environmental sensitivity index guidelines. Version 3.0. NOAA Technical Memorandum NOS OR&R, 11

Pulster EL, Gracia A, Snyder SM, Romero IC, Carr B, Toro-Farmer G, Murawski SA (2020) Polycyclic aromatic hydrocarbon baselines in Gulf of Mexico fishes (Chap. 15). In: Murawski SA, Ainsworth C, Gilbert S, Hollander D, Paris CB, Schlüter M, Wetzel D (eds) Scenarios and responses to future deep oil spills – fighting the next war. Springer, Cham

Romero AF, Abessa D, Fontes R, Silva G (2013) Integrated assessment for establishing an oil environmental vulnerability map: case study for the Santos Basin region, Brazil. Mar Pollut Bull 74:156–164

Sanchirico JN, Wilen JE (2005) Optimal spatial management of renewable resources: matching policy scope to ecosystem scale. J Environ Econ Manag 50:123–146

Santos CF, Carvalho R, Andrade F (2013) Quantitative assessment of the differential coastal vulnerability associated to oil spills. J Coast Conserv 17:25–36

Schwacke LH, Smith CR, Townsend FI, Wells RS, Hart LB, Balmer BC, Collier TK, De Guise S, Fry MM, Guillette LJ Jr (2013) Health of common bottlenose dolphins (*Tursiops truncatus*) in Barataria Bay, Louisiana, following the *Deepwater Horizon* oil spill. Environ Sci Technol 48:93–103

Sissine F (2007) Energy Independence and security act of 2007: a summary of major provisions. Washington, DC, Congressional Research Service (Library of Congress)

Smith EP, van Belle G (1984) Nonparametric estimation of species richness. Biometrics 40:119–129

Sutton T, Cook A, Moore J, Frank T, Judkins H, Vecchione M, Nizinski M, Youngbluth M. (2017) Inventory of Gulf oceanic fauna data including species, weight, and measurements. Meg Skansi cruises from Jan. 25–Sept. 30, 2011 in the northern Gulf of Mexico. [data set]. Gulf of Mexico Research Initiative Information and Data Cooperative (GRIIDC), Harte Research Institute, Texas A&M University – Corpus Christi. https://doi.org/10.7266/N7VX0DK2

Sutton T, Frank T, Judkins H, Romero IC (2020) As Gulf oil extraction goes deeper, who is at risk? Community structure, distribution, and connectivity of the deep-pelagic fauna (Chap. 24). In: Murawski SA, Ainsworth C, Gilbert S, Hollander D, Paris CB, Schlüter M, Wetzel D (eds) Scenarios and responses to future deep oil spills – fighting the next war. Springer, Cham

Szlafsztein C, Sterr H (2007) A GIS-based vulnerability assessment of coastal natural hazards, state of Brazil. J Coast Conserv 11:53e66

Tran T, Yazdanparast A, Suess EA (2014) Effect of oil spill on birds: a graphical assay of the *Deepwater Horizon* oil spill's impact on birds. Comput Stat 29:133–140. https://link.springer.com/content/pdf/10.1007%2Fs00180-013-0472-z.pdf

U.S. Bureau of Ocean Energy Management (BOEM) (2018) 2019–2024 National Outer Continental Shelf Oil and Gas Leasing Draft Proposed Program. Available at: https://www.boem.gov/NP-Draft-Proposed-Program-2019-2024, 380 pp

Appendix B: Finalized rasters for all resource components created in Chapter 3 and used as inputs in Chapter 4 and Chapter

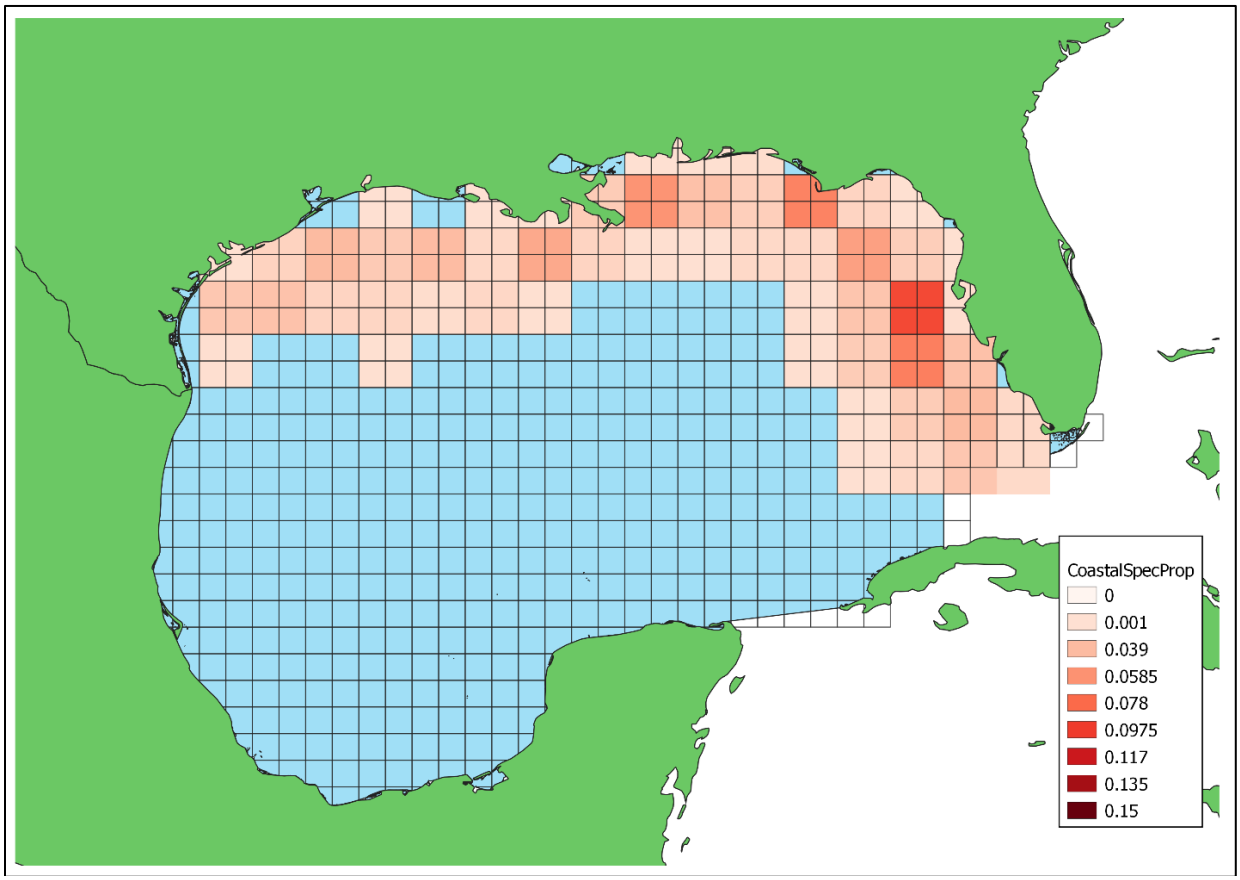

Figure B1 Raster of proportion of revenue for **Coastal Species** at 1°x1° latitude/longitude grid resolution. The values of this raster sum to 1 and is used in the created C-ESIs.

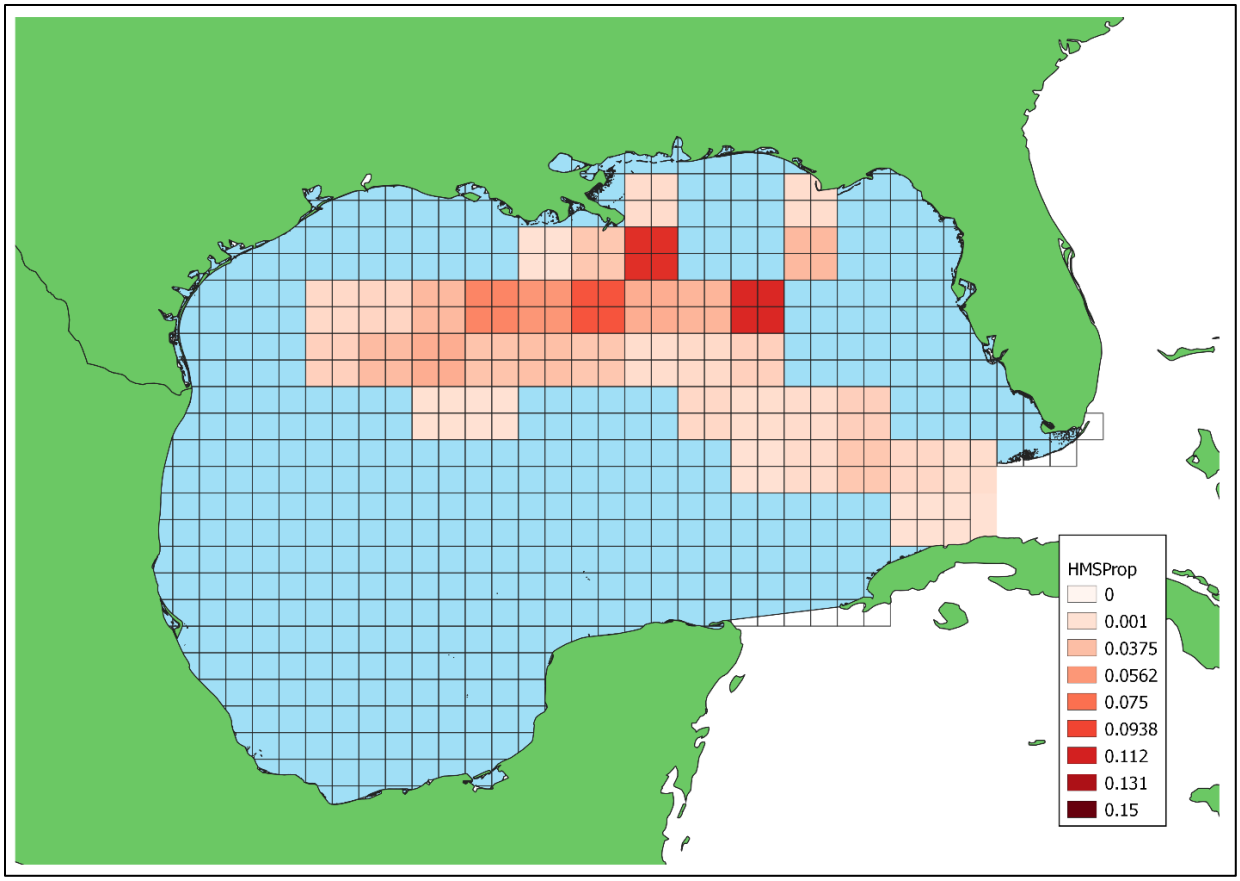

Figure B2 Raster of proportion of revenue index for **Highly Migratory Species** at 1°x1° latitude/longitude grid resolution. The values of this raster sum to 1 and is used in the created C-ESIs.

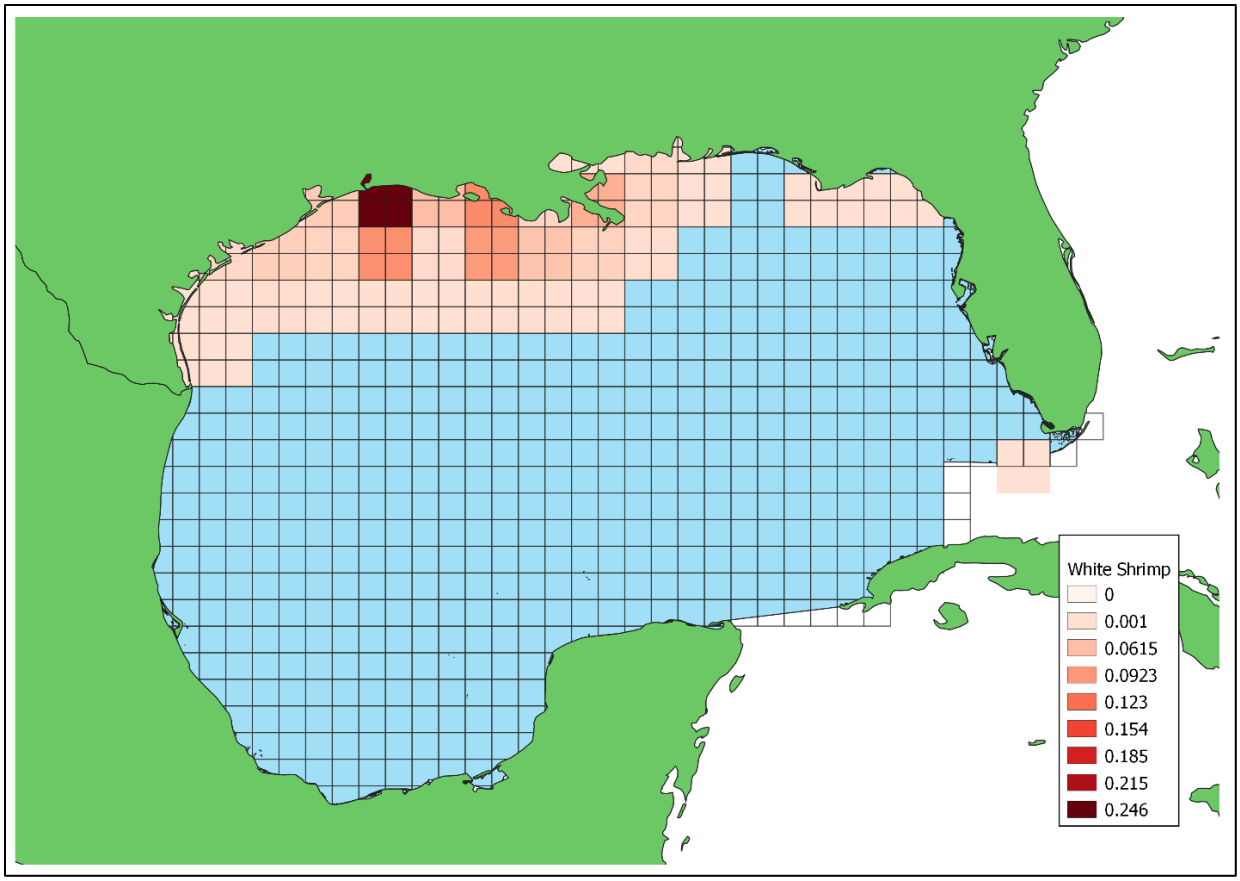

Figure B3 Raster of proportion of revenue index for **White Shrimp Species** at 1°x1° latitude/longitude grid resolution. The values of this raster sum to 1 and is used in the created C-ESIs.

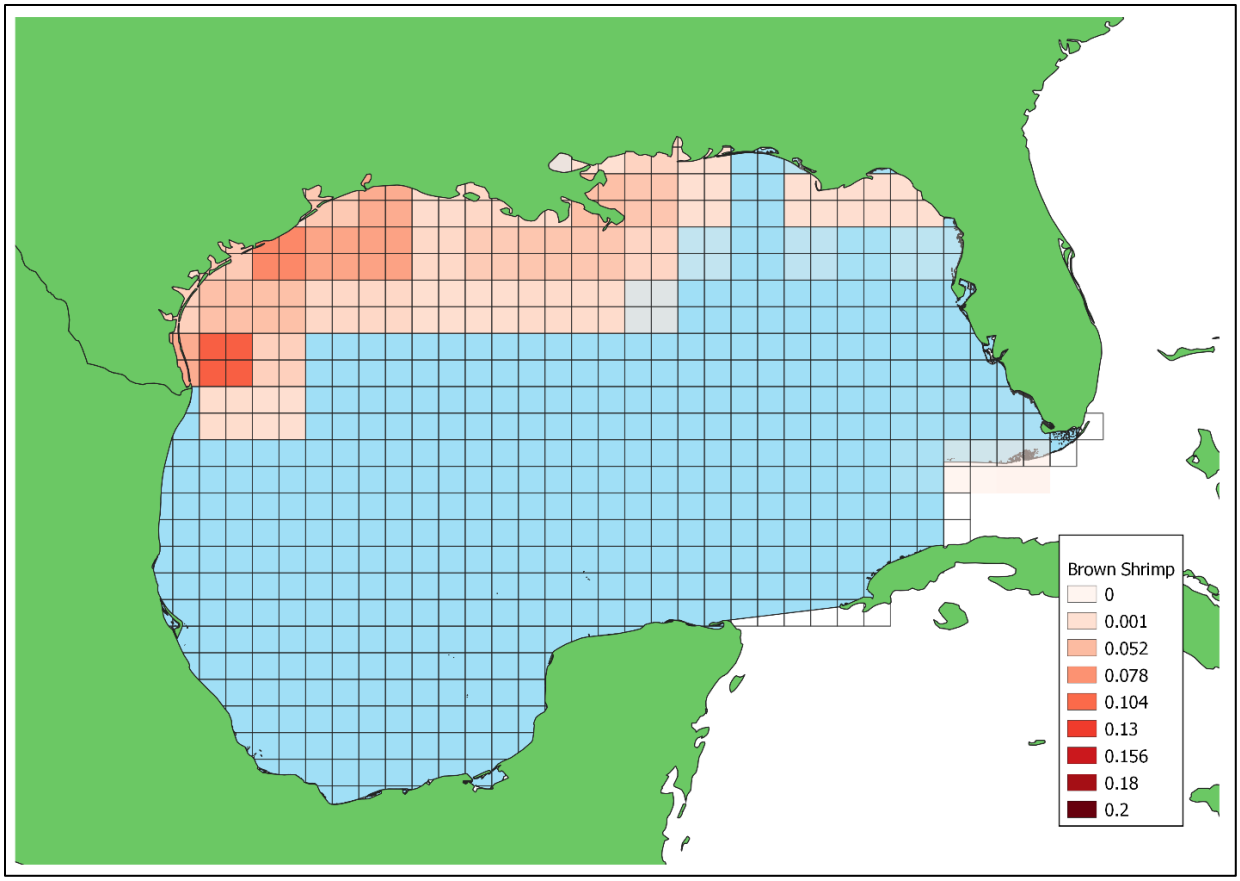

Figure B4 Raster of proportion of revenue index for **Brown Shrimp Species** at 1°x1° latitude/longitude grid resolution. The values of this raster sum to 1 and is used in the created C-ESIs.

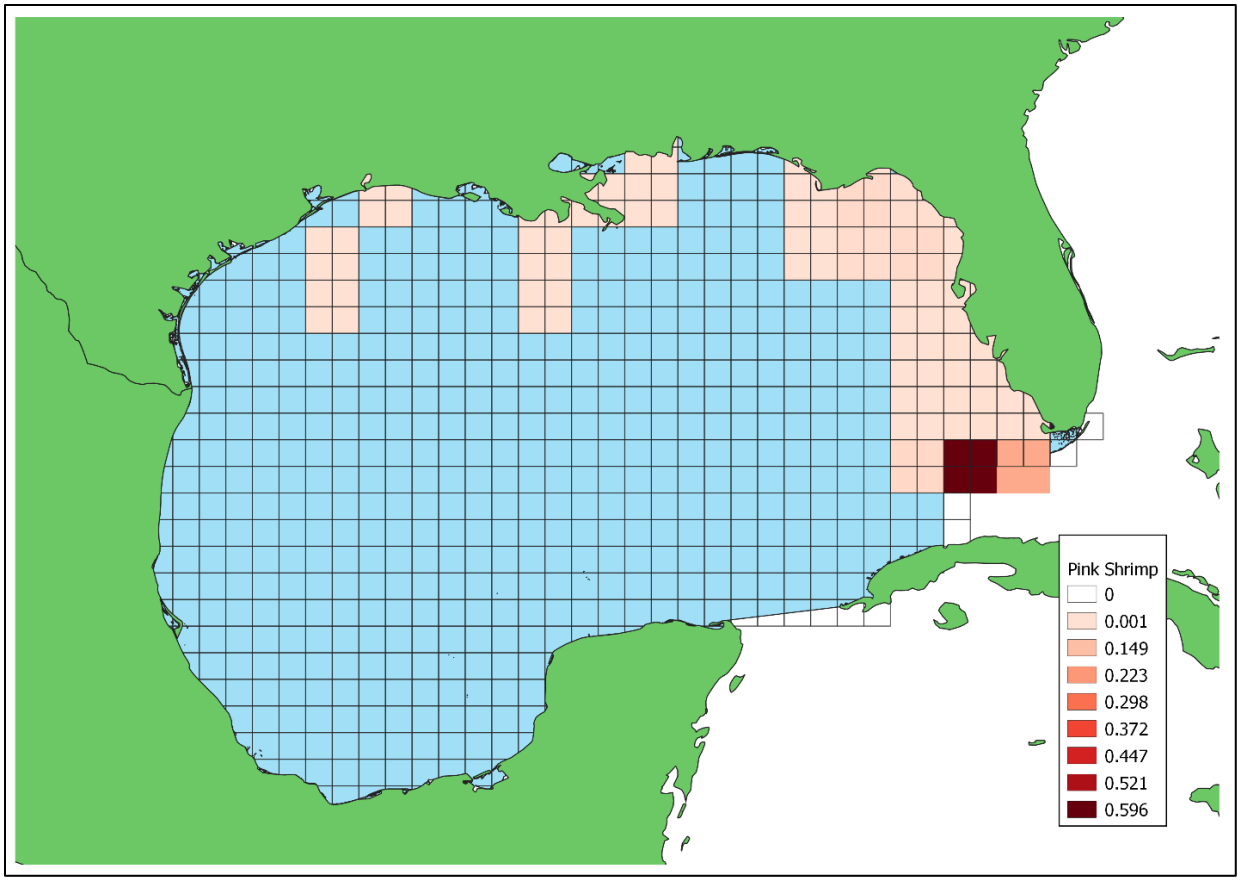

Figure B5 Raster of proportion of revenue index for **Pink Shrimp Species** at 1°x1° latitude/longitude grid resolution. The values of this raster sum to 1 and is used in the created C-ESIs.

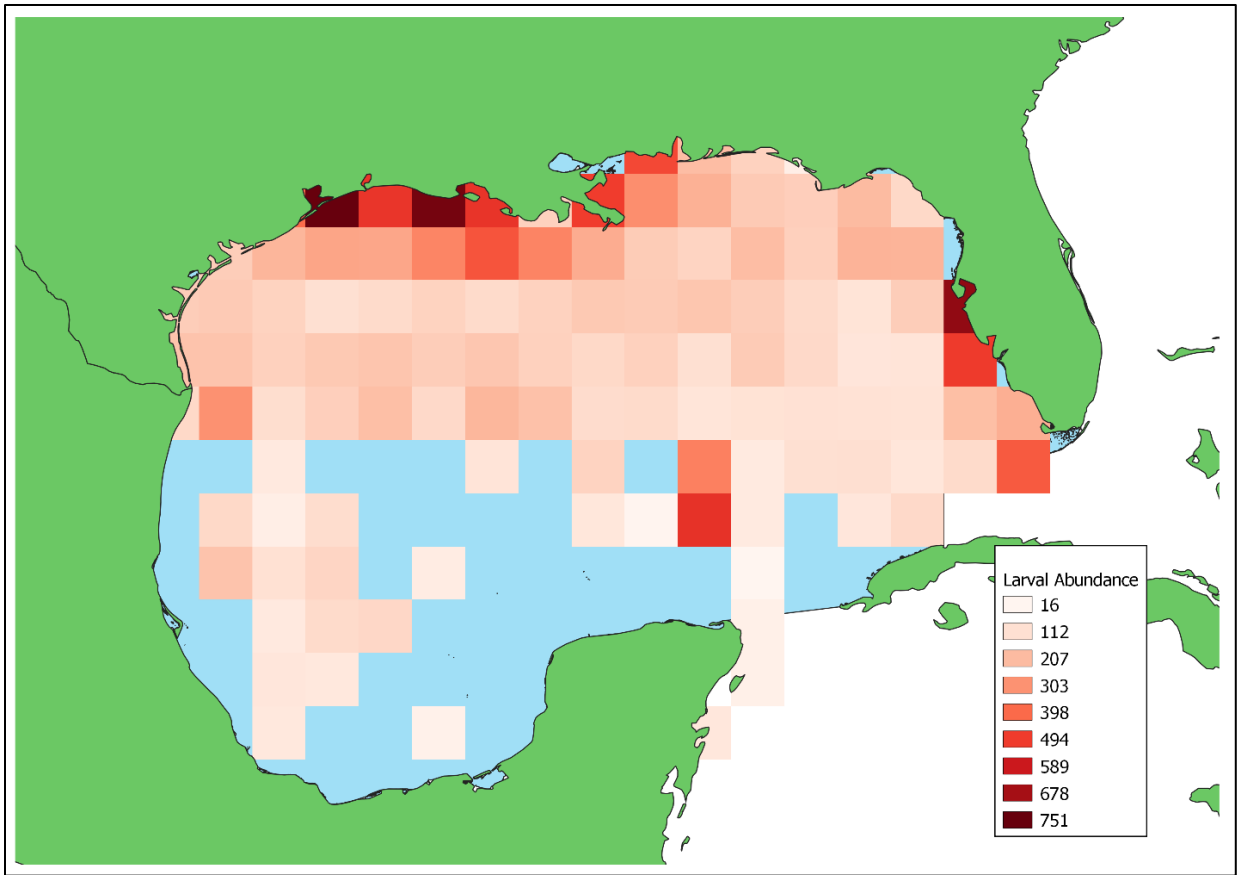

Figure B6 Raster of original standardized abundance of larval fish at 1°x1° latitude/longitude grid resolution.

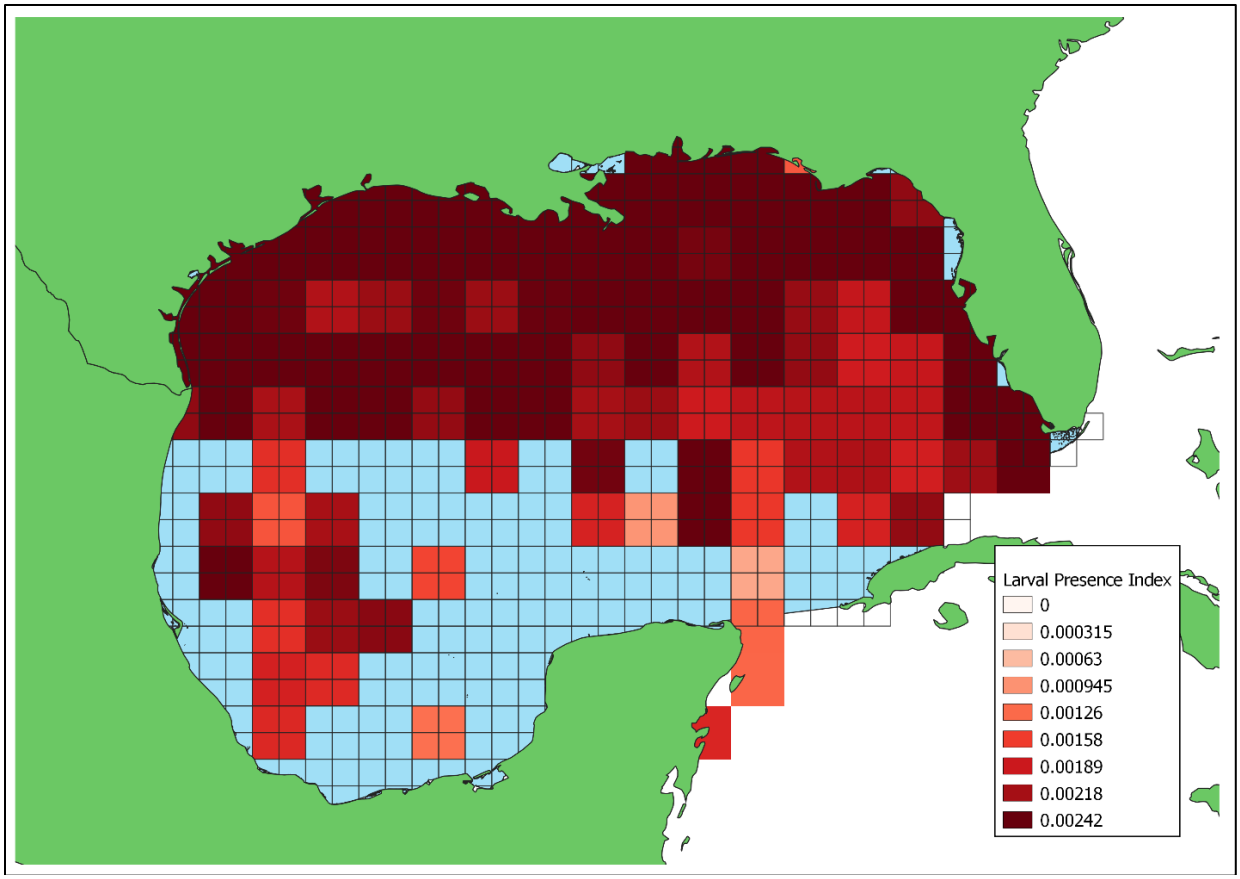

Figure B7 Raster of created presence index of larval fish at 0.5°x0.5° latitude/longitude resolution. The values of this raster sum to 1 and is used in the created C-ESIs.

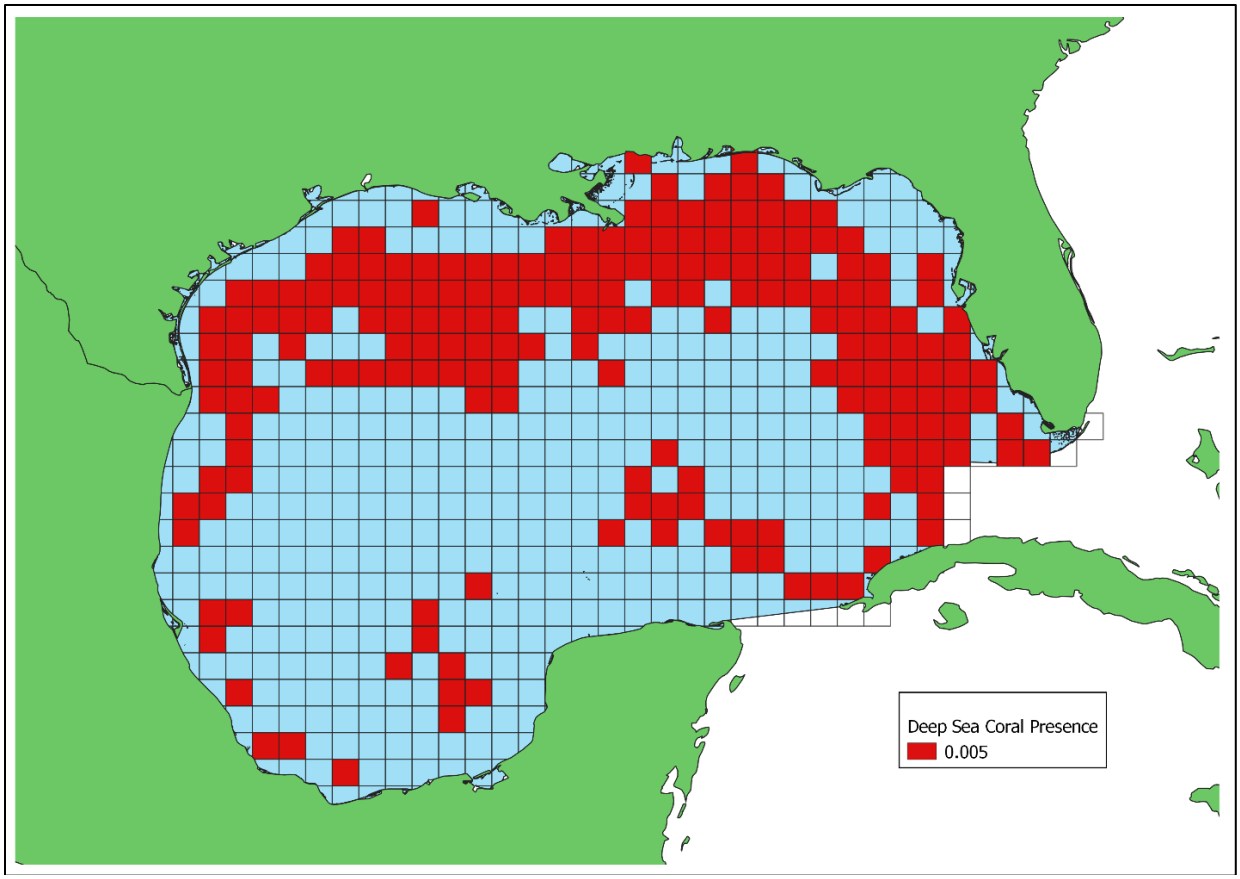

Figure B8 Raster of created presence index of the proportion of **deep-sea coral** habitat at 0.5°x0.5° latitude/longitude resolution. The values of this raster sum to 1 and is used in the created C-ESIs.

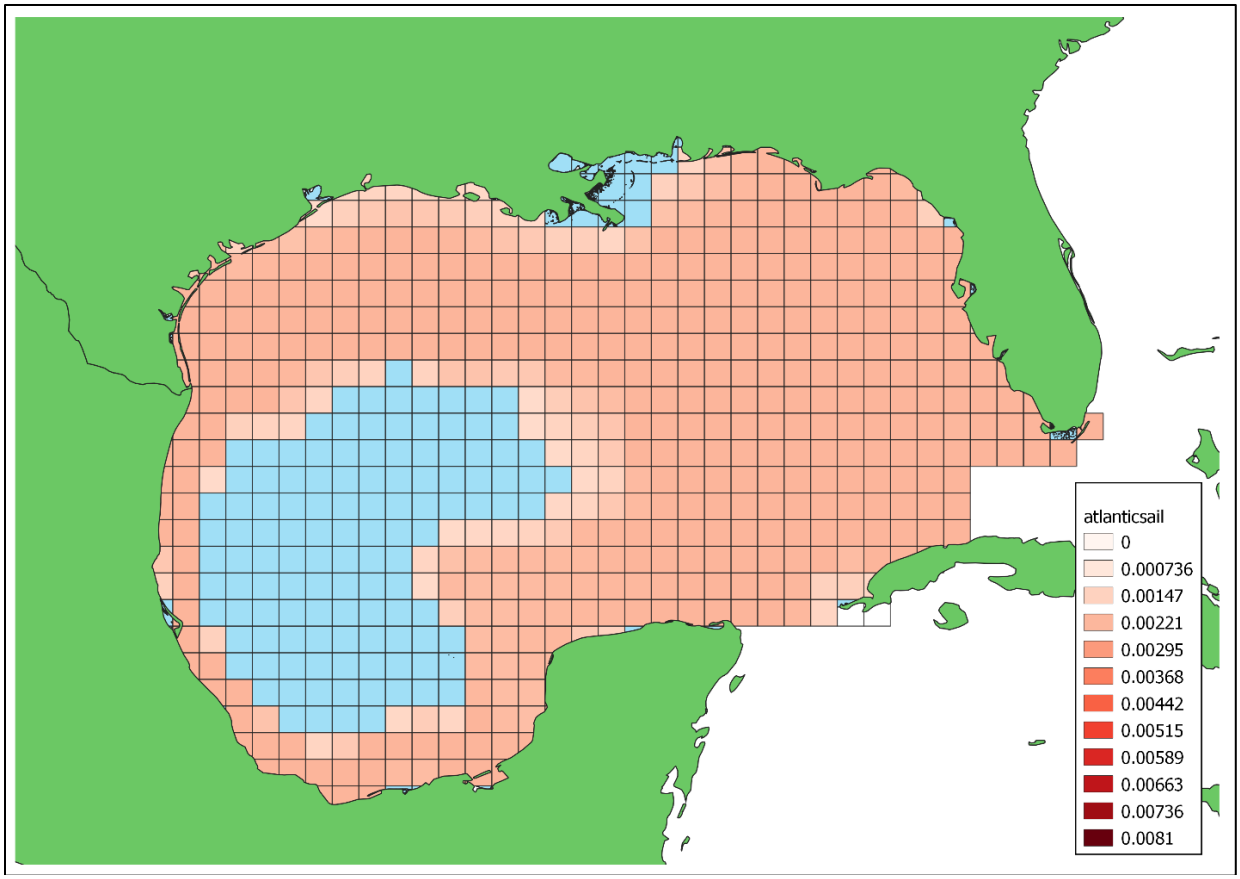

Figure B9 Raster of proportion of suitable habitat for Atlantic sailfish at 0.5°x0.5° latitude/longitude resolution. The values of this raster sum to 1 and is used in the created C-ESIs.

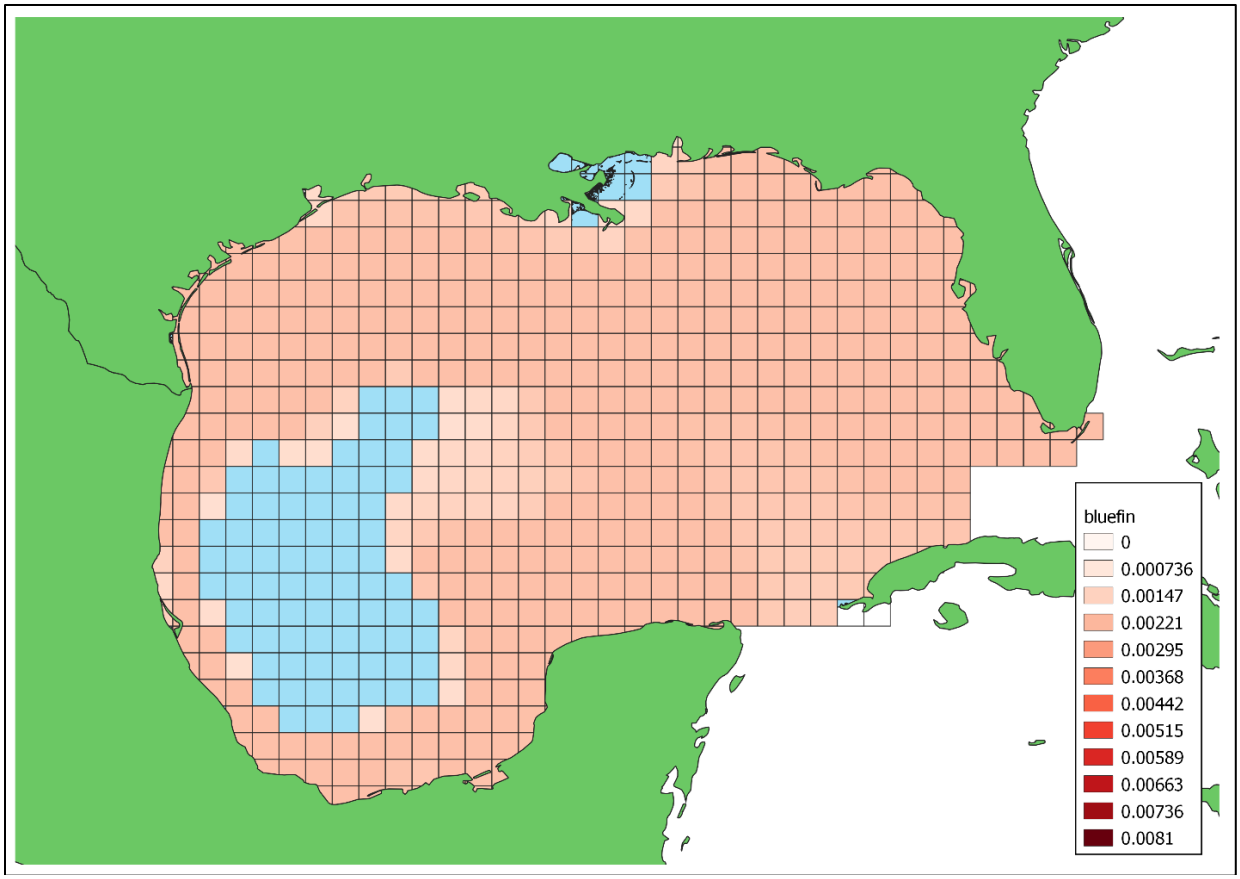

Figure B10 Raster of proportion of suitable habitat for Atlantic bluefin tuna at 0.5°x0.5° latitude/longitude resolution. The values of this raster sum to 1 and is used in the created C-ESIs.

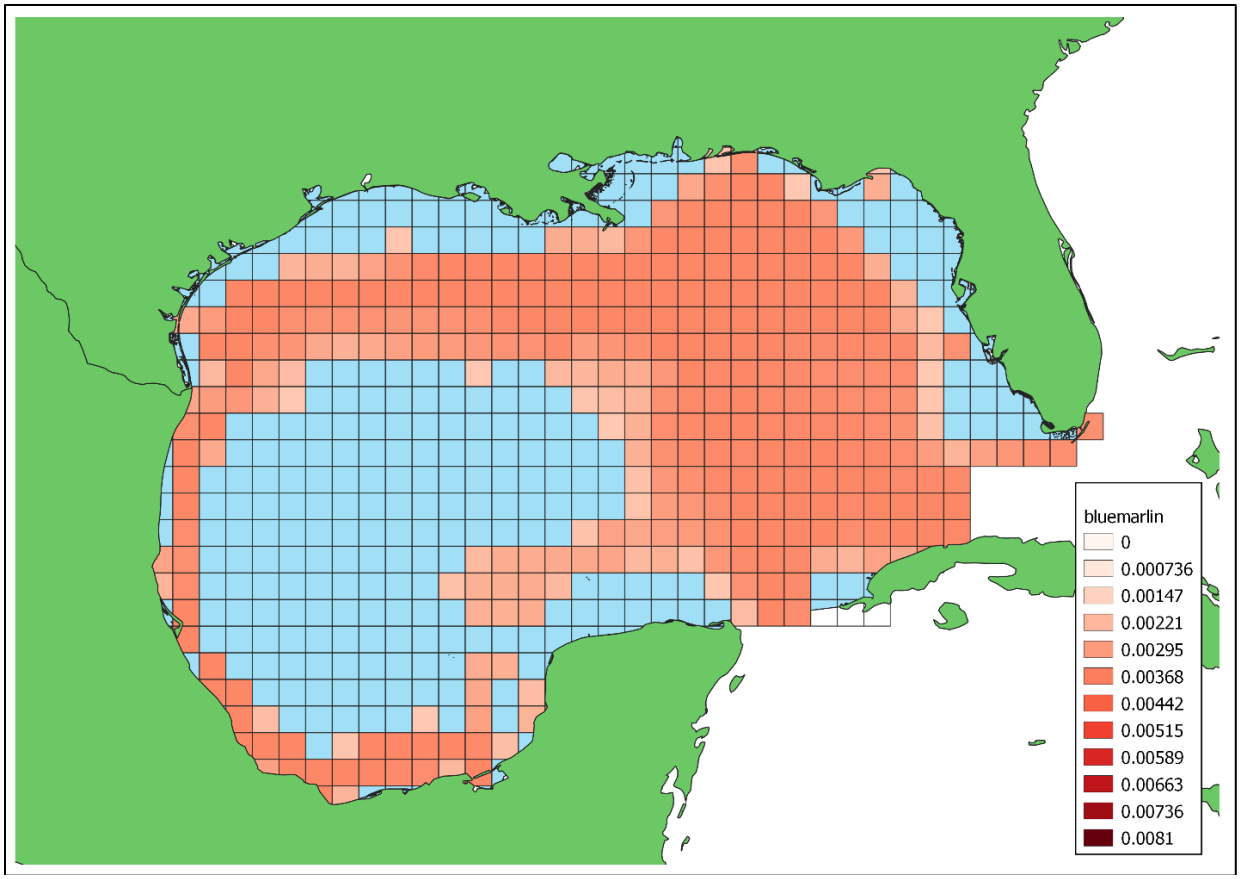

Figure B11 Raster of proportion of suitable habitat for Atlantic blue marlin tuna 0.5°x0.5° latitude/longitude resolution. The values of this raster sum to 1 and is used in the created C-ESIs.

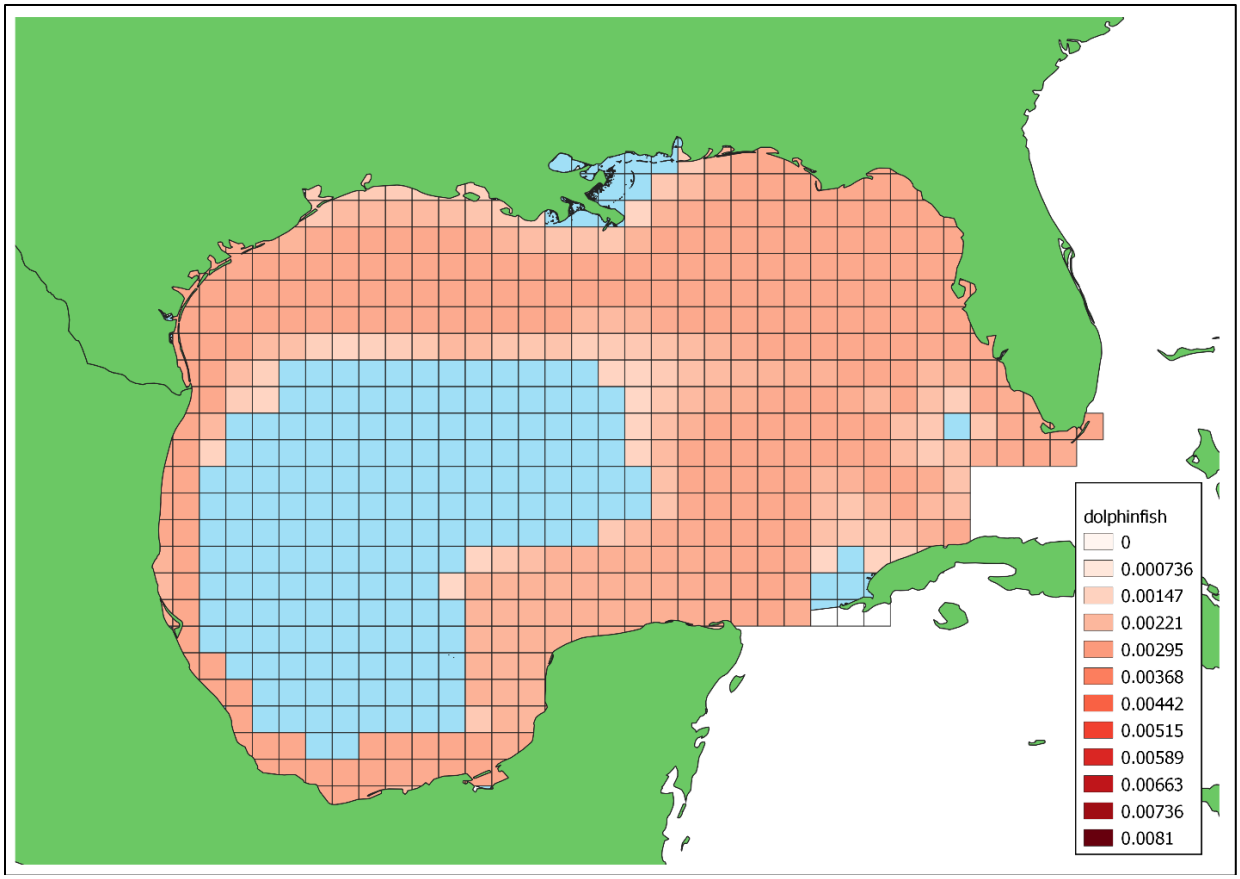

Figure B12 Raster of proportion of suitable habitat for Common dolphinfish at 0.5°x0.5° latitude/longitude resolution. The values of this raster sum to 1 and is used in the created C-ESIs.

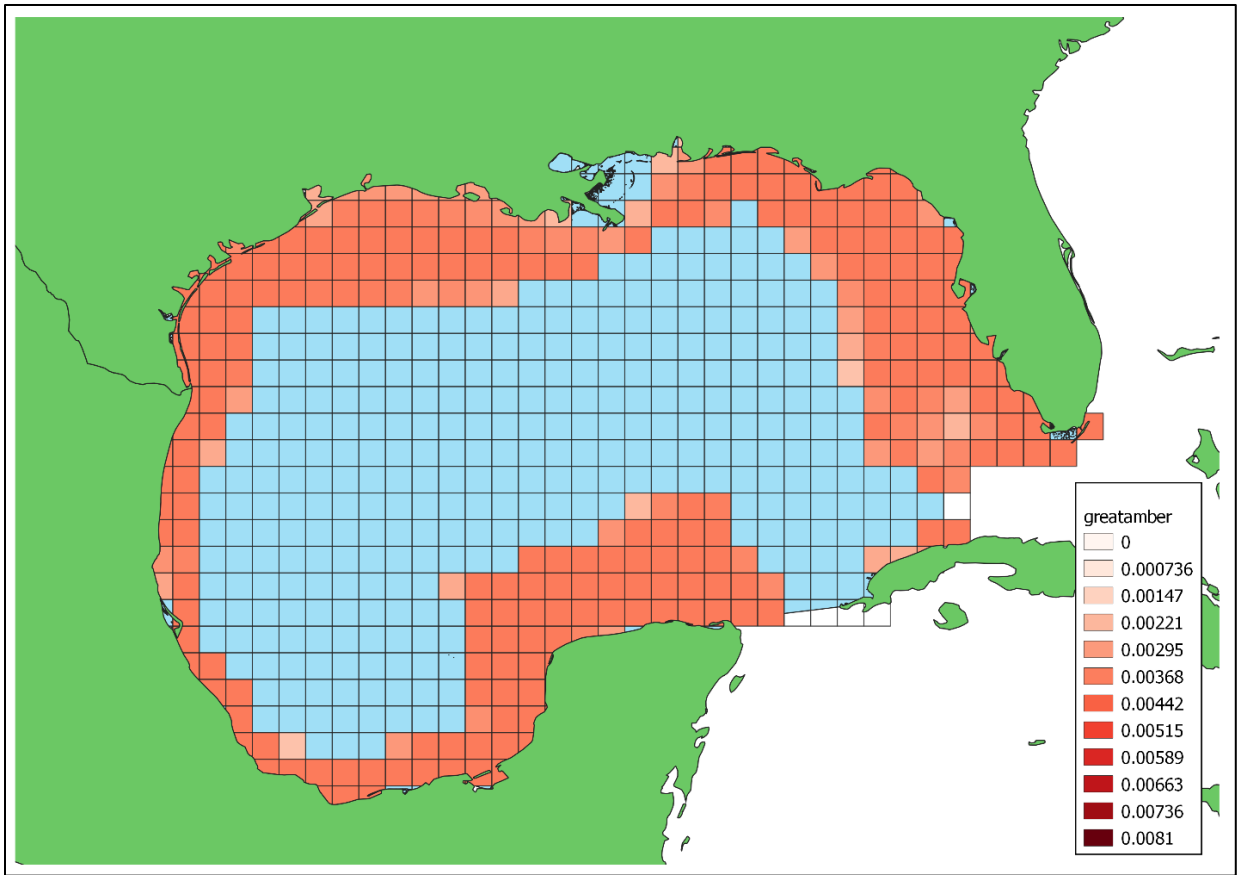

Figure B13 Raster of proportion of suitable habitat for Greater amberjack at 0.5°x0.5° latitude/longitude resolution. The values of this raster sum to 1 and is used in the created C-ESIs.

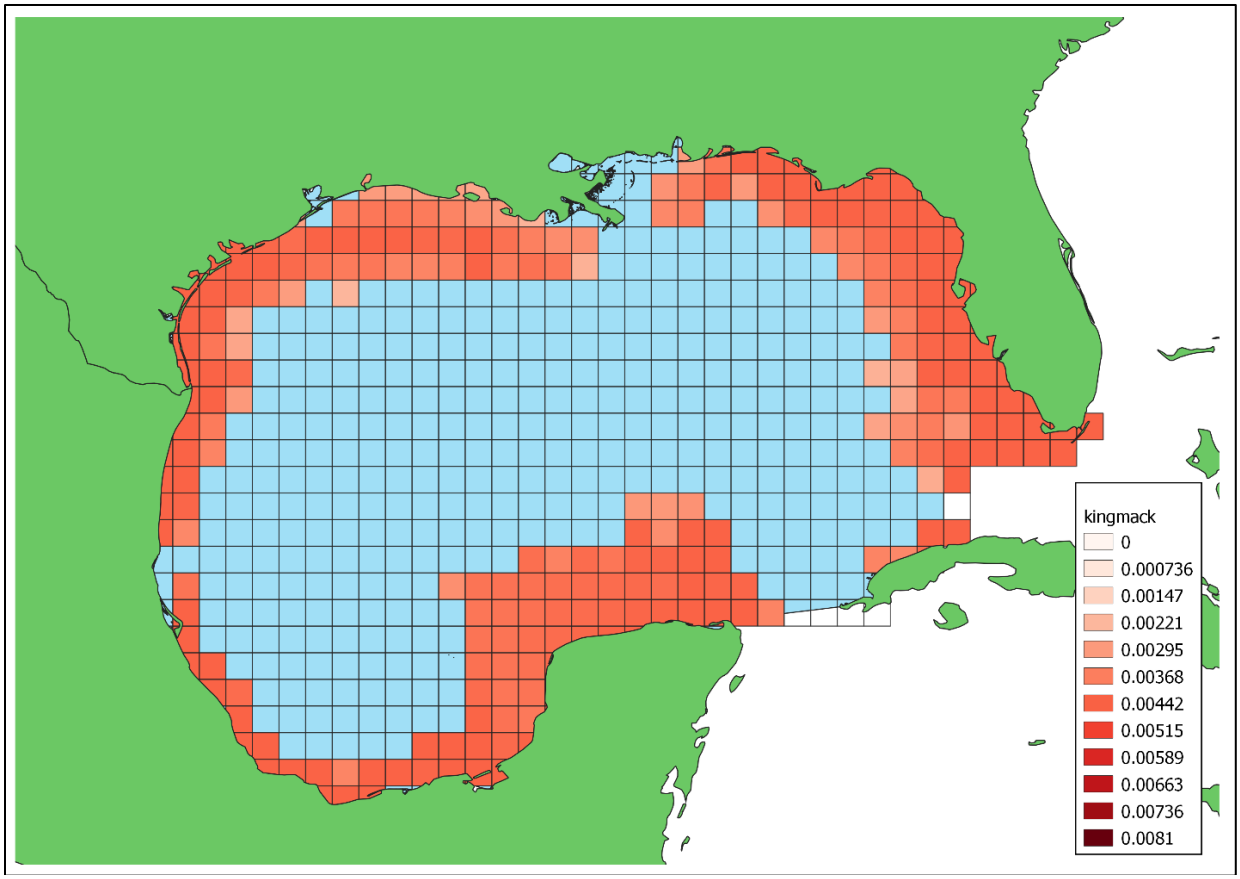

Figure B14 Raster of proportion of suitable habitat for King mackerel at 0.5°x0.5° latitude/longitude resolution. The values of this raster sum to 1 and is used in the created C-ESIs.

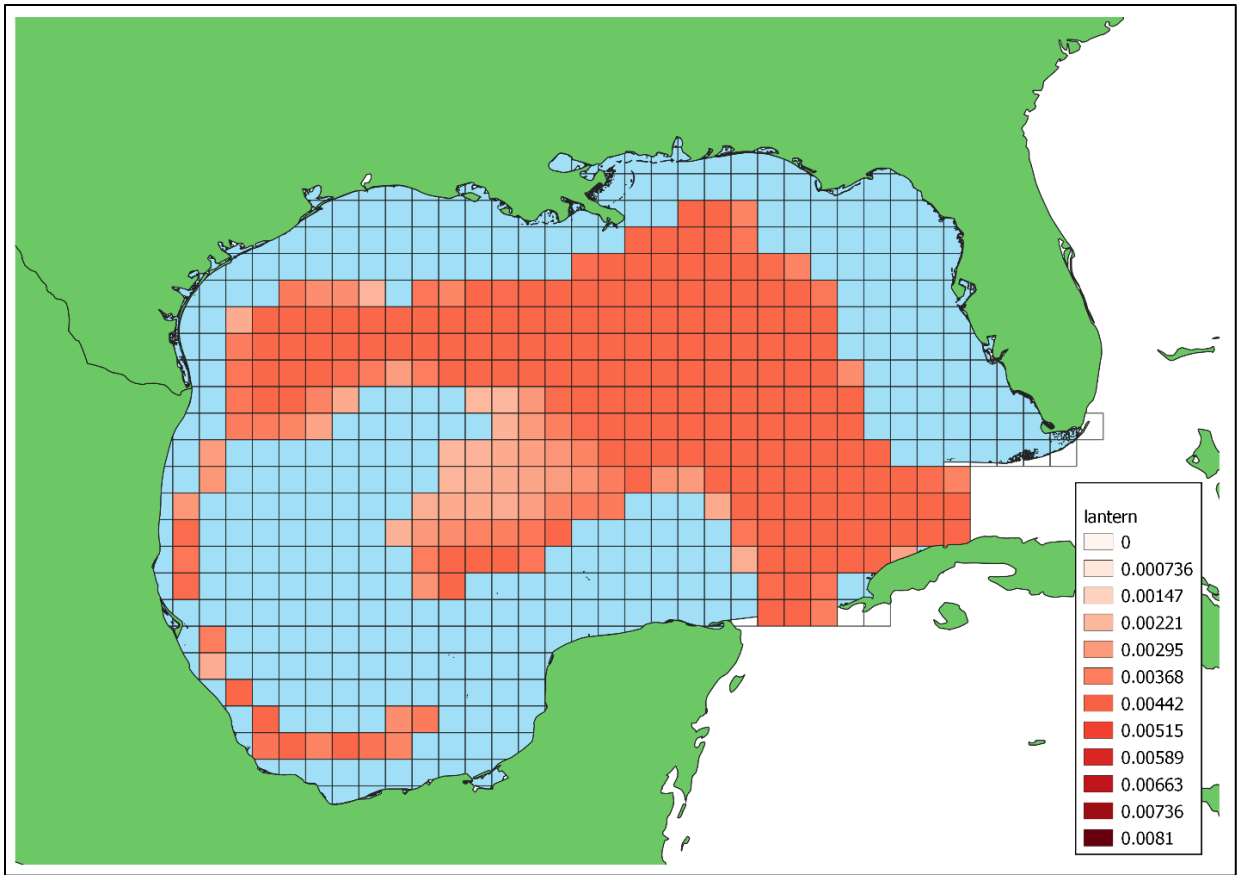

Figure B15 Raster of proportion of suitable habitat for Warmingii Lanternfish at 0.5°x0.5° latitude/longitude resolution. The values of this raster sum to 1 and is used in the created C-ESIs.

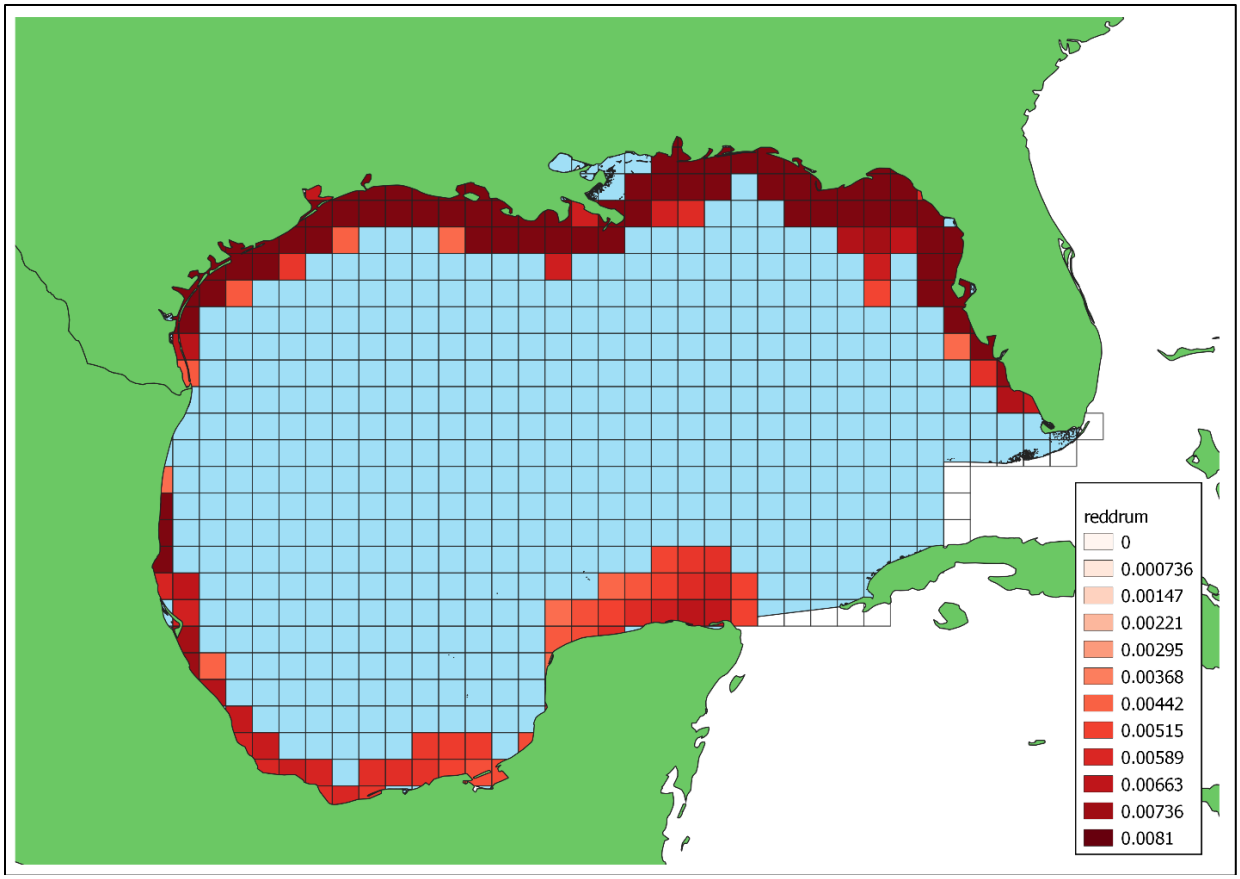

Figure B16 Raster of proportion of suitable habitat for Red drum at 0.5°x0.5° latitude/longitude resolution. The values of this raster sum to 1 and is used in the created C-ESIs.

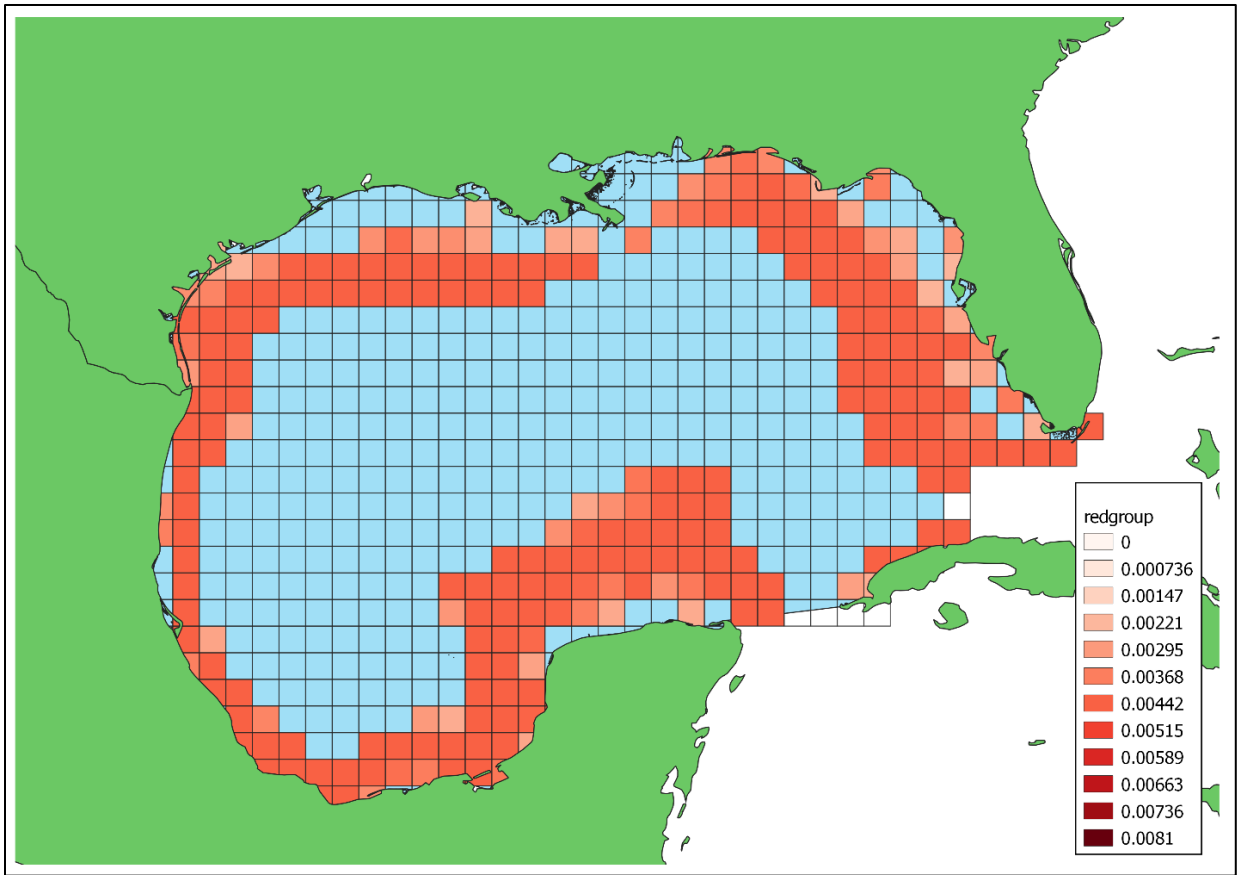

Figure B17 Raster of proportion of suitable habitat for Red grouper at 0.5°x0.5° latitude/longitude resolution. The values of this raster sum to 1 and is used in the created C-ESIs.

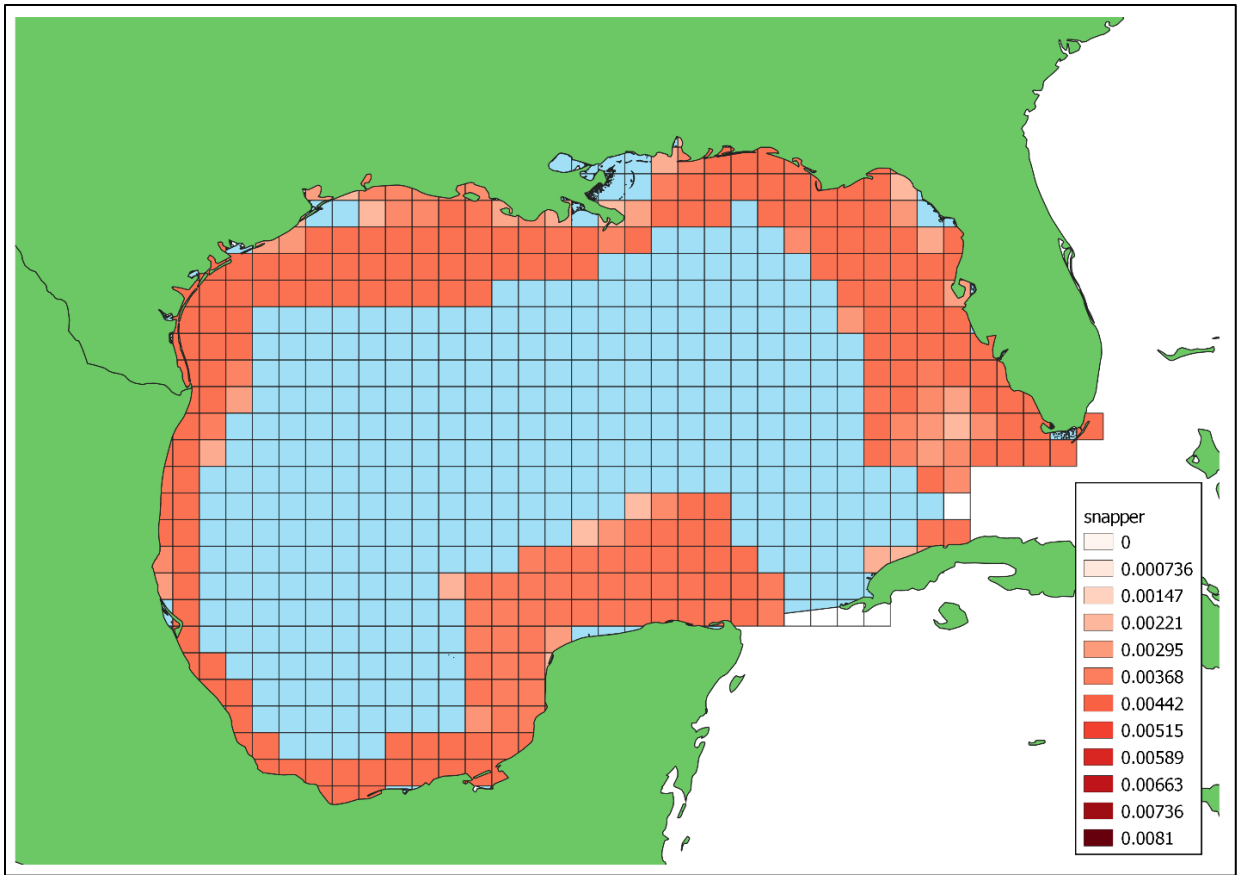

Figure B18 Raster of proportion of suitable habitat for Red snapper at 0.5°x0.5° latitude/longitude resolution. The values of this raster sum to 1 and is used in the created C-ESIs.

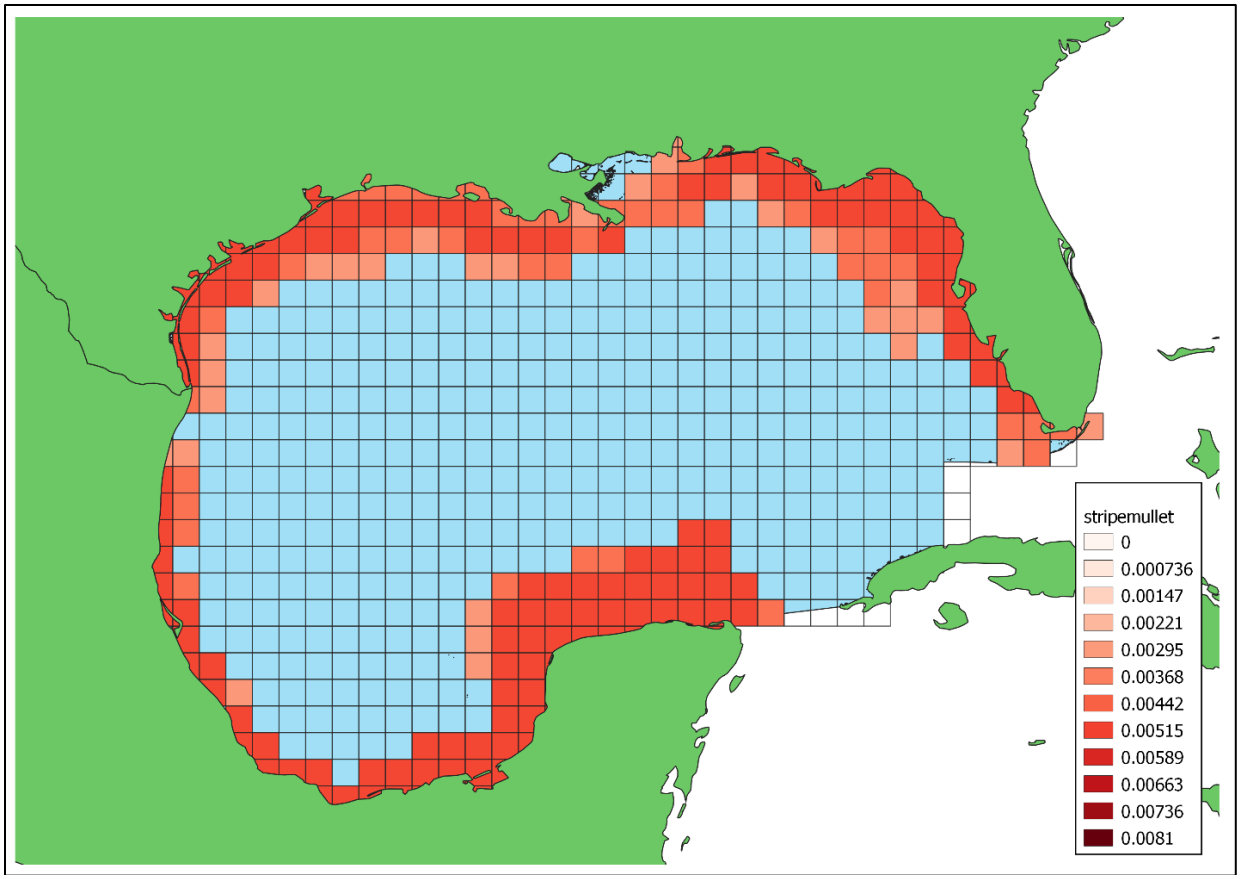

Figure B19 Raster of proportion of suitable habitat for Striped mullet at 0.5°x0.5° latitude/longitude resolution. The values of this raster sum to 1 and is used in the created C-ESIs.

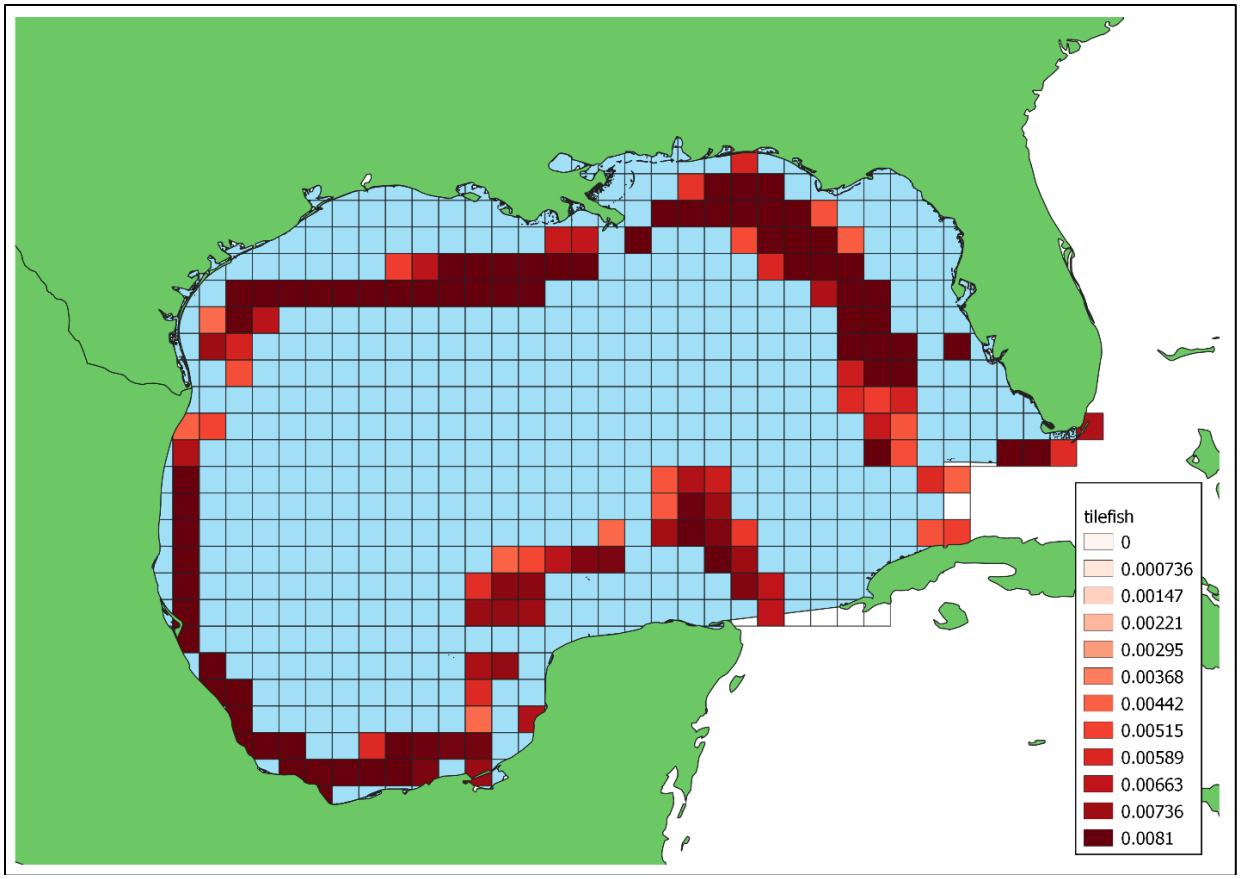

Figure B20 Raster of proportion of suitable habitat for Great northern tilefish at 0.5°x0.5° latitude/longitude resolution. The values of this raster sum to 1 and is used in the created C-ESIs.

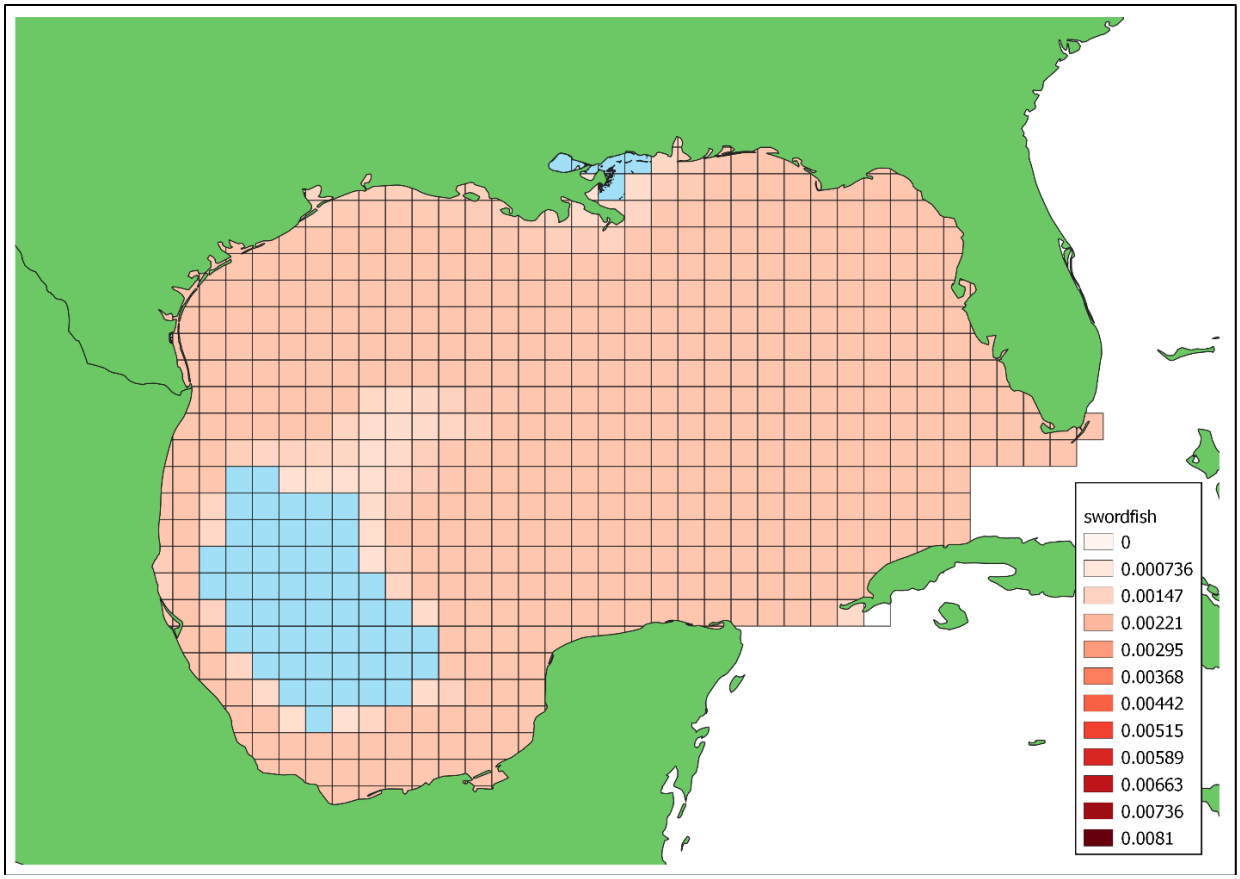

Figure B21 Raster of proportion of suitable habitat for Swordfish at 0.5°x0.5° latitude/longitude resolution. The values of this raster sum to 1 and is used in the created C-ESIs.

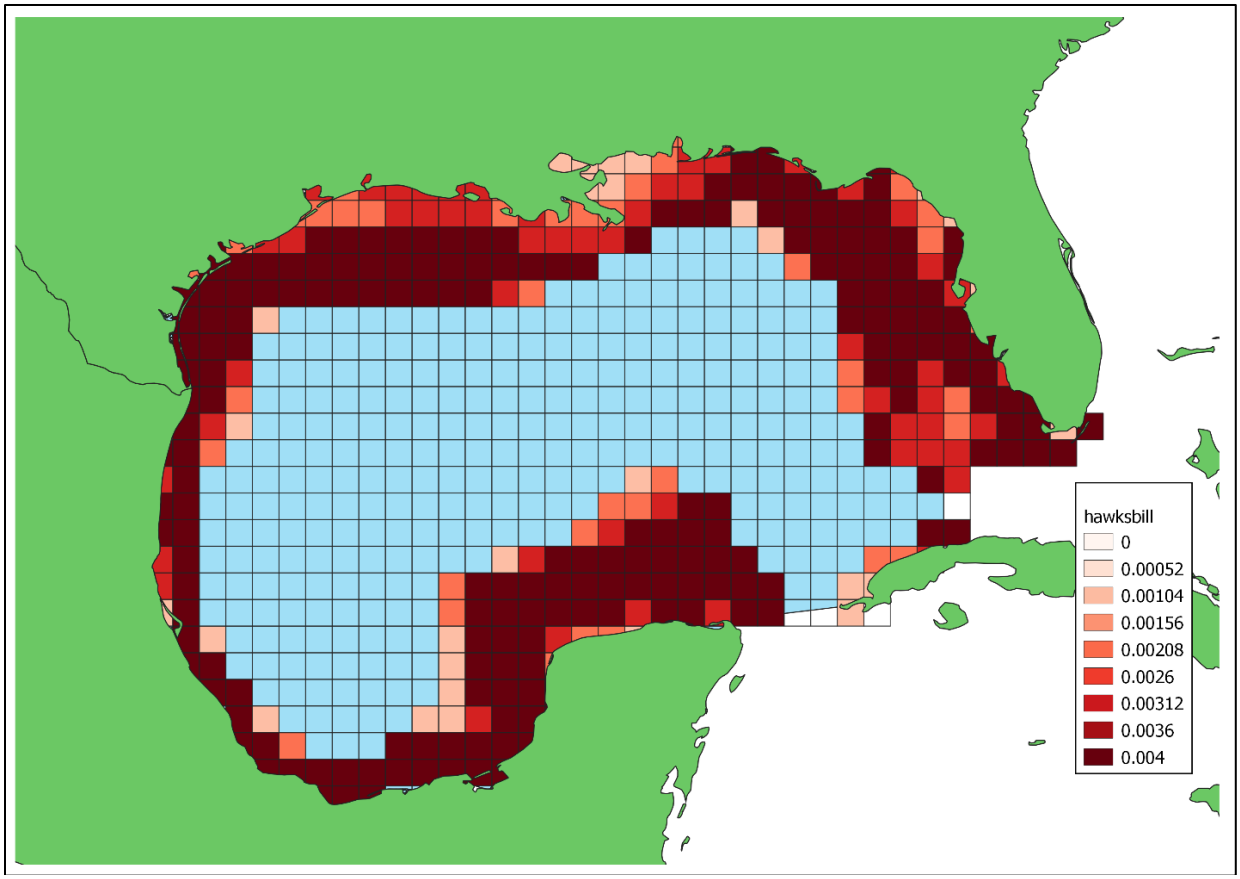

Figure B22 Raster of proportion of suitable habitat for Hawksbill sea turtle at 0.5°x0.5° latitude/longitude resolution. The values of this raster sum to 1 and is used in the created C-ESIs.

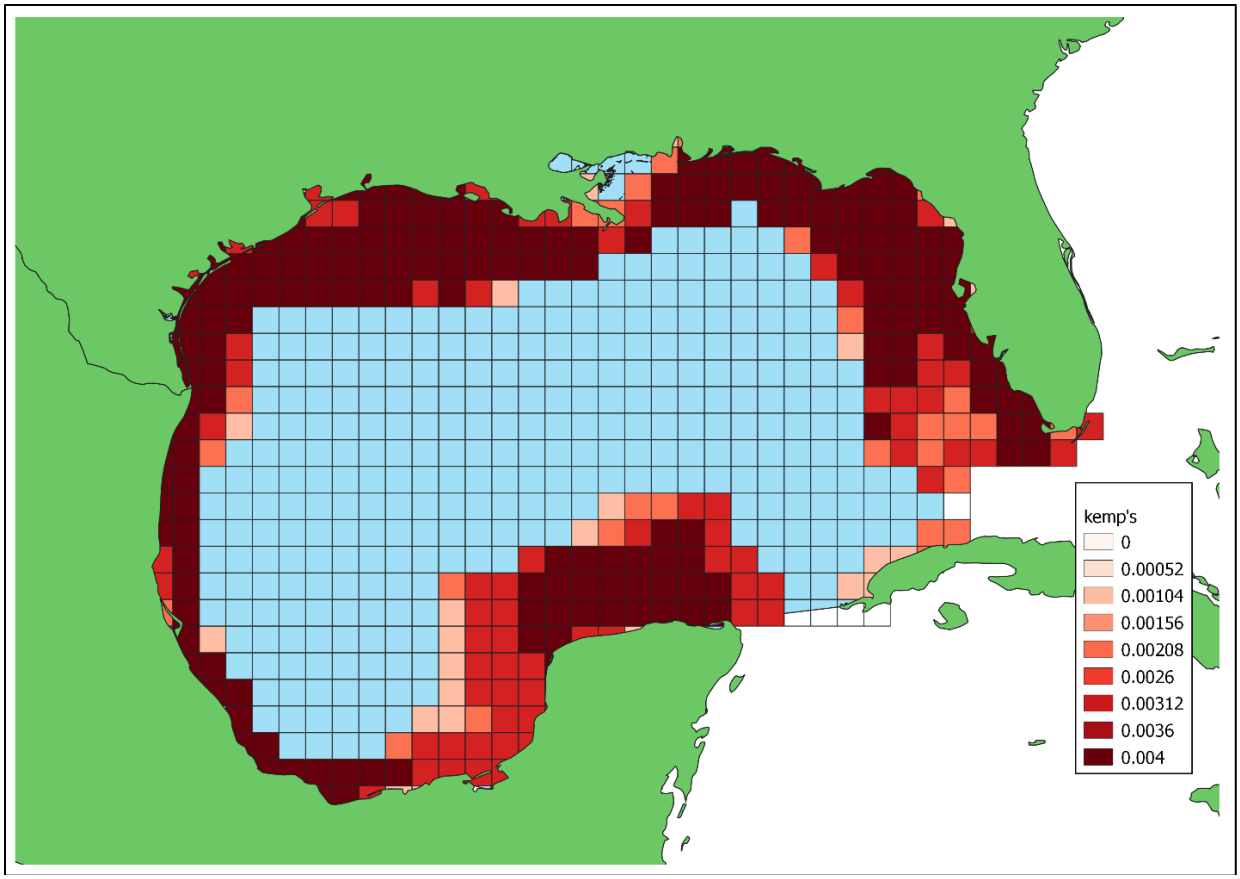

Figure B23 Raster of proportion of suitable habitat for Kemp's Ridley sea turtle at 0.5°x0.5° latitude/longitude resolution. The values of this raster sum to 1 and is used in the created C-ESIs.

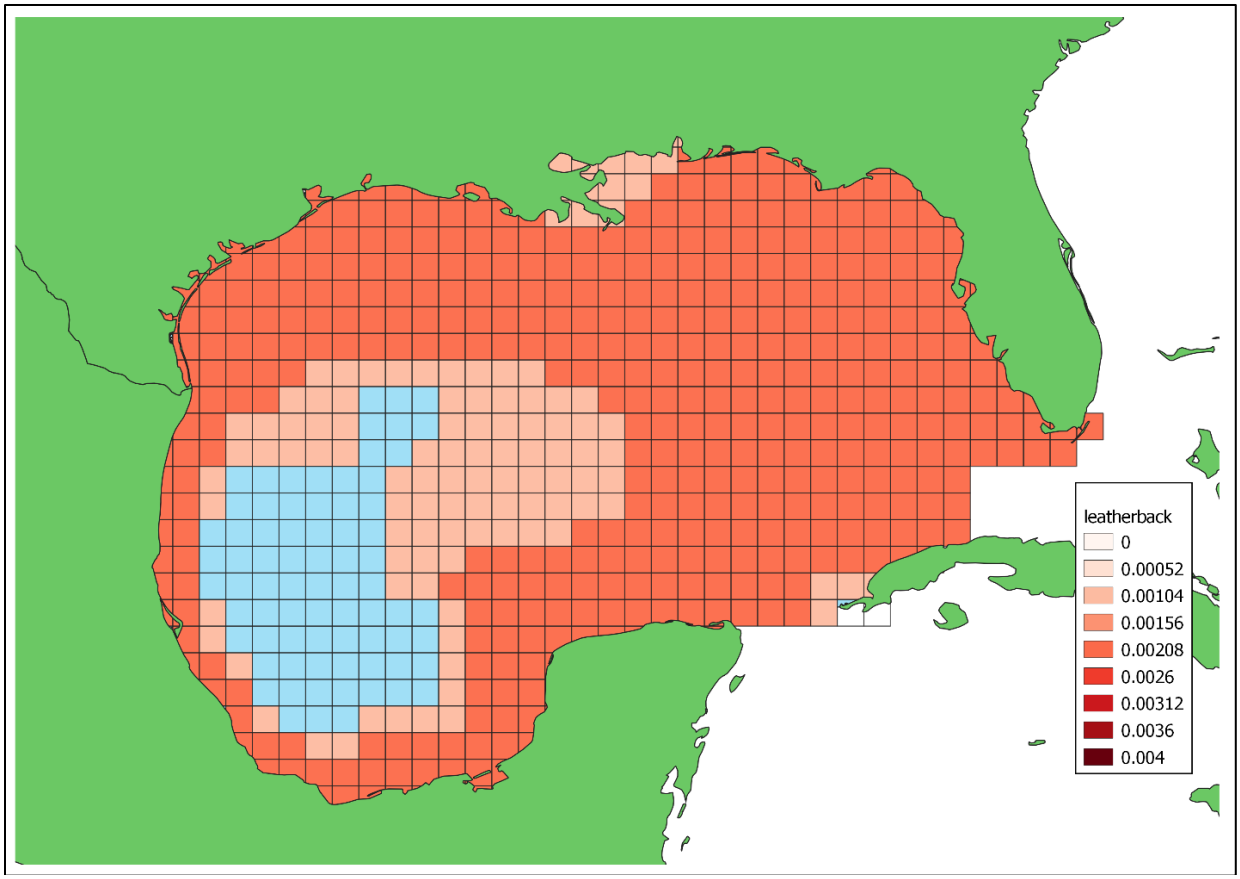

Figure B24 Raster of proportion of suitable habitat for Leatherback sea turtle at 0.5°x0.5° latitude/longitude resolution. The values of this raster sum to 1 and is used in the created C-ESIs.

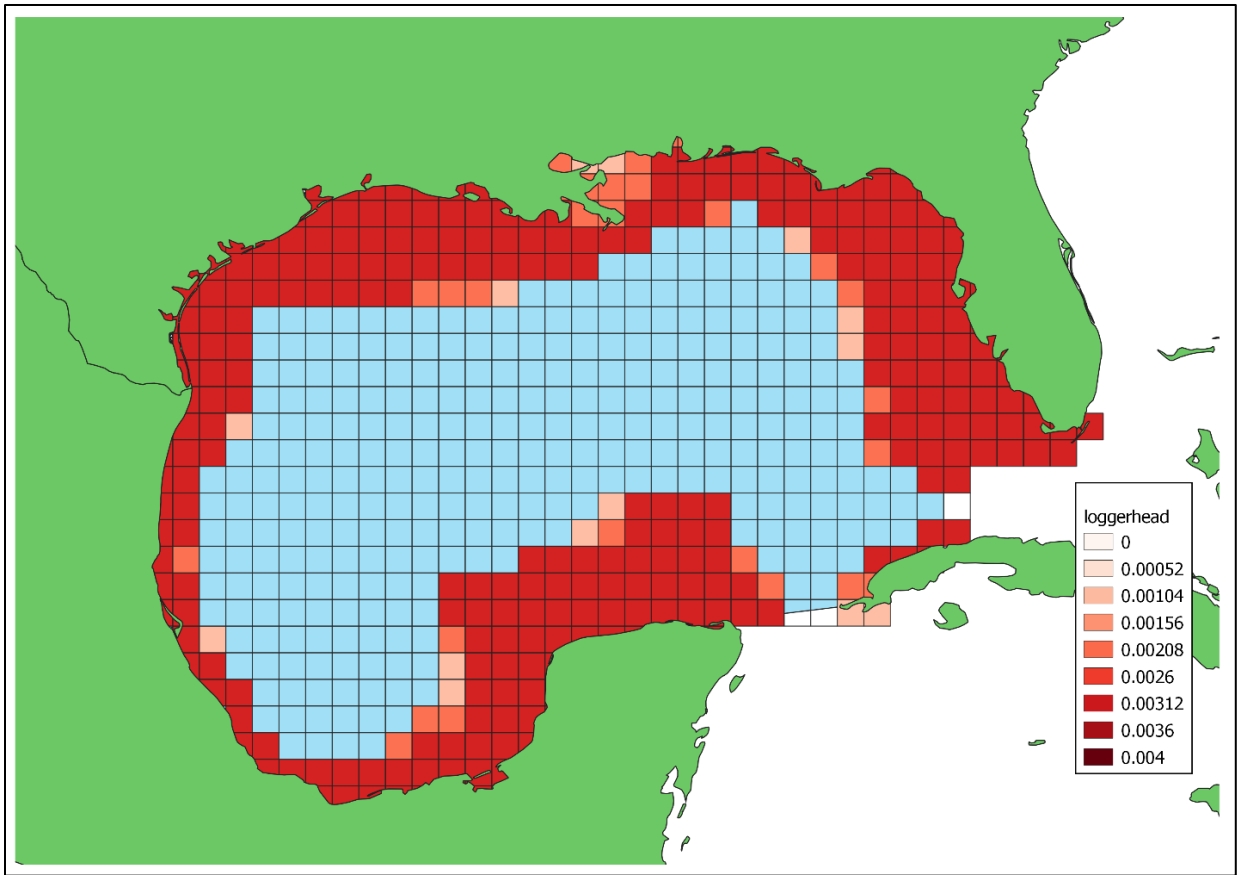

Figure B25 Raster of proportion of suitable habitat for Loggerhead sea turtle at 0.5°x0.5° latitude/longitude resolution. The values of this raster sum to 1 and is used in the created C-ESIs.

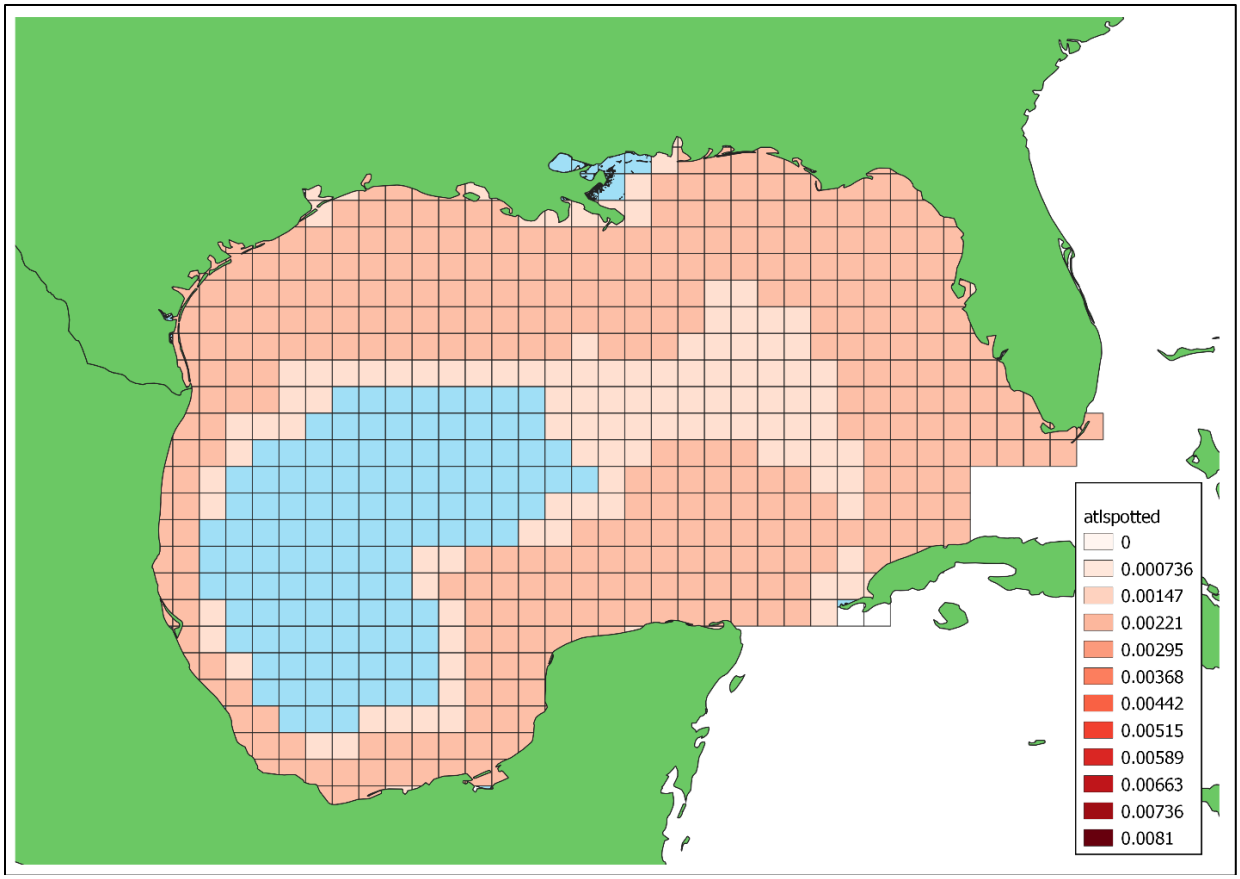

Figure B26 Raster of proportion of suitable habitat for Atlantic spotted dolphin 0.5°x0.5° latitude/longitude resolution. The values of this raster sum to 1 and is used in the created C-ESIs.

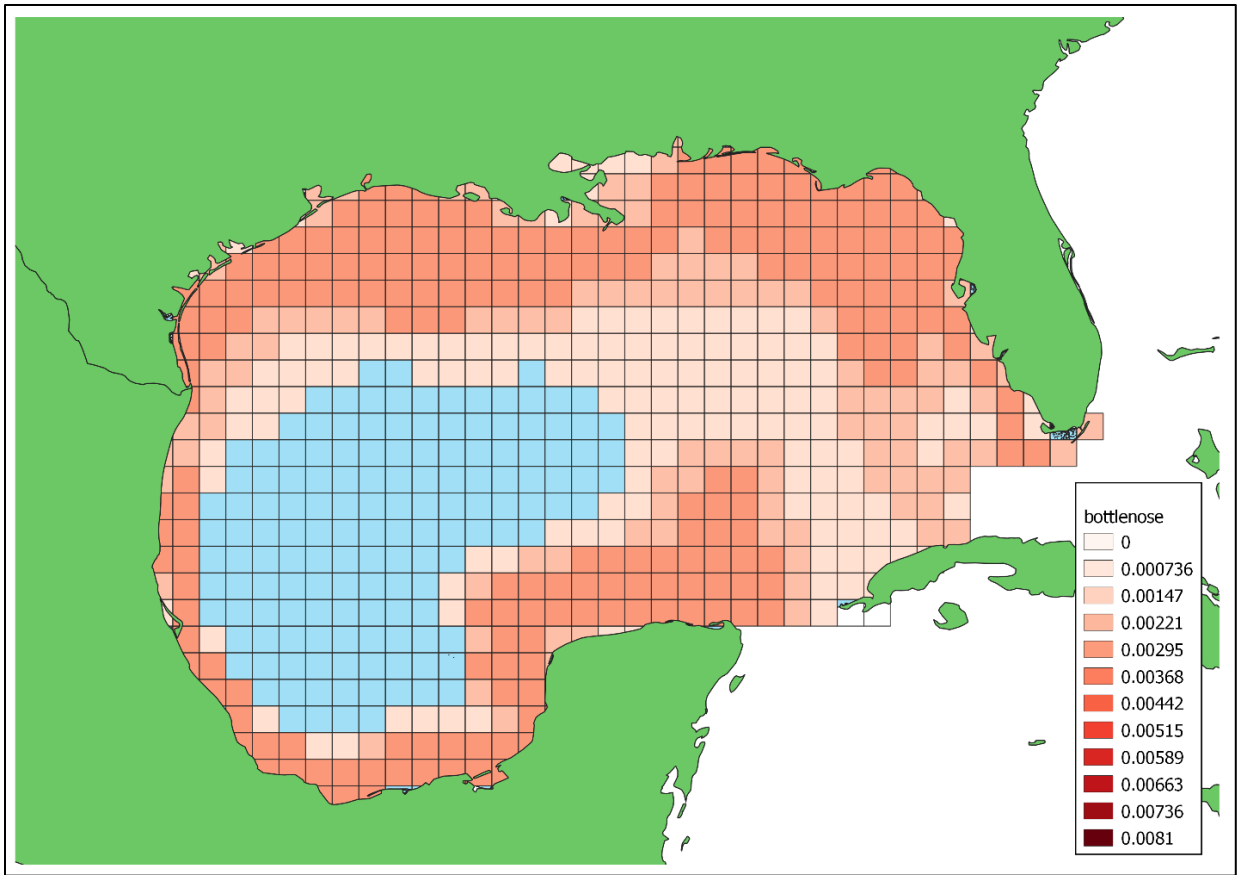

Figure B27 Raster of proportion of suitable habitat for Bottlenose dolphin at 0.5°x0.5° latitude/longitude resolution. The values of this raster sum to 1 and is used in the created C-ESIs.

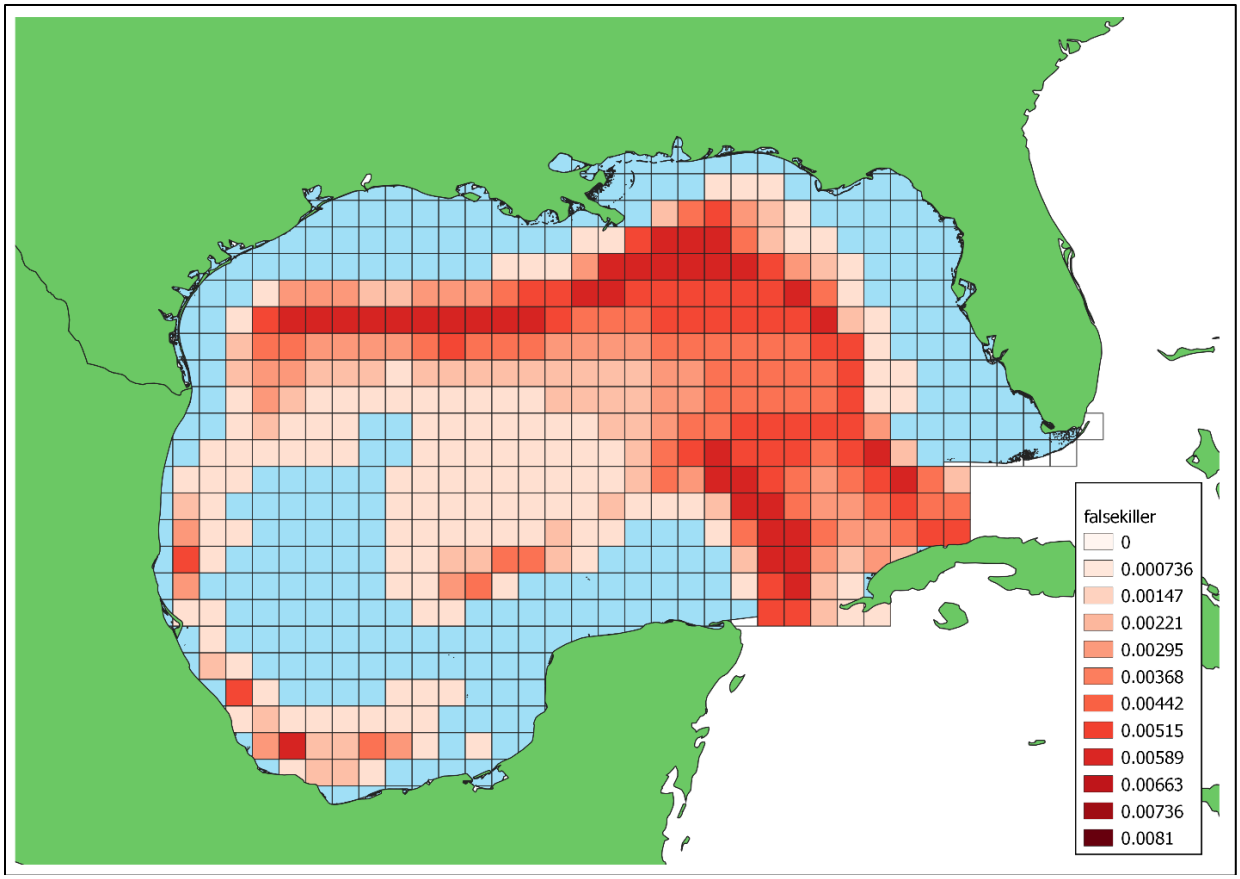

Figure B28 Raster of proportion of suitable habitat for False killer whale at 0.5°x0.5° latitude/longitude resolution. The values of this raster sum to 1 and is used in the created C-ESIs.

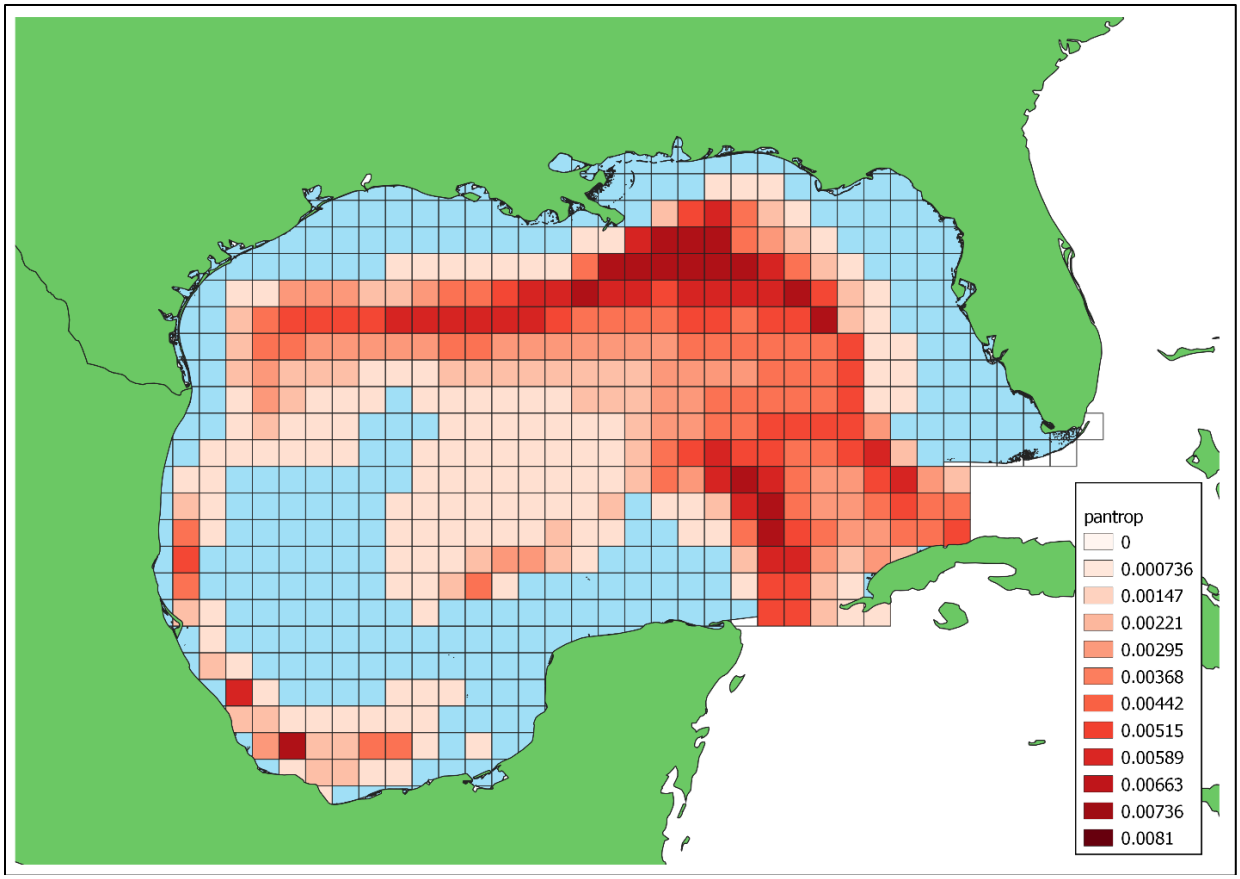

Figure B29 Raster of proportion of suitable habitat for Pantropical spotted dolphin at 0.5°x0.5° latitude/longitude resolution. The values of this raster sum to 1 and is used in the created C-ESIs.

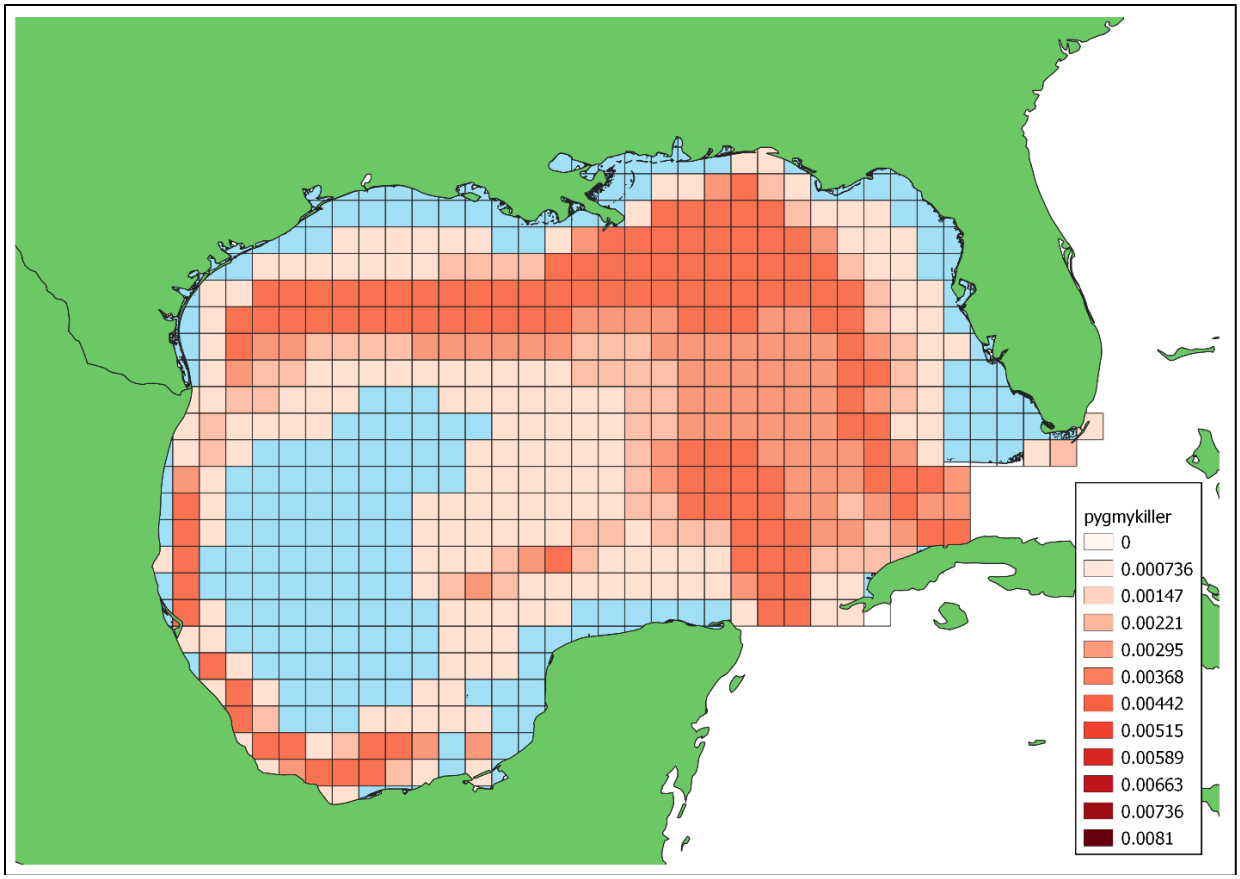

Figure B30 Raster of proportion of suitable habitat for Pygmy killer whale at 0.5°x0.5° latitude/longitude resolution. The values of this raster sum to 1 and is used in the created C-ESIs.

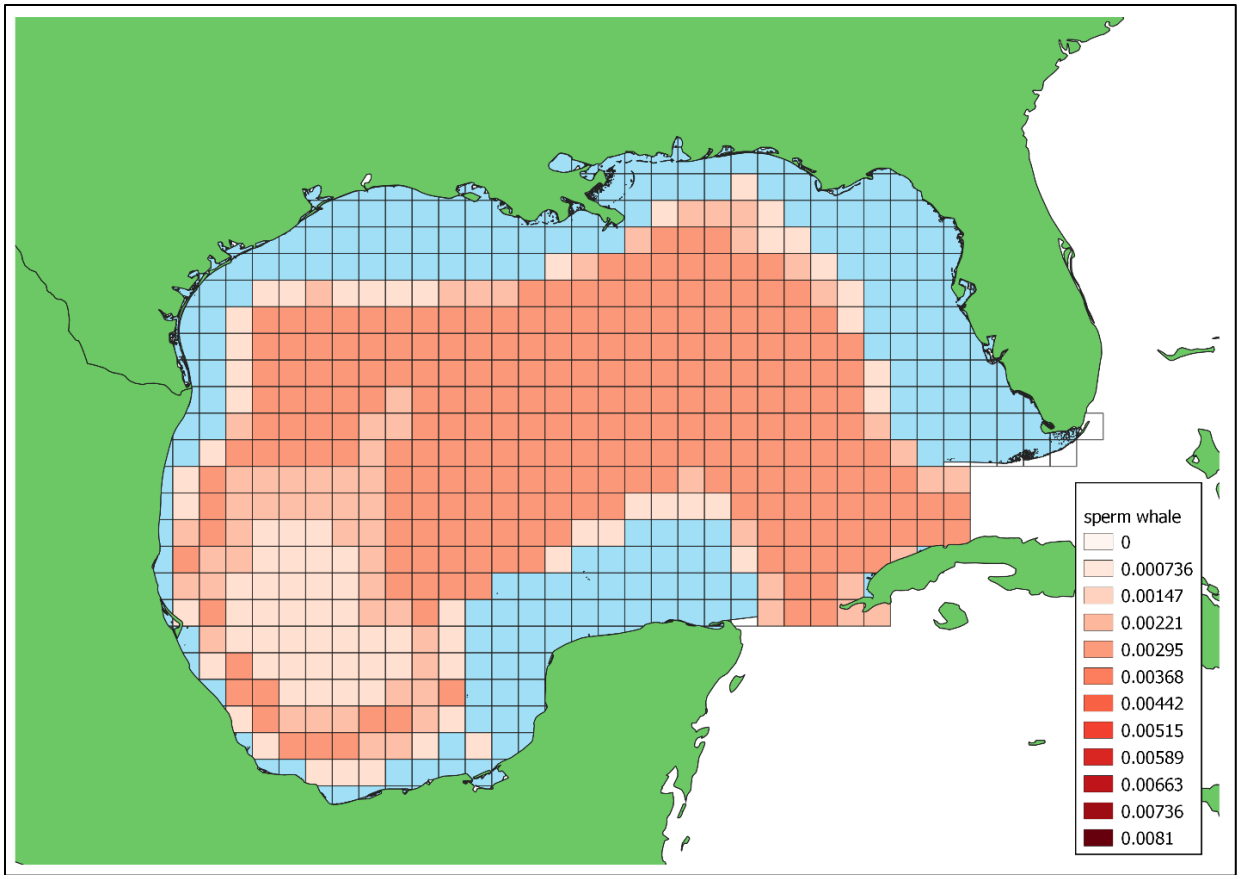

Figure B31 Raster of proportion of suitable habitat for Sperm whale at 0.5°x0.5° latitude/longitude resolution. The values of this raster sum to 1 and is used in the created C-ESIs.

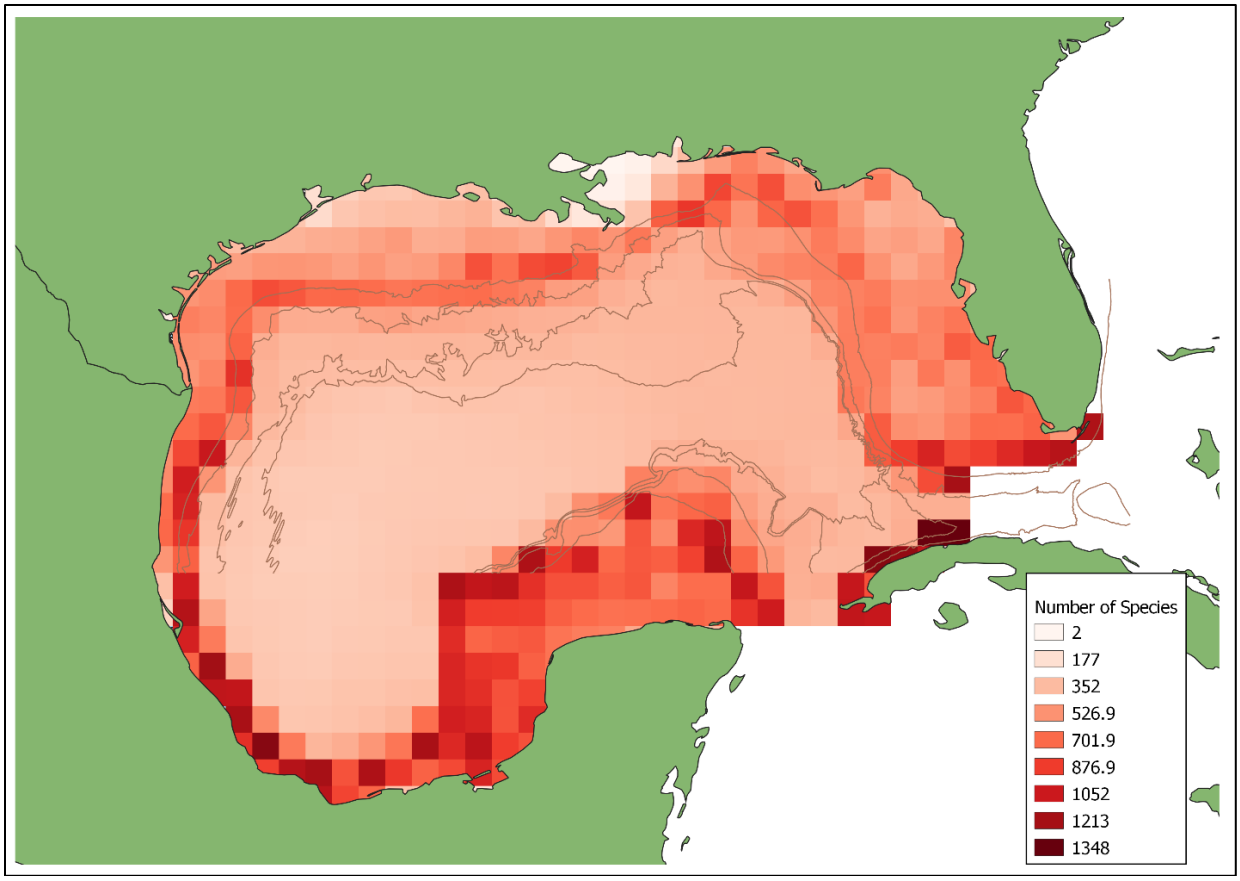

Figure B32 Raster of species richness for **ray finned fishes** at the 0.5°x0.5° latitude/longitude resolution. The values of this raster sum to 1 and the raster is used in the created C-ESIs.

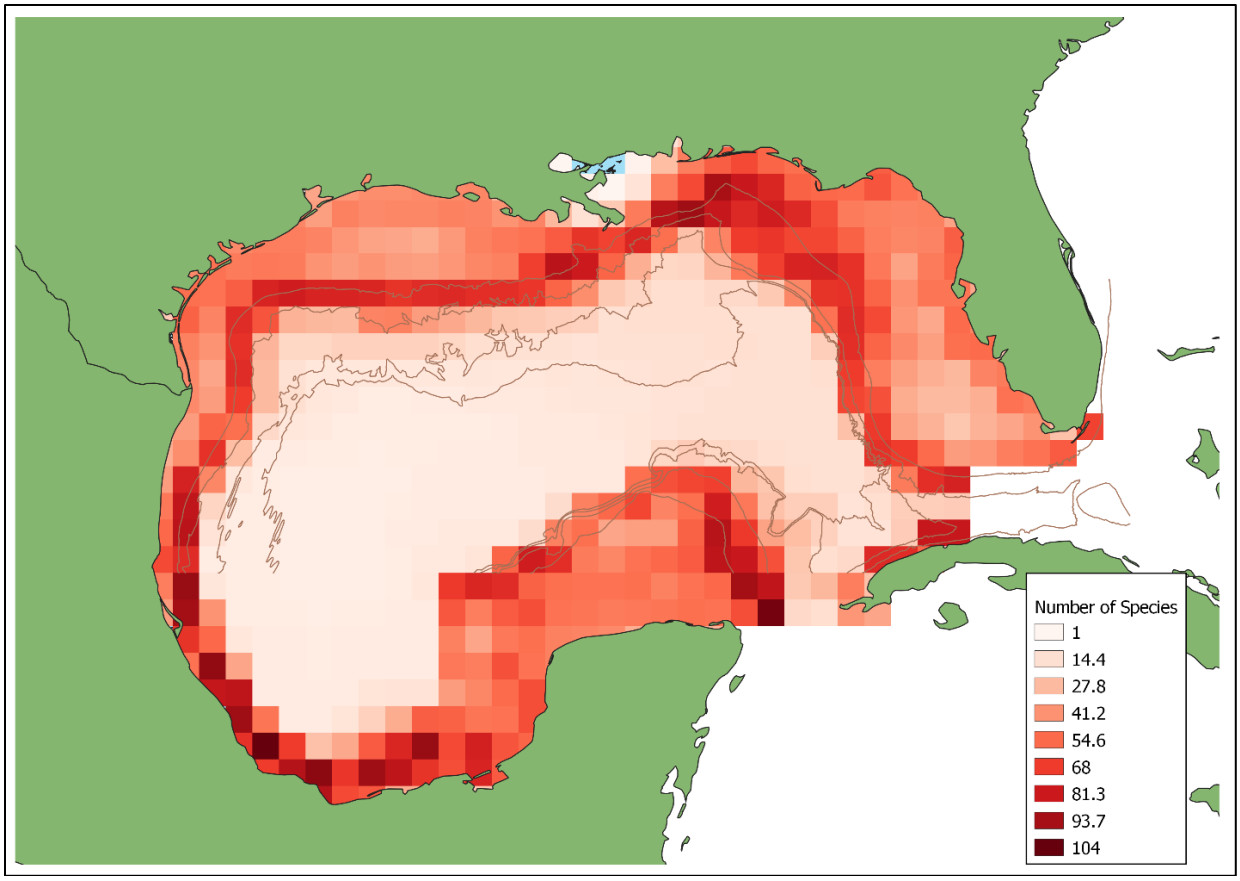

Figure B32 Raster of species richness for **sharks and rays** at the 0.5°x0.5° latitude/longitude resolution. The values of this raster sum to 1 and the raster is used in the created C-ESIs.

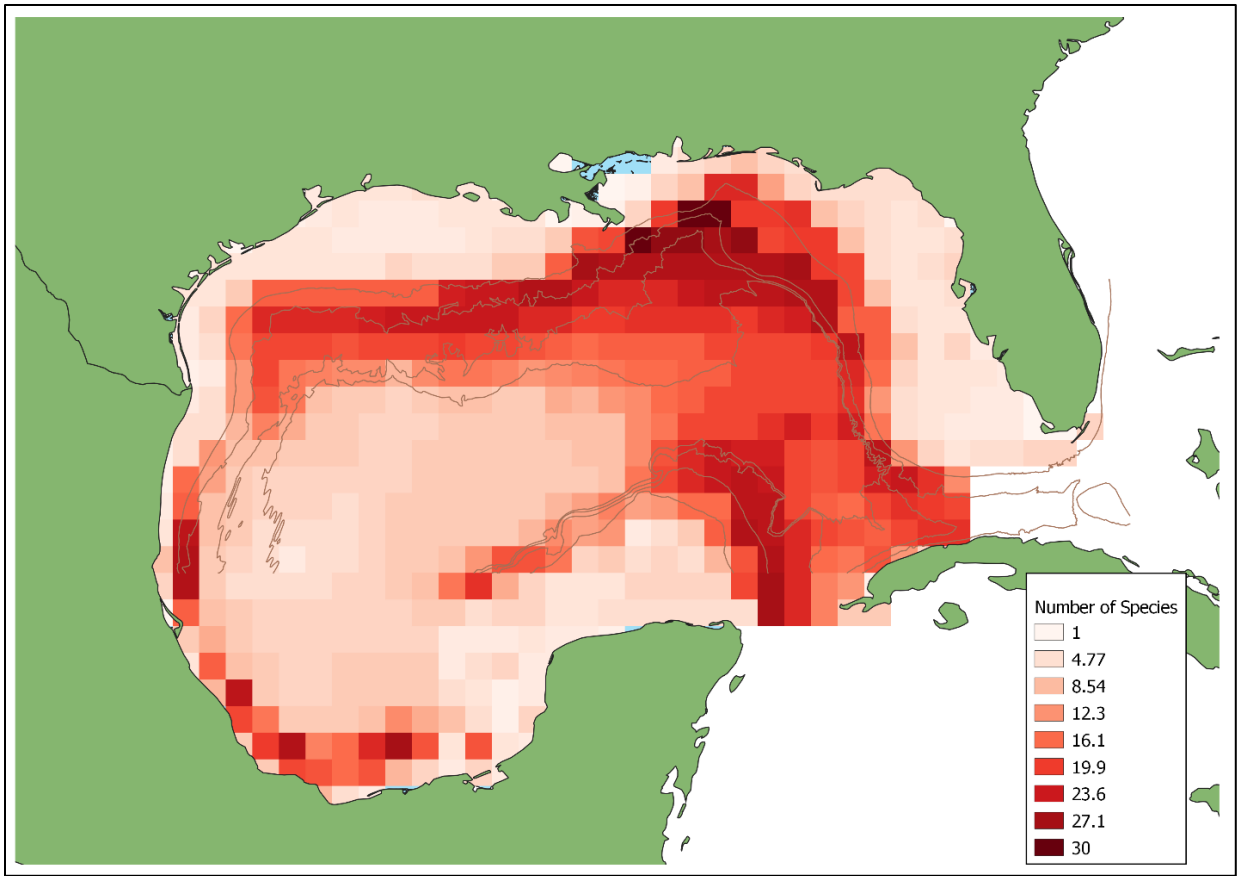

Figure B33 Raster of species richness for **mammals** at the 0.5°x0.5° latitude/longitude resolution. The values of this raster sum to 1 and the raster is used in the created C-ESIs.

Appendix C: Additional Tables and Figures from Running Marxan Spatial Planning Solver

Table C1 Initial Best Solution Summary **Scenario 1: Fisheries**.
Comparison of the best solutions from ten Marxan runs. Score (total score of the solution), Cost (sum of the costs of all the planning units), Planning_Units (number of planning units in solution), Connectivity (based on Connectivity), Penalty (from the Shortfall), Shortfall (Sum of unmet targets), Missing_Values (Number of features not met at 98%), MPM = minimum percent missing (the percent of the feature with the minimum covered). Based on the table below, Run9 was selected as the initial best with lowest score, connectivity, and missing values.

Run_Number	Score	Cost	Planning_Units	Connectivity	Penalty	Shortfall	Missing_Values	MPM
1	56548.74	51000	34	4368	5548.74	10021.33	2	0.763
2	56529.69	51000	34	4480	5529.69	9989.53	2	0.724
3	56041.02	51000	34	3920	5041.02	9252.97	2	0.758
4	56163.98	51000	34	4032	5163.98	9434.80	2	0.763
5	56018.9	51000	34	4144	5018.90	9231.06	1	0.759
6	55963.94	51000	34	4032	4963.94	9131.04	1	0.759
7	56163.98	51000	34	4144	5163.98	9434.80	2	0.763
8	55963.94	51000	34	4032	4963.94	9131.04	1	0.759
9	55963.94	51000	34	3920	4963.94	9131.04	1	0.759
10	56110.89	51000	34	4032	5110.89	9337.87	2	0.763

Table C2 Initial Best Solution by Feature **Scenario 1: Fisheries**.
Table from the initial Marxan Best solution before Boundary Length Modifier (BLM) and Species Penalty Factor (SPF) calibration for Marxan Scenario 1: Fisheries. Targets met for all conservation features except highly migratory species.

Conservation Feature	Target	Amount Held	Target Met	MPM
white shrimp	14852.79	15394.869	yes	1
brown shrimp	32834.88	32240.628	yes	0.981902
pink shrimp	4666.618	6430.221	yes	1
highly migratory	33833.21	25680.753	no	0.75904
coastal species	39743.58	39359.25	yes	0.99033

Table C3 Final Best Solution Summary **Scenario 1: Fisheries**.
Comparison of the best solutions from ten Marxan runs with modified BLM = 7.33 and SPF = 9.44. Best **Score** has risen from 55963 to 86950, **Planning Units** have increased from 34 to 41, all targets are met (MPM = 1). Based on the table below, Run9 was selected as the initial best with lowest score, connectivity, and missing values.

Run Number	Score	Cost	Planning Units	Connectivity	Penalty	Shortfall	Missing Values	MPM
1	87912.64	60000	40	3808	0	0	0	1
2	90375.52	60000	40	4144	0	0	0	1
3	91473.48	61500	41	4032	418.92	39.82	1	0.999
4	87091.68	60000	40	3696	0	0	0	1
5	87091.68	60000	40	3696	0	0	0	1
6	91285.25	60000	40	4256	88.76	7.41	1	1
7	91054.56	61500	41	4032	0	0	0	1
8	87912.64	60000	40	3808	0	0	0	1
9	86949.76	61500	41	3472	0	0	0	1
10	89598.08	61500	41	3584	1827.36	155.58	2	0.998

Table C4 Final Best Solution by Feature **Scenario 1: Fisheries**.
Table from the final Marxan Best solution with BLM = 7.33 and SPF = 9.44 for Marxan Scenario 1: Fisheries. Targets met for all conservation features.

Conservation Feature	Target	Amount Held	Target Met	MPM
white shrimp	14852.7918	16790.193	yes	1
brown shrimp	32834.8755	33111.162	yes	1
pink shrimp	4666.6179	6396.264	yes	1
highly migratory	33833.2113	34707.141	yes	1
coastal species	39743.5815	40381.047	yes	1

Table C5 Initial Best Solution Summary **Scenario 2: Mammals**
Comparison of the best solutions from ten Marxan runs. Score (total score of the solution), Cost (sum of the costs of all the planning units), Planning_Units (number of planning units in solution), Connectivity (based on Connectivity), Penalty (from the Shortfall), Shortfall (Sum of unmet targets), Missing_Values (Number of features not met at 100%), MPM = minimum percent missing (the percent of the feature with the minimum covered). Based on the table below, Run9 was selected as the initial best with lowest score. All runs meet feature targets with excess of 98% covered. No SPF calibration needed for this scenario.

Run_Number	Score	Cost	Planning_Units	Connectivity	Penalty	Shortfall	Missing Values	MPM
1	186890.8	186000	124	15232	890.81	1823.83	2	0.9956
2	188982.5	187500	125	17080	1482.53	3045.88	2	0.9929
3	187533.2	187500	125	16408	33.24	67.89	1	0.9997
4	188878.1	187500	125	16576	1378.09	2814.43	1	0.9889
5	187967.9	187500	125	17640	467.90	959.75	2	0.9982
6	189123.9	189000	126	17136	123.91	253.05	1	0.9990
7	186253.7	186000	124	16408	253.72	521.53	1	0.9985
8	187500	187500	125	17304	0.00	0.00	0	1.0000
9	186163.6	186000	124	16296	163.64	336.37	1	0.9991
10	186915.6	186000	124	16128	915.65	1879.37	3	0.9971

Table C6 Final Best Solution Summary **Scenario 2: Mammals**
Comparison of the best solutions from ten Marxan runs with modified BLM = 4.44 and SPF = 1. **Planning Units** and **Cost** are unchanged from the initial solution but **Connectivity** score of the best solution has decreased from 16296 to 5992. Based on the table below, Run1 was selected as the final best with lowest score.

Run Number	Score	Cost	Planning Units	Connectivity	Penalty	Shortfall	Missing Values	MPM
1	212604.5	186000	124	5992	0	0	0	1
2	218820.5	186000	124	7392	0	0	0	1
3	218331.4	187500	125	6944	0	0	0	1
4	212626.7	186000	124	5992	22.22	27.77	1	0.999922
5	214034.6	184500	123	6608	195.04	243.79	1	0.999318
6	213603	187500	125	5824	244.42	305.51	1	0.999146
7	214184.7	187500	125	5992	80.22	98.75	1	0.999612
8	213420.2	186000	124	6104	318.48	398.09	1	0.998887
9	213776.7	186000	124	6216	177.65	219.11	2	0.999247
10	212873.6	186000	124	5992	269.10	336.37	1	0.99906

Appendix D: Copyright Clearances

SPRINGER NATURE LICENSE TERMS AND CONDITIONS Nov 29, 2022
This Agreement between Emily Chancellor ("You") and Springer Nature ("Springer Nature") consists of your license details and the terms and conditions provided by Springer Nature and Copyright Clearance Center.

License Number 5438520845639 License date Nov 29, 2022

Licensed Content Publisher Springer Nature

Licensed Content Publication Springer eBook

Licensed Content Title Comparative Environmental Sensitivity of Offshore Gulf of Mexico Waters Potentially Impacted by Ultra-Deep Oil Well Blowouts

Licensed Content Author Emily Chancellor, Steven A. Murawski, Claire B. Paris et al

Licensed Content Date Jan 1, 2020 Type of Use Thesis/Dissertation

Requestor type academic/university or research institute

Format electronic Portion full article/chapter

Order reference number 31585731

License Number	5438520845639
License date	Nov 29, 2022

Printable Details

Licensed Content

Licensed Content Publisher	Springer Nature
Licensed Content Publication	Springer eBook
Licensed Content Title	Comparative Environmental Sensitivity of Offshore Gulf of Mexico Waters Potentially Impacted by Ultra-Deep Oil Well Blowouts
Licensed Content Author	Emily Chancellor, Steven A. Murawski, Claire B. Paris et al
Licensed Content Date	Jan 1, 2020

Order Details

Type of Use	Thesis/Dissertation
Requestor type	academic/university or research institute
Format	electronic
Portion	full article/chapter
Will you be translating?	no
Circulation/distribution	30 - 99
Author of this Springer Nature content	yes

About Your Work

Title	Quantifying Environmental Sensitivity of Marine Resources to Oil Well Blowouts in the Gulf of Mexico
Institution name	University of South Florida
Expected presentation date	Dec 2022

Additional Data

Order reference number	31585731